UNIVERSITY OF GAZİANTEP
GRADUATE SCHOOL OF
NATURAL & APPLIED SCIENCES

FINITE ELEMENT ANALYSIS OF KEYED CONNECTIONS UNDER TORSION AND BENDING

M. Sc. THESIS

IN

MECHANICAL ENGINEERING

BY

MUSTAFA MURAT YAVUZ

AUGUST 2010

Finite Element Analysis of Keyed Connections under Torsion and Bending

M. Sc. Thesis
in
Mechanical Engineering
University of Gaziantep

Supervisor
Assoc. Prof. Dr. Bahattin KANBER

by
Mustafa Murat YAVUZ
August 2010

T.C.
UNIVERSITY OF GAZİANTEP
GRADUATE SCHOOL OF
NATURAL & APPLIED SCIENCES
MECHANICAL ENGINEERING DEPARTMENT

Name of the thesis : Finite Element Analysis of Keyed Connections under Torsion and Bending
Name of the student : Mustafa Murat YAVUZ
Exam date : 04.08.2010

Approval of the Graduate School of Natural and Applied Sciences

Prof. Dr. Ramazan KOÇ
Director

I certify that this thesis satisfies all the requirements as a thesis for the degree of Master of Science.

Prof. Dr. L. Canan DÜLGER
Head of Department

This is to certify that we have read this thesis and that in our opinion it is fully adequate, in scope and quality, as a thesis for the degree of Master of Science.

Assoc. Prof. Dr. Bahattin KANBER
Supervisor

Examining Committee Members signature

Prof. Dr. Mustafa ÖZAKÇA _____

Assoc. Prof. Dr. Bahattin KANBER _____

Assist. Prof. Dr. Ahmet ERKLİĞ _____

ABSTRACT

FINITE ELEMENT ANALYSIS OF KEYED CONNECTIONS UNDER TORSION AND BENDING

YAVUZ, M. M.
M.Sc. in Mechanical Eng.
Supervisor: Assoc. Prof. Dr. Bahattin Kanber
August 2010, 149 pages

In this thesis, keyed connections are analysed using finite element method under torsion and bending. The effects of key edge geometries, the amount of torque, interference and friction on contact stresses between parts are investigated. ANSYS finite element package program is used in the analysis. Mapped mesh technique is used in all finite element models. The results are compared with available experimental results in the literature.

Key Words: key, keyway, keyed connections, stress, finite element method

ÖZET

KAMALI BAĞLANTILARIN EĞME VE BURMA ETKİSİ ALTINDA SONLU ELEMANLAR ANALİZİ

YAVUZ, M. M.
Yüksek Lisans Tezi, Mak Müh. Bölümü
Tez Yöneticisi: Doç. Dr. Bahattin KANBER
Ağustos 2010, 149 sayfa

Bu tezde kamalı bağlantılar, burulma ve bükülme yükleri altında sonlu elemanlar yöntemi kullanılarak incelenmiştir. Kama köşe geometrilerinin, farklı tork değerlerinin, parçalar arası sıkı geçmenin ve sürtünmenin temas yüzeyindeki gerilmeler üzerine etkileri araştırılmıştır. Çalışmada, ANSYS sonlu elemanlar paket programı kullanılmıştır. Sonlu eleman modellerinde, ölçekli ağ elde etme yöntemi uygulanmıştır. Analiz sonuçları literatürde var olan deneysel sonuçlarla kısaylanmıştır.

Anahtar Kelimeler: kama, kama yatağı, kamalı bağlantılar, gerilme, sonlu eleman yöntemi

ACKNOWLEDGMENTS

I express sincere appreciation to my supervisor Assoc. Prof. Dr. Bahattin Kanber for all helping. I cannot complete this thesis without his support and effort. His advices provide to continue and prevent plugging of my thesis in all steps.

Finally, I want to thank my family. My parents Nebi and Selma Yavuz, raised and always help me. They support morale and everything all my life.

CONTENTS

page

LIST OF FIGURES page

LIST OF TABLES page

LIST OF SYMBOLS

E : Young's modulus

G : Shear modulus

ε : Normal strain

γ : Shear strain

γ_y : Yield shear strain

γ_k : Mean shear strain

υ : Poisson's Ratio

I : Stress index; measured shear stress/nominal shear stress in shaft

I_1 : Principal stress index; measured principal stress/nominal stress in shaft

J : Stress index; measured shear stress/mean shear stress in key

β : Stress concentration factor of keyway

T : Applied torque

F : Applied force

M : Applied moment

Ty : Yield torque

τ : Shear stress

r : Radius of key edge fillet

r_s : Radius of shoulder fillet

R : Radius of keyway fillet

d : Diameter of shaft

D : Diameter of hub

b : Width of key

t : Thickness of models

Φ : Angular position in keyway fillet

α : Angular coordinate about shaft axis measured from plane of symmetry

Sb, Ss : Positions of measurement on keyway

Sr : Position of measurement between Sb and Ss on keyway

fc : Friction coefficient

x : Position at keyway edge profile

CHAPTER 1

INTRODUCTION

Keys are mostly used in machine elements for making connection of transmitting parts. Keys are placed in a slot which is called keyway between shafts and other machine parts like gears, discs, pulleys (for simplify, call all of them a general name; hub).

Different shapes and dimensions of keys and keyways are present and most of them have standards. End milled keyway, sled runner keyway and their keys are commonly used, due to their simple geometries and easy manufacturing properties. Also, different types of keys and keyways can be seen in commercial usage. Keys are widely used in connections of machine parts. They can be found from the most simple and small parts to complex and big parts connections. They can be used from toy cars to war tanks in the power transmitting parts. They are made of different materials with respect to connection parts. Plastic, brass, steel and other materials are some examples of its materials. Keys are mostly assembled with press fit or minimum clearance fit.

Keys and keyways are important design criteria of transmitting systems safety. If key is wanted to be stronger, key sizes can be increased. But for placing a larger key, keyway sizes should be increased and causes to decrease the strength of shaft and hub. If shaft and hub are wanted to be stronger from the effect of keyway's decreasing the strength, keyway and key sizes can be made small. However, key is weak at this time. Hence optimum key and keyway dimensions and geometries are required to satisfy the optimum safety of key, shaft and hub.

When a torque is applied to shaft or hub, it is transmitted mostly on key to the other part. From the using condition of keys, they are generally under all loading types. But mostly torsion and bending loadings are applied at keys. In proportional to the

key size to the shaft and hub sizes, key is smaller than shaft and hub. From these reasons, high stresses are expected to obtain at keys and keyways.

In this study, numerical method is used for investigating the keyed connections. The development of solution methods, fast computers and accuracy are some of the reasons for selecting the numerical analysis. Numerical technique is in spite of the experimental method, is an approximate solution technique. Results may not be direct solutions of real system analysis. But it has benefits like solution is fast by using computers; no experimental apparatus or mechanism is needed. If approximate solution results are acceptable, henceforth new solution tries are faster than experimental techniques.

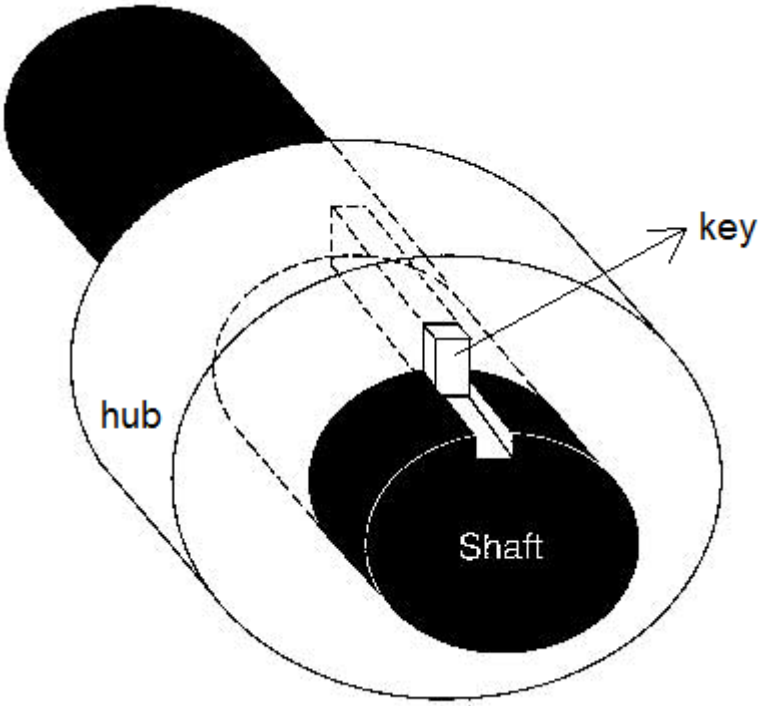

Figure 1.1. Transmitting system model of hub, shaft and key

This thesis mainly concerns the analysis of keyed connection under torsion and bending by using finite element analysis.

There are some studies on the literature about this subject. Some of them directly investigated keys and keyways by using experimental techniques. Other studies do

not directly investigate keys and keyways, but they show that key and keyway are important design criteria to prevent the failure of the system.

FEM models are compared with suitable experimental results. The contact algorithms of FEM are compared for different torques in section 5.3. FEM results of the effect of friction and key edge geometries are compared in section 5.4 with respect to the experimental study of Fessler and Appavoo [7] in 2D. FEM results of key edge geometries, frictions and torques are compared with Fessler and Appavoo's [7] study in section 5.5. Also the results of FEM on the effect of interferences and friction are compared with experimental study of Fessler and Eissa [4] in section 5.5. The effect of keyway fillet radius and applied torque is compared in section 5.6 with respect to experimental study of Okubo and colleagues [2]. In section 5.7, the FEM results of a shaft with keyway under torsion are compared with Fessler and colleagues [1] study. The FEM results of a shaft with keyway under bending are compared with experimental results of Fessler and colleagues [3] study. In section 5.9, FEM results are given for hub, shaft and key interaction under bending.

CHAPTER 2

LITERATURE SURVEY

2.1. Introduction

Because of theoretical complexity of shaft, key and hub interaction problem, the keyway stresses are generally studied experimentally. They are investigated under torsion, bending and axial loadings using different experimental techniques.

Fessler and co-workers [1] investigated the keyway end stresses of shouldered shafts using photoelastic techniques without considering key and hub interaction. They presented the principle stress indices in keyway fillets under direct and torsional loading.

Okubo and colleagues [2] studied stress concentration on keyways by using the electroplating method under torsional loading only. They fitted a shaft of carbon steel, plated with copper into a boss with a key. It was concluded that the keyway stress is concentrated at the corners of the keyway and it increases when the ratio of keyway corner fillet radius to shaft diameter decreases.

Fessler and colleagues [3] investigated the stresses at end milled keyways using the frozen-stress photoelastic technique for direct loading, bending and torsion. They observed that the peak stress in direct loading and bending is always in the fillet at the end of the keyway. They also reported that the peak stresses of combined loading of bending and torsion are less than pure torsion.

Fessler and Eissa [4] studied on the effect of fits and friction on the keyway stresses using frozen stress photoelastic technique. They used various metric and inched standard keyed shafts and hubs by applying different torques. They reported that high stresses occur mostly at the curvature of keyway and key surfaces. They also reported that the fit and friction between shaft and hub affect the torque transmission,

but do not affect the stress distribution around the key. Same authors [5] also investigated the effect of key and keyway shape with usual fits and friction. They reported that high stresses occur at the keyway contact surfaces and rounding the key chamfers decreases the keyway side stresses but increases at the edge stresses because of sliding. They showed that key slide is depended on the applied torque, key geometry and fit of the key in the shaft. The same photoelastic technique was used to obtain 3D stress distributions on keyways by the same authors [6]. The results showed that stresses are decreased on the key edge touched sides on keyway when decreasing the key width.

Fessler and Appavoo [7] extended the previous works by considering different shapes of key-edge. Study showed that increasing the chamfer dimensions causes decreasing the stresses. Increasing the torque also increases the peak stress. However it decreases the stress concentration factors because the nominal stresses are also increased. They reported that if key edges are rounded, the greatest stresses are obtained at the centre of the fillet radius.

Shaffer [8] studied theoretically on stresses between a circumferential key and its keyway. He applied the slip-line field theory of the plasticity in his study. He investigated the bearing stresses of the key and keyway shoulder and transverse shear of the key. He reported that the ability of key to withstand the bearing force calculated in his works is greater than that predicted by conventional engineering analysis.

Fessler and Warrior [9] reported the advantages of using cylindrical keys in torque transmission using photoelastic technique. They pointed out that the peak stresses in cylindrical keys are independent of the usual fits of the key and lubrication and decrease with increasing the key diameter. They also proved that the peak stress values on cylindrical keys lower than rectangular keys.

Çelik [10] studied on the deflection and stress analysis of a spur gear using the boundary element method. He pointed out that when the whole body model including the keyway is used in the analysis, the stress is concentrated around tooth contact point and keyway. Kanber [11] analysed spur gears with four different keyway

position using coupling of finite and boundary element methods. He concluded that stresses along the tooth fillet reach their maximum distributions when the nearest tooth to the keyway is loaded.

There are many studies in the literature reporting that the shaft failures generally start at the keyway areas. Vogwell [12] studied on a vehicle wheel shaft failure under fatigue loading. He concluded that the failure occurs at keyway slot and a fatigue crack is initiated at this point. Berndt and Bennekom [13] presented a collection of pump shaft failures. Study shows that one of the failures is caused by the stresses at the root of the key. Bhuamik and colleagues [14] researched the failure of a hollow power transmission shaft and they concluded that crack is initiated by fatigue at the keyway edges. They suggested that rounding the keyway sharp edges decreases the stress concentrations on keyway. Parida and colleagues [15] investigated the failure of a coal pulverizer mill shaft in fatigue loading. They proved that fatigue cracks originate from the keyway area, unusually from the top edge. Sekercioglu [16] investigated a polymer injection pump for polymer production under torsion. His study reports that fracture starts firstly gear keyway because sharp key corner is causing stress concentrations on gear keyway and small keyway fillet radius causes a notch effect. Göksenli and Eryürek [17] researched the failure of an elevator of 320 kg loading carry capacity's shaft under torsional and bending loading. His study concluded that failure occurs at the keyway and stresses are affected by radius of curvature of the keyway.

Vidner and Leidich [18] used the Ruiz criterion for the evaluation of crack initiation in contact subjected to fretting fatigue. In their study, the fatigue fretting damage parameters are discussed for key, hub and shaft connections using both experimental and numerical methods. They reported that fatigue failure of crack initiates at directly in key groove radius and one of the maximum stresses occurs in the key groove radius between shaft and key.

Yang and Tong [19] studied analytically splines and keys profiles performances on power transmission. They gave three different design conditions for optimization of performance: Uniform hub deformation, maximum transmission load capacity and

optimum capacity. Study concluded that spline and key profiles are an important factor for power transmission.

2.2. Conclusion of literature survey

The literature review shows that keyed connections are very important. They are widely used in connected parts. Almost all studies pointed out that high stresses occur at keyways. Therefore, most of the failures are started at the keyways.

Most of the studies in the literature investigate the keyway stresses using photo-elastic experimental techniques. Because of complexity of the problem, numerical studies such as finite and boundary element methods are not used. Therefore, this study offers an alternative method to investigate keyway stresses.

Bending analysis of hub, shaft and key interaction is not presented in literature. Commonly a single shaft with keyway is investigated under bending. In this study, it is investigated in details considering shaft, hub and key interaction.

CHAPTER 3

EXPERIMENTAL STUDIES

BY FESSLER-COLLEAGUES AND OKUBO-COLLEAGUES

3.1. Introduction

The FEM is a method to approximate the solution of governing differential equation of elasticity with appropriate boundary conditions. The amount of approach of results to the accurate results requires an error analysis or comparing the results of some other methods. If the analytical solutions of the problem are available, the FEM solutions can be compared with them. However, it is not always possible. The analytical solution of key, shaft and hub interaction problem studied in this work, for example, is very difficult without any simplification. It is already not exist in the literature. Therefore, the FEM solutions are compared with the results of experimental studies in the literature. In this chapter, some information is given about experimental studies of Fessler-colleagues and Okubo-colleagues.

3.2. Experimental study of Fessler and Appavoo [7]

Fessler and Appavoo investigate the effect of key edge shape on keyway stress distribution in shafts under torsional loading. They use photoelastic experimental technique in this investigation. In their study, they investigate how various key edge geometries and various torques affect the keyway edge stresses.

In their experimental study, hub and shaft geometries are kept constant and not changed in all experiments as shown in Figure 3.1. Only key edge dimensions are changed. All parts have a constant thickness of 3 mm. The shaft has a diameter of 125 mm. There is a hole of 10 mm at the centre of shaft. Four 5 mm diameter holes are used at the shaft. They are used for applying force couples to obtain a pure torque with a circular distance of 50 mm. Shaft has a keyway with a width of 32 mm and a height of 8.5 mm. Keyway edges are rounded. Hub has an outside diameter of 250

mm and inside diameter of 125 mm. Twelve 6 mm diameter holes are present at hub; used for fixing the hub with a circular distance of 220 mm. Hub has a keyway with a width of 32 mm and a height of 8.5 mm. Keyway edges are rounded. Key dimensions are kept constant; however, key edge dimensions are changed as shown in the Table 3.1. Keys have a width of 32 mm and height of 17 mm. Key edges are cut or rounded with variable dimensions with respect to the experimental studies. They are assembled with minimum clearance fit.

Table 3.1. Key edge dimensions in the experiment of Fessler and Appavoo [7]

Test no	Chamfer width, w (mm)	Chamfer height, h (mm)	Radius of key edge fillet, r (mm)
fa-1	1.00	0.84	-
fa-2	1.00	3.00	-
fa-3	0.70	0.70	-
fa-4	1.00	1.00	-
fa-5	1.30	1.30	-
fa-6	3.00	3.00	-
fa-7	1.00	1.00	1.00
fa-8	1.30	1.30	1.30
fa-9	3.00	3.00	3.00

Fessler and Appavoo [7] observe and measure changes in the fringe orders in a diffused light polariscope. They convert the results to maximum shear stresses. They use photoelastic materials for all parts in the experiments; however, all results are calibrated for a typical steel material.

In their experimental study, a pure torque is applied from the shaft to the hub. The torque is determined from the yield shear strain of a typical steel for torsion. It can be calculated as;

$$\tau = \gamma_y * G \tag{3.1}$$

where;

γ_y is the yield shear strain of a typical steel and it is equal to 0.0035.

G is shear modulus of a typical steel and it is used as $80 * 10^9$ Pa.

Shear stress can be obtained from Eq. 3.1 as 280 MPa. It is equal to the nominal shear stress in the shaft and can be written in terms of applied torque as follows

$$\tau = \frac{16*T}{\pi*d^3} \tag{3.2}$$

Where, T is applied torque and d is diameter of shaft which is equal to 0.125 m in their study. Using Eq. 3.2, the torque can be calculated as **T = 107.37** Nm.

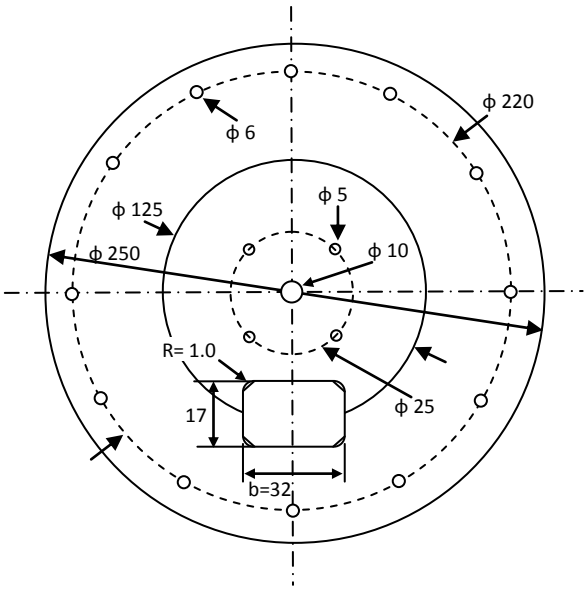

Figure 3.1. Experimental model of Fessler and Appovoo

They give the results by stress indices which is the ratio of measured maximum shear stress to applied nominal shear stress in the shaft. The Sb point on the keyway is the datum or starting point of the stress results taken (Figure 3.2). The positive direction is from Sb to Ss. The position of Sb and Ss change with respect to the key edge chamfer dimensions. Sr is the centre of keyway fillet.

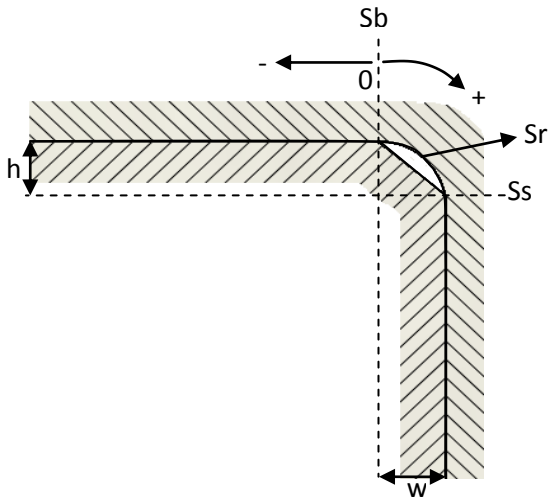

Figure 3.2. Key edge and keyway of shaft

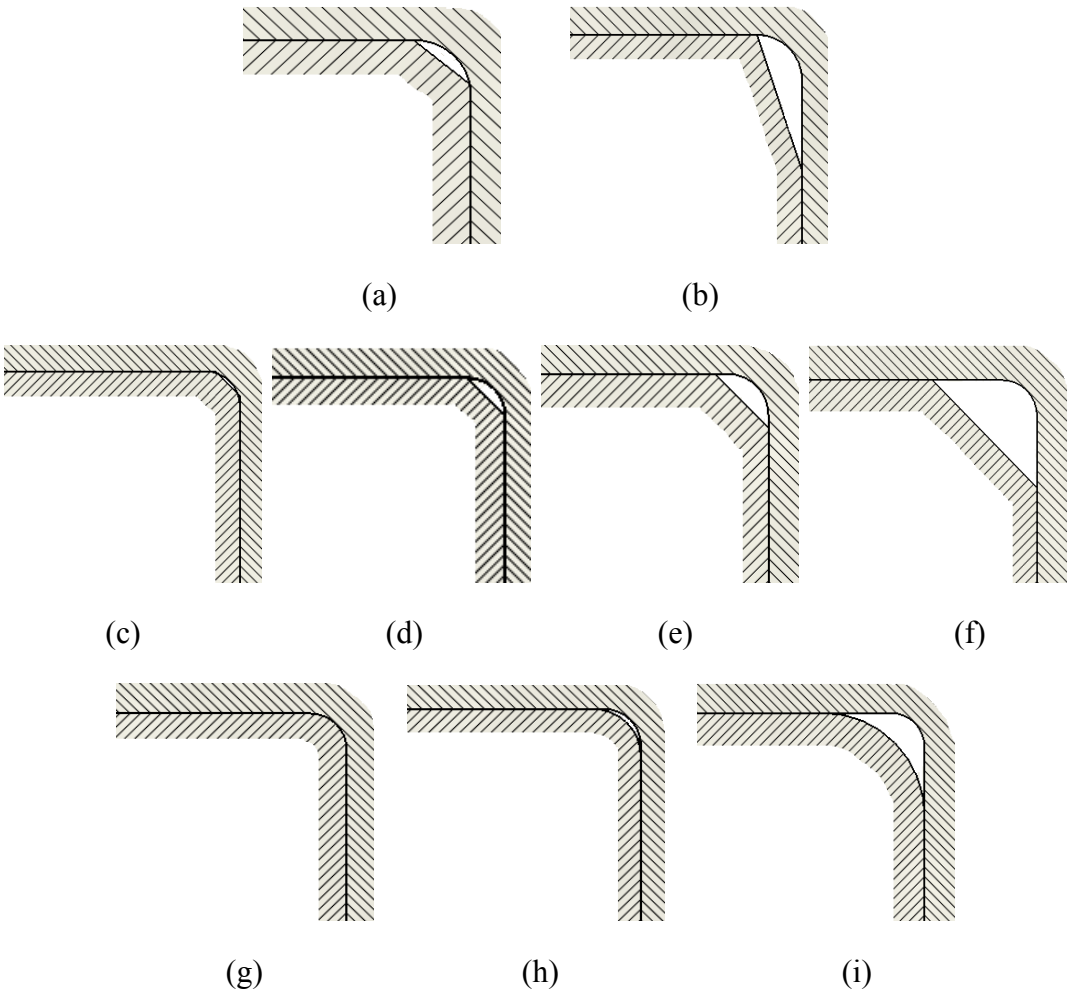

Figure 3.3. Test number and key edge dimensions, (a) Test no fa-1, (b) Test no fa-2, (c) Test no fa-3, (d) Test no fa-4, (e) Test no fa-5, (f) Test no fa-6, (g) Test no fa-7, (h) Test no fa-8, (i) Test no fa-9

3.3. Experimental study of Fessler and Eissa [4]

Fessler and Eissa investigate the effect of fits and friction at keyed connections. They analyse the hub-shaft-key interaction problem under torsional loading by using photoelastic experimental technique. Their experimental model is nearly as same as Fessler and Appavoo's [7] experimental model. It can be seen in Figure 3.1. But key has a height of 18 mm in study of Fessler and Eissa [4]. All other dimensions of models and conditions are same. Different fits and frictions are applied in model and they can be seen in Table 3.2 for analysing the effect of fits and friction at keyed connections. Positive values show that the clearances between parts and negative values show that the interference between parts in the Table 3.2.

Table 3.2. Clearances and friction coefficients in the experiment of Fessler and Eissa [4]

Test no	Clearance of shaft in hub (mm)	Clearance of key in shaft (mm)	Clearance of key in hub (mm)	Coefficient of friction
fe-1	+0.06	+0.06	+0.31	0.15
fe-2	+0.06	+0.06	+0.31	0.27
fe-3	+0.06	-0.08	+0.17	0.14
fe-4	+0.03	-0.07	+0.18	0.27
fe-5	+0.03	-0.16	+0.17	0.27
fe-6	-0.06	-0.08	+0.17	0.35

Experimental results are given by stress indices J;

$$J=\frac{T}{\frac{d}{2}\times b\times t} \tag{3.3}$$

where;

T is applied torque and d is diameter of shaft which is 125 mm. b is width of key and t is the model thickness. Applied torque calculation is as same as Fessler and Appovoo's [7] experimental study which is given in Equation 3.2.

3.4. Experimental study of Fessler and colleagues [3]

Fessler and colleagues investigate the stresses at end milled keyways in plain shafts in tension, bending and torsion. Also the effect of combine loading of tension,

bending and torsion is investigated in their experimental analysis. Only a shaft with keyway is investigated by using frozen-stress photoelastic technique experimentally. Shaft model is made of CT200 / HT907 photoelastic material in their analysis. Their experimental models have different dimensions like width, depth and fillet radius of keyway in tension, bending and torsion analyses. In tension analysis, 3 inch diameter shaft is used which has 15 inch length and 1/16 inch keyway fillet radius. Only a tension load is applied to the shaft from ends of shaft in their tension analysis. Same shaft dimensions of tension model are used in bending analysis. A standard bending test is applied from four points in their bending analysis. In their torsion analysis, 6 inch diameter shaft is used which has 19 inch length and 1/8 inch keyway fillet radius. Shaft is fixed from one end and twisted from other end by using a dead weight pulley system.

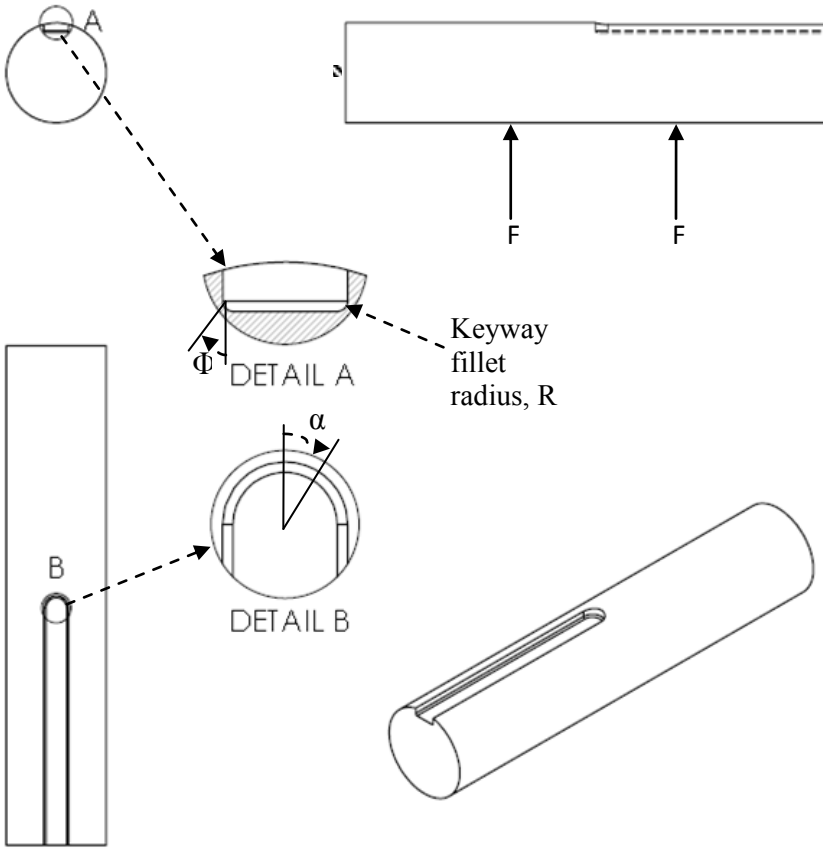

Figure 3.4. Analysis model of Fessler and colleagues [3] for bending

Their experimental results are given as principal stress indices which is the ratio of measured principal stresses to applied bending stress. The calculation of principal stress indices in bending is given as;

$$I_1 = \frac{\sigma_1}{\frac{32*M}{\pi*d^3}} \quad (3.4)$$

Where σ_1 is principal stress, M is applied bending moment and d is diameter of shaft.

Fessler and colleagues [1] also investigate stresses at keyway ends near shoulders in another experimental study by using photoelastic stress analysis. Only a shouldered shaft with keyways is investigated under tension and torsion loading in their analysis. Also the effect of change of shoulder fillet radius is investigated. Shaft model can be seen in Figure 3.5.

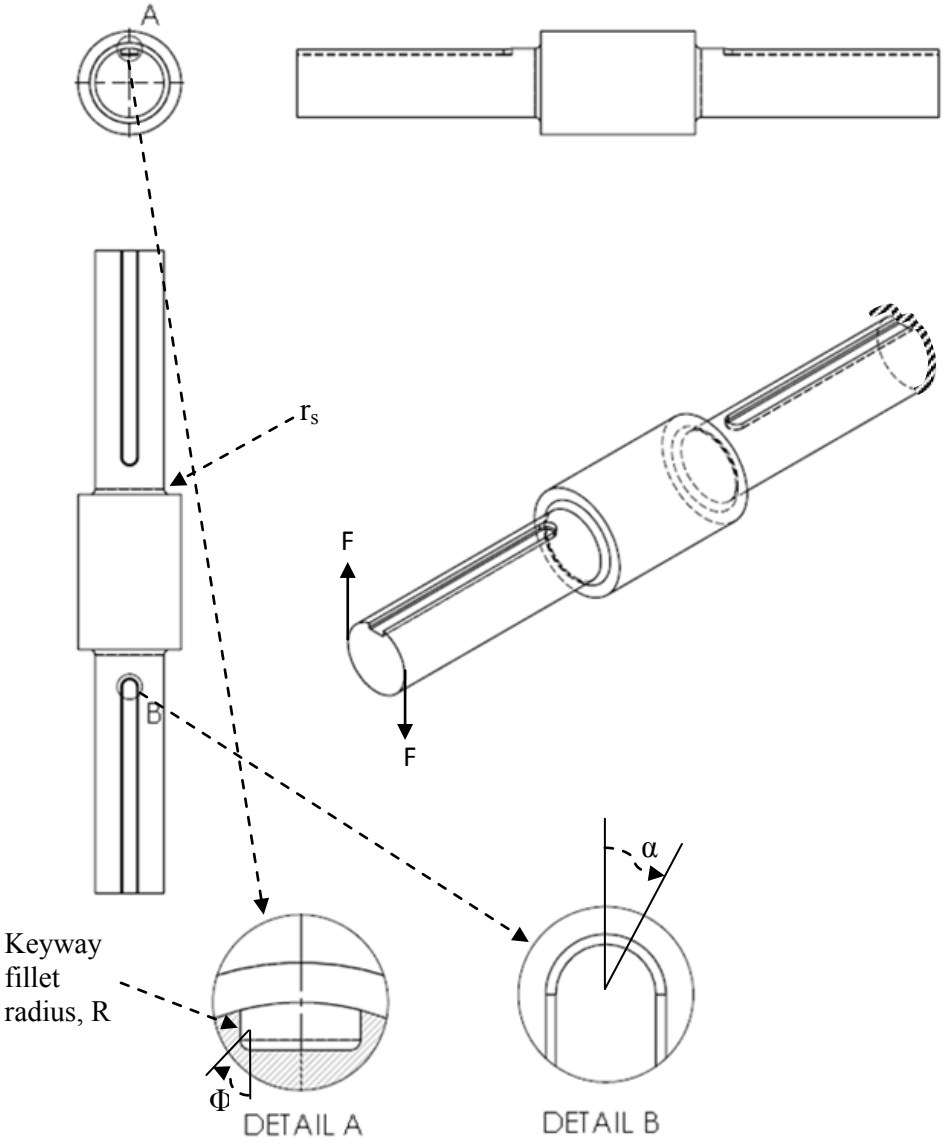

Figure 3.5. Analysis model of Fessler and colleagues [1] for torsion

Shaft has 28 inch length and 3 inch diameter. There is a shoulder at the centre of shaft and it has 4.5 inch diameter and 6.75 inch length. Distance between keyway and shoulder fillet is 0.25 inch. Shoulder fillet radius and keyway fillet radius are 0.063 inch. Shoulder fillet radius and distance between keyway and shoulder fillet are changed in some steps of their experiments. Shaft is made of Araldite CT200 / HT907 photoelastic material in their analysis. Shaft is loaded in air with position of vertical axis in direct loading from its ends. Also shaft is fixed from one end and twisted from other end at the same position in their torsion analysis. Fessler and colleagues [1] ignore the gravity effect from their experiments when their experimental loading is made at vertical axis position. Stress results are read from slices which are cut from keyway surface. They read fractional fringe orders in polariscope with a mercury lamp in their photoelastic experiment. Experiment results are given in principal stress indices which are the ratio of measured principal stresses to nominal shear stress of shaft and it is given in Equation 3.5 for torsion.

$$I_1 = \frac{\sigma_1}{\frac{16*T}{\pi*d^3}} \tag{3.5}$$

3.5. Experimental study of Okubo and colleagues [2]

Okubo and colleagues investigate stress concentration in keyways when torque is transmitted through keys. They use electroplating method of strain analysis to investigate the keyway stresses at the corner of keyway. Key, hub and shaft are used in their analyses which are made of typical carbon steel.

Two different shaft diameters are used in their analysis. Key and hub dimensions are changed with respect to the shaft diameters. In their experiments, one of the shafts has dimensions of 10 mm diameter and 106 mm length. An end milled keyway is obtained at the shaft and has dimensions of 74 mm length, 1 mm depth and 2.5 mm width. In the other experiment, the shaft has dimensions of 12 mm diameter and 106 mm length. An end milled keyway has dimensions of 74 mm length, 2.4 mm depth and 4 mm width. The keyway corners are rounded with different dimensions to see the effect of keyway fillet in their experiments. The keyway is obtained at one end side of shaft and the other end side of shaft has no keyway in their experimental shaft model. Hub and key are mounted on the shaft at the end of keyway as shown in

Figure 3.6. A rectangular key with chamfered bottom edges has dimensions of 25 mm length, 2.66 mm height and 2.5 mm width. Chamfer dimensions of bottom key corners are equal to 0.333 mm. A hub is placed on the shaft which is the same length of key. Torque is increased as shown in the Table 3.3. Hub is fixed from its outside circumferential areas and a pure torque is applied from shaft's other end surface. Stresses are measured from key top edge contact point on the keyway fillet of shaft.

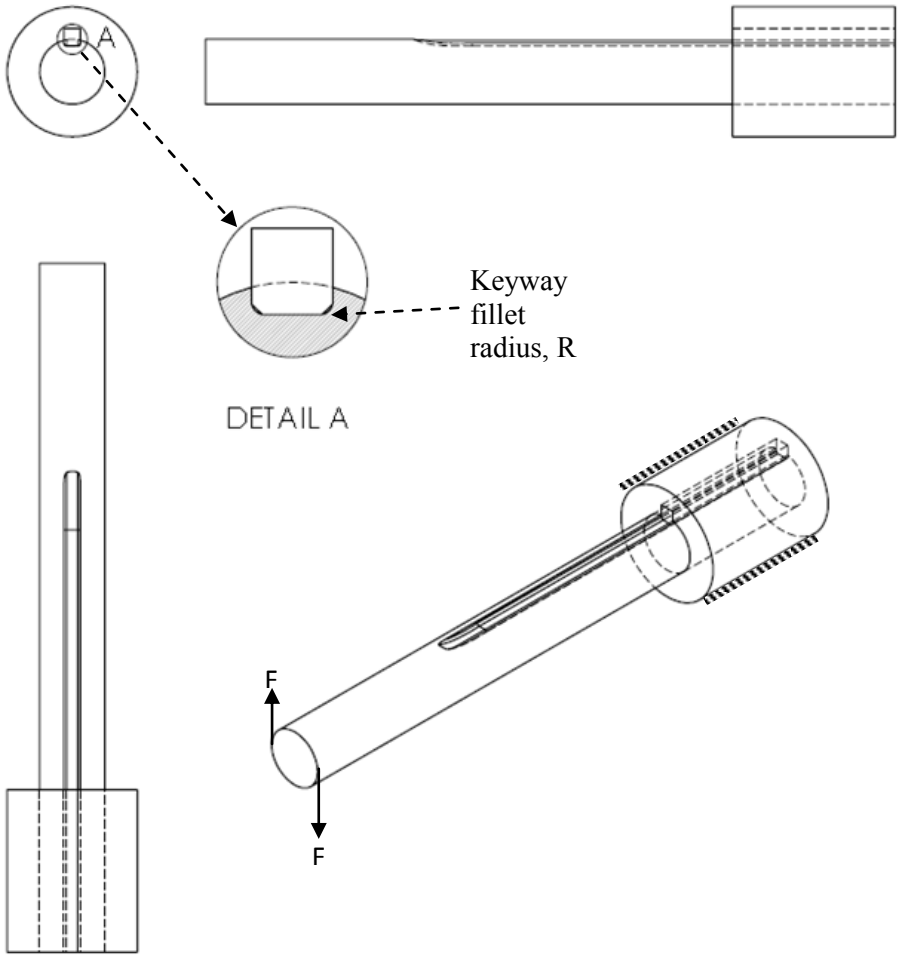

Figure 3.6. Analysis models of Okubo and colleagues [2] with hub and key

Stresses are given as stress concentration factor (β) which is the ratio of measured shear stress to nominal shear stress of shaft. The stress concentration factor (β) is calculated from;

$$\beta = \frac{\pi * d^3 * G * \gamma}{16 * T} \tag{3.6}$$

where;

d is diameter of shaft and it is equal to 10 mm.

G is modulus of rigidity and it is used as 80 GPa for a typical steel.

γ is shear strain and it is taken from the Table 3.3 with respect to experimental study of Okubo and colleagues.

Table 3.3. Experimental properties of Okubo and colleagues' [2] study

Test no	r (mm)	r/d (mm)	T (kg.m)	γ (x10^{-3})
oh-1	0.06	0.006	0.50	1.061
oh-2	0.08	0.008	0.50	1.009
oh-3	0.12	0.012	0.60	1.082
oh-4	0.19	0.019	0.68	1.061
oh-5	0.26	0.026	0.73	1.040
oh-6	0.28	0.028	0.73	1.027
oh-7	0.40	0.040	0.81	1.044

Okubo and colleagues use Tereda's [20] experimental analysis results to compare their results with ignoring the key effect. It can be estimated that only a shaft with keyway can be analysed under torsion when ignoring the key effect.

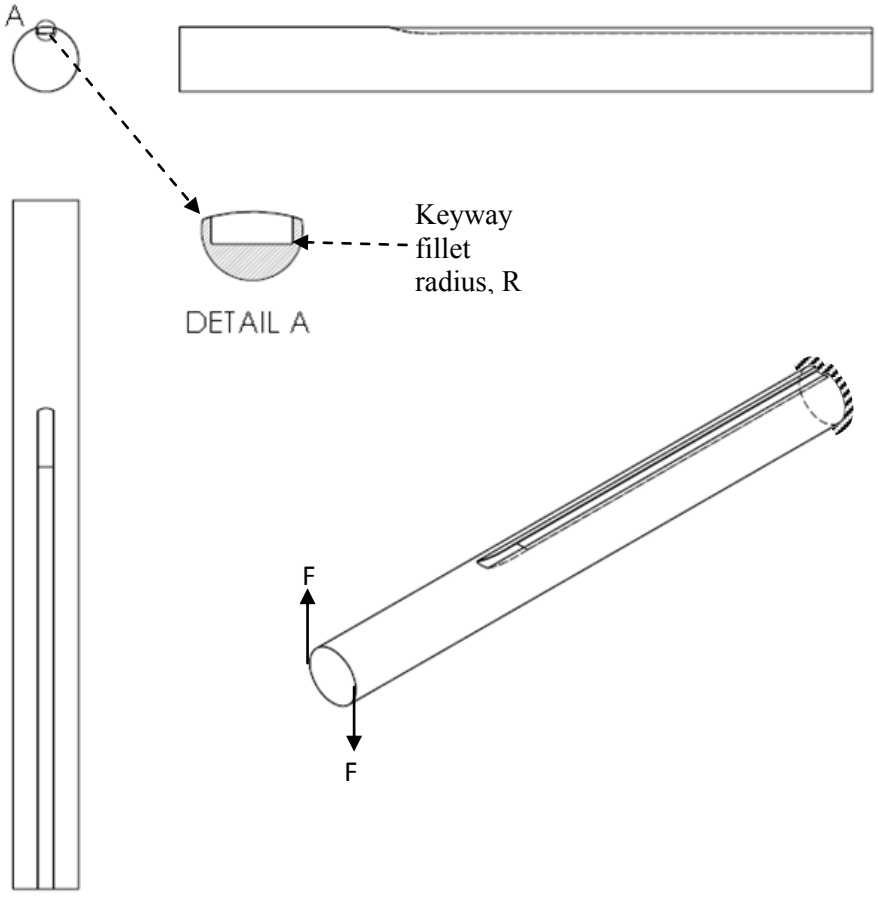

Figure 3.7. Analysis model of Okubo and colleagues [2] without hub and key

The model of the shaft is given in Figure 3.7. Shaft has a diameter of 10 mm and a length of 106 mm. An end milled keyway is obtained at the shaft and has a depth of 1 mm, length of 74 mm and width of 2.5 mm. Its results are compared with Terada's [20] experimental results.

3.6. Conclusion of experimental studies by Fessler-colleagues and Okubo-colleagues

In general, experimental studies of Fessler-colleagues and Okubo-colleagues are mentioned in this chapter. These studies are foremost and one of suitable experimental studies about related subject. They show the way of how to make the analyses of keyed connections. Their studies give lots of information and assistance, later using finite element technique about keyed connection analysis.

Fessler and colleagues generally make their experiments with photoelastic experimental technique and use polariscope to see the results. Okubo and colleagues use electroplating method strain analysis to see the result.

Their analyses mainly concern the keyway stresses. They give information experimental technique properties and boundary conditions of experiments. They point out the critical and interested locations of the keyed connection analyses. Models dimensions, analysis and boundary conditions, interaction of parts and other required properties are taken from their studies to make finite element models of numerical analysis.

CHAPTER 4

FINITE ELEMENT MODELS IN ANSYS

4.1. Introduction

Different techniques can be used for analysing parts or systems. Finite element analysis is one of the analysing techniques which is used in this thesis. Several finite element analysis package programs are present in commercial usage. In this analysis, ANSYS finite element analysis package program is used. It is one of the most using analysing programs in the literature and it is capable of solving the problems of static/dynamic structural (both linear and non-linear), heat transfer, fluid dynamics, contact pair, acoustic and electromagnetic analysis. Pre-processor, solving and post-processor of analyses are made in ANSYS. Some of models are prepared in SOLIDWORKS 3D modelling program for pre-processor modelling step and imported to ANSYS as parasoid file form.

The common points of all finite element models are discussed in this section. Some information are further discussed in subsections of the related finite element models.

Finite element models in ANSYS contain three main parts which are pre-processor, solving and post-processor. Defining the finite element type, material properties, modelling of parts, material properties assignments to the parts, meshing and contact pair definition are done in pre-processor step. Defining the boundary conditions, applying forces and solving operation are done in solving step. Plotting and listing the analysis results are made in post-processor step.

A linear elastic isotropic carbon steel A1040 is selected in all finite element models for material selection of finite element analysis, which has properties of Young's modulus (E) 200 GPa and Poisson's Ratio (υ) 0.30.

Meshing is required in finite element analyses. Meshing can be explained that dividing of the each part with small elements like cubes, prisms, pyramid and/or other geometry types of elements are called finite elements. Elements have nodes and these nodes are connected with mesh lines. The dividing of solid part to small finite elements is only for using finite element analysis and is not a real dividing or separation of whole part.

Meshing is an important part of convergence of solution. Good mesh can provide good convergence, less iterations, more accuracy, saves time and decrease computer system trouble. Bad or poor mesh can cause divergence, more iteration, less accuracy, more CPU time and increase computer system trouble.

The number of elements can directly influence the solution results and accuracy. Analysis results are taken from nodes in nodal solution. If enough nodes are not present at required place, insufficient numbers of data are taken. This will affect the results' sensitivity. If much various and rapidly change conditions exist in analysis, more finite element usage is better. For this purpose, mapped meshing technique is used in all finite element models. High stress regions of parts are meshed more elements. However low stress regions are meshed less but enough elements.

Increasing the number of elements is good but how many elements can be increased in analysis. It is generally known that the increase of elements can cause to more CPU time and increase the round off errors. If the increment of number of elements is not dominant to change results, the numbers of elements are enough. Also this element number satisfaction can be called mesh convergence.

Five different contact algorithms are present in ANSYS in contact library. Augmented Lagrange, Lagrange, Lagrange-Penalty, MPC and Penalty algorithms are the contact algorithms. All contact algorithms have different properties and functions. Augmented Lagrange is used in 2D analyses. Lagrange-Penalty contact algorithm is used in 3D analyses.

On the contrary to the surface forces, concentrated forces are applied in force applying section of the analyses. This will make high stresses at force applied points

and nearby locations. However critical and interested locations like contact surfaces of key and keyway have enough distance from applied concentrated forces. Hence the concentrated forces do not dominantly influence the stress results of related locations with respect to Saint Venant's principle in the analyses. Also it can be seen that the effect of the concentrated forces causes peak stresses at the applied points in results of the solution. However the stress values are not extremely high and get an expected stress distribution far away from the concentrated force locations. Different finite element models are obtained with respect to the experimental studies.

4.2. 2D Finite element models of hub, shaft and key under torsion [7]

2D hub, shaft and key finite element models are obtained with respect to the experimental models of Fessler and Appovoo [7] as shown in Figure 4.1. Especially when looking the thickness of the experimental study; the hub, shaft and key interaction problem can be analysed with 2D. Model geometry sizes show that thickness is less than other dimensions. It can be assumed that this type of analysis can be made as plane stress analysis. 2D models are obtained on x-y plane in ANSYS. Modelling, meshing, contact options defining, applying boundary conditions and solving steps are needed for finite element analysing.

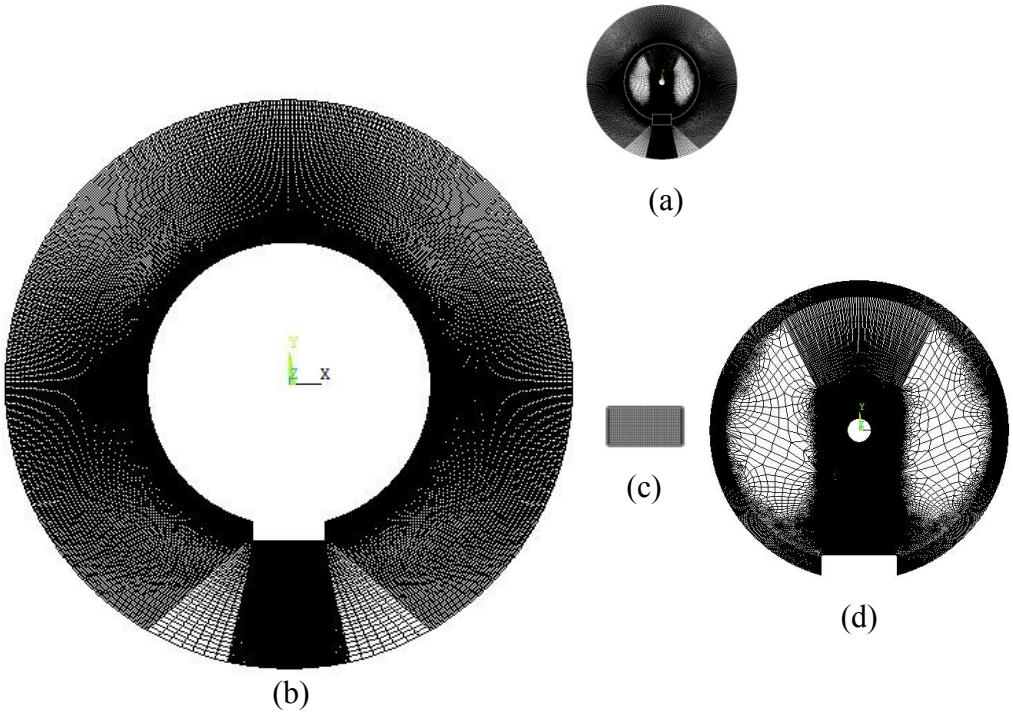

Figure 4.1. 2D hub, shaft and key FEM models of Fessler and Appovoo [7], (a) Assembled parts, (b) Shaft, (c) Key, (d) Hub

Models are constructed from areas in 2D modelling. Areas are obtained from lines and arcs. Lines and arcs can be modelled with keypoints which is a helping point for line or arc creating and not used in finite element. Keypoints are placed to suitable places where line or arc start or end locations. When modelling is finished, meshing is required.

4.2.1. Mesh technique

Finite element type must be determined for meshing. There are different finite element types in ANSYS. Mainly PLANE42 and PLANE82 finite element types are suitable for 2D stress analyses. They can be used at plane stress, plane strain, axisymmetric and plane stress with thickness options. Their nodes have two degrees of freedom in x and y coordinates. PLANE42 and PLANE82 elements are same properties however PLANE82 element is higher order element. PLANE42 element is 2D finite element type and has four nodes for quadrilateral and three nodes for triangular shapes. PLANE82 element has eight nodes for quadrilateral and six nodes for triangular shapes. Hence PLANE82 element has more accurate results than PLANE42 element with respect to the analysing conditions. However more and enough number of PLANE42 elements can give the near or same result of PLANE82 elements. Hence PLANE42 2D finite elements are used in the finite element model for solving time and memory sufficiency of computer. Higher order elements need high memory and much CPU time.

CONTA172 and TARGE169 elements are two of contact elements in ANSYS. CONTA172 element is a 2D contact element and placed between contact lines of parts. It has three nodes. TARGE169 element is a target segment element or contact target element, placed opposite side of CONTA172 contact element. It has different number of nodes. When CONTA172 and TARGE169 elements touch or penetrate with each other, the contact occurs. They can slip with respect to Coulomb friction law in the analysis.

4.2.2. Contact algorithm

Augmented Lagrange contact algorithm which is the default contact algorithm in ANSYS is used in 2D stress analyses. Augmented Lagrange contact algorithm has

normal penalty stiffness, penetration tolerance and pinball region properties which can be set up by ANSYS or user.

Friction coefficient between contact and target surfaces is taken 0.1 with respect to a typical steel surface friction coefficient and experimental conditions of Fessler and Appavoo [7].

Behaviour of contact surface is set up to standard surface contact type which allows to elastic slip. Other types of contact surface like rough, no separation and bonded do not provide real conditions of the analyses. Other properties are not changed and default options are used in the analyses.

4.2.3. Boundary conditions

Hub is fixed from its' outside circumferential lines in the analyses with respect to Fessler and Appavoo's [7] experimental study. A pure torque is applied by using force couples in the analyses. Four concentrated forces are applied from four nodes on shaft area to obtain a pure torque. The results of finite element analyses are given as stress indices, which are the ratio of the reading maximum shear stress to nominal shear stress.

4.3. 3D Finite element models of hub, shaft and key with constant thickness under torsion [4, 7]

3D hub, shaft and key finite element models are obtained with respect to the experimental models of Fessler and Appavoo [7]. All modelling and analyses are made in ANSYS. Modelling of shaft, key and hub are made directly in ANSYS pre-processor step for the analyses. Model geometries can be seen in Figure 4.2.

When modelling of parts, different modelling techniques can be applied to make 3D solid models. Two ways are commonly followed in modelling of parts. Modelling the solid parts directly from volumes is one of the ways. From the shape of solid model, adding or subtracting volumes to construct the wanted geometrical solid model.

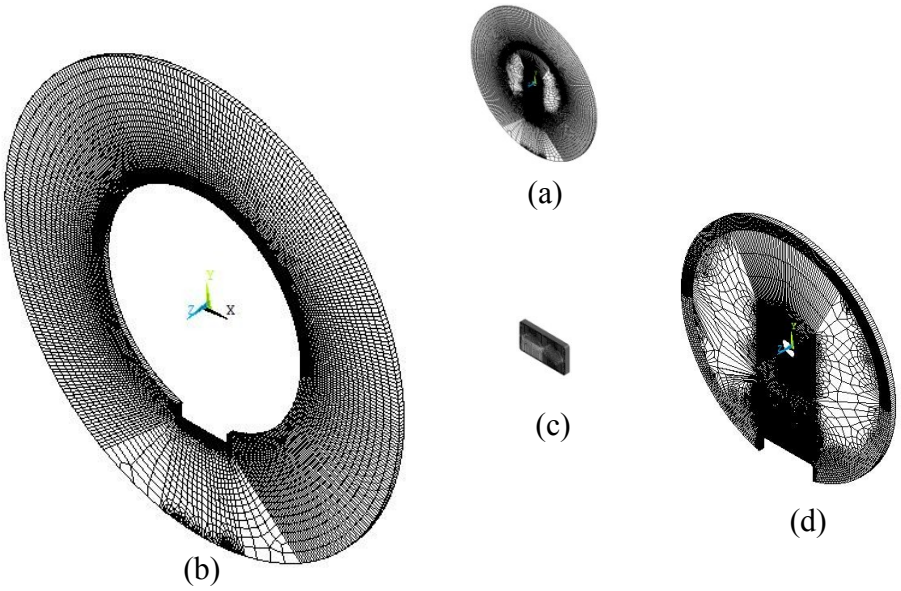

Figure 4.2. 3D hub, shaft and key FEM models of Fessler and Appovoo [7], (a) Assembled parts, (b) Shaft, (c) Key, (d) Hub

In the other way, modelling of solid parts can be obtained by a serial modelling technique. Volumes can be constituted from extruding the areas. Areas can be obtained from lines and/or arcs. Lines and arcs can be obtained from keypoints. Keypoints are constituted with respect to the geometries of model. This modelling technique takes more time; however complex geometrical models can be modelled and mapped meshing technique can be applied easier. At the end of this modelling way, there is not a separate of the solid part to small parts. Still solid model is modelled with only a single volume model for each part. Surface models are meshed and extruded to normal direction to make 3D finite element models.

Same modelling, meshing and other finite element analysing method steps are applied to obtain the finite element model of Fessler and Eissa [4] study. Only key has a height of 18 mm for ensuring the same geometrical model dimensions of Fessler and Eissa [4] experimental model. Also some clearance and interference tolerances are applied in modelling step and friction coefficient is changed in Fessler and Eissa [4] study. The clearances and friction coefficients can be seen in Table 3.2.

Also the effect of different clearances and friction coefficients are investigated in finite element analyses which are not given by Fessler and Eissa [4]. They are given

in Table 4.1. All other model dimensions and conditions of FEM models are as same as experimental study of Fessler and Eissa [4].

Table 4.1. Different clearances and friction coefficients of finite element models

Test no	Clearance of shaft in hub (mm)	Clearance of key in shaft (mm)	Clearance of key in hub (mm)	Coefficient of friction
fem-1	-0.06	-0.08	0.17	0.27
fem-2	-0.03	-0.08	0.17	0.27
fem-3	0.06	-0.16	0.17	0.14
fem-4	0.06	-0.16	0.17	0.27
fem-5	0.06	-0.16	-0.17	0.14
fem-6	-0.03	-0.08	-0.06	0.27

4.3.1. Mesh technique

The element type must be determined before meshing of parts. Different finite element types and their properties are present in ANSYS. PLANE42, SOLID45, CONTA174 and TARGE170 elements are some of finite elements which are used in this analysis. Areas are meshed with PLANE42 2D finite elements. When meshing of areas are finished with PLANE42 elements, PLANE42 elements are extruded in z-direction to obtain SOLID45 3D finite elements. SOLID45 element is a 3D brick element and used for 3D stress analysis. It has eight nodes for cubic and six nodes for prismatic shapes. Their nodes have three degrees of freedom in x, y and z coordinates. When SOLID45 elements are obtained by extruding the PLANE42 elements, PLANE42 elements are removed and only SOLID45 elements are left in 3D analysis.

On the contrary to high order elements like SOLID95 elements, SOLID45 3D finite elements are used in meshing. SOLID95 element is a cubic element and has 20 nodes. 8 nodes of element are found at edges and other 12 nodes are at centre of lines. Finite element analyses are made better with SOLID95 elements at the same element number of SOLID45 elements with respect to the analyse conditions. However, enough number of SOLID45 elements satisfies nearly the same analysis results. Hence SOLID45 elements are used in analysis for solution time and

computer memory. Mapped meshing technique is used for setting the number of finite elements.

CONTA174 and TARGE170 elements are used for defining the contact elements. CONTA174 element is a 3D contact element and placed between the contact surfaces of parts. It has eight nodes for quadrilateral shape or six nodes for triangular shape. TARGE170 element is a target segment element or contact target element, placed opposite side of CONTA174 contact element. It has different shapes and number of nodes. When CONTA174 and TARGE170 elements touch or penetrate between themselves, the contact occurs. They can slip with respect to Coulomb friction law.

One finite element is used at thickness, because increasing the number of elements at thickness elements gets more execution time and needs more computers RAM.

The aspect ratio of finite elements is tried to equal. However, all opposite lines of the parts are divided at same element length in same direction and this will cause that small area lines and large area lines are divided both divisions. This will cause to aspect ratio is more than one. Big sized elements are far away from critical locations like keyway surfaces. Hence the results of analysis are not extremely influenced from the aspect ratio of finite elements.

Mainly, five different contact types occur between parts in contact; Node-to-node, node-to-surface, surface-to-surface, line-to-line and line-to-surface. They have different properties and capabilities. In this analysis, most of the contact occurs at surface area of parts. Hence surface-to-surface contact type is used.

Contact and target elements are placed on the shaft, key and hub surface with an order. In the analysis, the contact elements are mainly used on the force applied parts. Target elements are used on the force transmitting or the fixed parts. Contact elements are placed on shaft contact surface where contacts to the key surface and target elements are placed on key surface where contacts to the shaft surface. Contact elements are placed on key contact surface where contacts to the hub surface and target elements are placed on hub surface where contacts to the key surface. Contact

elements are placed on shaft contact surface where contacts to the hub surface and target elements are placed on hub surface where contacts to the shaft surface.

4.3.2. Contact algorithm

Lagrange-Penalty contact algorithm is used in this analysis. Basic properties of Lagrange-Penalty method involve allowable tensile contact pressure, penetration tolerance and pinball region which can be set up by ANSYS software or the user.

In most of the analyses, default options are used which are determined by ANSYS. But if much penetration occurs between parts under loading, it will influence the contact elements with respect to model geometries and contact conditions. Hence convergence is influenced and solver makes more iterations. From these reasons, allowable tensile contact pressure and penetration tolerance are determined by user in some cases.

Friction coefficient between contact and target surfaces is taken 0.1 with respect to a typical steel surface friction coefficient and experimental study of Fessler and Appavoo [7].

Behaviour of contact surface is set up to standard which can allow elastic slip. Other properties are not changed and default options are used in the analysis.

4.3.3. Boundary conditions

In 3D finite element model, hub is fixed from its outside circumferential areas with respect to Fessler and Appavoo [7] experimental study. Decreasing iterations and numerical errors; shaft, key and hub are fixed along the z-axis from four symmetric nodes at back and front surfaces. These z-constraints do not affect the stress distribution but helps convergence drastically. The z-axis fixing nodes have enough distance to critical locations like contact surfaces and force applied points.

A symmetric boundary condition is applied to inside circumferential areas of the shaft at the centre to prevent the movement of all shaft x-y-z coordinates. It only

allows the rotation of shaft at the centre and obtains same conditions of experimental study of Fessler and Appavoo [7].

A pure torque is applied by using force couples in the analysis. Four concentrated forces are applied from four nodes at each front and back surface of shaft to obtain a pure torque. When carrying the forces to the centre of the shaft, the summation of all forces is equal to the zero and only a pure torque remains. Analysis results are given as stress indices, which are the ratio of the reading maximum shear stress to nominal shear stress.

4.4. 3D Finite Element Models of hub, shaft and key with different thicknesses under torsion [2]

3D hub, shaft and key finite element models with different thicknesses are obtained with respect to Okubo and colleagues [2] study as shown in Figure 4.3. Models are obtained in SOLIDWORKS program and imported to ANSYS as parasoid file form. All parts are in a position of minimum clearance fit.

Also only a single shaft finite element model is prepared and analysed for obtaining the results without key and hub interaction as in Terada's [20] experimental study. The FEM model is shown in Figure 4.4.

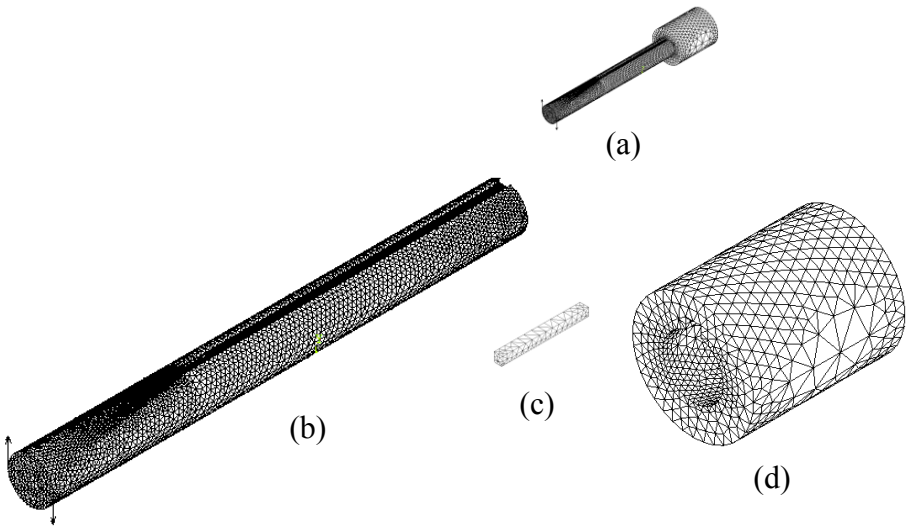

Figure 4.3. 3D hub, shaft and key FEM models of Okubo and colleagues [2] with different thickness, (a) Assembled parts, (b) Shaft, (c) Key, (d) Hub

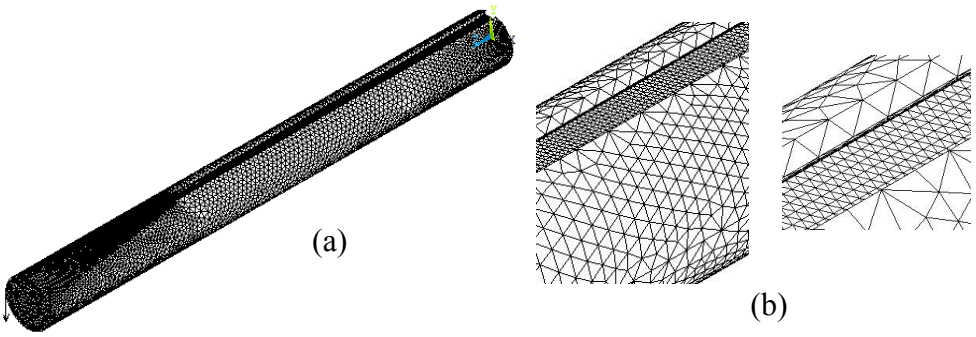

Figure 4.4. 3D shaft FEM models of Terada [20], (a) Shaft, (b) Magnifying views of keyway on the shaft

4.4.1. Mesh Technique

SOLID45 finite elements are used in meshing. Surface area edges are divided with suitable sizes for mapped meshing. Also mesh refinement technique, which is the increment the number of finite elements in a determined location of model, is used on important locations like keyway fillet and key edges.

CONTA174 and TARGE170 contact elements are used in the hub, shaft and key interaction analysis for contact element assignment. Surface-to-surface standard contact type is selected.

No contact elements are used at the single shaft analysis. Because no interaction of parts are available.

4.4.2. Contact Algorithm

Lagrange-Penalty contact algorithm is used. All parts are in full contact and penetration is not allowed between parts. Friction coefficient is selected to 0.1 with respect to typical steel. Default contact options are used in contact algorithm and standard surface type is selected.

4.4.3. Boundary Conditions

In the hub, shaft and key interaction analysis, hub is fixed from its outside circumferential areas. A force couple is applied from shaft end edges to obtain a torque.

In single shaft analysis, shaft is fixed from one end edge surface and a force couple is applied from other end edge surface to obtain a torque.

The applied concentrated forces have enough distances to the interested and critical locations like keyway fillet in both shaft keyway stresses analysis with and without involving of hub and key.

4.5. 3D Finite Element Models of a stepped shaft without keys under torsion [1]

Finite element model of a single stepped shaft is obtained with respect to experimental study of Fessler and colleagues [1] as shown in Figure 4.5. Model is obtained in SOLIDWORKS and imported to ANSYS as parasoid file form.

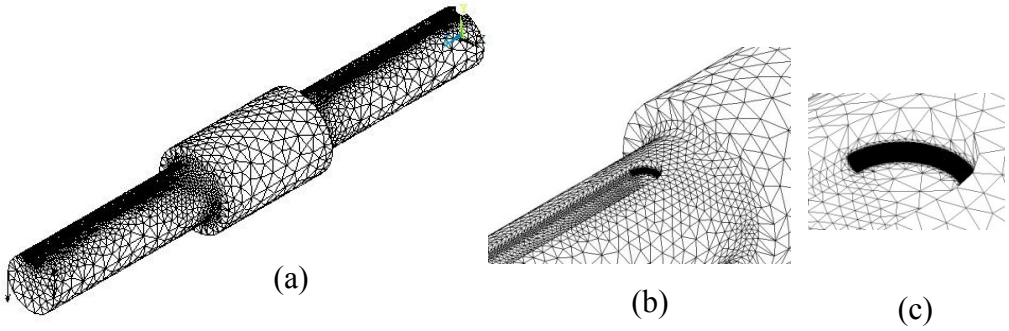

Figure 4.5. 3D shaft FEM models of Fessler and colleagues [1], (a) Shaft, (b) Magnifying view of keyway on the shaft, (c) Magnifying view of keyway fillet

4.5.1. Mesh Technique

SOLID45 brick element is used in meshing. Surface area edges are divided with suitable sizes for mapped meshing. Also mesh refinement is applied to increase the number of finite elements in wanted locations like keyway fillet of shaft. SOLID45 finite elements transform into pyramid geometry in meshing.

4.5.2. Contact Algorithm

No contact algorithm is used in this analysis because only a single shaft is analysed.

4.5.3. Boundary Conditions

For torsion analysis of the model, model is fixed from one end surface and a force couple is used for making a pure torque from other end surface edges. Concentrated forces are applied which have enough distances to the interested and critical locations.

4.6. 3D Finite Element Models of plain shaft without keys under bending [3]

In bending analysis of the shaft without keys and hub, the study is carried by Fessler and colleagues [3] is used to verify the FEM results. A single shaft is modelled in SOLIDWORKS and imported to ANSYS as parasoid file form. The FEM model is shown in Figure 4.6.

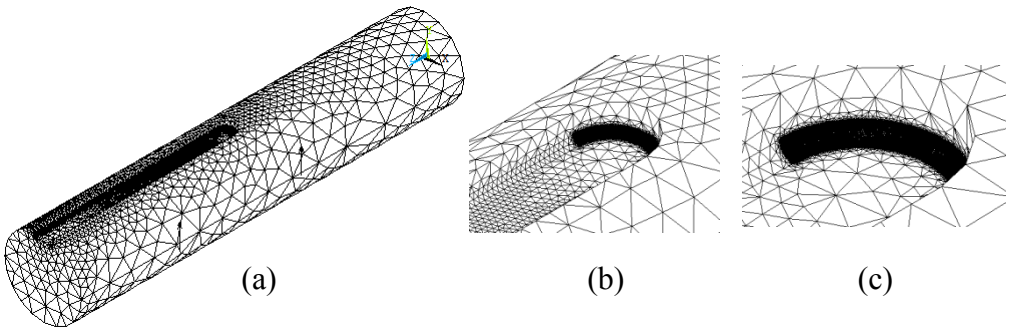

Figure 4.6. 3D shaft FEM models of Fessler and colleagues [3], (a) Shaft, (b) Magnifying view of keyway on the shaft, (c) Magnifying view of keyway fillet

4.6.1. Mesh Technique

SOLID45 finite element is used in meshing. Mapped meshing technique is applied by dividing the surface area edges of shaft model with required dimensions. Also mesh refinement is applied at shaft keyway. SOLID45 finite elements transform into pyramid during meshing of the shaft.

4.6.2. Contact Algorithm

Contact algorithm is not used in this analysis, because of only a single shaft is present.

4.6.3. Boundary Conditions

For bending analysis of the model, model is fixed from two points at two end surface edges and two forces are applied from bottom of the shaft which have equal distance between them. Force directions pass though the centre of shaft and only a bending load is obtained. The applied concentrated forces have enough distances to the interested and critical locations.

4.7. 3D Finite Element Models of hub, shaft and key under bending

Six different finite element models of hub, shaft and key are obtained with different geometric shapes. Models are obtained and assembled in SOLIDWORKS and imported to ANSYS as parasoid file form. Hub is located at the mid-length of the shaft. All parts surfaces are minimum clearance fit with respect to the assembly. Three of them have sled runner keyways at shafts and others have end milled keyways at shafts. Shaft has a length of 381 mm and a diameter of 76.2 mm in all models. Also hub has an inside diameter of 76.2 mm, an outside diameter of 152.4 mm and a length of 76.2 mm. Key has a length of 88.85 mm and width of 19.05 mm. Solid and finite element models are shown in Figures from 4.7 to 4.18. The hatches in the Figures show the fixing locations of the models. Forces are applied for producing bending and they are shown as “F” label in the Figures.

4.7.1. Mesh Technique

SOLID45 3D finite element is used in meshing. Model surface area edges are divided with suitable sizes for mapped meshing. Also mesh refinement is applied to increase the number of finite elements at required locations like shaft keyway fillet. SOLID45 elements take pyramid geometry form from the geometry of shaft.

4.7.2. Contact Algorithm

Lagrange-Penalty contact algorithm is used. Friction coefficient is selected to 0.1 with respect to typical steel. Default contact options are used in contact algorithm. Contact elements penetrate very much with respect to the geometry of the models in any loading which may be very small. Hence, allowable tensile contact pressure and penetration tolerance are determined by user.

4.7.3. Boundary Conditions

Shaft is fixed from its end surfaces and two forces are applied on the hub end surface edges to obtain a standard four point bending analysis. Force directions are passes through the centre of shaft and only a bending loading is obtained. Applied concentrated forces have enough distances to the interested and critical locations of the models.

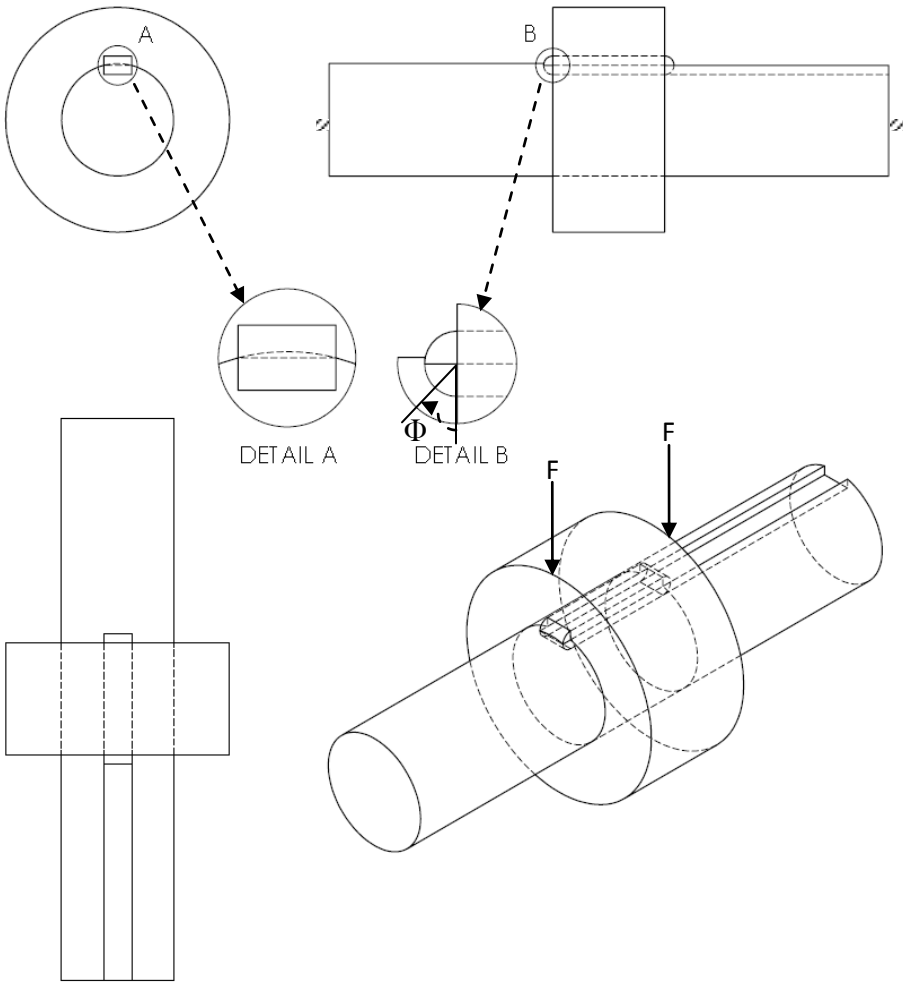

Figure 4.7. Bending model of hub, key and shaft with sled runner keyway

One of the hub, shaft and key bending model is obtained and it can be seen in Figure 4.7. Shaft has a sled runner keyway. Keyway is opened from one end of the shaft. Key top corners are filleted with a radius of 6.3246 mm and keyways have no fillet. FEM models of Figure 4.7 are shown in Figure 4.8.

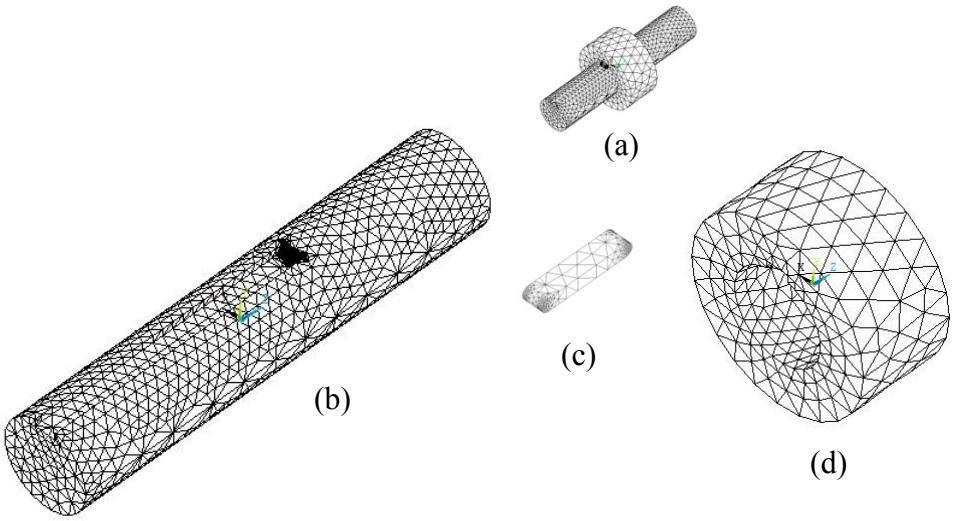

Figure 4.8. FEM model of bending model of hub, key and shaft with sled runner keyway, (a) Assembled parts, (b) Shaft, (c) Key, (d) Hub

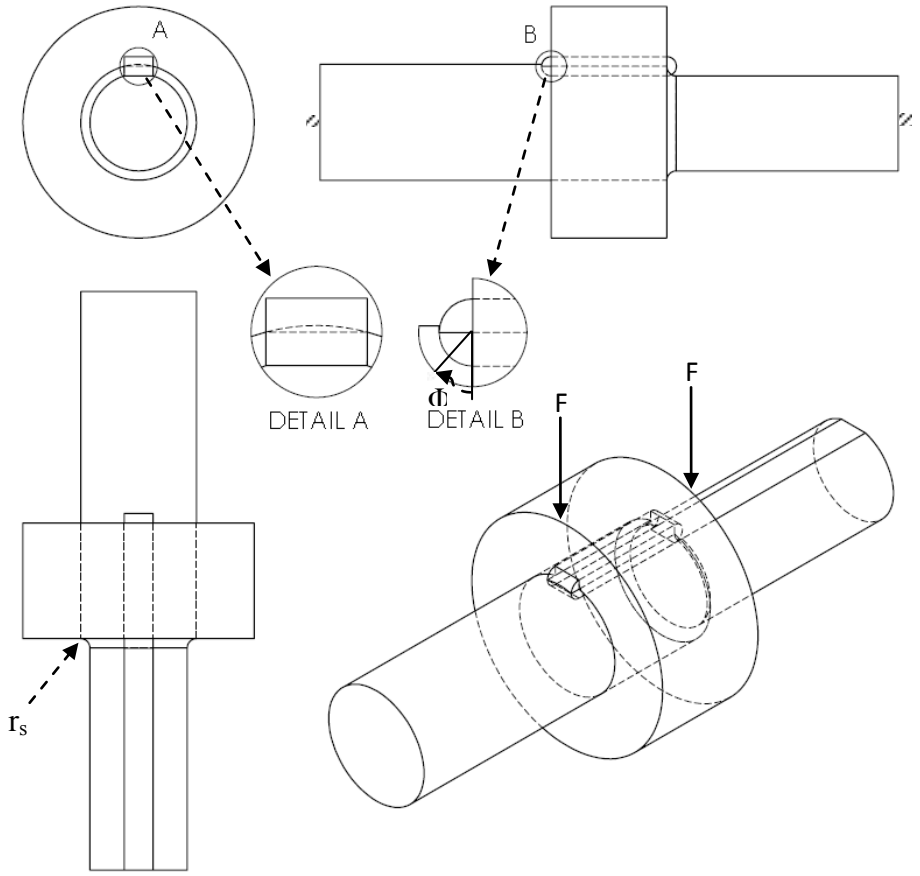

Figure 4.9. Bending model of hub, key and a stepped shaft with sled runner keyway

Another bending model can be seen in Figure 4.9. Hub, key and a stepped shaft with sled runner keyway are used in the analyses. Shaft stepped side has a diameter of 64.1 mm. The shoulder of the shaft is rounded with a radius (r_s) of 6.08 mm. Key top corners are rounded with a radius of 6.3246 mm and keyways have no fillet. FEM model of Figure 4.9 is shown in Figure 4.10.

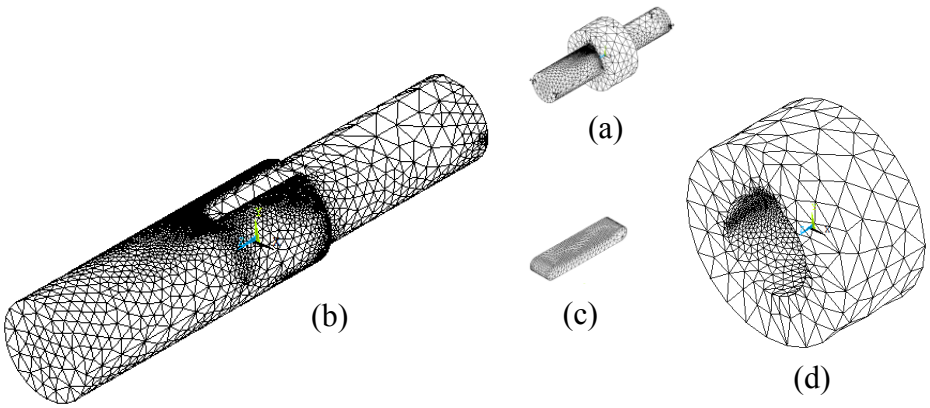

Figure 4.10. FEM model of bending model of hub, key and a stepped shaft with sled runner keyway, (a) Assembled parts, (b) Shaft, (c) Key, (d) Hub

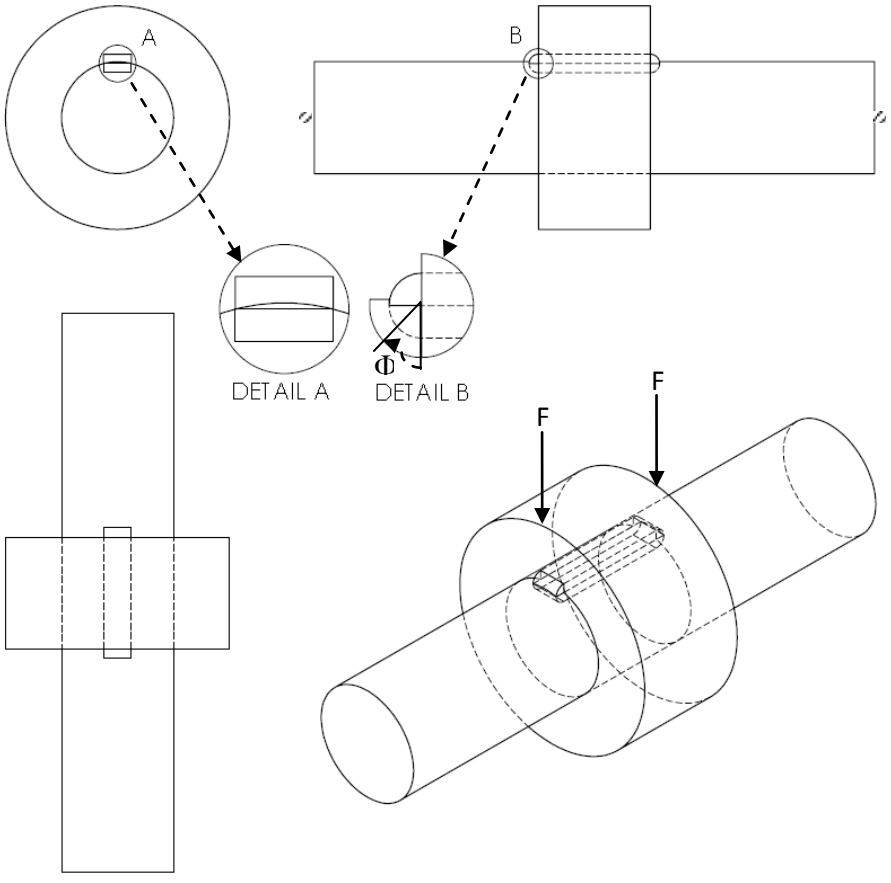

Figure 4.11. Bending model of hub, key and shaft with sled runner keyway

The third of sled runner keyway bending model can be seen in Figure 4.11. Parts are placed with minimum clearance fit. Other dimensions and properties are as same as other sled runner keyway bending models. FEM models of Figure 4.11 are shown in Figure 4.12.

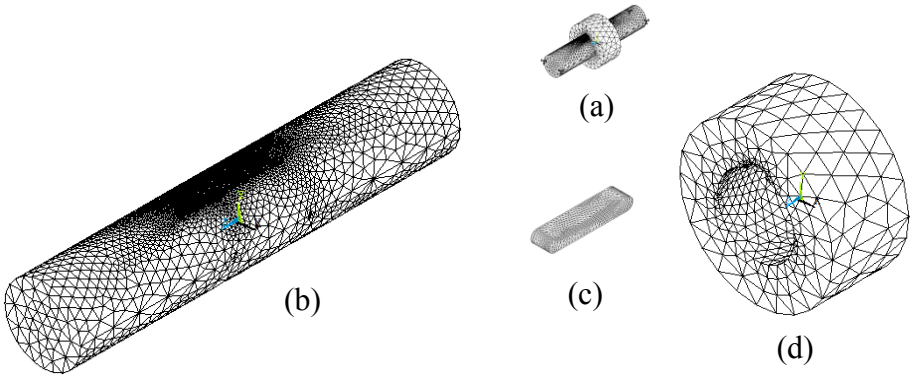

Figure 4.12. FEM model of bending model of hub, key and shaft with sled runner keyway, (a) Assembled parts, (b) Shaft, (c) Key, (d) Hub

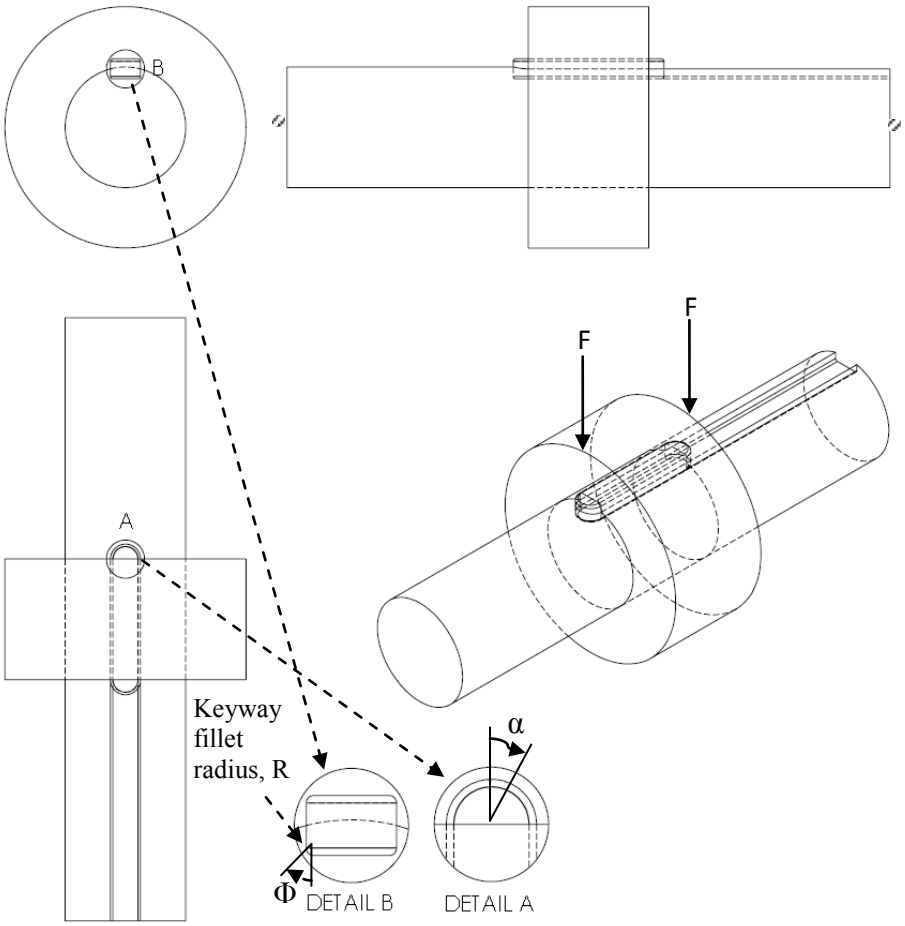

Figure 4.13. Bending model of hub, key and shaft with end milled keyway

One of the end milled keyway bending model can be seen in Figure 4.13. Shaft has an end milled keyway at one side and it is opened from one end of the shaft. Shaft and hub keyway are filleted with a radius of 1.58 mm and same fillet radius is used for rounding the key edges. Key top edges are rounded with a radius of 9.525 mm. FEM models of Figure 4.13 are shown in Figure 4.14.

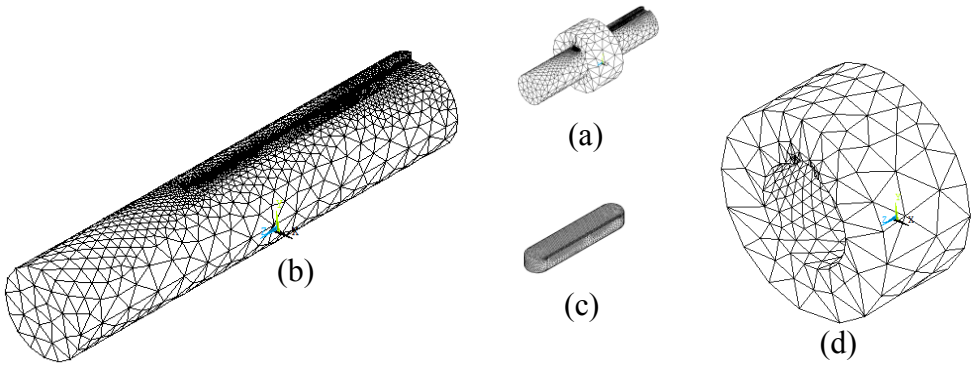

Figure 4.14. FEM model of bending model of hub, key and shaft with end milled keyway, (a) Assembled parts, (b) Shaft, (c) Key, (d) Hub

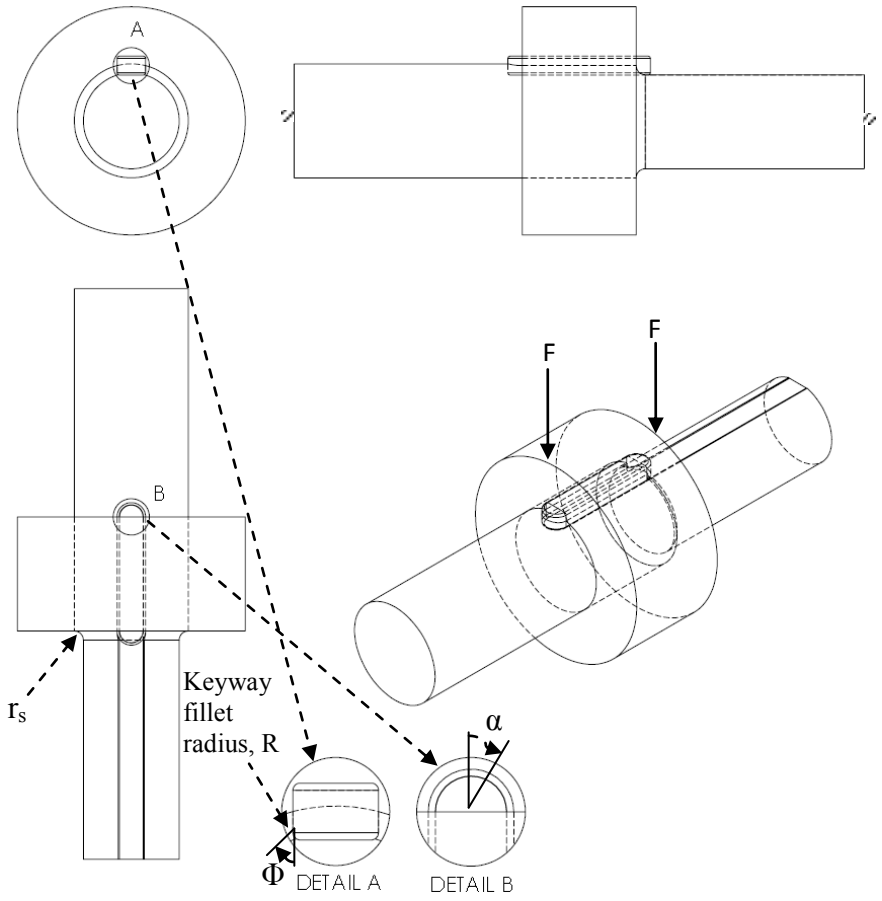

Figure 4.15. Bending model of hub, key and a stepped shaft with end milled keyway

Another end milled keyway stepped shaft is used with hub and key in Figure 4.15. A keyway is opened from one end of shaft. Stepped side of shaft has a diameter of 64.1 mm. The shoulder fillet (r_s) is 6.08 mm. Key edges, shaft and hub keyway are rounded with a radius of 1.58 mm. Key top edges are rounded with a radius of 9.525 mm as same as Figure 4.13. FEM models of Figure 4.15 are shown in Figure 4.16.

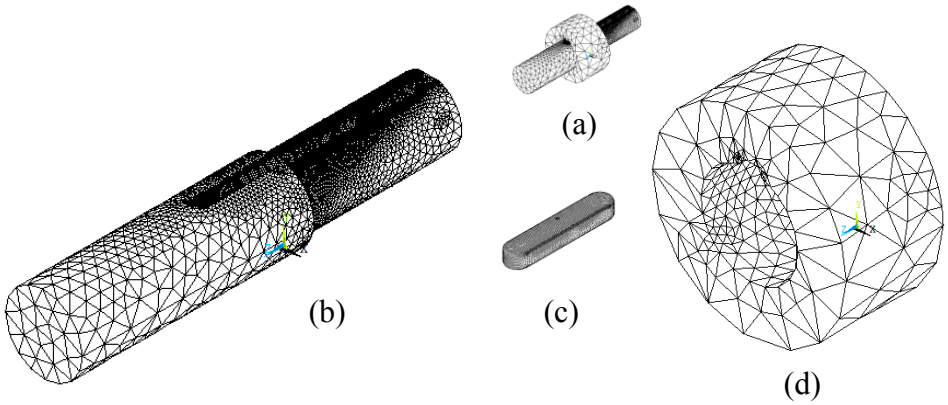

Figure 4.16. FEM model of bending model of hub, key and a stepped shaft with end milled keyway, (a) Assembled parts, (b) Shaft, (c) Key, (d) Hub

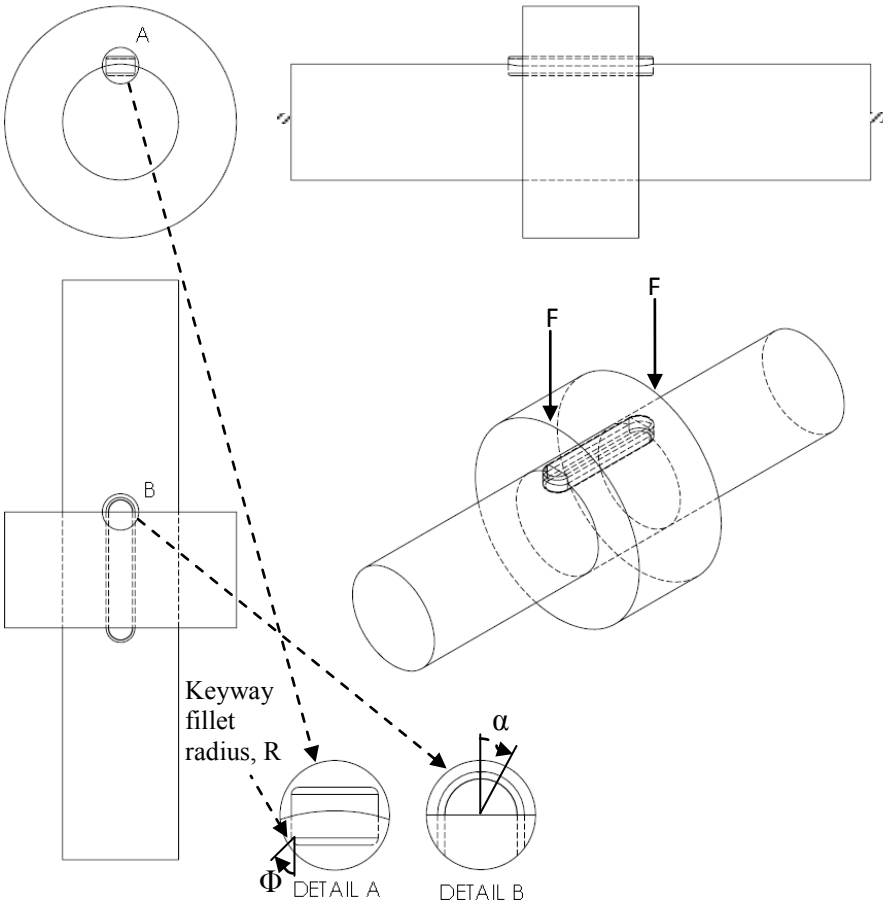

Figure 4.17. Bending model of hub, key and shaft with end milled keyway

Same fillet radius is used in Figure 4.17 as other end milled keyway bending models. FEM models of Figure 4.17 are shown in Figure 4.18.

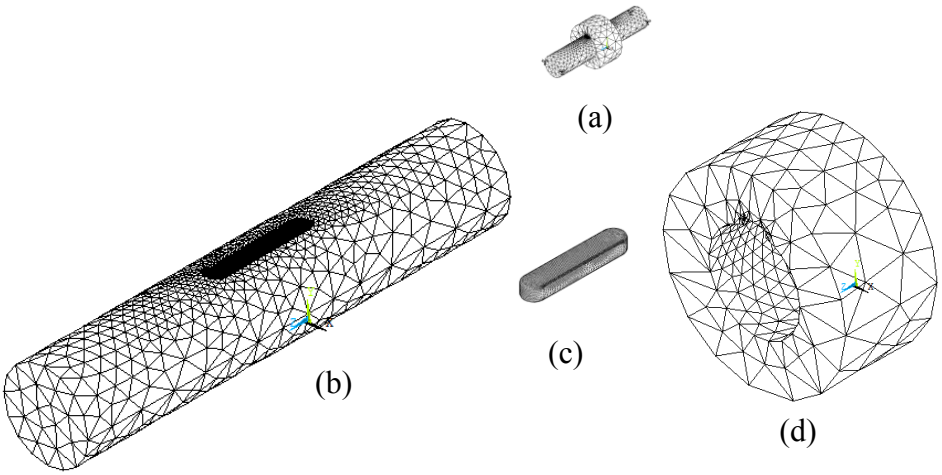

Figure 4.18. FEM model of bending model of hub, key and shaft with end milled keyway, (a) Assembled parts, (b) Shaft, (c) Key, (d) Hub

CHAPTER 5

RESULTS AND DISCUSSIONS

5.1. Introduction

Finite element models of keyed connections are investigated under torsion with respect to the experimental models. Also some different types of hub, shaft and key interaction finite element models are obtained and analysed under bending. The results of analyses are given as stress indices for providing the same analyse results of experimental studies. The effect of key edge geometries, friction and interference between parts are investigated. The results of different contact algorithms are also investigated and their results are given.

5.2. The properties of the computers used in solutions

All finite element solutions are carried out using two different computers. The speed of the CPU is 2.4 GHz and RAM is 3 GByte. The operating system is Windows Vista with 32 bits. In some solutions, the virtual memory is used in harddisc. The harddisc capacity is 250 GByte. All solutions are stored as database in harddisc.

5.3. Comparison of contact algorithms used in 3D solutions

The Augmented Lagrange, Penalty, Lagrange and Lagrange-Penalty contact algorithms are compared in 3D solutions for the keyway edge stress distributions. All contact algorithms are used with their default options. All contact algorithms have penetration tolerance, pinball region, contact surface behaviour, friction coefficient and allow to elastic slip options.

Augmented Lagrange and Penalty contact algorithm are the same properties and characteristics. Only Augmented Lagrange contact algorithm is less sensitive about contact stiffness. They both have normal penalty stiffness, tangent penalty stiffness and contact opening stiffness options which are determined automatically by

ANSYS. Also another important property of Augmented Lagrange and Penalty contact algorithm is that the contact stiffness can be updated with each load step, sub step or iteration. In other contact algorithms, it cannot be able to update. Lagrange-Penalty contact algorithm has allowable tensile contact pressure and tangent penalty stiffness options. They are determined automatically by ANSYS. Lagrange contact algorithm has same properties of Lagrange-Penalty contact algorithm. Only it cannot be able to determine tangent penalty stiffness automatically. Without these options, other properties are nearly same. Friction coefficient is accepted and taken 0.1 with respect to a typical steel friction coefficient for all analyses if friction coefficient is not mentioned in subsections. Also elastic slip is allowed in the analyses.

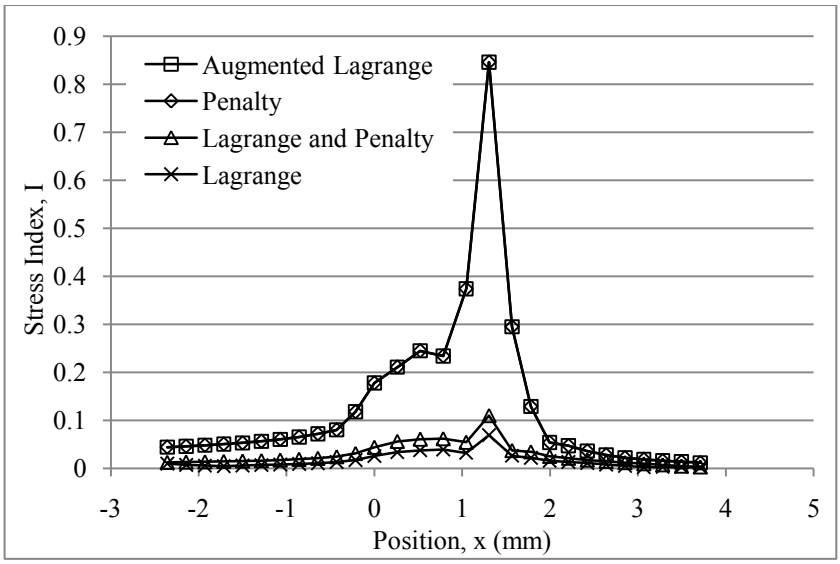

Figure 5.1. Comparison of 3D contact algorithms for the stresses along keyway edge profiles (test no fa-1, T=Ty/10000, fc=0.1)

Different contact algorithm stress distributions are given in Figure 5.1 as stress indices. Position (x) is given in Figure 3.2 and it changes with respect to keyway edge profile. The applied torque is calculated from Equation 3.2 and it is equal to 1/10000 of yield torque in Figure 5.1. Augmented Lagrange and Penalty contact algorithms give the same stress distributions. Lagrange and Lagrange-Penalty contact algorithms give less stress values than Augmented Lagrange and Penalty contact algorithms. Especially the value of stress peak point is much higher at Augmented Lagrange and Penalty contact algorithms than the others. But stress distribution of all contact algorithms looks like same. The peak point location and stress distribution with respect to the position (x) are similar.

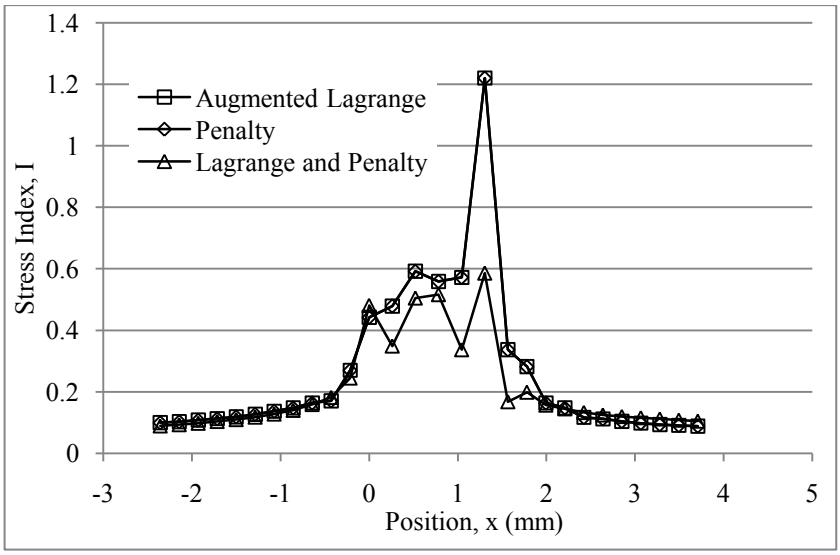

Figure 5.2. Comparison of 3D contact algorithms for the stresses along keyway edge profiles (test no fa-1, T=Ty/1000, fc=0.1)

When the amount of torque is increased, stress indices of contact algorithms increase and they can be seen in Figure 5.2. Lagrange contact algorithm does not converge when increasing the torque. Augmented Lagrange and Penalty contact algorithms give same stress distributions again. There is one stress peak point occurs at Augmented Lagrange and Penalty contact algorithms. Lagrange-Penalty contact algorithm solutions give less stress values at some positions, especially at the keyway fillet. There are three stress peak points occur when looking the stress distribution of Lagrange-Penalty contact algorithm.

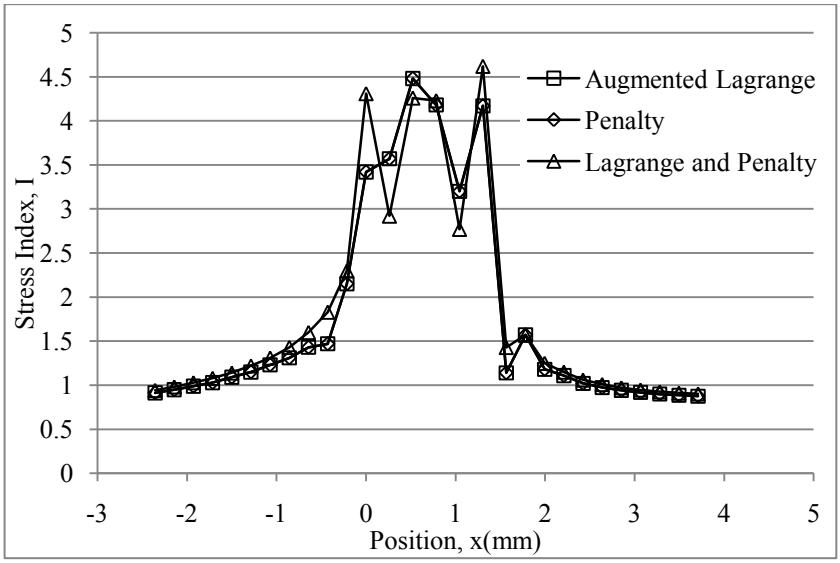

Figure 5.3. Comparison of 3D contact algorithms for the stresses along keyway edge profiles (test no fa-1, T=Ty/100, fc=0.1)

When applied torque is increased, Lagrange contact algorithm does not converge again. The stress distributions of contact algorithms can be seen in Figure 5.3. Augmented Lagrange and Penalty contact algorithm give same stresses again. Lagrange-Penalty contact algorithm stress distribution becomes more similar to Augmented Lagrange and Penalty contact algorithms when applying 1/100 of yield torque. However when the stress distributions are observed, Lagrange-Penalty contact algorithm has three stress peak points. But Augmented Lagrange and Penalty contact algorithms have two stress peak points.

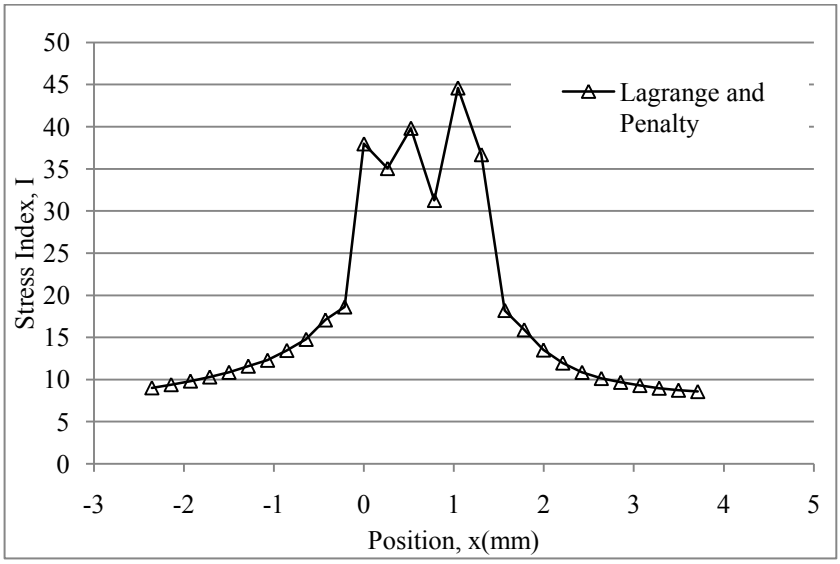

Figure 5.4. Comparison of 3D contact algorithms for the stresses along keyway edge profiles (test no fa-1, T=Ty/10, fc=0.1)

When ten percent of yield torque is applied, only Lagrange-Penalty contact algorithm converges and gives result. It can be seen in Figure 5.4. The stress indices are getting higher. When looking the stress distribution, three stress peak points can be seen.

As a result, some convergence problems occur at contact algorithms under different torques. When increasing the torque, some contact algorithms cannot converge. Lagrange contact algorithm gives results at the lower torques. When increasing the torque, Lagrange contact algorithm does not converge. Augmented Lagrange and Penalty contact algorithms give same results in all analyses. But Augmented Lagrange and Penalty contact algorithms cannot converge, when ten percent of yield torque is applied in the analyses. Only Lagrange-Penalty contact algorithm gives

results when applying 1/10 of yield torque. Hence Lagrange-Penalty contact algorithm is used in further analyses.

5.4. Analysis of hub, shaft and key interaction problem under torsion using 2D finite element models

The keyway stresses of keyed connections are investigated in 2D FEM analyses under torsion. Also the effect of friction is investigated by applying different friction coefficients.

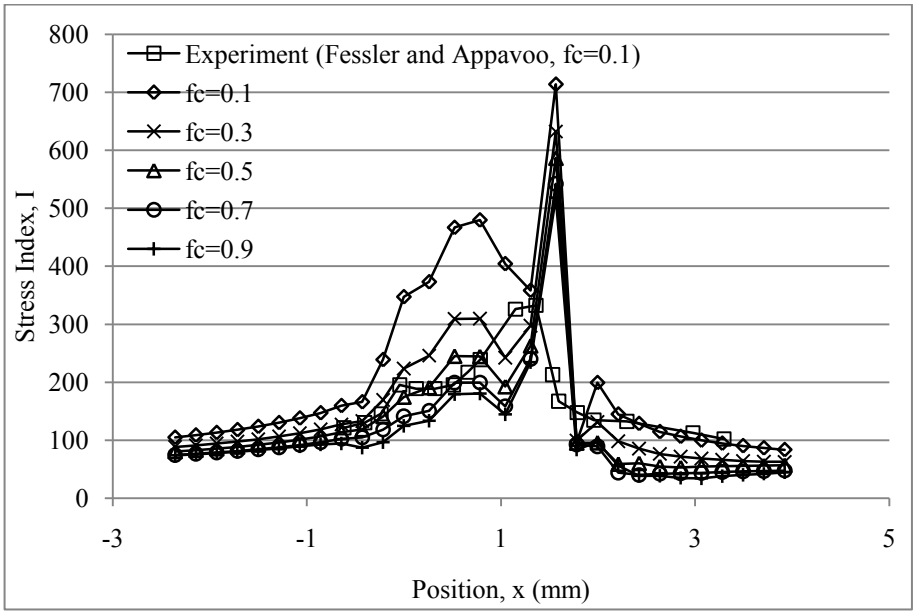

Figure 5.5. Comparison of the effect of friction in 2D analysis for the stresses along keyway edge profiles (test no fa-1, T=Ty)

The effect of friction can be seen in Figure 5.5 for key edge dimensions of w=1 mm and h=0.84 mm in 2D analyses. The stress indices change with respect to the friction. Not all of the torque is transmitted directly from key. Some of torque is transmitted by means of friction between parts, especially between shaft and hub surfaces. When friction coefficient is increased, the torque transmission of friction increases. This will cause to decrease the torque transmission from key. Hence less stresses are occurred at key and keyway locations. When decreasing the friction coefficient between parts, the torque transmission from key increases. So the stresses increase at key and keyways.

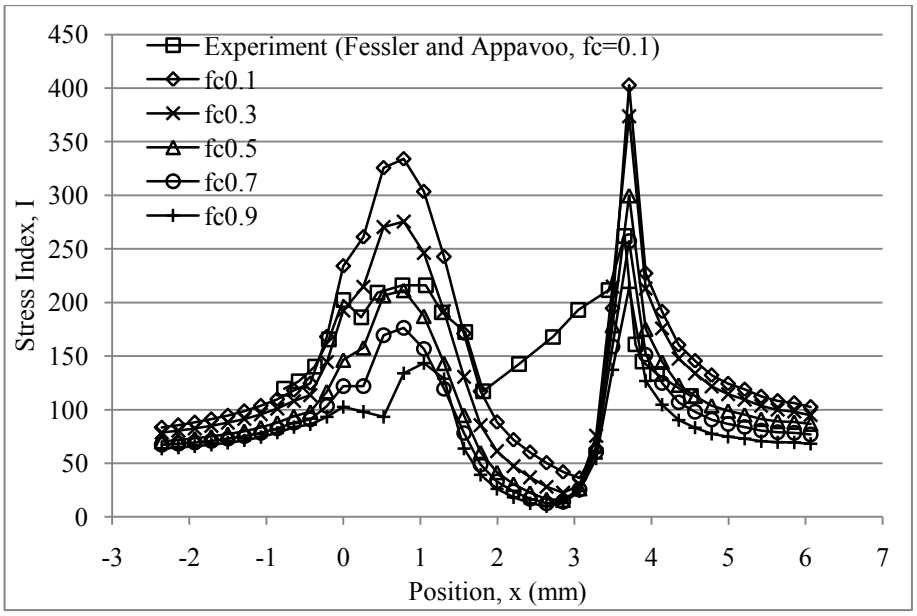

Figure 5.6. Comparison of the effect of friction in 2D analysis for the stresses along keyway edge profiles (test no fa-2, T=Ty)

Same friction coefficient effects can be seen in Figure 5.6 for key edge dimensions of w=1 mm and h=3 mm in 2D analyses. When the friction coefficient decreases, the stresses increase at keyway of shaft. High friction between parts decreases the torque transmission from the key.

Hence friction coefficient affects the stresses and it can be seen in Figure 5.5 and Figure 5.6. However, stress distribution is generally similar with respect to position change on keyway edge profile.

5.5. Analysis of hub, shaft and key interaction problem under torsion using 3D finite element models with constant thickness

The finite element analyses of hub, shaft and key interaction are investigated under different conditions with respect to experimental study of Fessler and Appavoo [7]. Finite element results are given in subchapters of this topic. Also the effect of clearances and friction between parts are investigated by using finite element analyses with respect to experimental study of Fessler and Eissa [4]. Their results are given.

Also stress contour plots of some FEM analyses are given to see the stress contour distribution and where the high stresses are obtained. Stress intensity is used in contour plots. Because the maximum shear stress of FEM models are calculated from stress intensity values.

5.5.1. Effects of key geometry on stress distributions along keyway edge profile

The stress distributions along keyway edge profile are investigated with different key edge geometries. The horizontal (w) and vertical (h) dimensions of the key edge are shown in Figure 3.3 and given in the Table 3.1.

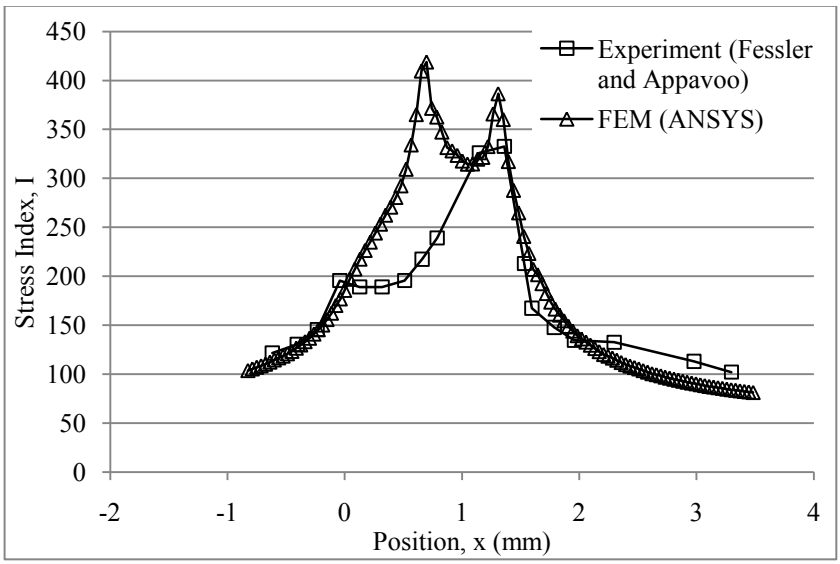

Figure 5.7. Comparison of FEM and experimental results for stress distributions along keyway surface (test no fa-1, T=Ty, fc=0.1)

The FEM stress distribution can be seen in Figure 5.7 and it is compared with the experimental result. The stress distributions look similar at most locations. However, two stress peak points are observed in FEM when comparing the FEM results to experimental results. They may be obtained from the edges of key.

Stress contours are shown in Figure 5.8. The high stresses occur at the keyway fillet of shaft. The range of stresses at this region is between 157 GPa and 235 GPa. Also slip of parts can be seen.

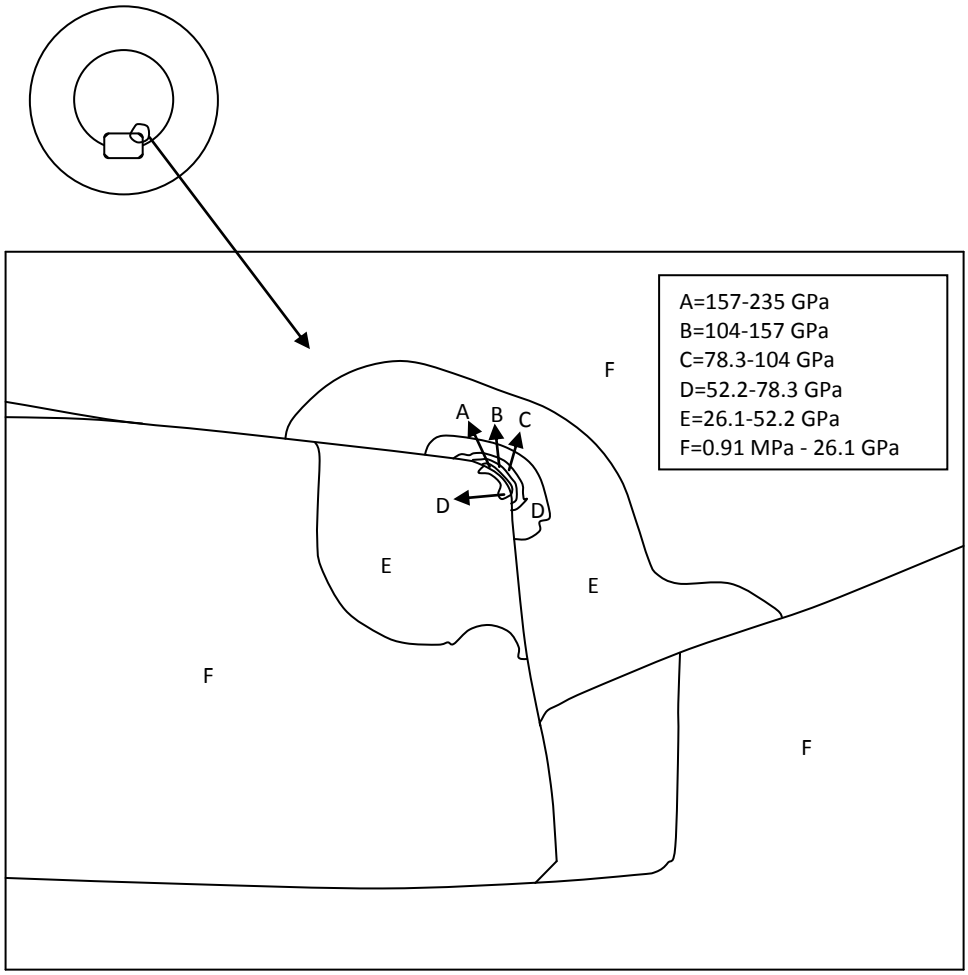

Figure 5.8. Stress contours at key and keyway corner (test no fa-1, T=Ty, fc=0.1)

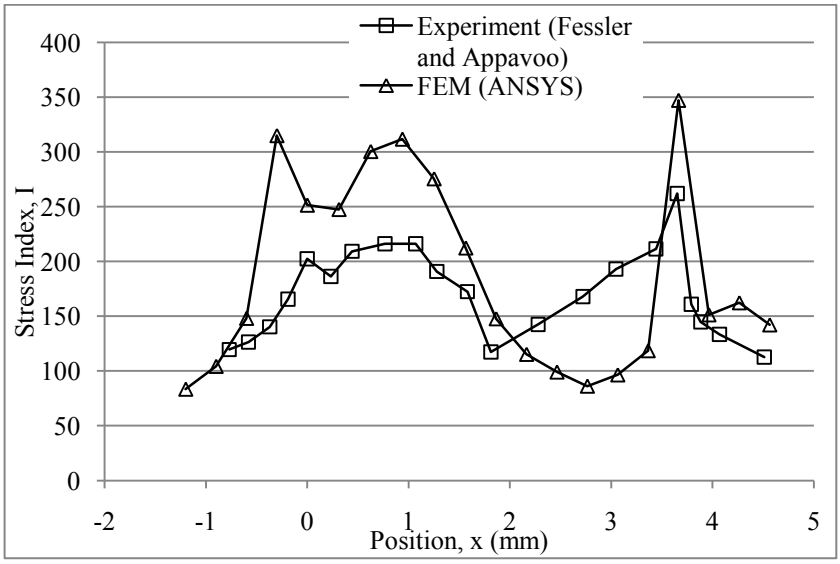

Figure 5.9. Comparison of FEM and experimental results for stress distributions along keyway surface (test no fa-2, T=Ty, fc=0.1)

FEM stress distribution can be seen in Figure 5.9 for key edge dimensions of w=1 mm and h=3 mm. It is compared with the experimental result. Stress distribution of FEM looks similar to the experimental results at most positions. The peak stresses occur at same positions. However peak stresses of FEM analysis are higher than experimental results.

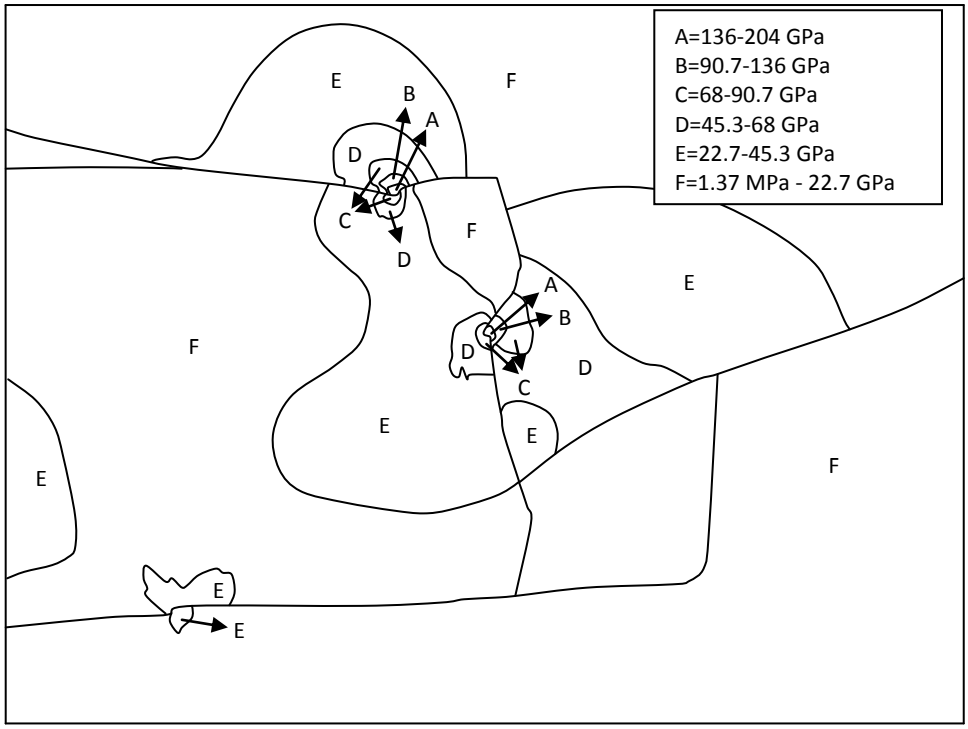

Figure 5.10. Stress contours at key and keyway corner (test no fa-2, T=Ty, fc=0.1)

Stress contours can be seen in Figure 5.10. A wide range of stresses are obtained at key and keyway locations. Key edge dimensions may cause this stress distribution. It may be obtained from the gap between key edge and keyway of the shaft. The gap between shaft keyway and key edge in test no 2 is larger than test no 1. High stresses have a stress range from 157 GPa to 235 GPa.

The stress distribution of FEM results can be seen in Figure 5.11. Stresses are getting higher in a small position range. This may be caused from the edge dimensions which have a height of 0.7 mm and a width of 0.7 mm. Two stress peak points are obtained.

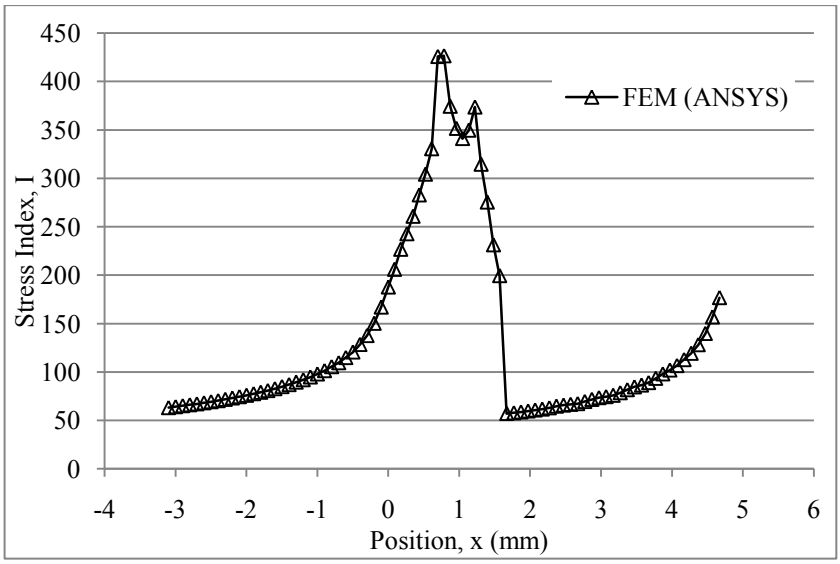

Figure 5.11. Stress distributions along keyway surface (test no fa-3, T=Ty, fc=0.1)

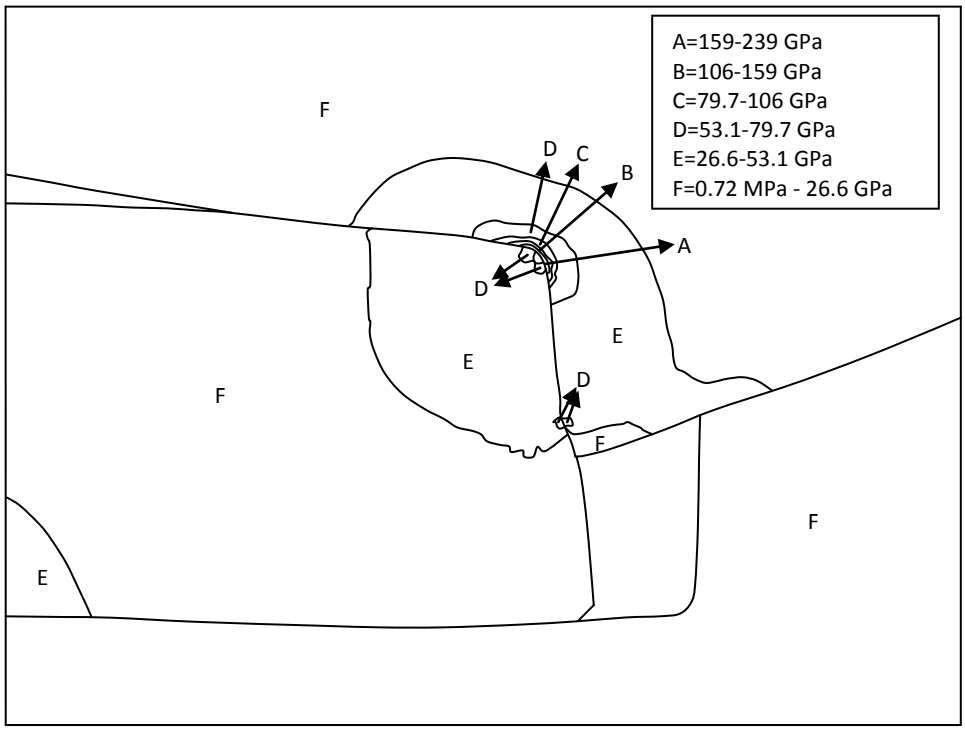

Figure 5.12. Stress contours at key and keyway corner (test no fa-3, T=Ty, fc=0.1)

Stress contours are shown in Figure 5.12. Edges of key are initially in a position of interference with keyway corners. But when applying the torque, the parts deform and slip. High stresses are obtained at shaft keyway and have a stress range from 159 GPa to 239 GPa.

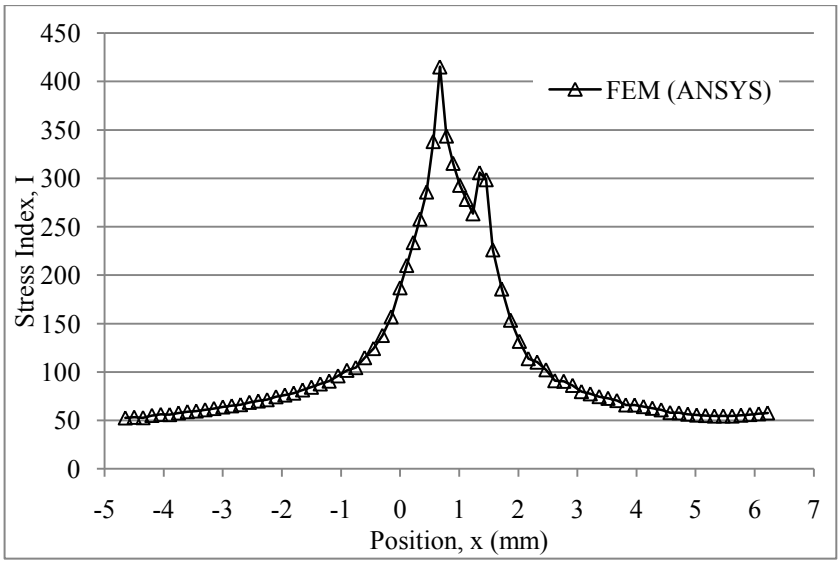

Figure 5.13. Stress distributions along keyway surface (test no fa-4, T=Ty, fc=0.1)

Stress distribution of FEM can be seen in Figure 5.13. The position difference between two stress peak points is increasing. Because key edge dimensions of test no fa-4 are higher than key edge dimensions of test no fa-3. Two stress peak points are obtained.

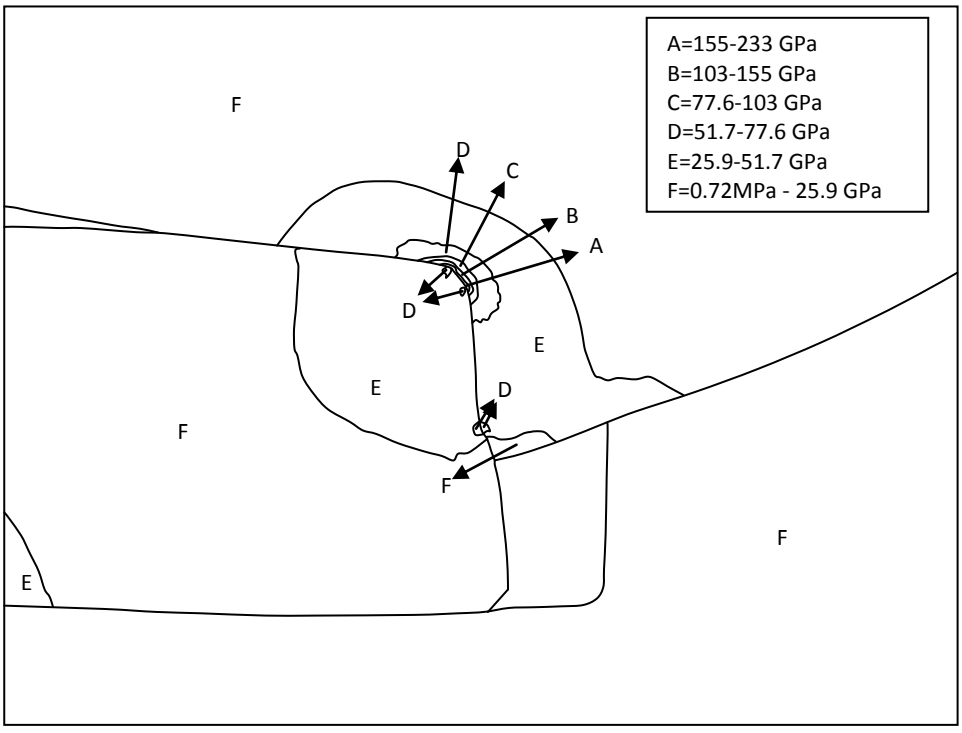

Figure 5.14. Stress contours at key and keyway corner (test no fa-4, T=Ty, fc=0.1)

Stress contours of test no fa-4 can be seen in Figure 5.14. High stresses are obtained at keyway fillet of shaft and have a stress range between 155 GPa and 233 GPa. Other locations of key, shaft and hub have low stresses than keyway of the shaft.

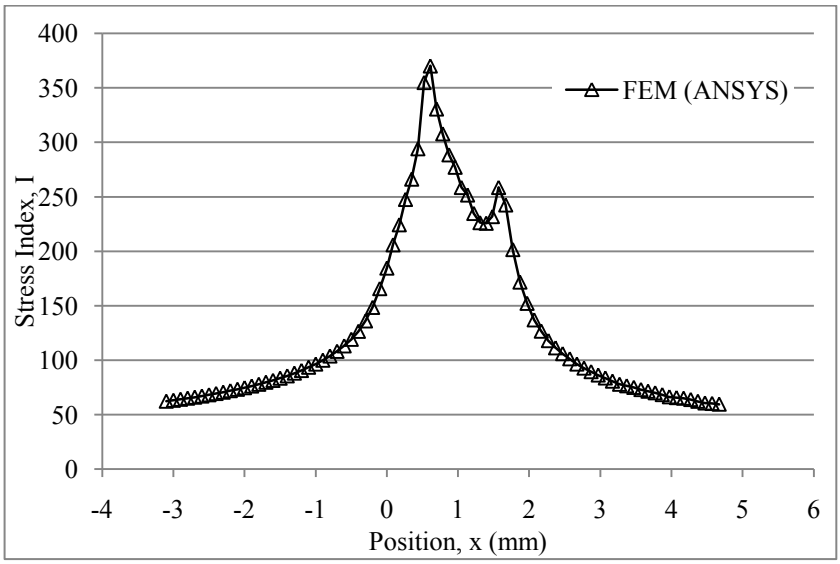

Figure 5.15. Stress distributions along keyway surface (test no fa-5, T=Ty, fc=0.1)

Stress distribution of test no 5 is given in Figure 5.15. Two stress peak points are seen. General stress distributions of test no 3, test no 4 and test no 5 are similar.

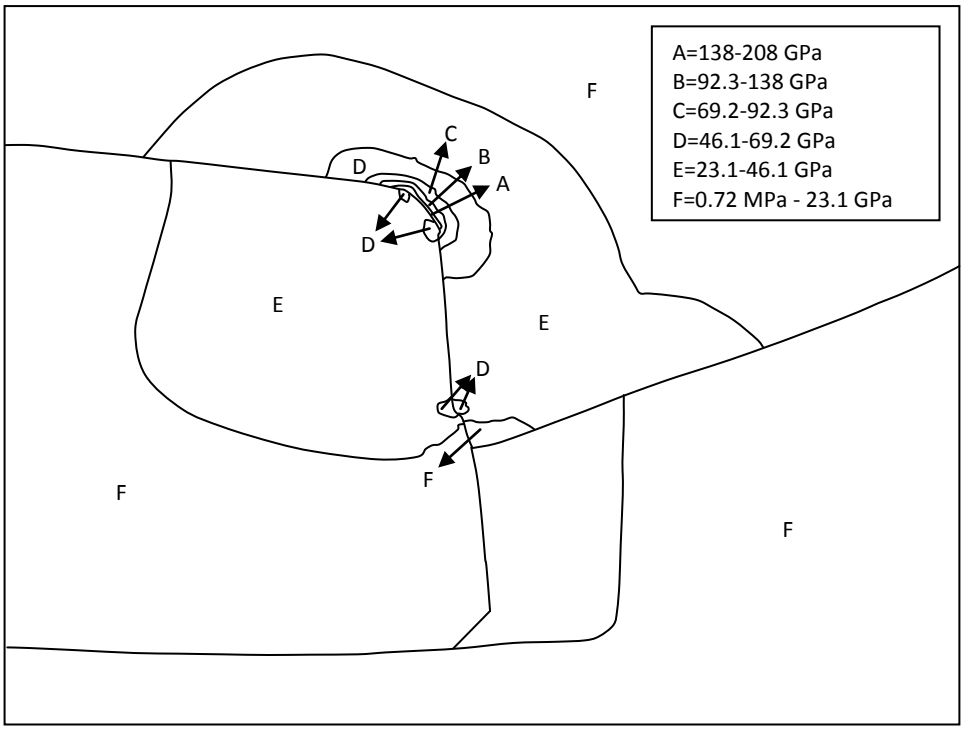

Figure 5.16. Stress contours at key and keyway corner (test no fa-5, T=Ty, fc=0.1)

Stress contours of test no 5 can be seen in Figure 5.16. High stresses are obtained at shaft keyway fillet and have a stress range from 138 GPa to 208 GPa.

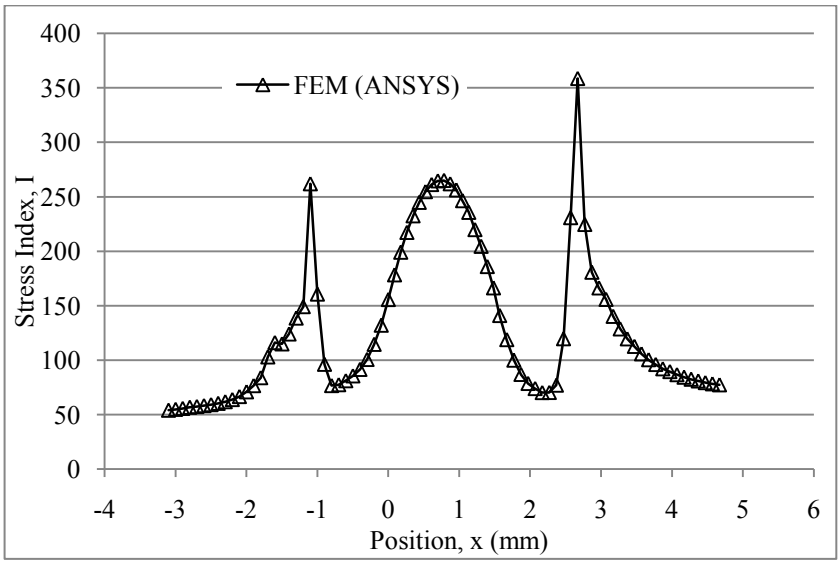

Figure 5.17. Stress distributions along keyway surface (test no fa-6, T=Ty, fc=0.1)

The stress distribution of test no 6 can be seen in Figure 5.17. Different stress distribution occurs from other tests in test no fa-6. Not only two stress peak points are obtained but also a high stress location can be seen at keyway fillet.

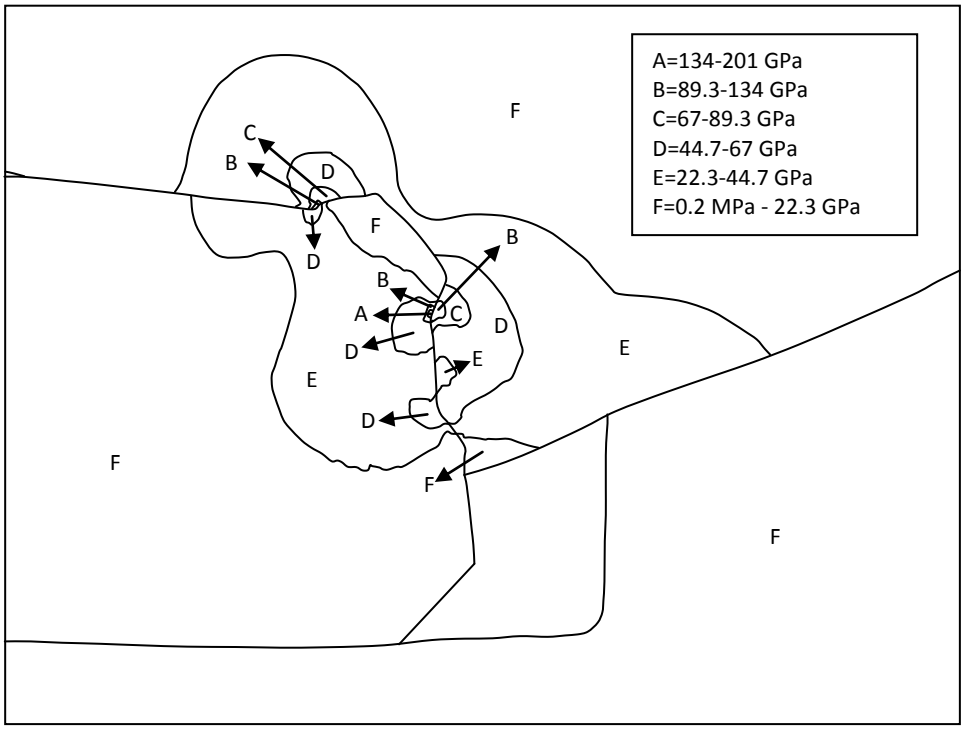

Figure 5.18. Stress contours at key and keyway corner (test no fa-6, T=Ty, fc=0.1)

The contours of test no 6 can be seen in Figure 5.18. High stresses are obtained at one of the key edges. They have a stress range between 134 GPa and 201 GPa. Also high stresses are obtained at shaft keyway which have a stress range between 89.3 GPa and 134 GPa.

When analysing the effect of different key edges, it's seen that the maximum stress indices occur at test no fa-3 which has a key edge dimensions of w=0.7 mm and h=0.7 mm. Maximum stress indices of test no fa-2 and test no fa-4 have as near values as test no fa-3 but not same or high. Test no fa-2 and test no fa-3 key edges are in a position of interference fit with shaft and hub keyways. This may cause to make the biggest stress indices occur at test no fa-2 and test no fa-3. However key edges are not in a position of interference fit in test no fa-4. Key edge dimensions of test no fa-4 is equal to keyway fillet of shaft and in a position of minimum clearance fit. Any sliding may cause high interference fit and occurs high stresses at keyway of shaft.

The lowest stress index peak points occur at test no fa-2 and test no fa-6 which have the biggest key edge chamfer dimensions and there is not initially interference between key edges and keyways. The lowest stresses are obtained at test no 6 which have a key edge dimensions of w=3 mm and h= 3 mm.

5.5.2. Effects of friction on stress distributions along keyway edge profile

The effect of friction is investigated by chancing the friction coefficient. Hub, shaft and key interaction surfaces have same friction coefficients. Five different friction coefficients are applied.

The effect of friction can be seen in Figure 5.19 for key edge dimensions of w=0.7 mm and h=0.7 mm in 3D analysis. Nearly same stress change characteristics of 2D can be seen in 3D analyses. When the friction coefficient is increased, the stress indices decrease. Friction transmits some of torques. If friction coefficient is increased, more torque is transmitted by means of friction. Hence stress indices decrease at the keyway of shaft.

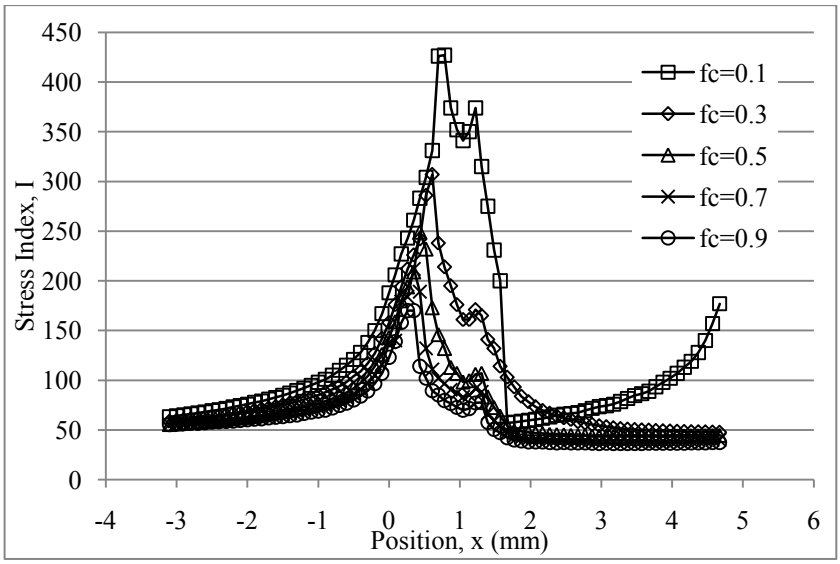

Figure 5.19. Comparison of the effect of friction in 3D analysis for the stresses along keyway edge profiles (test no fa-3, T=Ty)

5.5.3. Effects of interference fit on stress distributions along keyway edge profile

The effect of interference fits between parts is investigated by increasing the interference between parts.

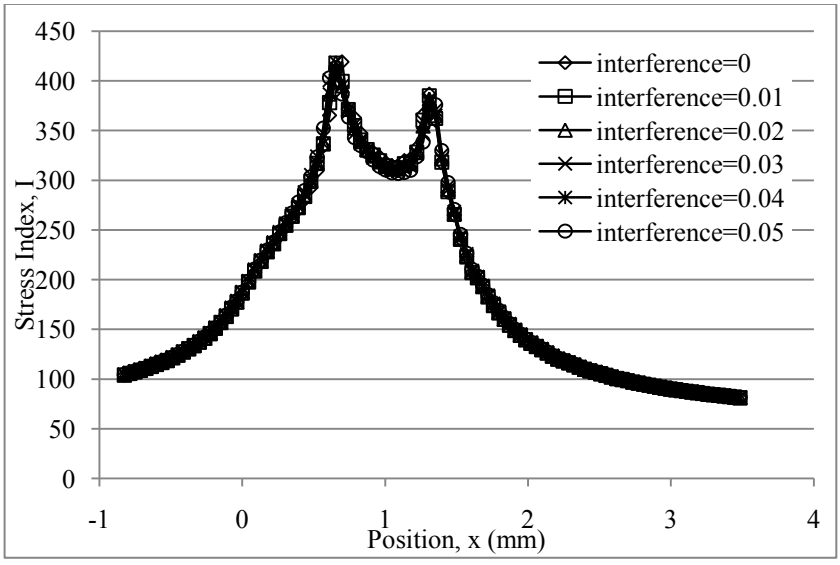

Figure 5.20. The effect of interference fit with a step size of 0.01 mm in 3D analysis for the stresses along keyway edge profiles (test no fa-1, T=Ty, fc=0.1)

The effect of interference fit can be seen in Figure 5.20 for key edge dimensions of w=1 mm and h=0.84 mm in 3D analysis. The interference is obtained both dimensions of key height and width with an increment the step size of 0.01 mm. When looking the Figure 5.20, the effect of interference on the stress distribution causes to increase the stresses, but the increase of stresses are very low.

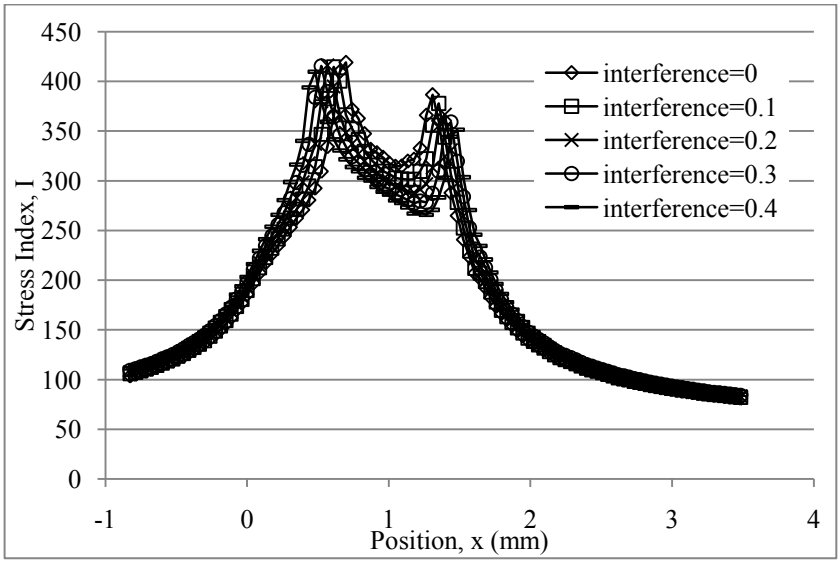

Figure 5.21. The effect of interference fit with a step size of 0.1 mm in 3D analysis for the stresses along keyway edge profiles (test no fa-1, T=Ty, fc=0.1)

Effect of interference can be seen in Figure 5.21 with a step size of 0.1 mm. It can be seen that small interferences are not dominant at the change of stresses. It is expected that the stress increase is much high, but the analyses show that the stresses increase is not high, only a little stress increase is seen under the effect of interference fit and its effect can be neglected.

5.5.4. Effects of torque on stresses at the point Ss with different key edge geometries

The stresses at point Ss can be seen for different key edge dimension under effect of various torques. Also stress contours of analyses are given.

The effect of torque can be seen in Figure 5.22 at the point Ss on keyway edge profile. The FEM result is compared with experimental result. It is seen that stress indices are decreasing when increasing the torque.

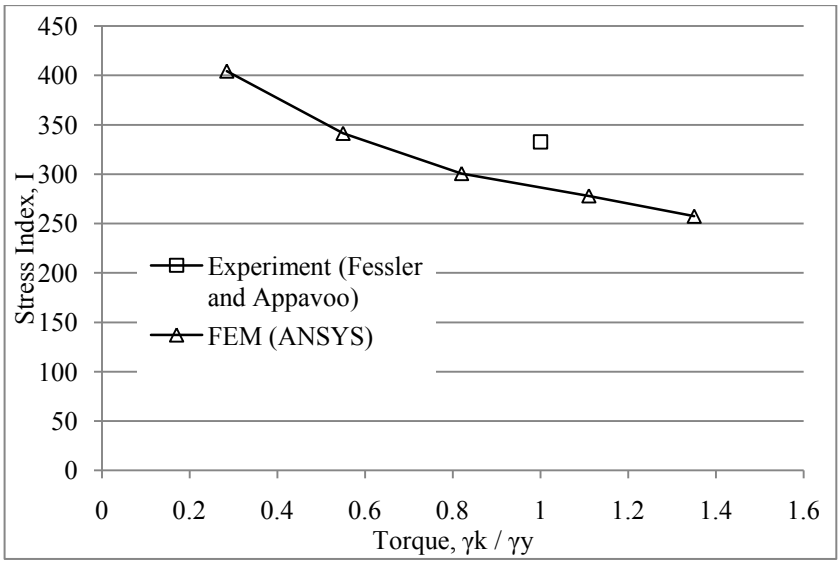

Figure 5.22. Variations of stress index, I, at the point Ss for different torques (test no fa-1, fc=0.1)

Stress contours of FEM results are given from Figure 5.23 to Figure 5.27 for test no fa-1 with different torques. The behaviour of torque effect can be seen in stress contours.

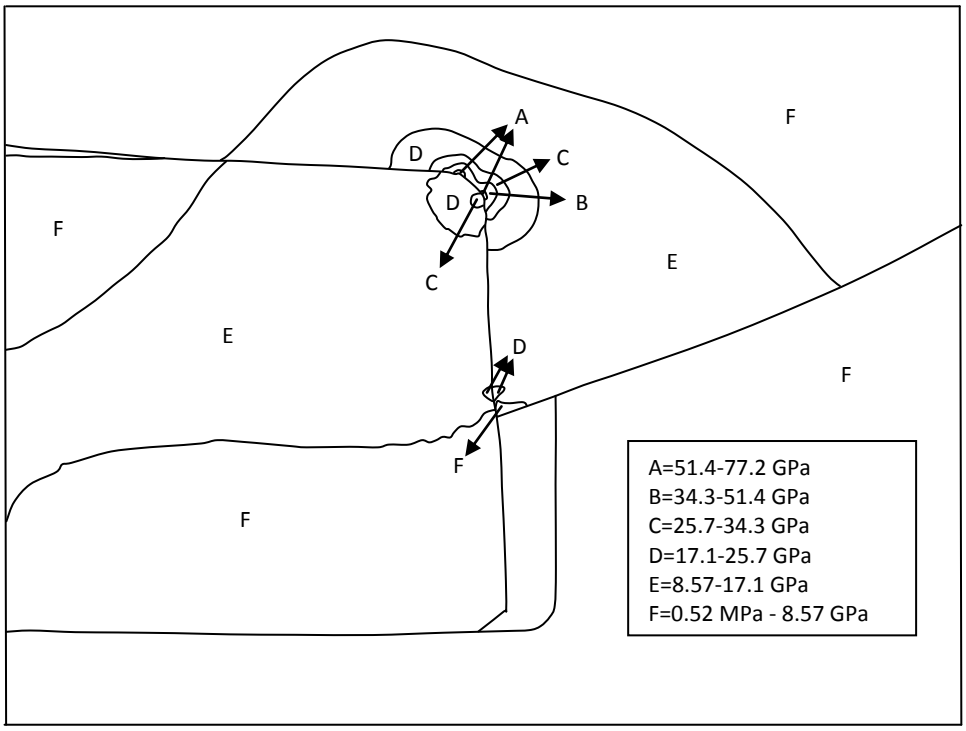

Figure 5.23. Stress contours at key and keyway corner (test no fa-1, T=0.285*Ty, fc=0.1)

Stress contours of FEM results can be seen in Figure 5.23 when applying 0.285 of yield torque. A wide range of stresses are obtained in Figure 5.23. High stresses are obtained at keyway of shaft, especially at the fillet location. It can be estimated that the key edges cause to make two high stress locations on keyway fillet of shaft. Highest stress values are obtained in a stress range from 51.4 GPa to 77.2 GPa.

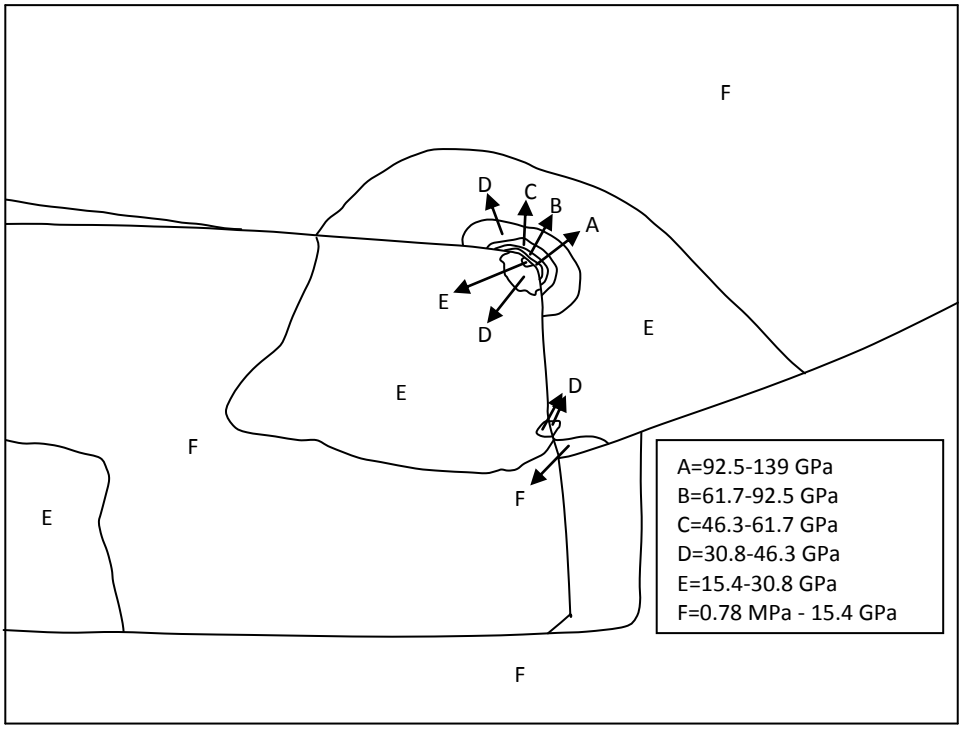

Figure 5.24. Stress contours at key and keyway corner (test no fa-1, T=0.55*Ty, fc=0.1)

Stress contours of FEM results can be seen in Figure 5.24 when increasing the torque to 0.55 of yield torque. The rotation of shaft is increasing and causes to more compress the key between shaft and hub keyway. High stresses are obtained at keyway fillet of shaft with a stress range between 92.5 GPa and 139 GPa.

When 0.82 of yield torque is applied, stress contours of FEM can be seen in Figure 5.25. The slip of parts is increasing more. High stresses are obtained at shaft keyway fillet and have a stress range from 126 GPa to 190 GPa.

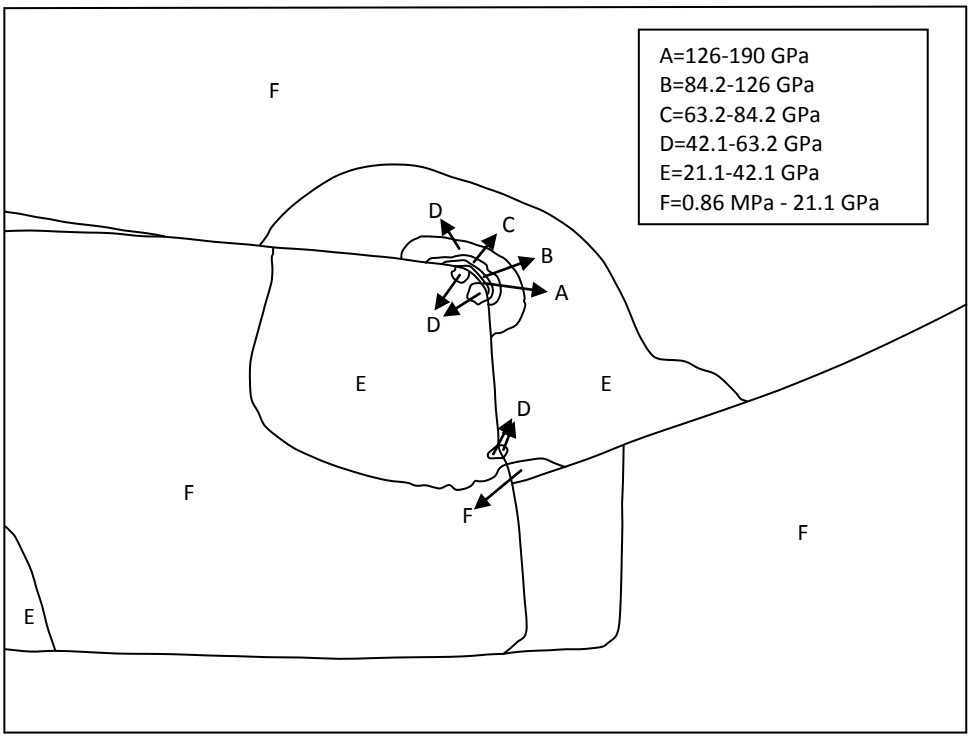

Figure 5.25. Stress contours at key and keyway corner (test no fa-1, T=0.82*Ty, fc=0.1)

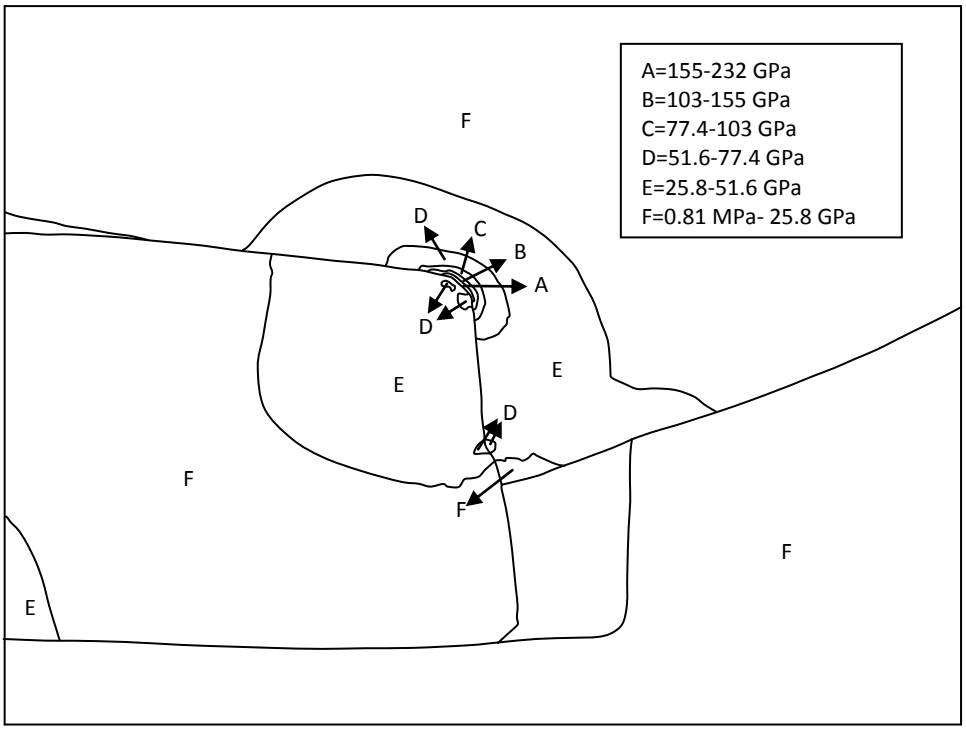

Figure 5.26. Stress contours at key and keyway corner (test no fa-1, T=1.11*Ty, fc=0.1)

Stress contours are shown in Figure 5.26 when applying 1.11 of yield torque. Highest stresses are obtained at keyway fillet of shaft and have a stress range between 155 GPa and 232 GPa.

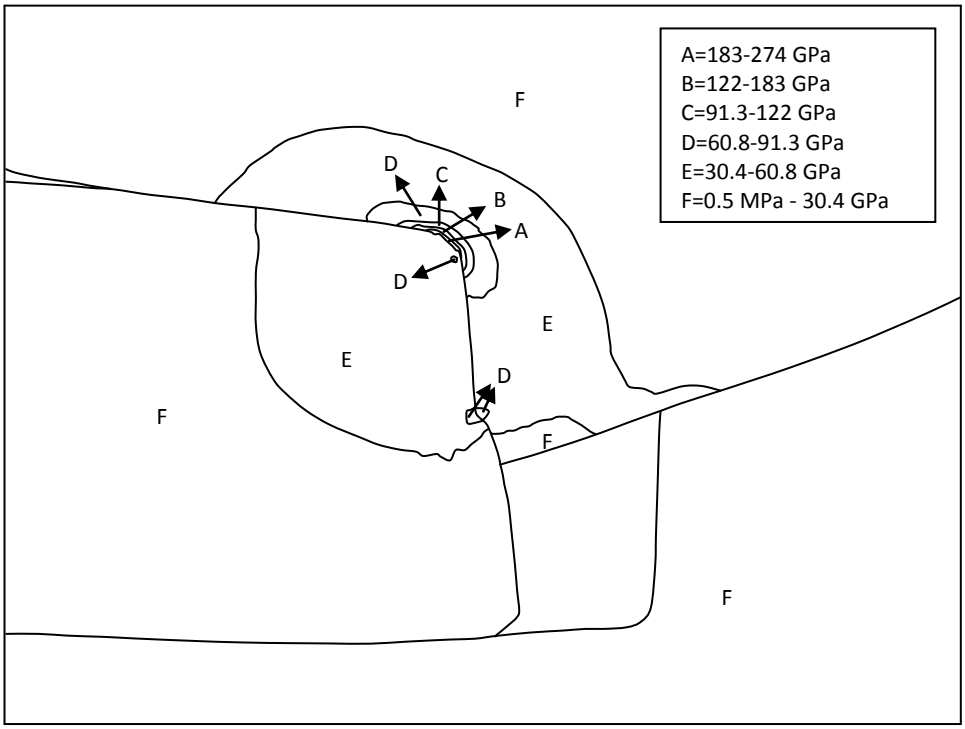

Figure 5.27. Stress contours at key and keyway corner (test no fa-1, T=1.35*Ty, fc=0.1)

Last increasing the torque to 1.35 of yield torque, FEM stress contours can be seen in Figure 5.27. High stresses are obtained at shaft keyway fillet and have a stress range from 183 GPa to 274 GPa.

Stress indices of test no fa-2 can be seen in Figure 5.28 and they are compared with the experimental result. It is seen that the FEM stress result is lower than the experimental result at yield torque. Key edges have dimensions of w=1 mm and h=3 mm. The slip of key and shaft may influence the FEM results.

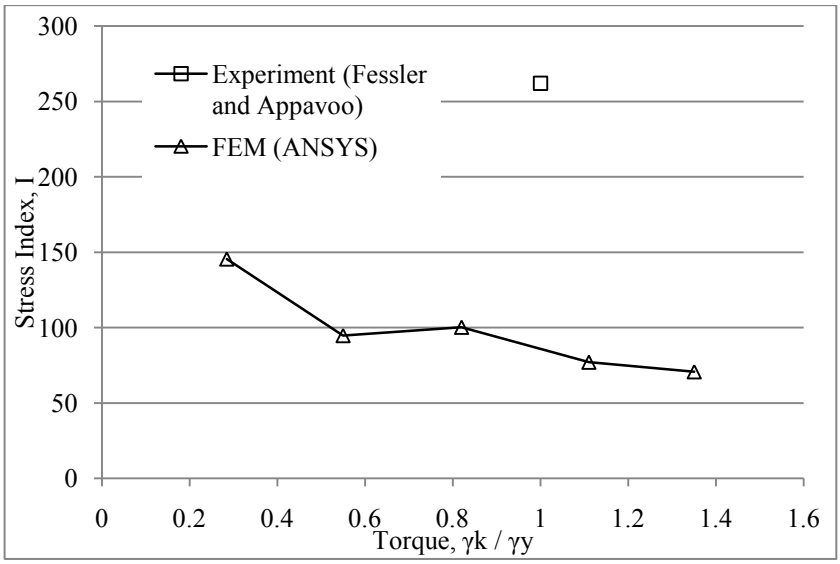

Figure 5.28. Variations of stress index, I, at the point Ss for different torques (test no fa-2, fc=0.1)

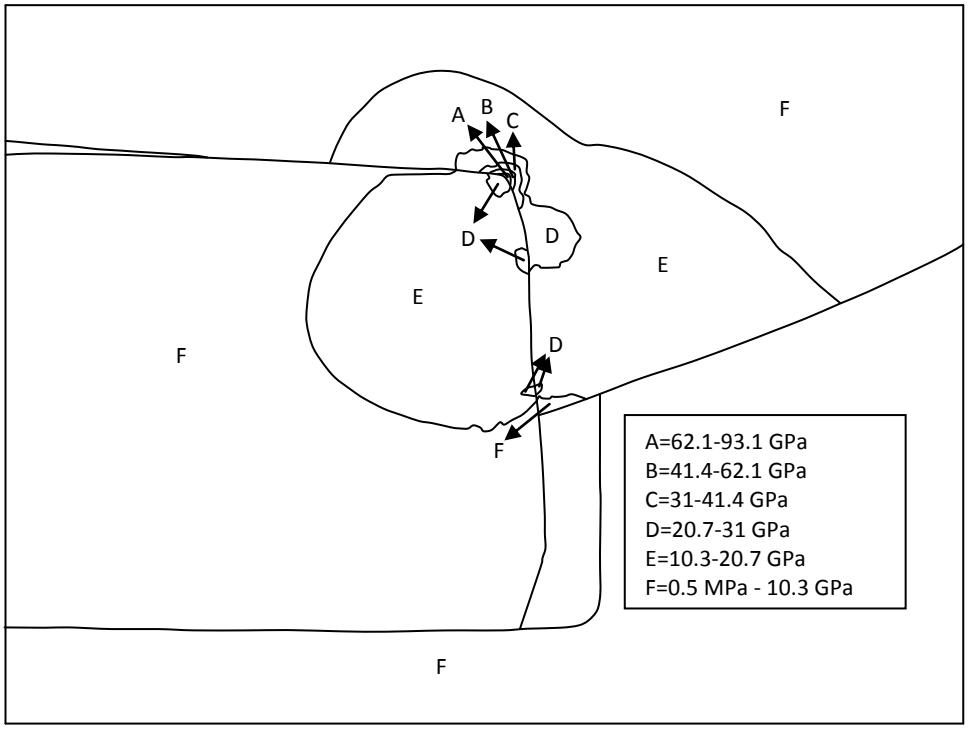

Figure 5.29. Stress contours at key and keyway corner (test no fa-2, T=0.285*Ty, fc=0.1)

Stress contours of FEM can be seen in Figure 5.29 for 0.285 of yield torque. High stresses are obtained at shaft keyway fillet and have a stress range between 62.1 GPa and 93.1 GPa. The slip of shaft and key can be seen.

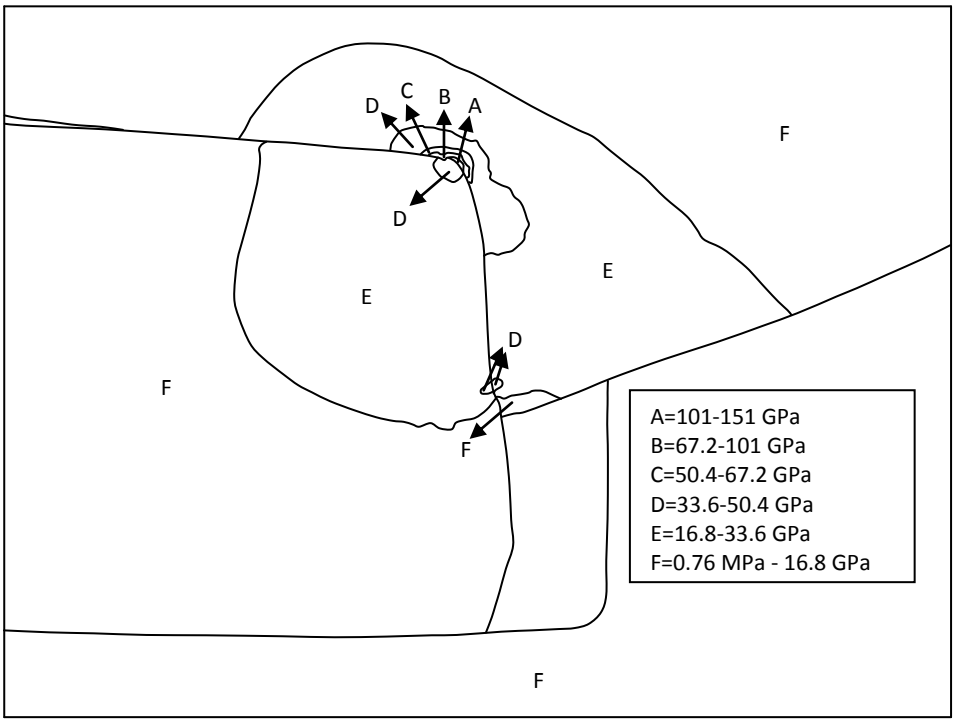

Figure 5.30. Stress contours at key and keyway corner (test no fa-2, T=0.55*Ty, fc=0.1)

Stress contours of FEM results can be seen in Figure 5.30 when increasing the applied torque to 0.55 of yield torque. High stresses have a stress range between 101 GPa and 151 GPa.

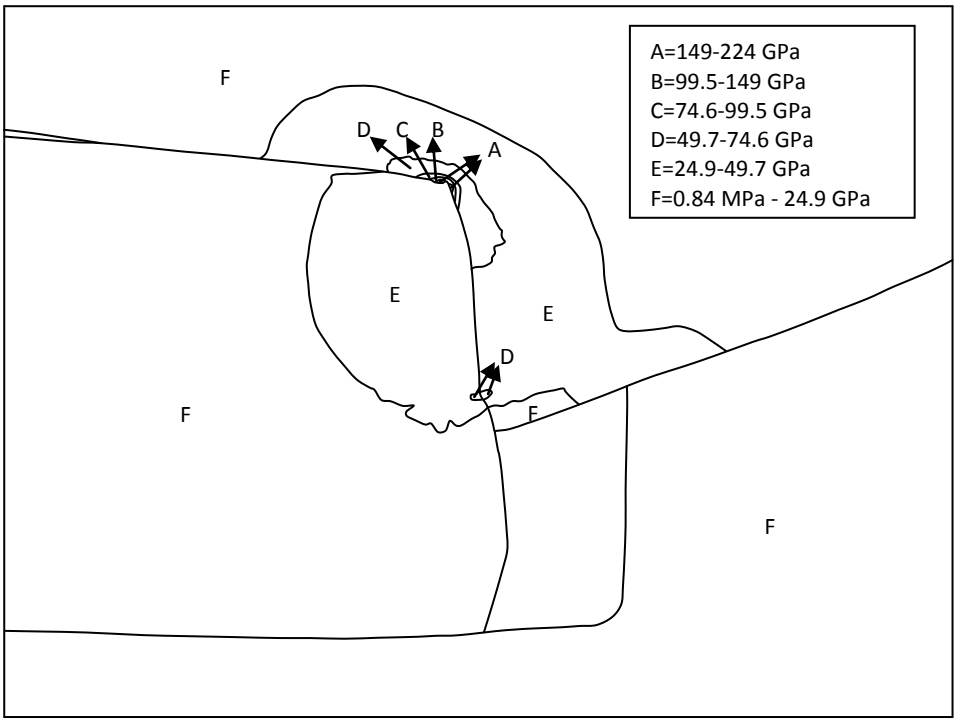

Figure 5.31. Stress contours at key and keyway corner (test no fa-2, T=0.82*Ty, fc=0.1)

Further increasing the applied torque to 0.82 of yield torque, stress contours of FEM are as shown in Figure 5.31. High stresses are obtained at the keyway fillet of the shaft and have a stress range between 149 GPa and 224 GPa at shaft keyway.

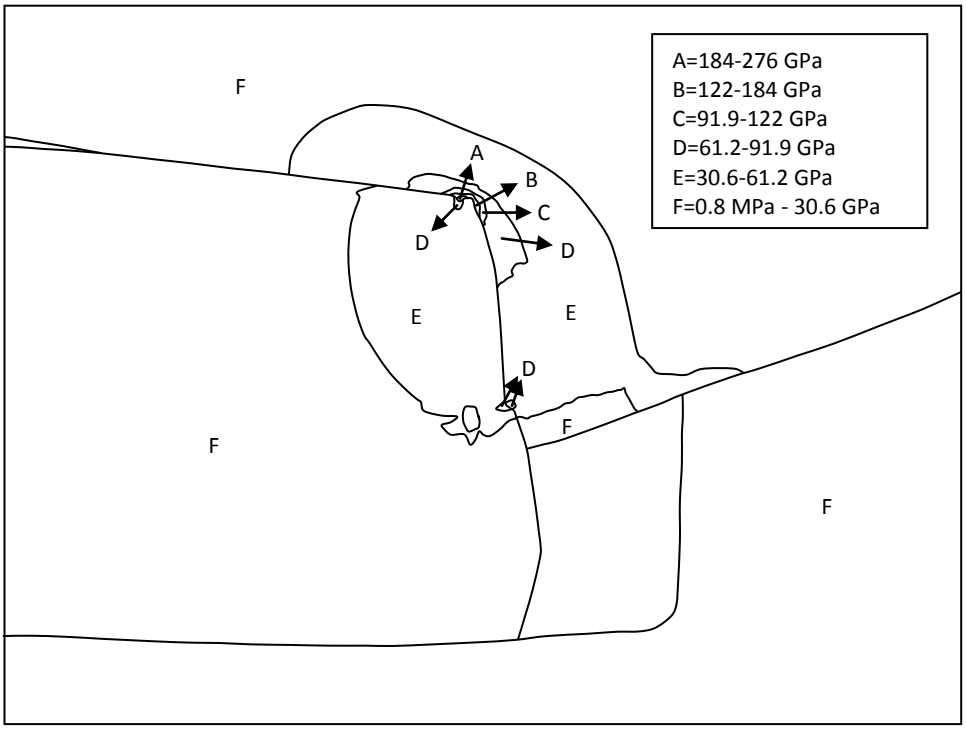

Figure 5.32. Stress contours at key and keyway corner (test no fa-2, T=1.11*Ty, fc=0.1)

Stress contours are shown in Figure 5.32, when applying 1.11 of yield torque. High stresses are obtained at shaft keyway and have a stress range from 184 GPa to 276 GPa.

Stress contours of FEM results can be seen in Figure 5.33 at the 1.35 of yield torque. High stresses are obtained shaft keyway fillet and stresses are obtained between 211 GPa and 317 GPa.

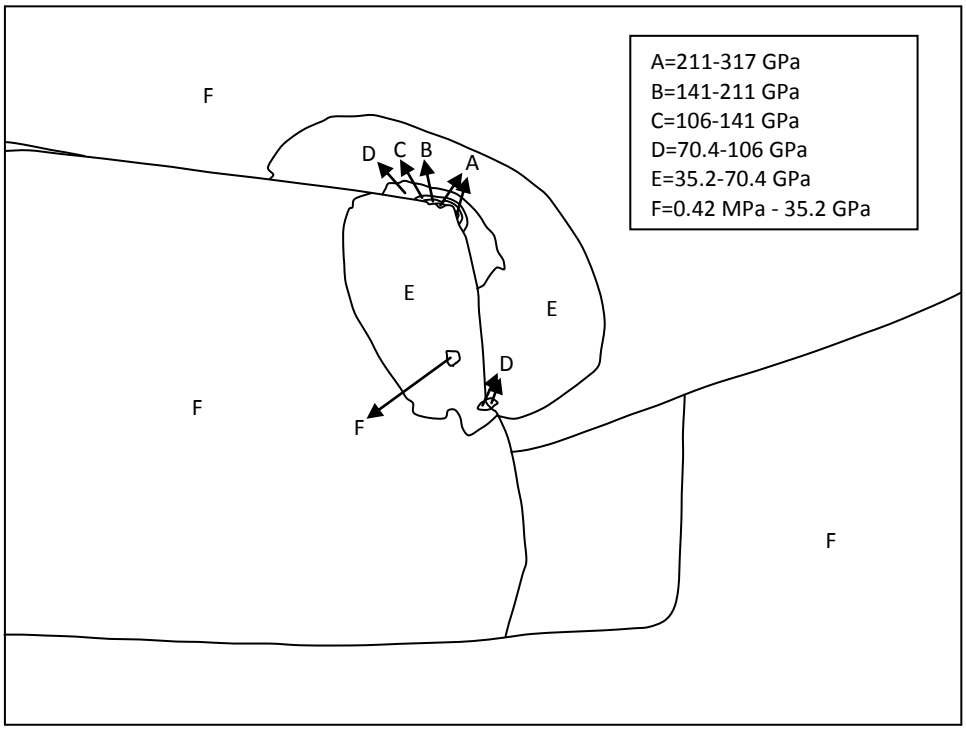

Figure 5.33. Stress contours at key and keyway corner (test no fa-2, T=1.35*Ty, fc=0.1)

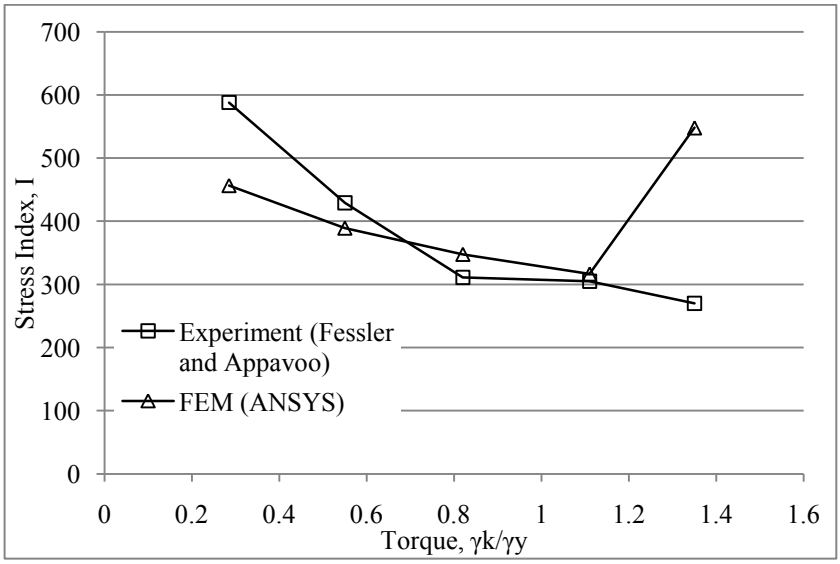

Figure 5.34. Variations of stress index, I, at the point Ss for different torques (test no fa-3, fc=0.1)

Stress indices of test no fa-3 can be seen in Figure 5.34 at Ss point and they are compared with experimental results. General stress distributions are similar. But

when applying 1.35 of yield torque, FEM results are getting higher. This may be caused from the slip of shaft and key.

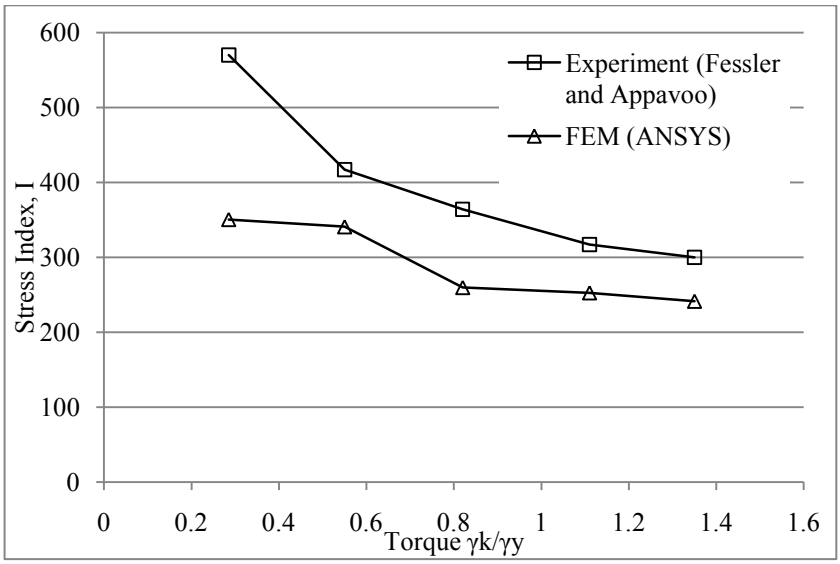

Figure 5.35. Variations of stress index, I, at the point Ss for different torques (test no fa-4, fc=0.1)

Stress distribution of FEM can be seen in Figure 5.35 for test no fa-4 and it is compared with experimental result. When increasing the torque, stress indices are decreasing. The difference between FEM and experimental result is high at 0.285 of yield torque. Other results of FEM and experimental results are similar.

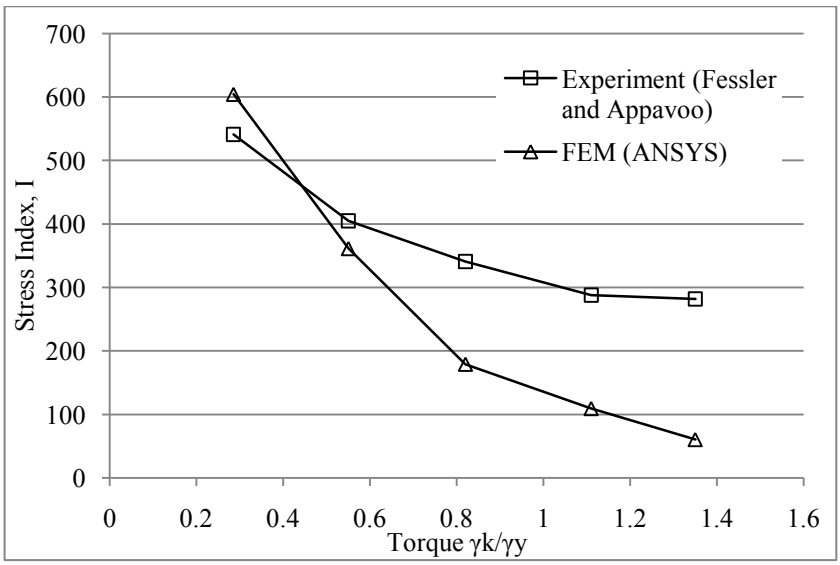

Figure 5.36. Variations of stress index, I, at the point Ss for different torques (test no fa-5, fc=0.1)

Stress distribution of FEM can be seen in Figure 5.36 for test no fa-5 and it is compared with experimental result. FEM results are decreasing when increasing the torque. It may be caused from the slip of key and shaft. Especially key slip can mostly influence the stress distribution.

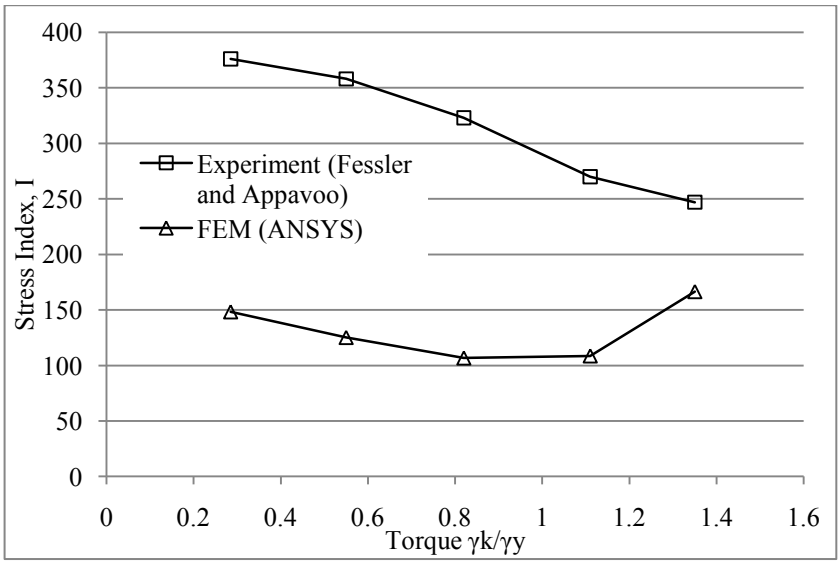

Figure 5.37. Variations of stress index, I, at the point Ss for different torques (test no fa-6, fc=0.1)

Stress distribution of test no fa-6 can be seen in Figure 5.37 at the point Ss. FEM result is less than experimental result. The reason of this difference can be caused from the slip of the key. Key edges have a dimensions of w=3 mm and h=3 mm. The gap between shaft keyway and key edge is more than before models. Hence slip occurs more.

5.5.5. Effects of torque on stresses at the point Sb with different key edge geometries

The stresses at the point Sb are investigated for different key edge geometries with various torques and they are compared with experimental results.

Stress indices of test no fa-1 at point Sb can be seen in Figure 5.38 and they are compared with experimental results. The FEM and experimental results are similar at the yield torque. When increasing the torque, the stress indices of FEM results are decreasing.

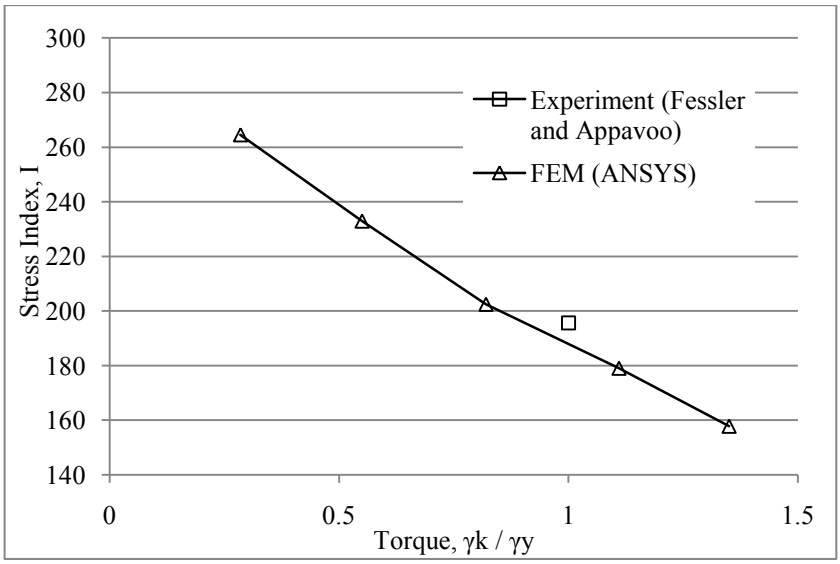

Figure 5.38. Variations of stress index, I, at the point Sb for different torques (test no fa-1, fc=0.1)

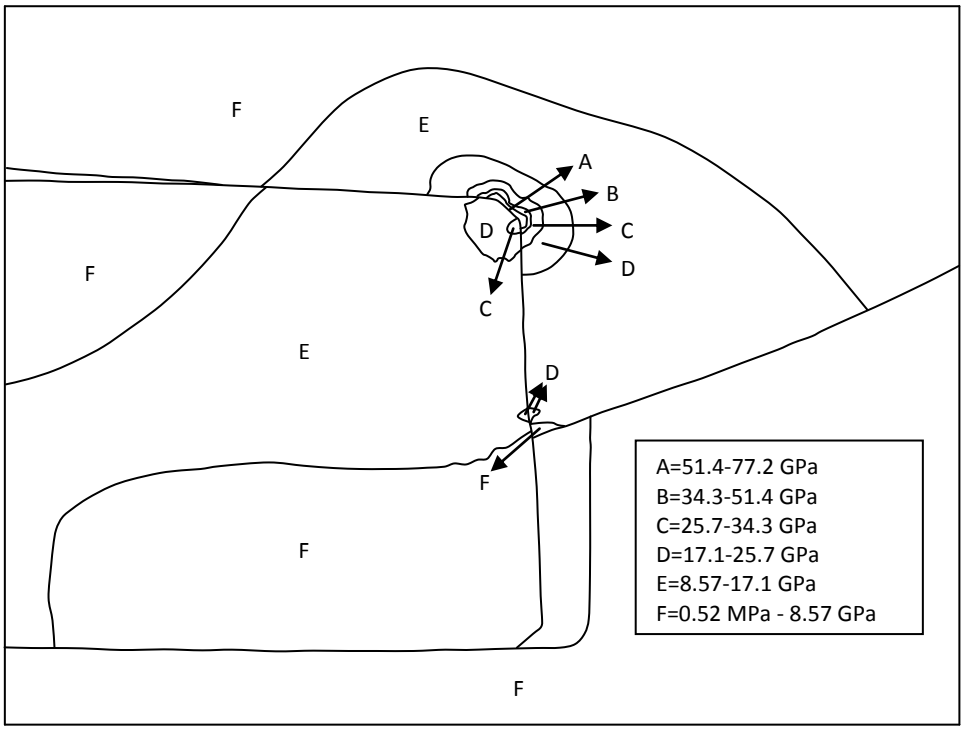

Figure 5.39. Stress contours at key and keyway corner (test no fa-1, T=0.285*Ty, fc=0.1)

Stress contours of test no fa-1 can be seen in Figure 5.39 when applying 0.285 of yield torque. It is seen that high stresses are obtained at keyway fillet of shaft and have a stress range from 51.4 GPa to 77.2 GPa. Also the slip of key and shaft can be seen.

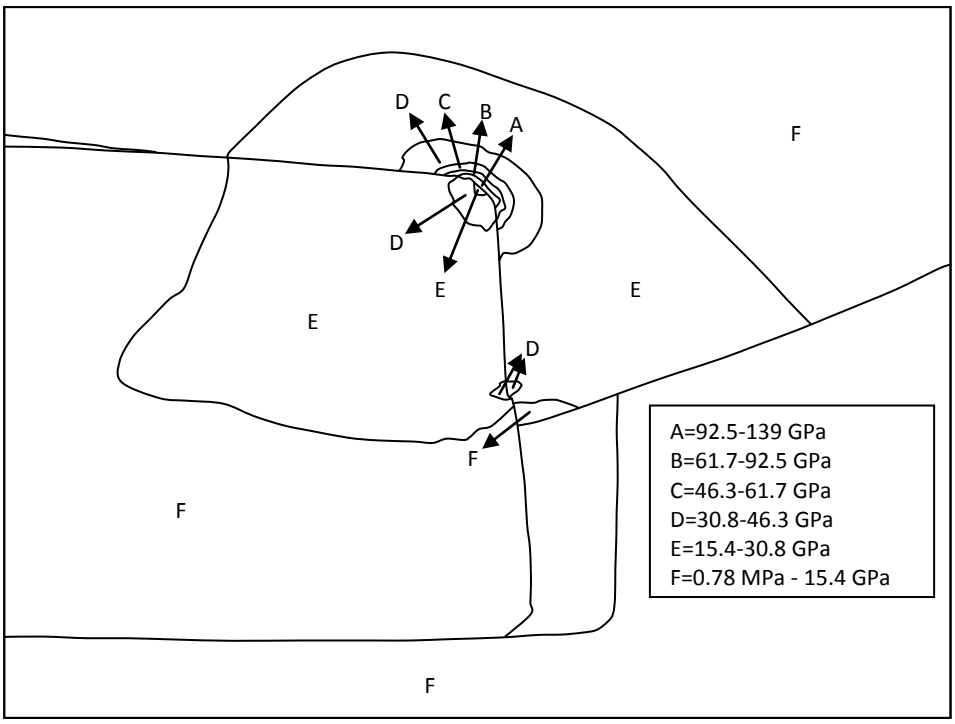

Figure 5.40. Stress contours at key and keyway corner (test no fa-1, T=0.55*Ty, fc=0.1)

When increasing the torque to 0.55 of yield torque, stresses are getting higher and the highest stress values are obtained in a stress range from 92.5 GPa to 139 GPa. They exist at the keyway fillet of the shaft.

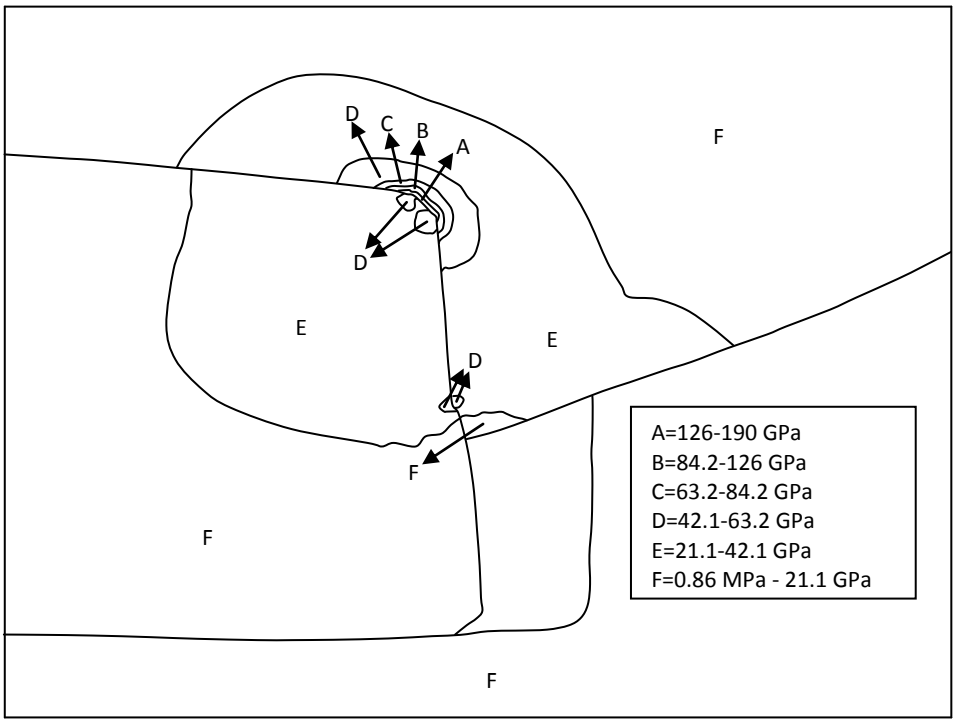

Figure 5.41. Stress contours at key and keyway corner (test no fa-1, T=0.82*Ty, fc=0.1)

Further increasing the torque to the 0.82 of yield torque, the stress contours become as given in Figure 5.41. High stresses are obtained at the keyway fillet of the shaft and have a stress range from 126 GPa to 190 GPa.

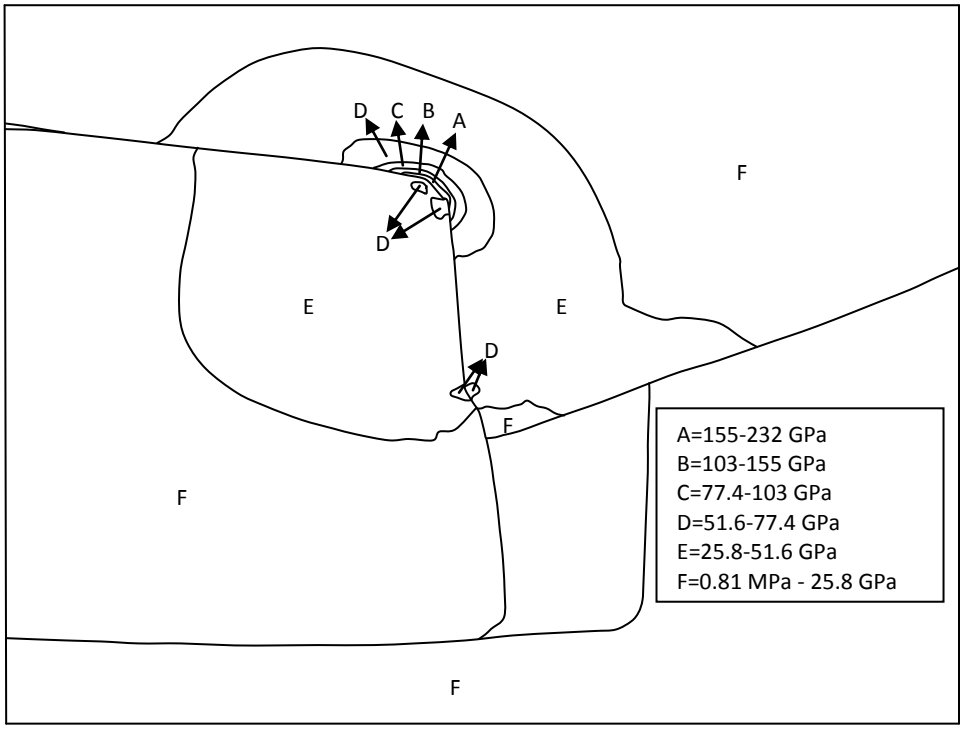

Figure 5.42. Stress contours at key and keyway corner (test no fa-1, T=1.11*Ty, fc=0.1)

Stress contours of test no fa-1 can be seen in Figure 5.42 when applying 1.11 of yield torque. High stresses are obtained at shaft keyway and have a stress range between 155 GPa and 232 GPa.

Stress contours can be seen in Figure 5.43 when increasing the torque to 1.35 of yield torque. High stresses have a stress range between 183 GPa and 274 GPa. Hub has low stresses than key and shaft.

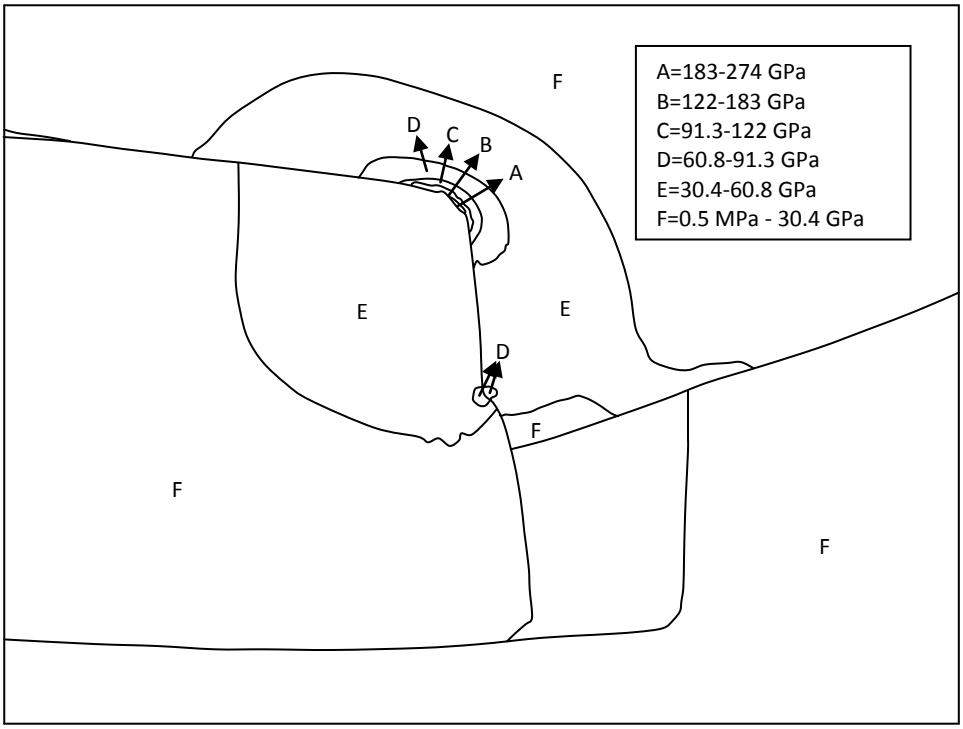

Figure 5.43. Stress contours at key and keyway corner (test no fa-1, T=1.35*Ty, fc=0.1)

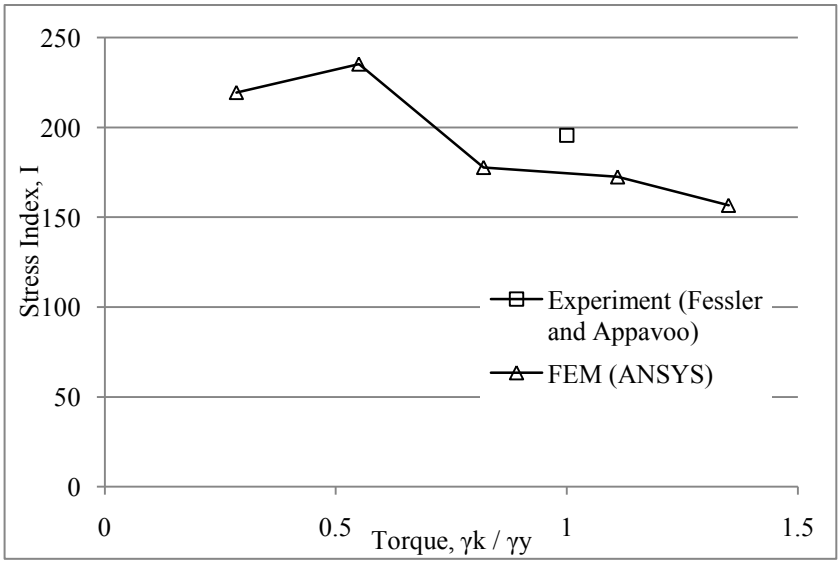

Figure 5.44. Variations of stress index, I, at the point Sb for different torques (test no fa-2, fc=0.1)

Stress distribution of test no fa-2 at point Sb can be seen in Figure 5.44. The FEM result is near the experimental result at same torques. When looking the stress

distribution of FEM, it is firstly increasing and then decreasing with respect to increasing the torque.

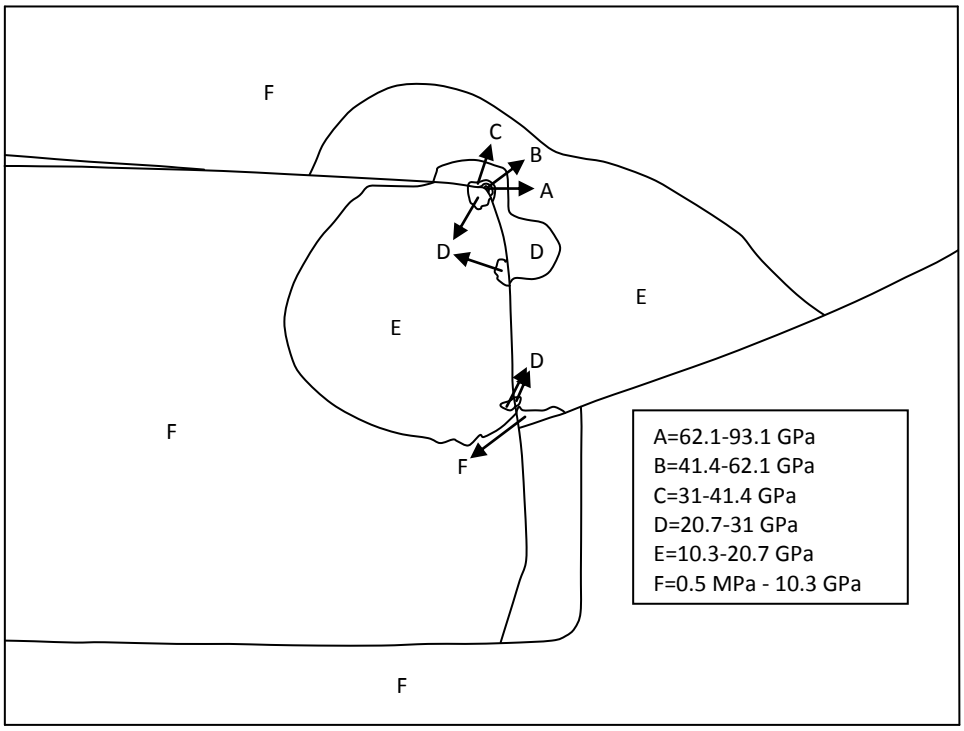

Figure 5.45. Stress contours at key and keyway corner (test no fa-2, T=0.285*Ty, fc=0.1)

Stress contours of test no fa-2 can be seen in Figure 5.45 when applying 0.285 of yield torque. Maximum stresses are obtained at shaft keyway fillet and have a stress range between 62.1 GPa and 93.1 GPa.

When increasing the torque to 0.55 of yield torque, stresses are increasing. Stress contours can be seen in Figure 5.46. High stresses have a stress range between 101 GPa and 151 GPa.

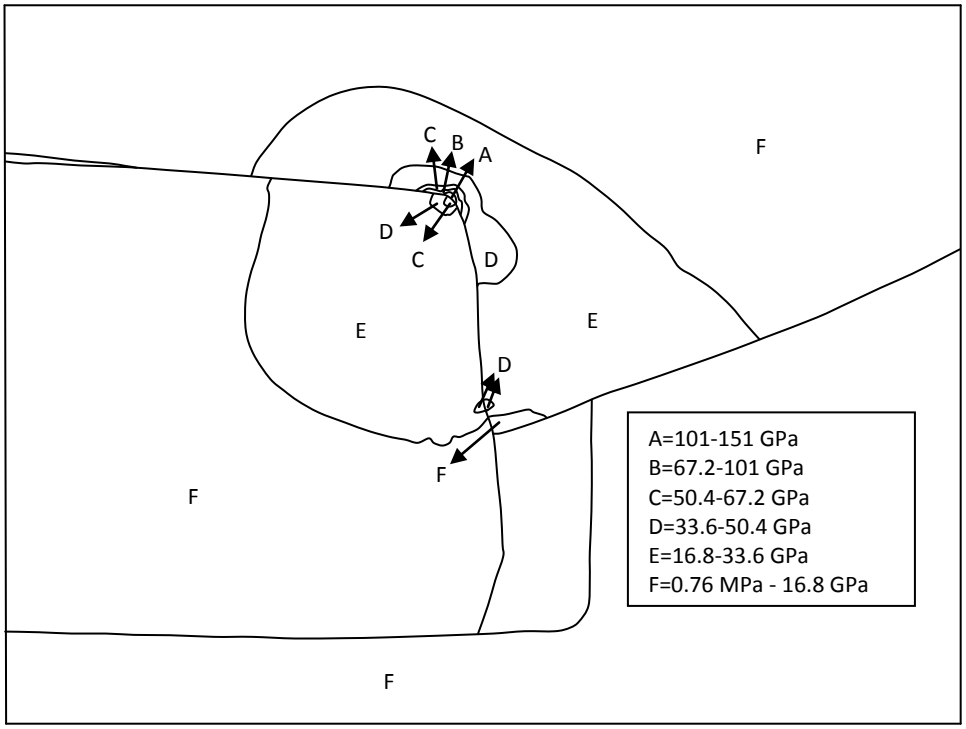

Figure 5.46. Stress contours at key and keyway corner (test no fa-2, T=0.55*Ty, fc=0.1)

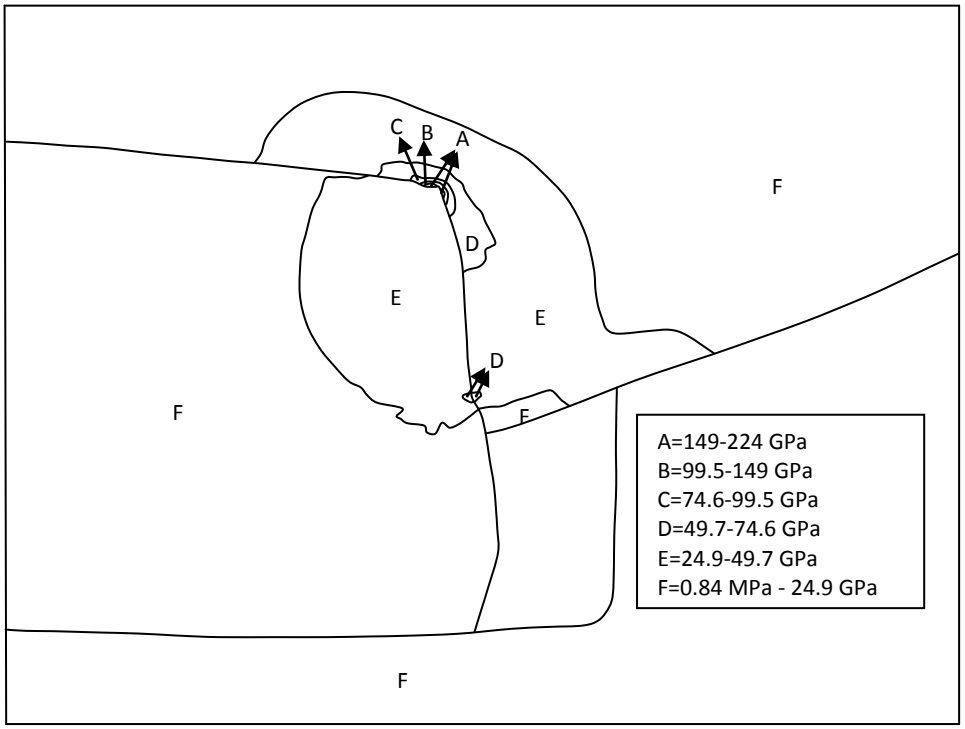

Figure 5.47. Stress contours at key and keyway corner (test no fa-2, T=0.82*Ty, fc=0.1)

Further increasing the torque, stress contours become as given in Figure 5.47. High stresses are obtained in shaft keyway fillet and have a stress range between 149 GPa and 224 GPa.

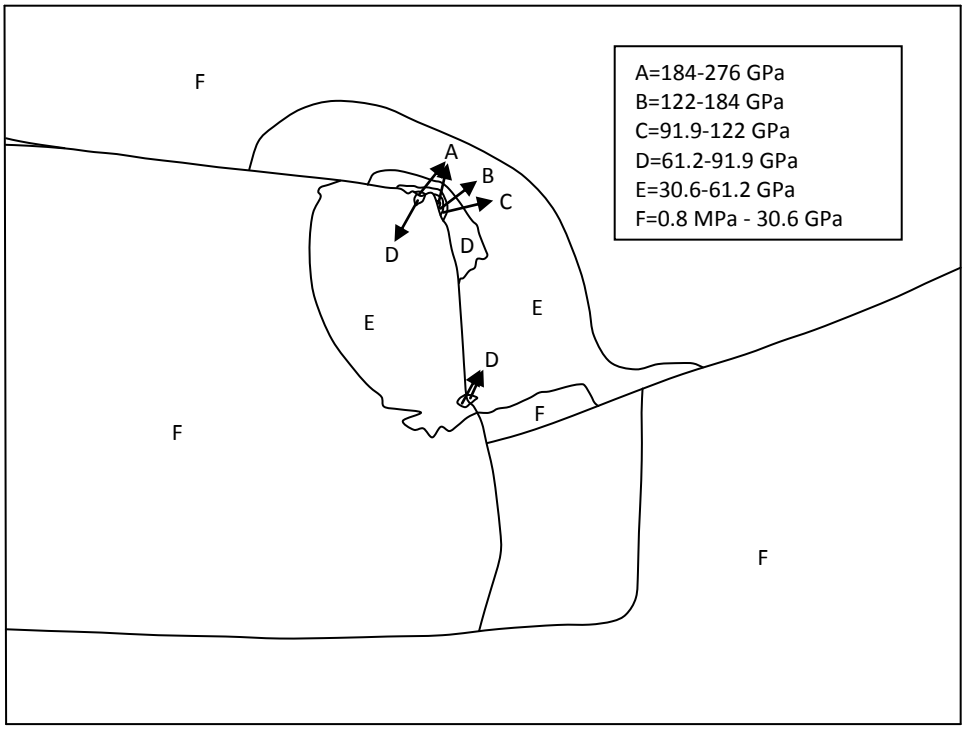

Figure 5.48. Stress contours at key and keyway corner (test no fa-2, T=1.11*Ty, fc=0.1)

When increasing the torque to 1.11 of yield torque, stress contours become as shown in Figure 5.48. Maximum stresses are obtained at keyway fillet of the shaft and have a stress range between 184 GPa and 276 GPa.

When the torque is equal to 1.35 of yield torque, the stress contours become as shown in Figure 5.49. High stresses are found at shaft keyway fillet and have a stress range from 211 GPa to 317 GPa.

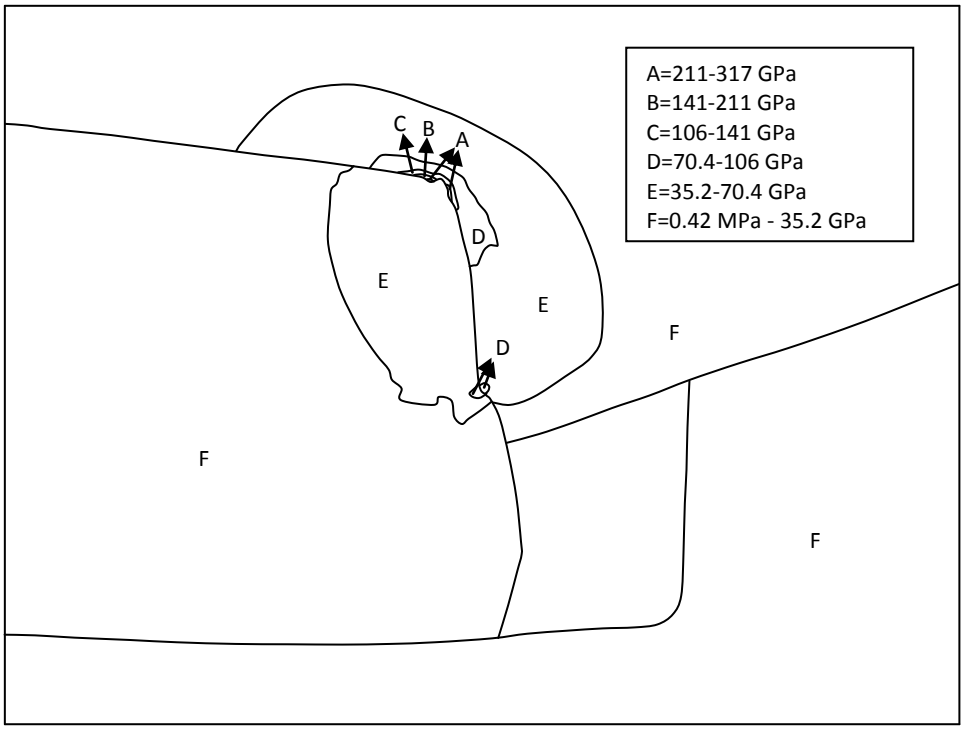

Figure 5.49. Stress contours at key and keyway corner (test no fa-2, T=1.35*Ty, fc=0.1)

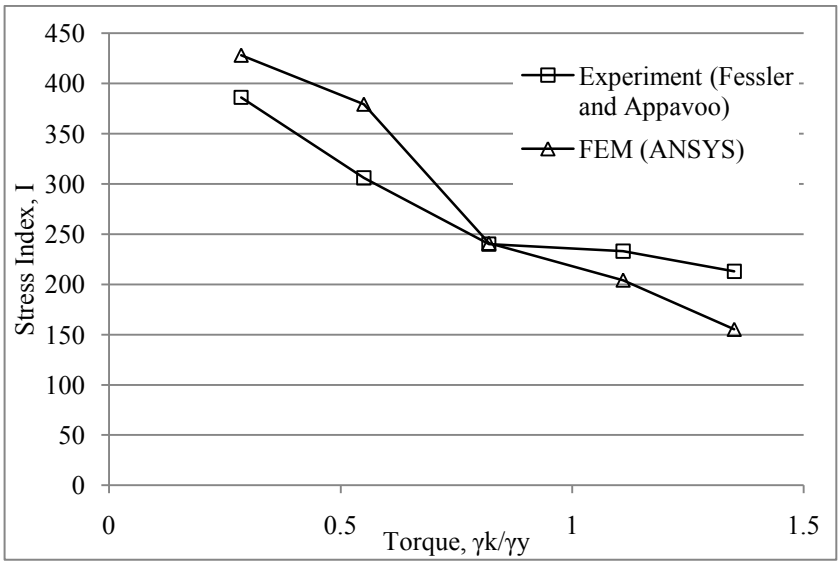

Figure 5.50. Variations of stress index, I, at the point Sb for different torques (test no fa-3, fc=0.1)

Stress distribution of test no fa-3 at point Sb can be seen in Figure 5.50 with respect to changing torque. FEM result is similar to the experimental result. When increasing the torque, stress indices are decreasing.

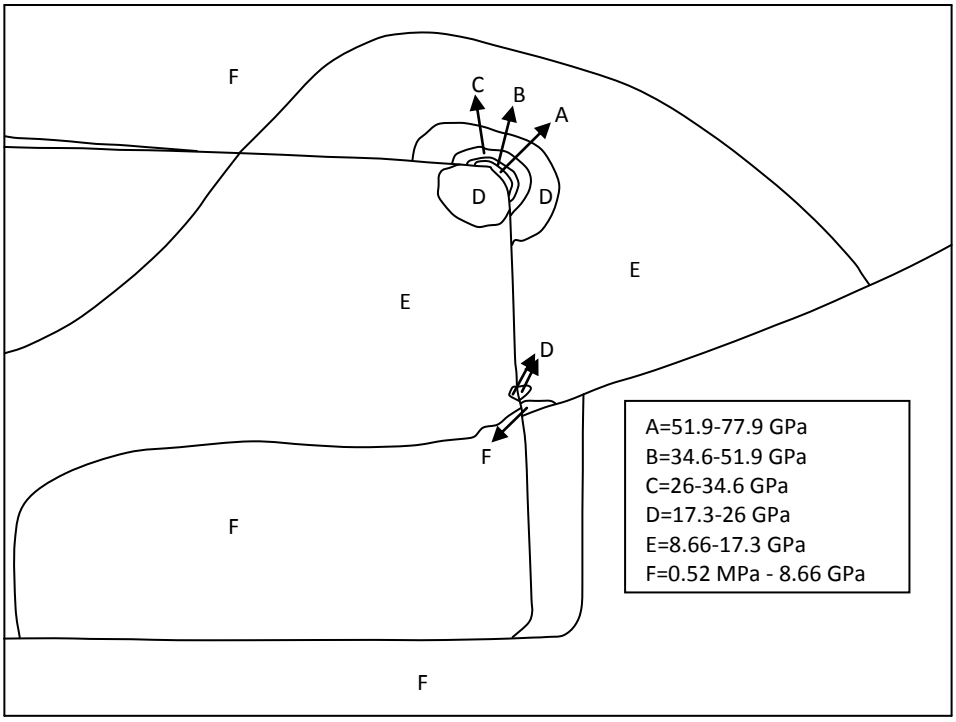

Figure 5.51. Stress contours at key and keyway corner (test no fa-3, T=0.285*Ty, fc=0.1)

Stress contours of test no fe-3 can be seen in Figure 5.51 when applying 0.285 of yield torque. Maximum stresses are obtained at shaft keyway and have a stress range between 51.9 GPa and 77.9 GPa.

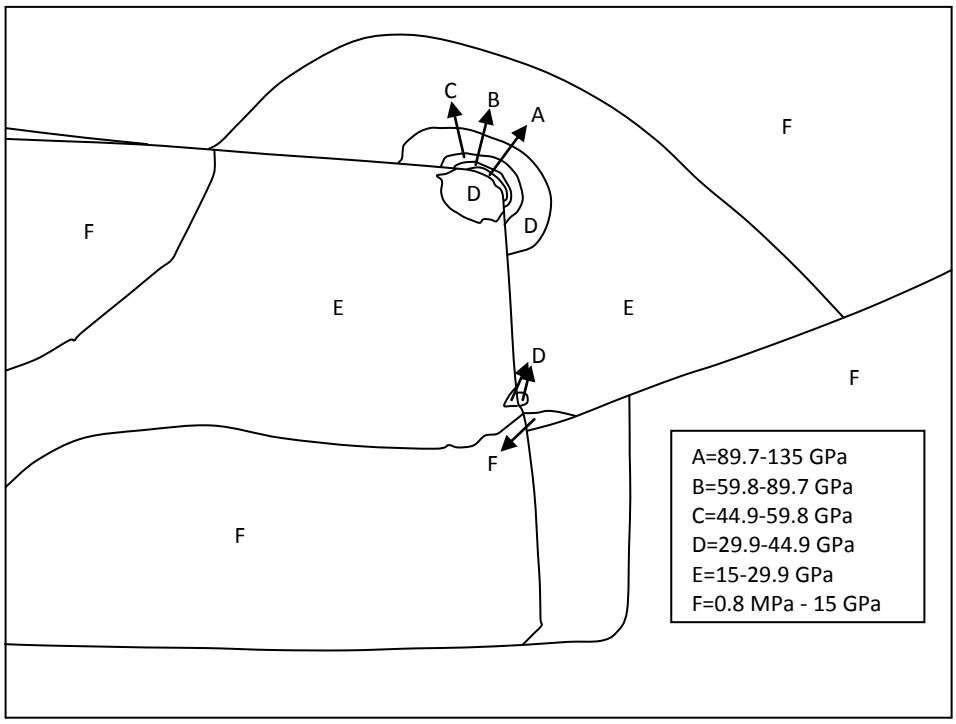

Figure 5.52. Stress contours at key and keyway corner (test no fa-3, T=0.55*Ty, fc=0.1)

Increasing the torque causes to more slip of the key and also increases the stresses. It can be seen in Figure 5.52. Maximum stresses have a stress range from 89.7 GPa to 135 GPa.

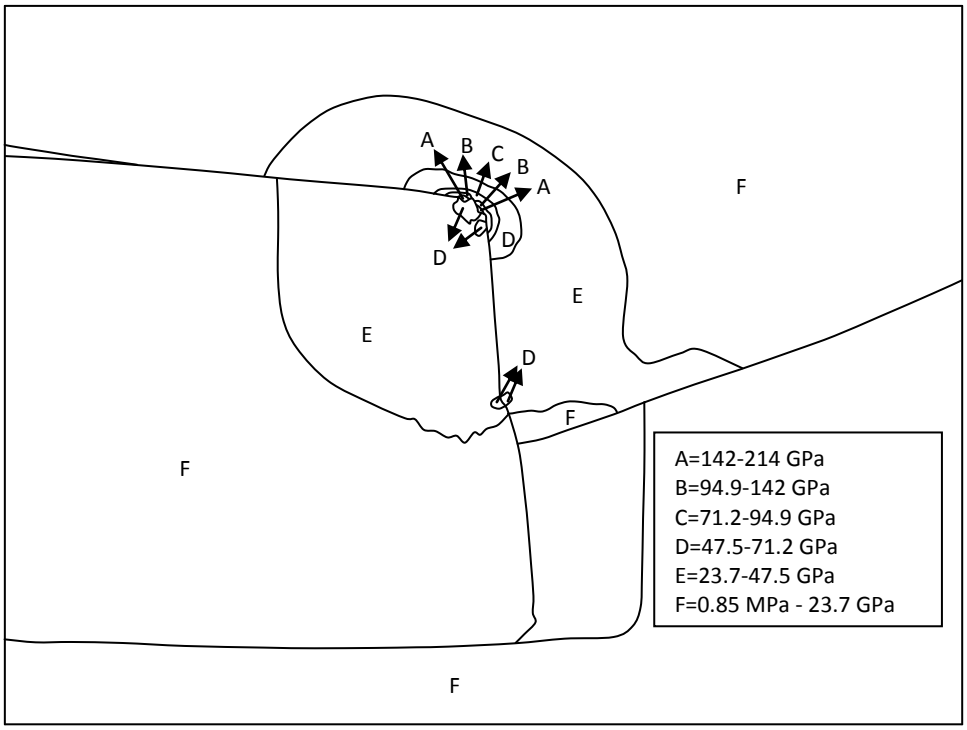

Figure 5.53. Stress contours at key and keyway corner (test no fa-3, T=0.82*Ty, fc=0.1)

When applying 0.82 of yield torque, stress contours of test no fa-3 can be obtained in Figure 5.53. Maximum stresses are obtained shaft keyway edge and have a stress range from 142 GPa to 214 GPa.

Stress contours of FEM can be seen in Figure 5.54, when increasing the torque to 1.11 of yield torque. Maximum stresses have a stress range between 181 GPa and 272 GPa.

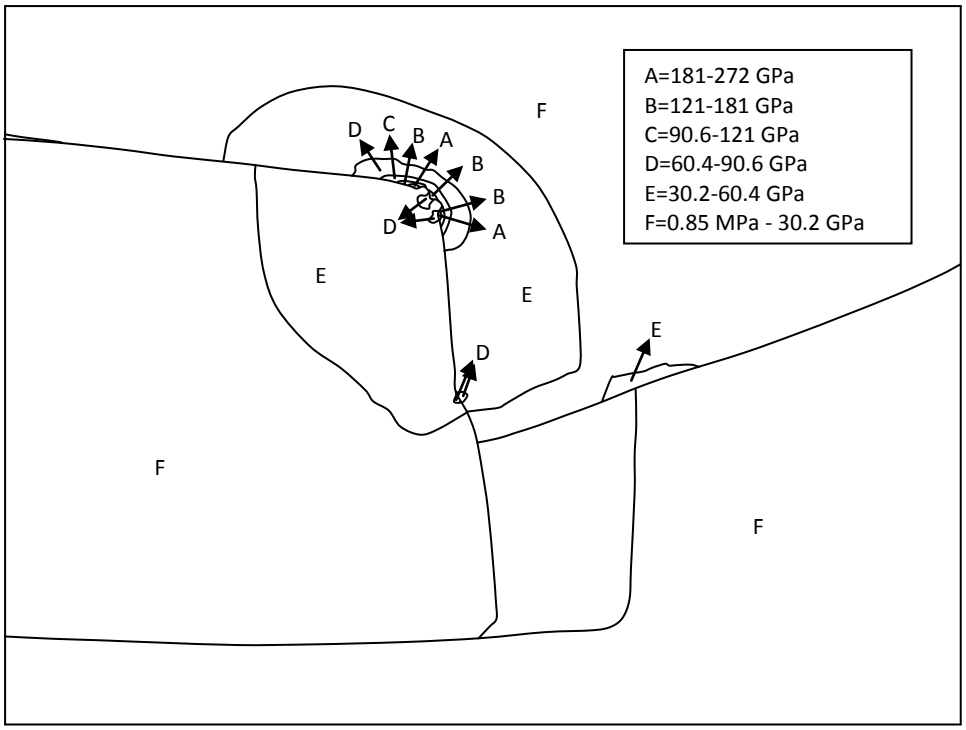

Figure 5.54. Stress contours at key and keyway corner (test no fa-3, T=1.11*Ty, fc=0.1)

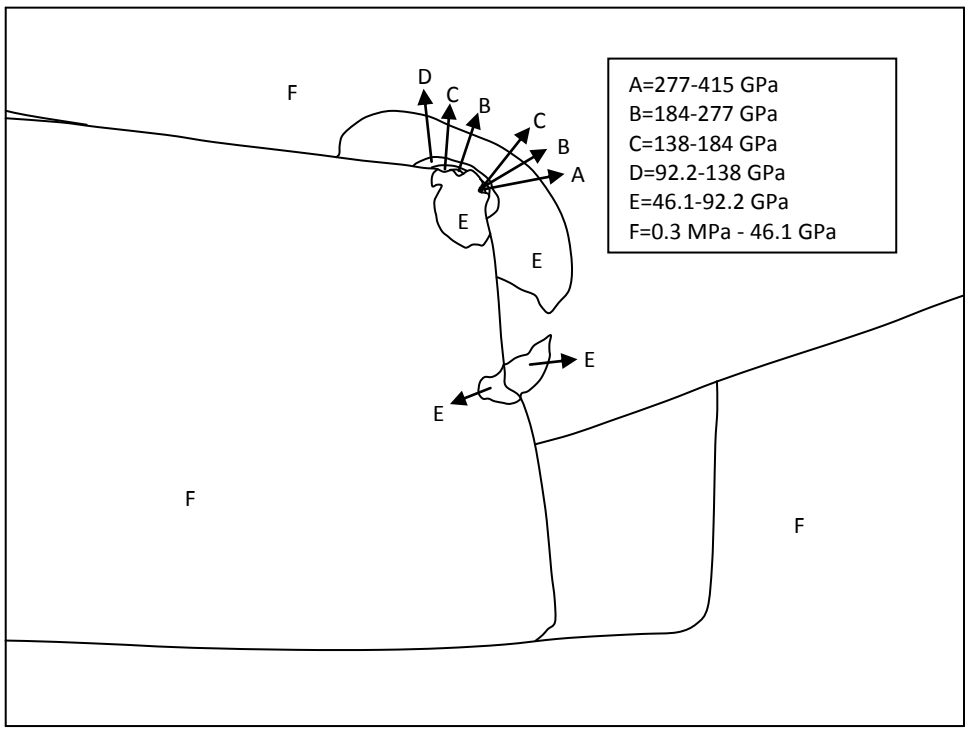

Figure 5.55. Stress contours at key and keyway corner (test no fa-3, T=1.35*Ty, fc=0.1)

Stress contours can be seen in Figure 5.55 when 1.35 of a yield torque is applied. High stresses are obtained at keyway fillet of the shaft and have a stress range from 277 GPa to 415 GPa.

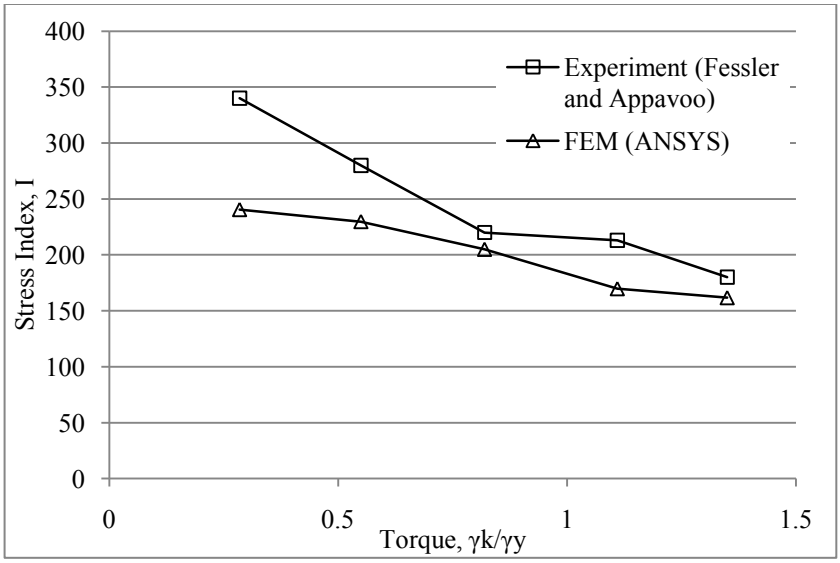

Figure 5.56. Variations of stress index, I, at the point Sb for different torques (test no fa-4, fc=0.1)

Stress indices of point Sb are given in Figure 5.56 with respect to different torques. FEM results are similar to the experimental results. Stress indices are decreasing when increasing the torque.

Stress contours of test no fa-4 can be seen in Figure 5.57 when applying 0.285 of yield torque. Different range of stresses is obtained in Figure 5.57. It can be seen that high stresses are obtained at the keyway fillet of the shaft and have a stress range between 50.2 GPa and 75.3 GPa. The slip of key and shaft can be seen.

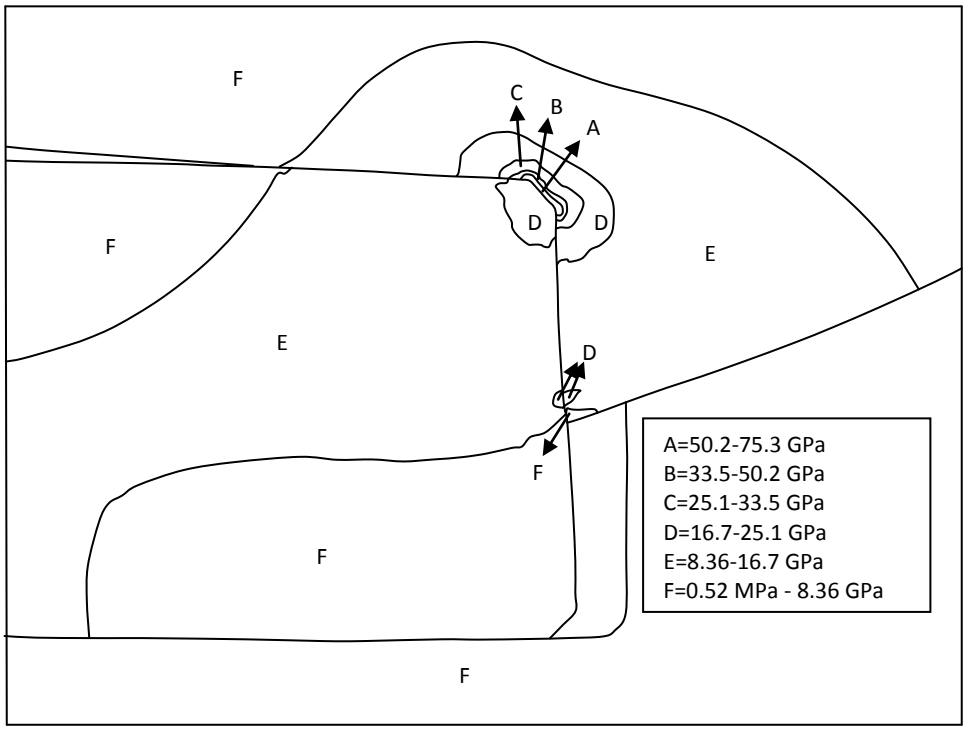

Figure 5.57. Stress contours at key and keyway corner (test no fa-4, T=0.285*Ty, fc=0.1)

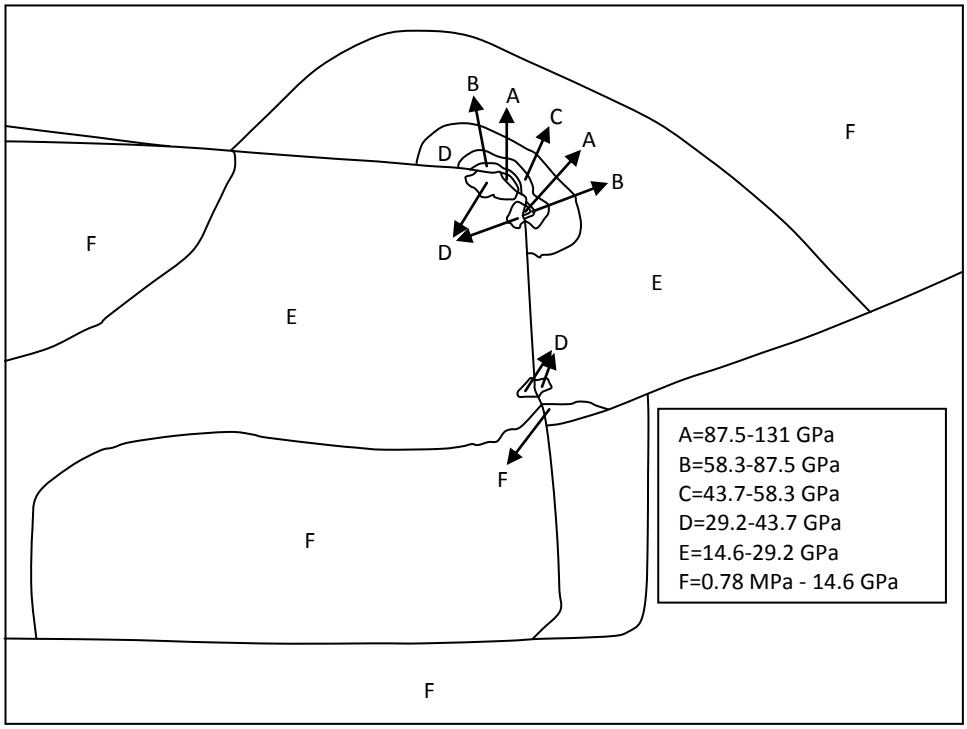

Figure 5.58. Stress contours at key and keyway corner (test no fa-4, T=0.55*Ty, fc=0.1)

When applying 0.55 of yield torque, stresses become as given in Figure 5.58. High stresses are obtained at keyway fillet of the shaft again and have a stress range from 87.5 GPa to 131 GPa.

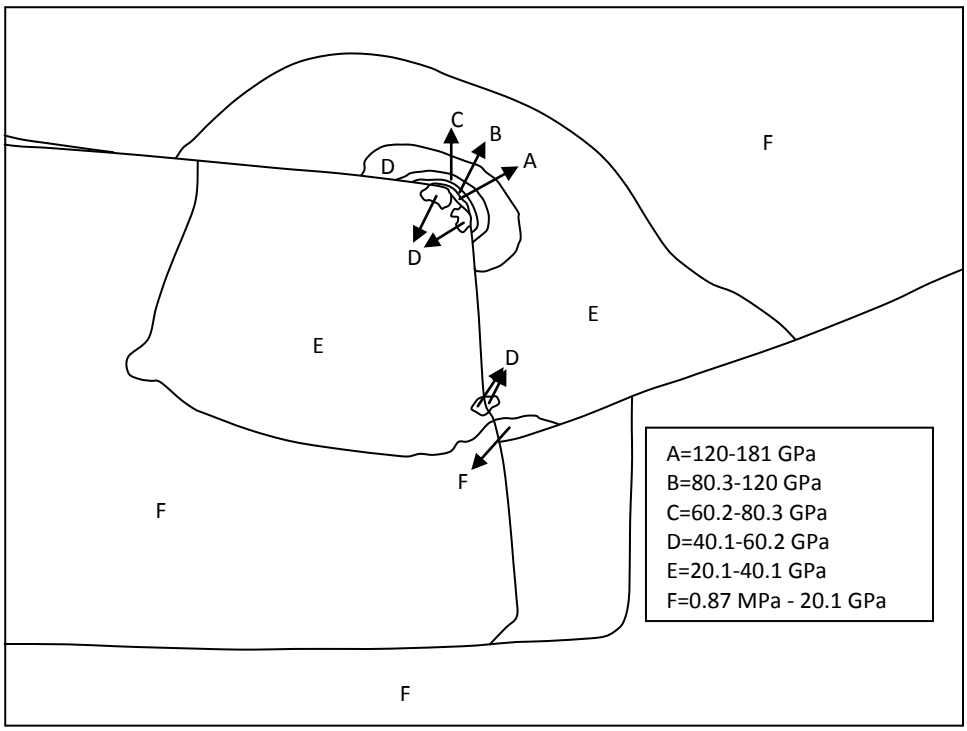

Figure 5.59. Stress contours at key and keyway corner (test no fa-4, T=0.82*Ty, fc=0.1)

Stresses are shown in Figure 5.59 when increasing 0.82 of yield torque. High stresses are obtained at keyway fillet of the shaft and have a stress range between 120 GPa and 181 GPa.

Stress contours of test no fa-4 can be seen in Figure 5.60 when applying 1.11 of yield torque. The slip of shaft and key are increasing. High stresses are obtained at the keyway fillet of shaft and have a stress range between 147 GPa and 220 GPa.

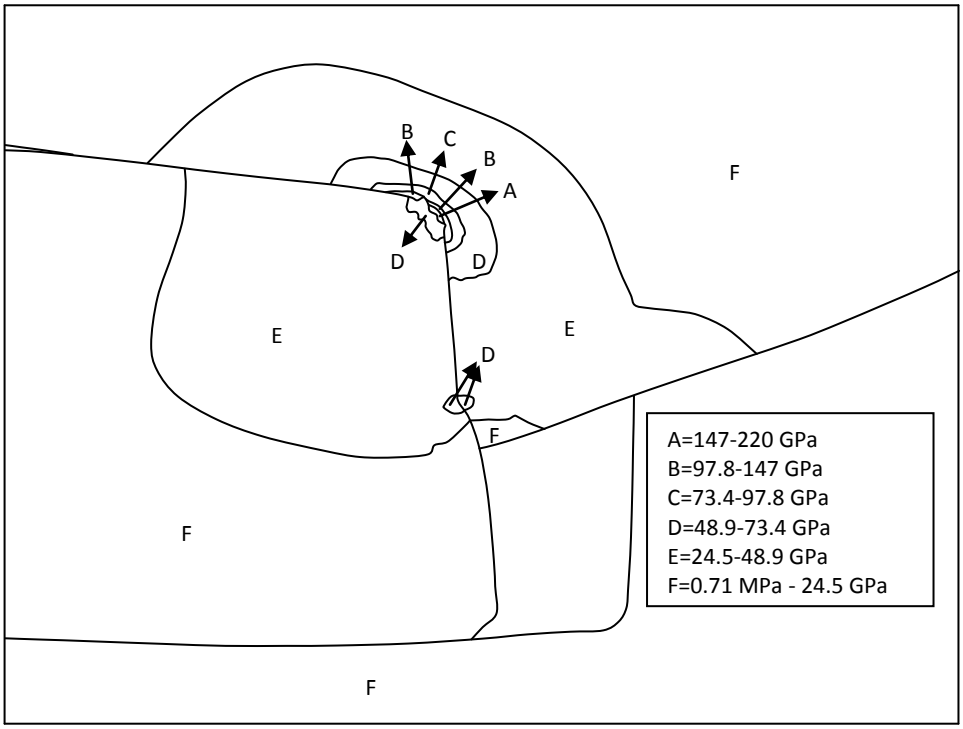

Figure 5.60. Stress contours at key and keyway corner (test no fa-4, T=1.11*Ty, fc=0.1)

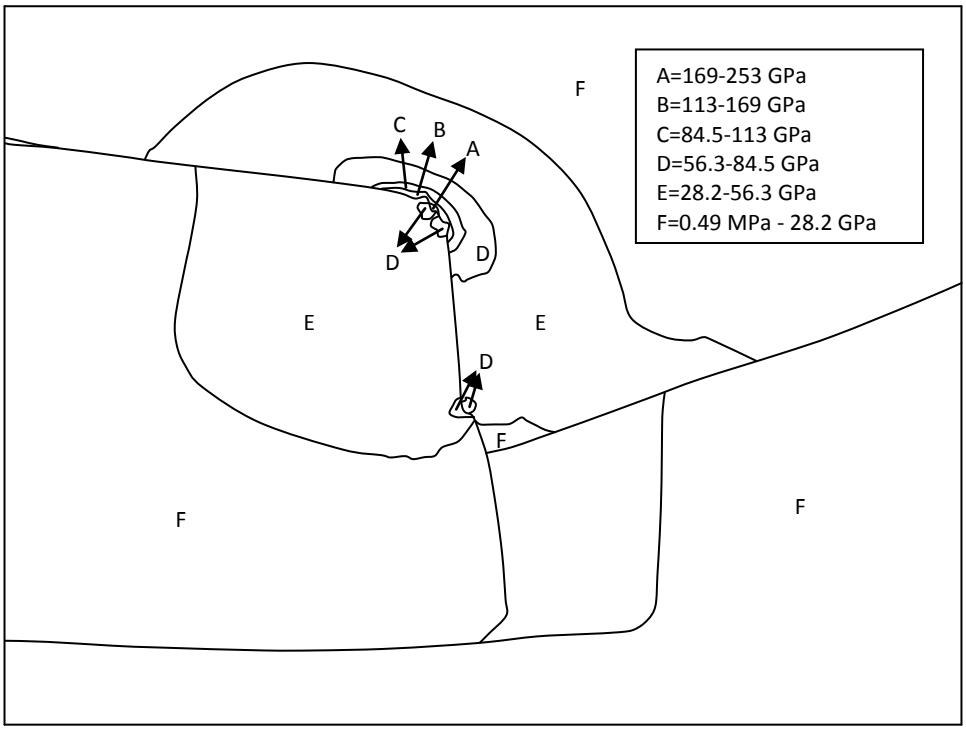

Figure 5.61. Stress contours at key and keyway corner (test no fa-4, T=1.35*Ty, fc=0.1)

Stress contours of FEM results are given in Figure 5.61 when applying 1.35 of yield torque. High stresses are obtained at the keyway fillet of the shaft. They have a stress range between 169 GPa and 253 GPa.

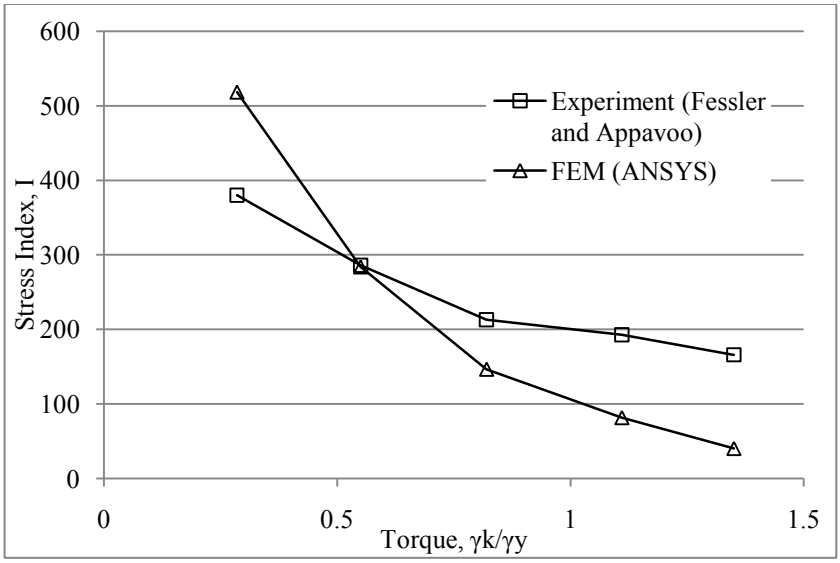

Figure 5.62. Variations of stress index, I, at the point Sb for different torques (test no fa-5, fc=0.1)

Stress indices of Sb are given in Figure 5.62 when applying different torques. Both FEM and experimental results are decreasing when increasing the torque. The FEM results are rapidly decreasing when starting to increase the torque.

Stress contours of FEM results are given in Figure 5.63 when 0.285 of yield torque is applied. High stresses are obtained at keyway fillet of the shaft and have a stress range between 45.9 GPa and 68.9 GPa. Key edges have less stresses than keyway fillet of the shaft and have a stress range between 30.6 GPa and 45.9 GPa.

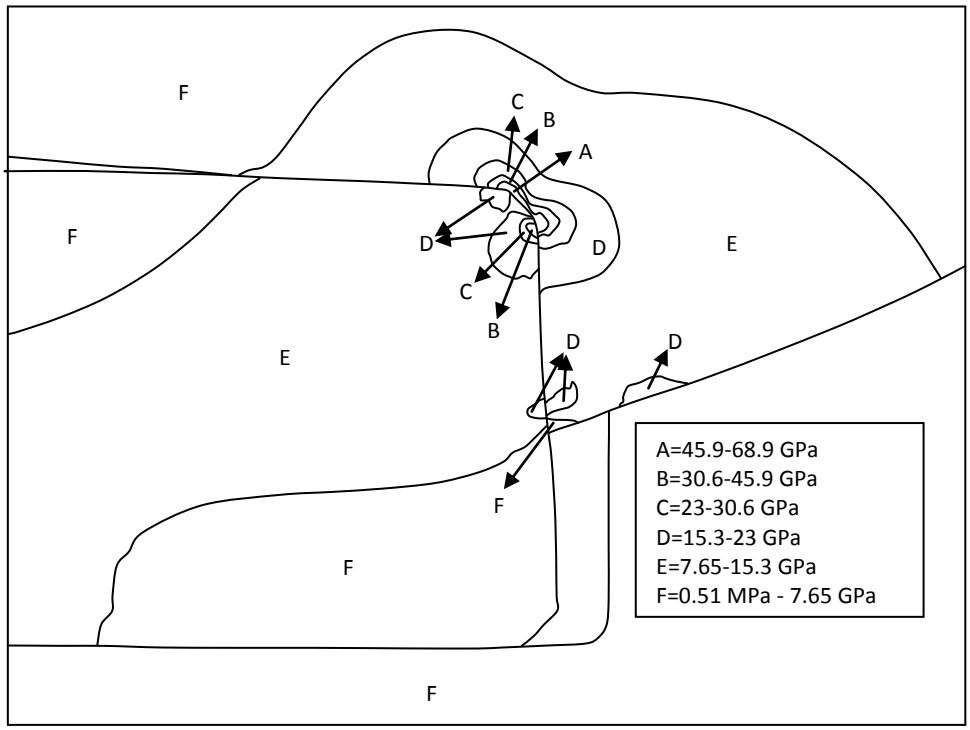

Figure 5.63. Stress contours at key and keyway corner (test no fa-5, T=0.285*Ty, fc=0.1)

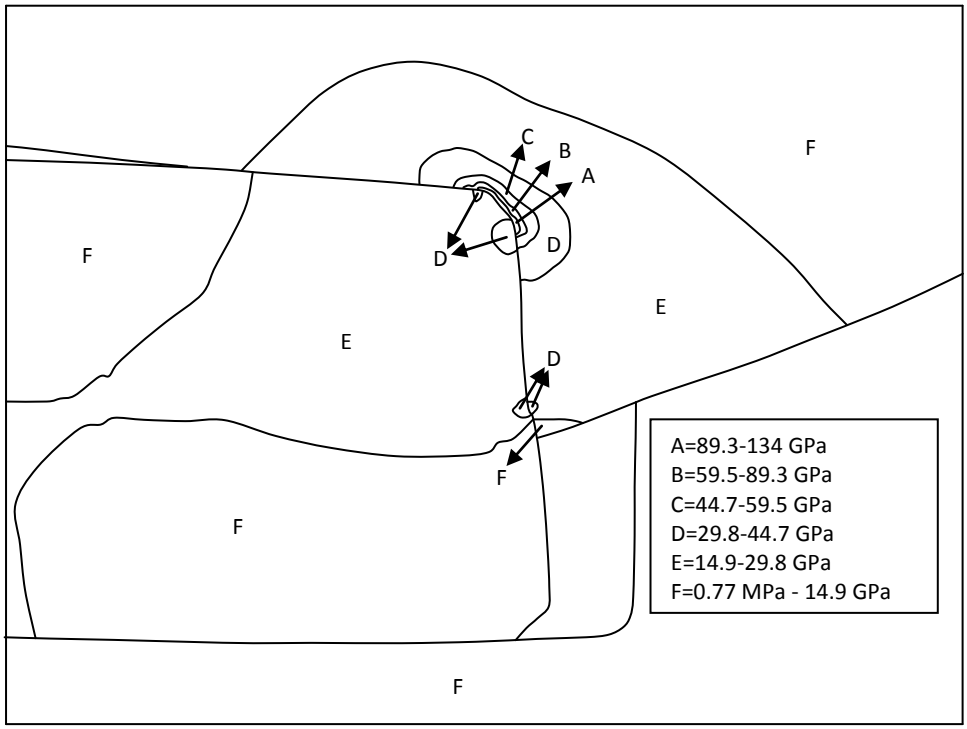

Figure 5.64. Stress contours at key and keyway corner (test no fa-5, T=0.55*Ty, fc=0.1)

When applying 0.55 of yield torque, stress contours of FEM can be seen is Figure 5.64. High stresses are obtained at keyway fillet of the shaft and have a stress range from 89.3 GPa to 134 GPa. Key edges have a stress range from 29.8 GPa to 44.7 GPa.

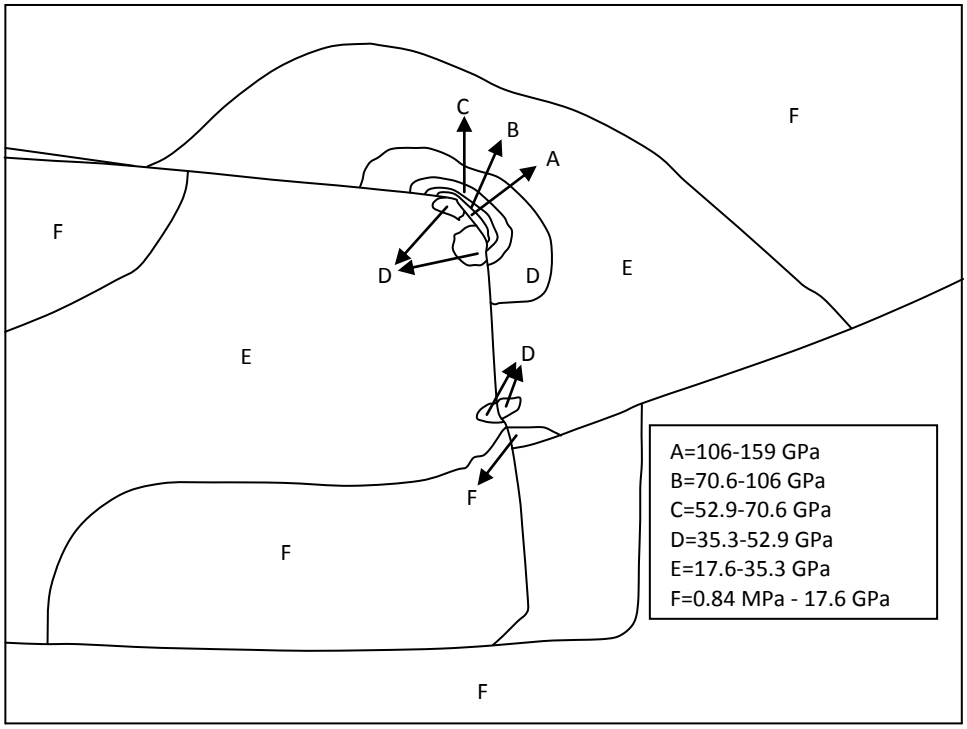

Figure 5.65. Stress contours at key and keyway corner (test no fa-5, T=0.82*Ty, fc=0.1)

When increasing the torque to 0.82 of yield torque, stress contours become as given in Figure 5.65. The gap between key and hub keyway side is increasing. High stresses are obtained at the keyway fillet of the shaft and they have a stress range between 106 GPa and 159 GPa.

By further increasing the torque to 1.11 of yield torque, stress contours of FEM results become as shown in Figure 5.66. High stresses are obtained at the keyway fillet of the shaft and have a stress range from 139 GPa to 209 GPa.

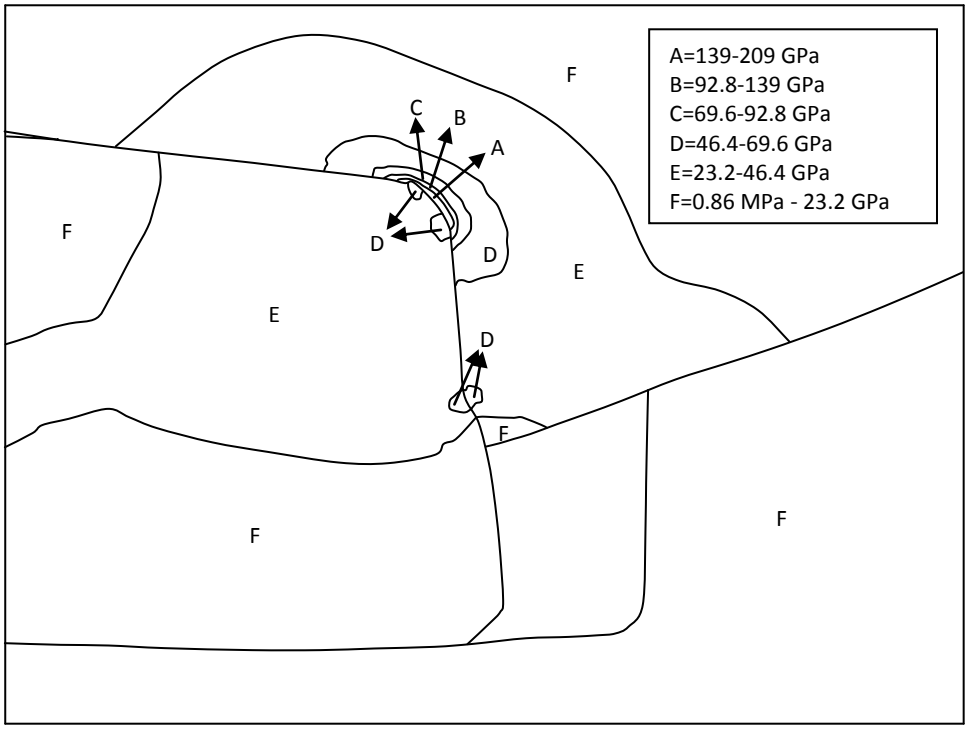

Figure 5.66. Stress contours at key and keyway corner (test no fa-5, T=1.11*Ty, fc=0.1)

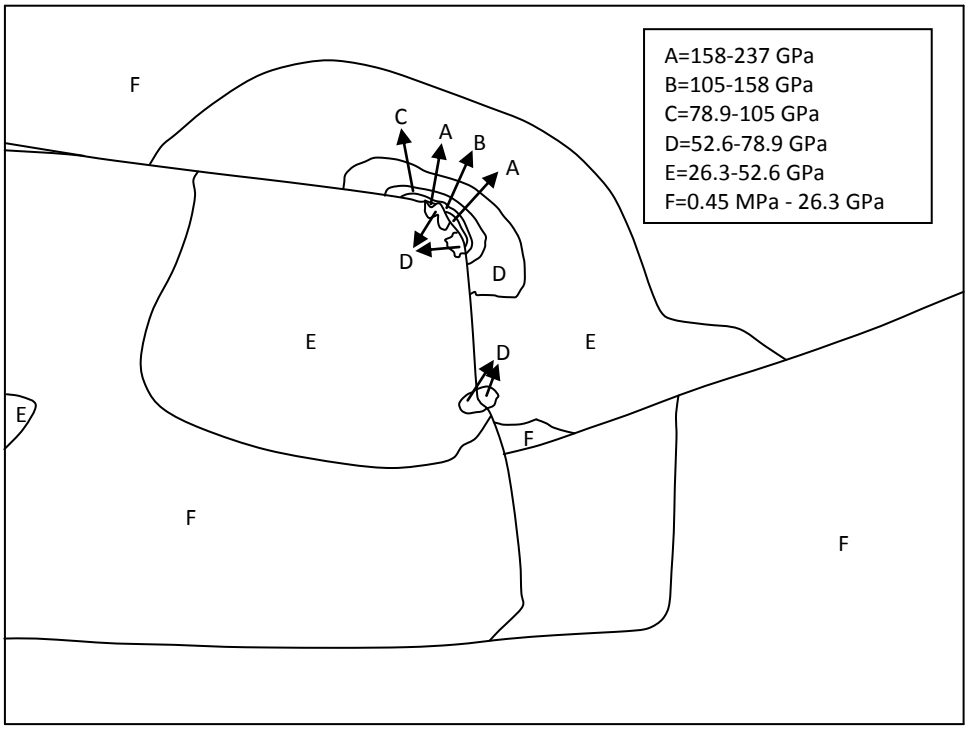

Figure 5.67. Stress contours at key and keyway corner (test no fa-5, T=1.35*Ty, fc=0.1)

Stress contours are shown in Figure 5.67 when applying 1.35 of yield torque. The slip of key and shaft is increasing. High stresses are obtained at the keyway fillet of the shaft. They have a stress range between 158 GPa and 237 GPa.

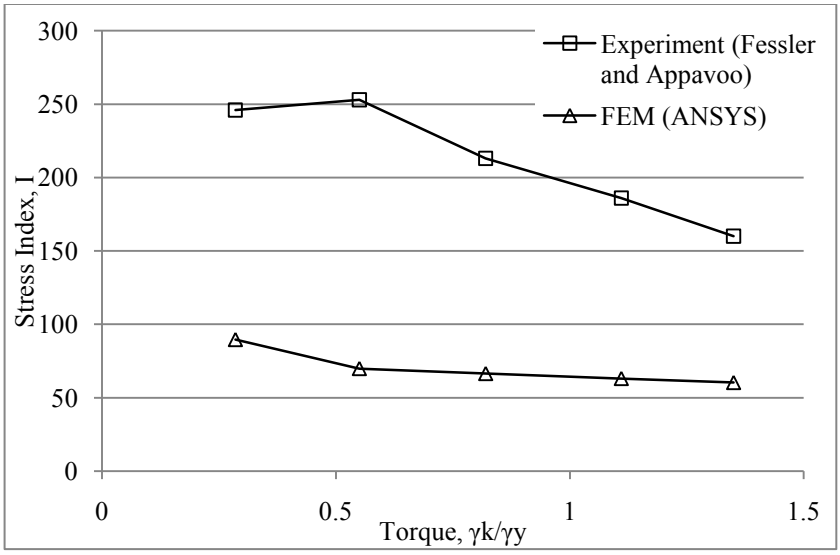

Figure 5.68. Variations of stress index, I, at the point Sb for different torques (test no fa-6, fc=0.1)

Stress indices of test no fa-6 are shown in Figure 5.68 for point Sb. FEM results are compared with the experimental results. When the torque is increased, stress indices of FEM decrease. Then FEM results become nearly not change or a little decreasing. However in experimental results, stress indices are firstly increasing then decreasing when increasing the torque. Key edge have dimensions of w=3 mm and h=3 mm. The gap is the biggest gap between in all keyed connection models in Table 3.1. Hence any slip of key causes to change the key edge which generally causes to obtain high stresses or peak stresses.

Stress contours are given in Figure 5.69 for test no fa-6 when applying 0.285 of yield torque. It is seen that a wide range of stresses are obtained at the keyway of shaft and key edges. High stresses are obtained at the keyway of shaft and key edges which have a stress range between 34.9 GPa and 52.3 GPa.

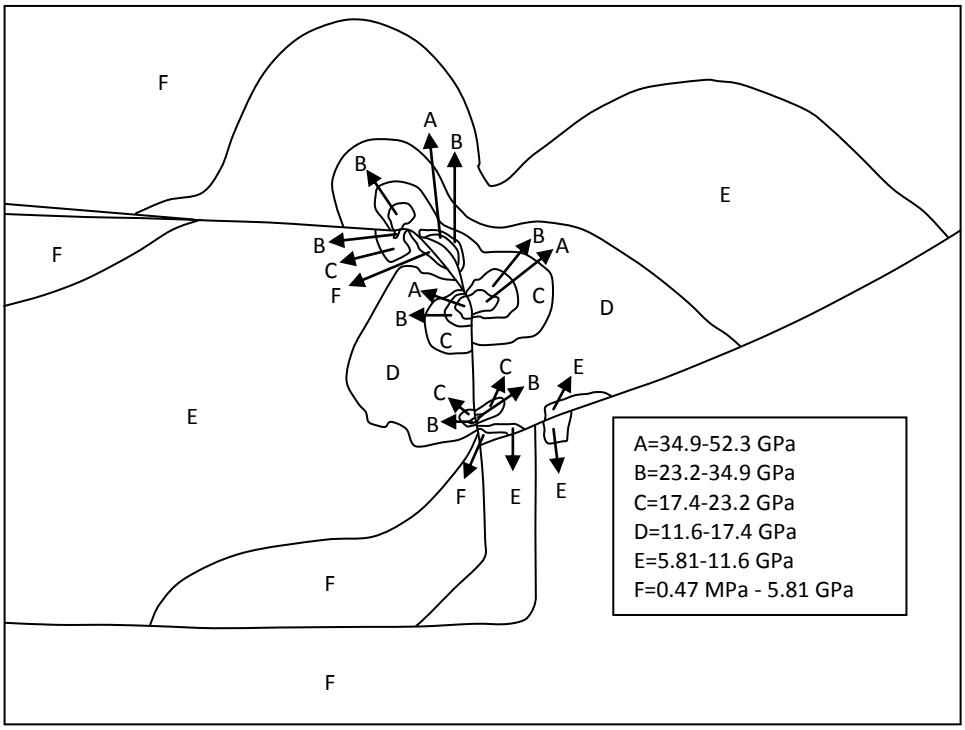

Figure 5.69. Stress contours at key and keyway corner (test no fa-6, T=0.285*Ty, fc=0.1)

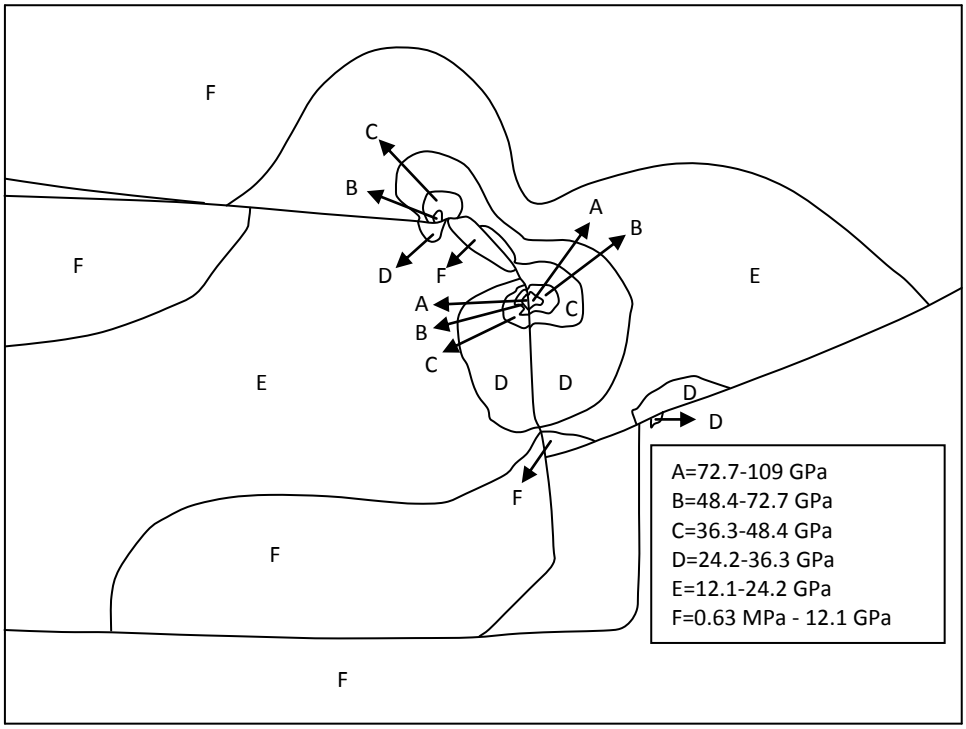

Figure 5.70. Stress contours at key and keyway corner (test no fa-6, T=0.55*Ty, fc=0.1)

Stress contours are shown in Figure 5.70 when applying 0.55 of yield torque. High stresses are obtained at one of the key edge and keyway of the shaft. They have a stress range between 72.7 GPa and 109 GPa.

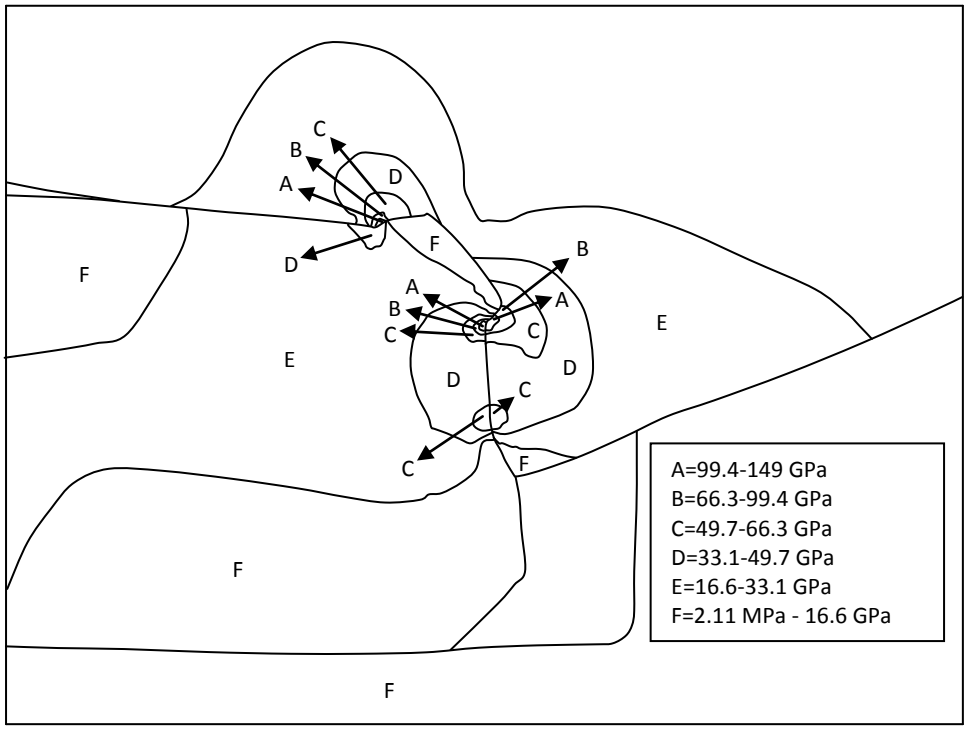

Figure 5.71. Stress contours at key and keyway corner (test no fa-6, T=0.82*Ty, fc=0.1)

Stress contours are given in Figure 5.71 when increasing the torque to 0.82 of yield torque. High stresses are obtained at the keyway of the shaft and one of the key edges. They have a stress range from 99.4 GPa to 149 GPa.

When applying 1.11 of yield torque, stresses are increasing and they can be seen in Figure 5.72. One of the key edge and keyway fillet of the shaft have high stresses. High stresses have a stress range between 108 GPa and 162 GPa.

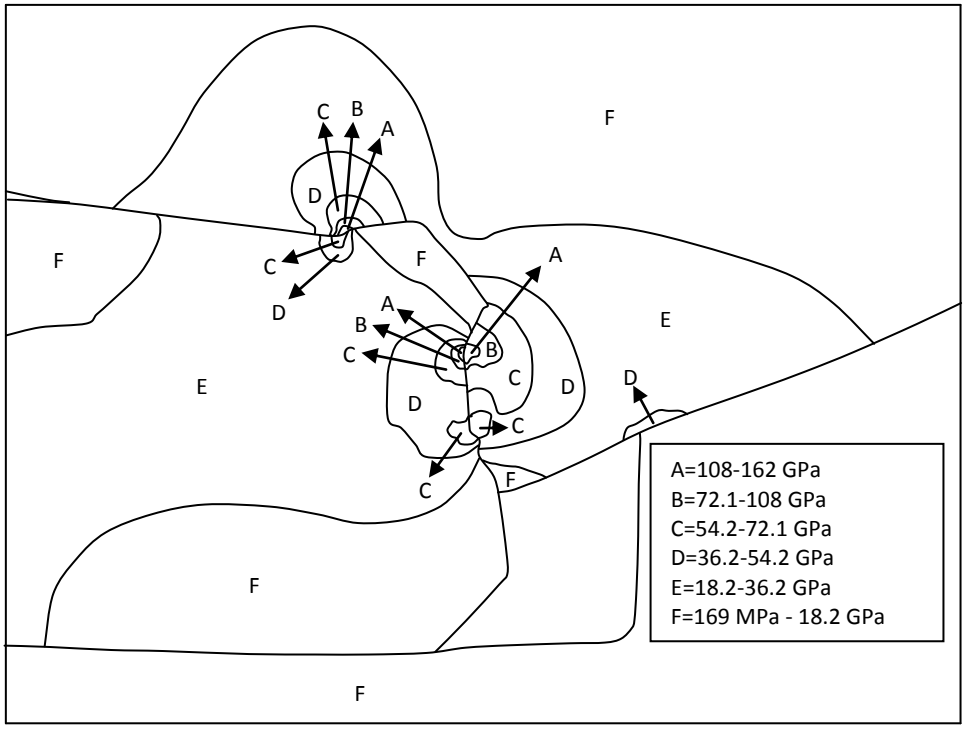

Figure 5.72. Stress contours at key and keyway corner (test no fa-6, T=1.11*Ty, fc=0.1)

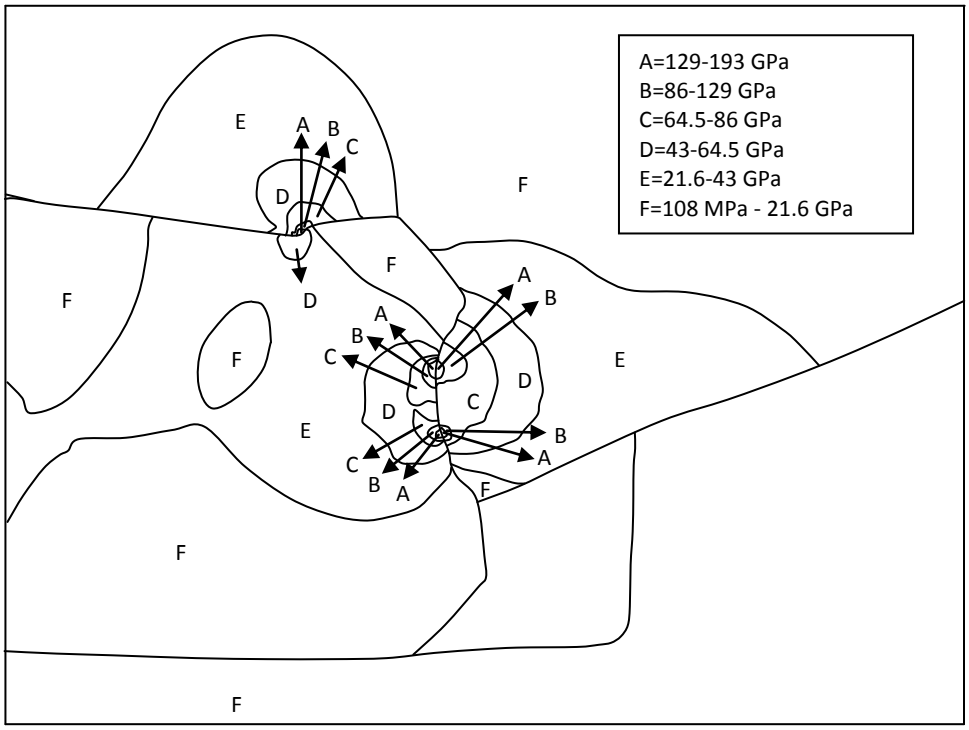

Figure 5.73. Stress contours at key and keyway corner (test no fa-6, T=1.35*Ty, fc=0.1)

Stress contours can be seen in Figure 5.73 when applying 1.35 of yield torque. It is seen that high stresses are obtained at the side of key and keyway of the shaft. They have a stress range from 129 GPa to 193 GPa.

5.5.6. Effect of sizes of chamfer at the point Ss with different torques

The effect of sizes of chamfer is investigated for the point Ss when applying different torques. The FEM results are compared with the experimental results.

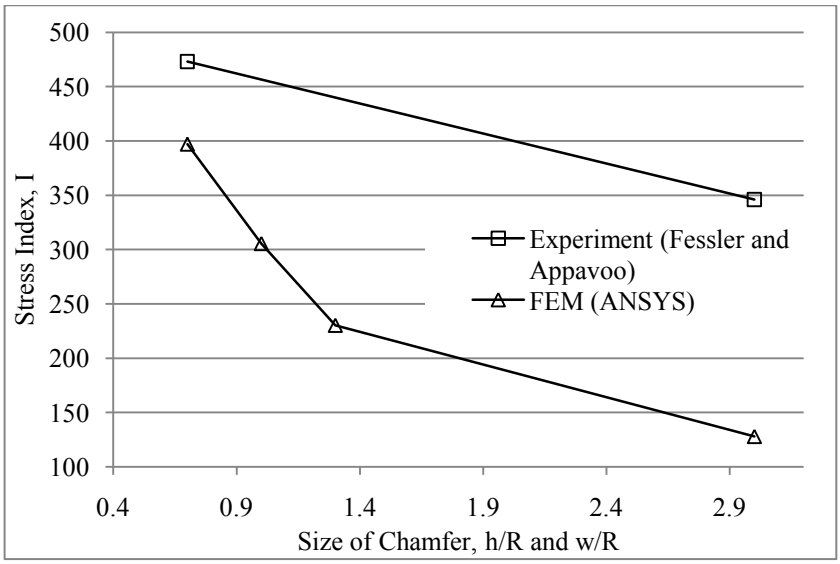

Figure 5.74. The effect of size of chamfer on stress at side of keyway for $\gamma_k/\gamma_y = 0.5$

The effect of size of chamfer can be seen for the point Ss in Figure 5.74 when applying 0.5 of yield torque. It is seen that stress indices are rapidly decreasing when increasing the size of the chamfer. Then the decrease of stress indices of FEM is similar to the experimental result. The smallest size of chamfer result is as near as the experimental result. The difference between FEM and experimental result may be caused from the slip of parts, especially the slip of the key.

Stress contours of test no fa-3 are given in Figure 5.75 when applying 0.5 yield torque. It is seen that high stresses are obtained at the keyway fillet of the shaft and have a stress range from 82.7 GPa to 124 GPa. The slip of the key can be seen.

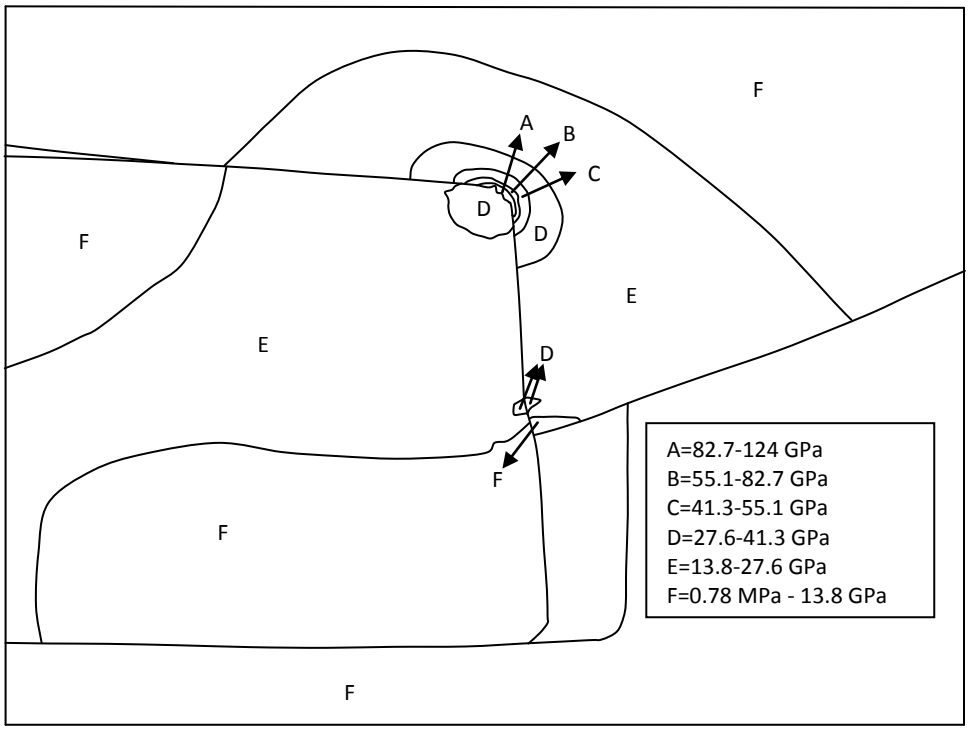

Figure 5.75. Stress contours at key and keyway corner (test no fa-3, T=0.5*Ty, fc=0.1)

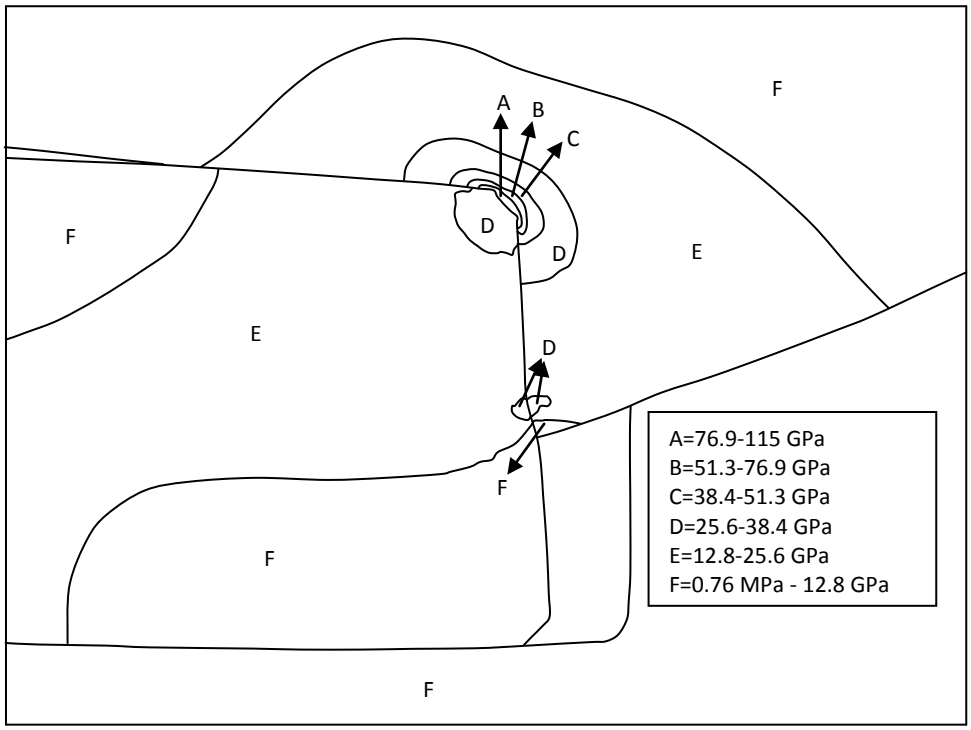

Figure 5.76. Stress contours at key and keyway corner (test no fa-4, T=0.5*Ty, fc=0.1)

Stress contours of test no fa-4 can be seen in Figure 5.76 when applying 0.5 of yield torque. High stresses are obtained at keyway fillet of shaft and have a stress range between 76.9 GPa and 115 GPa.

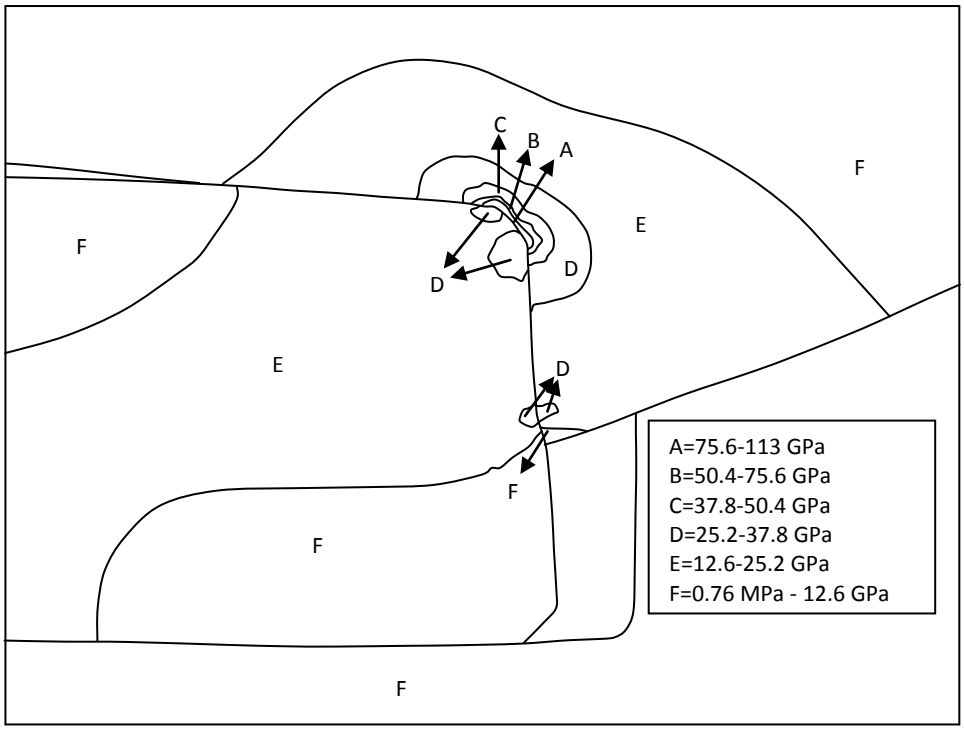

Figure 5.77. Stress contours at key and keyway corner (test no fa-5, T=0.5*Ty, fc=0.1)

Stress contours can be seen in Figure 5.77 for test no fa-5 when applying 0.5 of yield torque. High stresses are obtained at keyway fillet of the shaft and have a stress range between 75.6 GPa and 113 GPa.

Stress contours of test no fa-6 can be seen when applying 0.5 of yield torque. High stresses are obtained at one of the key edge and keyway of shaft. They have a stress range from 36 GPa to 54 GPa.

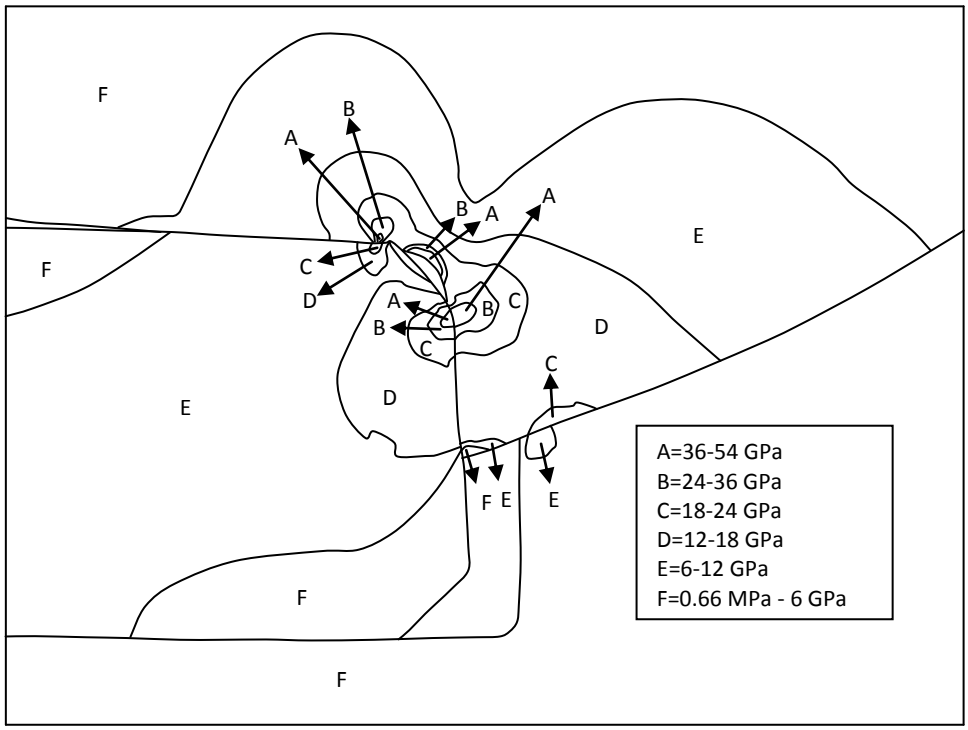

Figure 5.78. Stress contours at key and keyway corner (test no fa-6, T=0.5*Ty, fc=0.1)

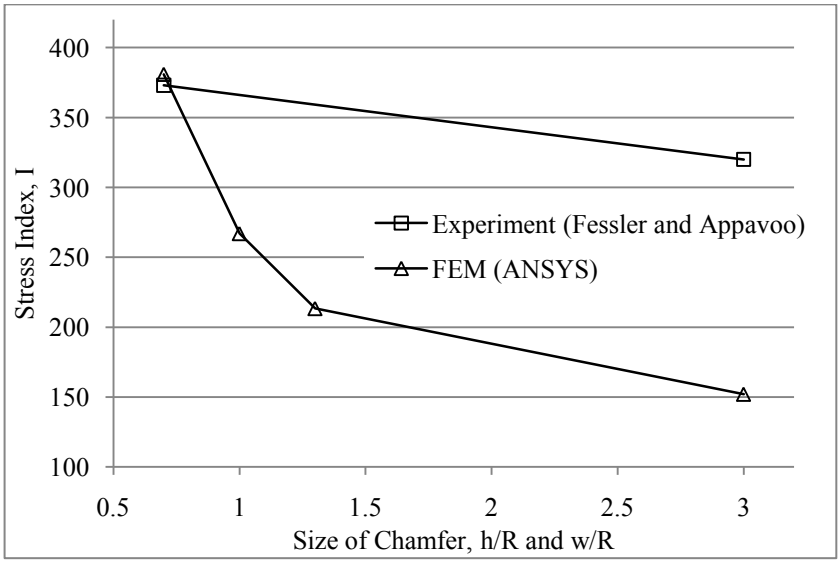

Figure 5.79. The effect of size of chamfer on stress at side of keyway for $\gamma_k/\gamma_y = 0.75$

The effect of size of chamfer can be seen for the point Ss in Figure 5.79 when applying 0.75 of yield torque. It seen that stress indices are same at the lowest size of chamfer. However when increasing the size of chamfer, FEM results are

decreasing rapidly. Then the change of FEM results is similar to the experimental result when the sizes of chamfers are between 1.3 mm and 3 mm.

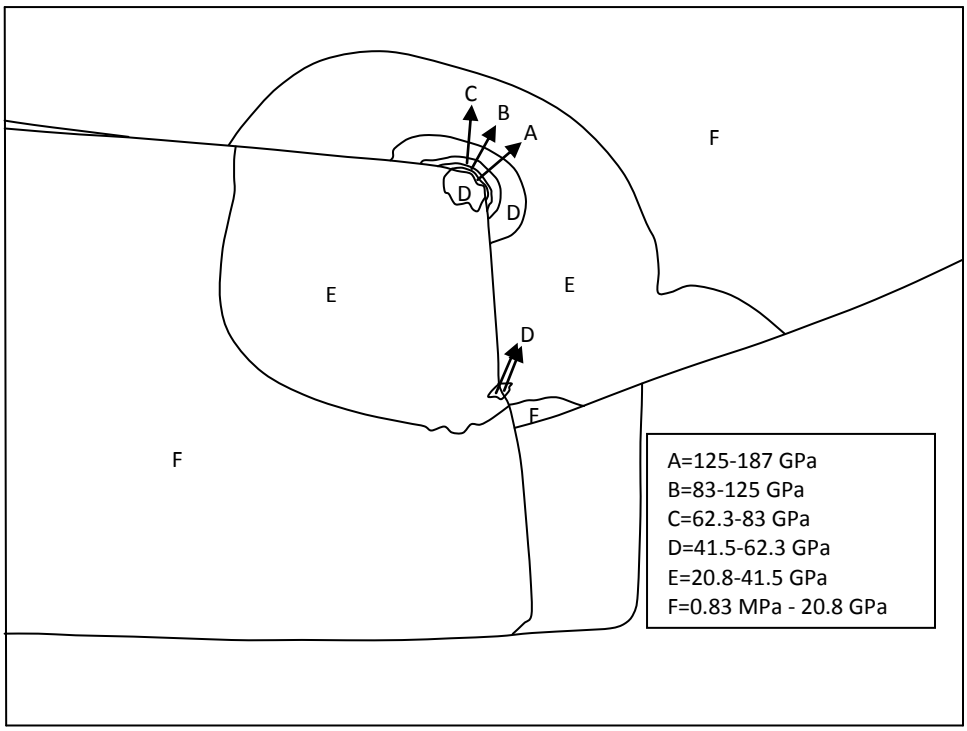

Figure 5.80. Stress contours at key and keyway corner (test no fa-3, T=0.75*Ty, fc=0.1)

Stress contours of test no fa-3 are given in Figure 5.80, when applying the 0.75 of yield torque. It is seen that the slip of key and shaft is increasing. High stresses are obtained at the fillet of the shaft and have a stress range between 125 GPa and 187 GPa.

Stress contours are given in Figure 5.81 for test no fa-4 when applying 0.75 of yield torque. High stresses are obtained at the keyway fillet of the shaft and have a stress range from 112 GPa to 168 GPa.

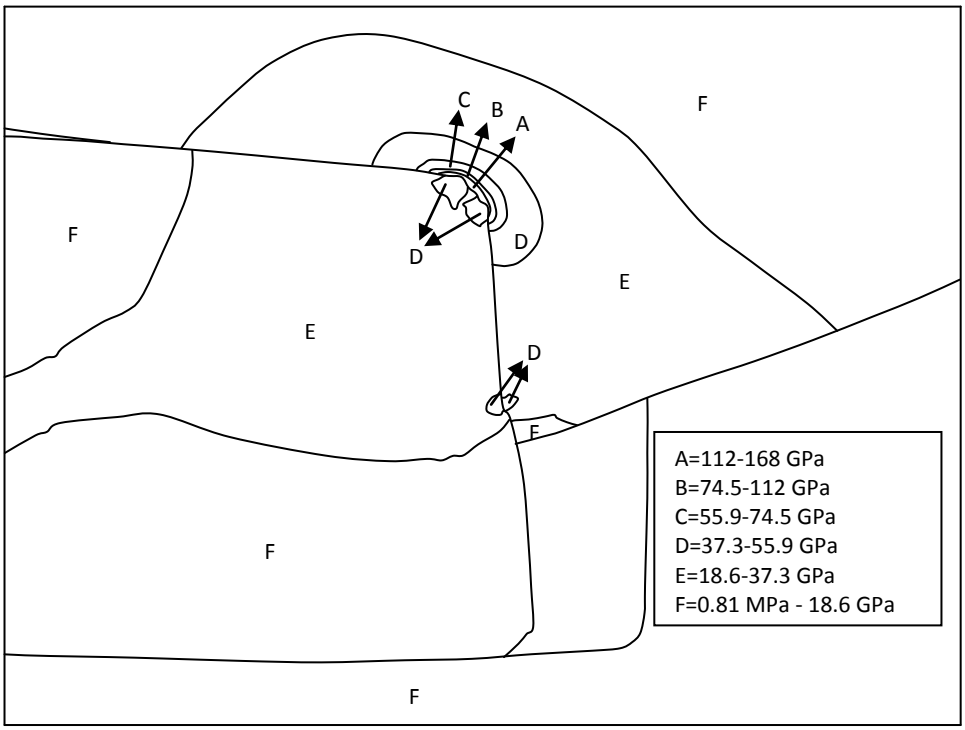

Figure 5.81. Stress contours at key and keyway corner (test no fa-4, T=0.75*Ty, fc=0.1)

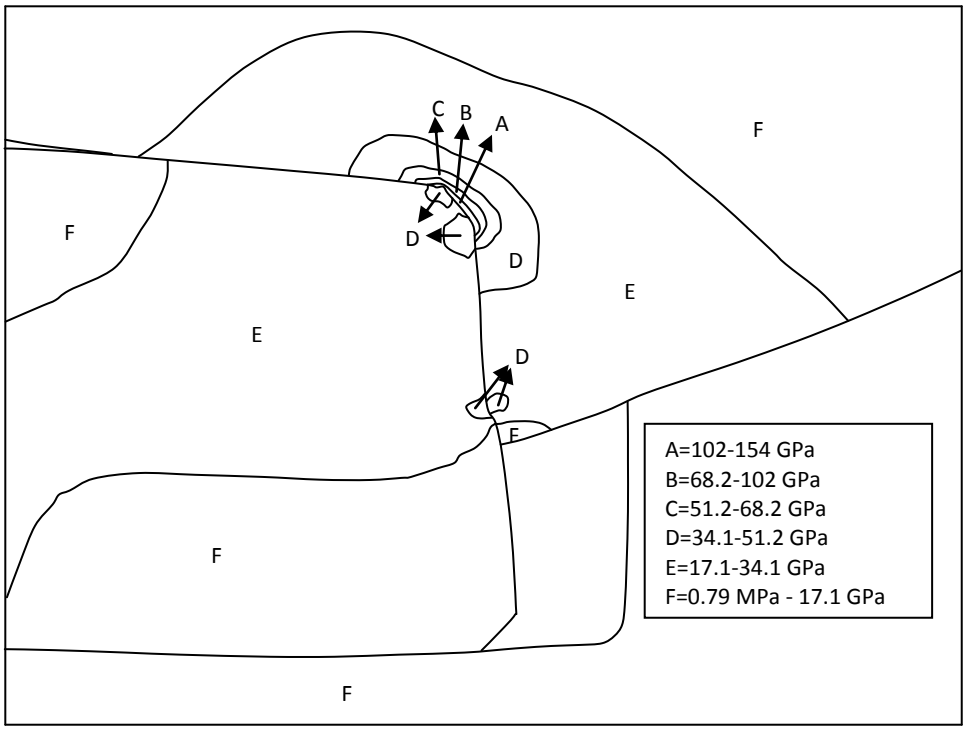

Figure 5.82. Stress contours at key and keyway corner (test no fa-5, T=0.75*Ty, fc=0.1)

Stress contours of test no fa-5 are given in Figure 5.82 when applying 0.75 of yield torque. High stresses are obtained at the keyway of the shaft which have a stress range from 102 GPa to 154 GPa.

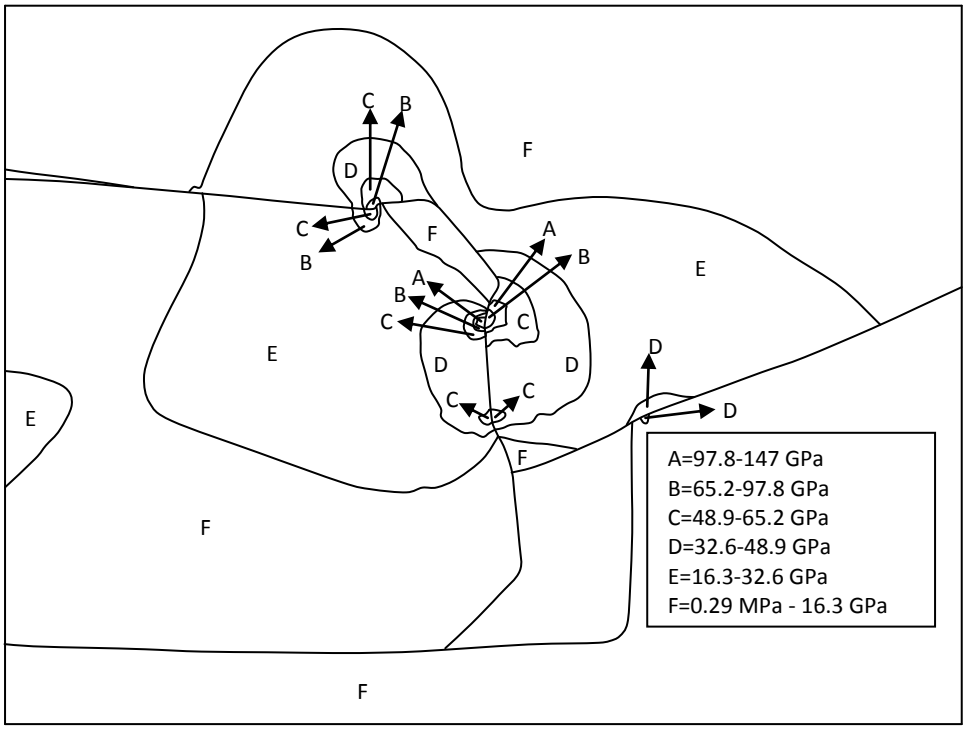

Figure 5.83. Stress contours at key and keyway corner (test no fa-6, T=0.75*Ty, fc=0.1)

Stress contours are given in Figure 5.83 for test no fa-6. High stresses have a stress range from 97.8 GPa to 147 GPa. They are obtained at one of the key edge and keyway of shaft.

The effect of size of chamfer is given for the point Ss in Figure 5.84 when applying yield torque. It is seen that FEM and experimental results are near at the small chamfer sizes of the key. When increasing the size of the chamfer, stress indices are decreasing rapidly in FEM results rather than experimental results. Low stress indices occur at big chamfer sizes. Stress contours of Figure 5.84 chamfer dimensional analyses are given in Figure 5.12, Figure 5.14, Figure 5.16 and Figure 5.18 when applying yield torque.

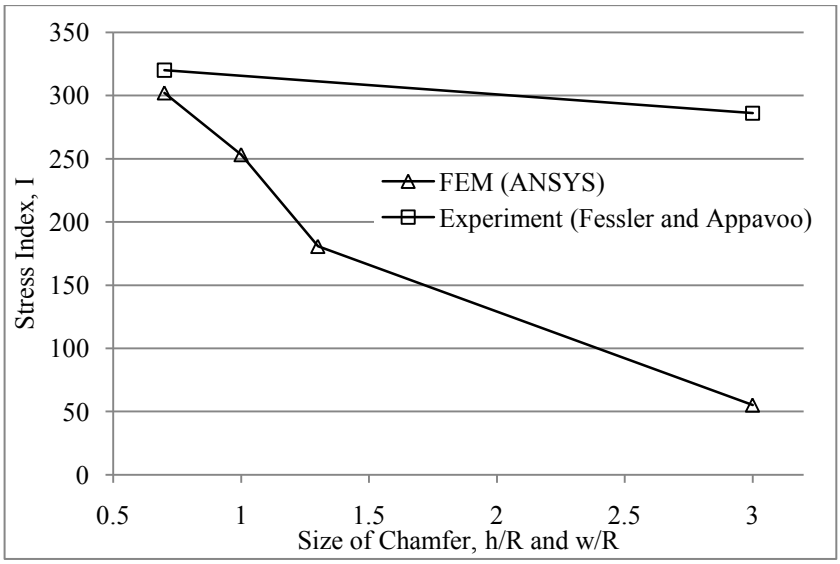

Figure 5.84. The effect of size of chamfer on stress at side of keyway for $\gamma_k/\gamma_y = 1$

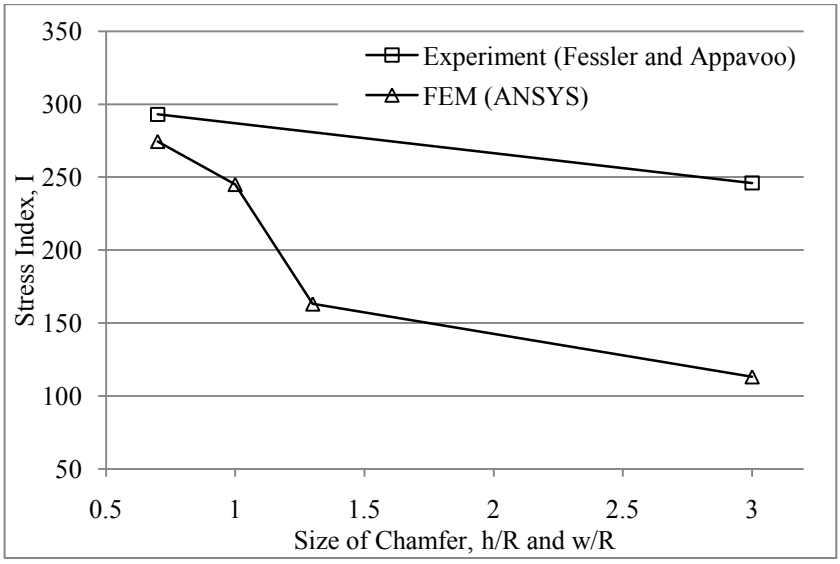

Figure 5.85. The effect of size of chamfer on stress at side of keyway for $\gamma_k/\gamma_y = 1.25$

The effect of size of chamfer can be seen for the point Ss in Figure 5.85 when applying 1.25 of yield torque. It can be seen that FEM and experimental results are near at the lowest size of chamfers. When increasing the size of chamfer, both FEM and experimental results are decreasing.

Stress contours of test no fe-3 are given in Figure 5.86 when applying 1.25 of yield torque. It is seen that high stresses are obtained at the keyway fillet of the shaft and have a stress range from 204 GPa to 307 GPa.

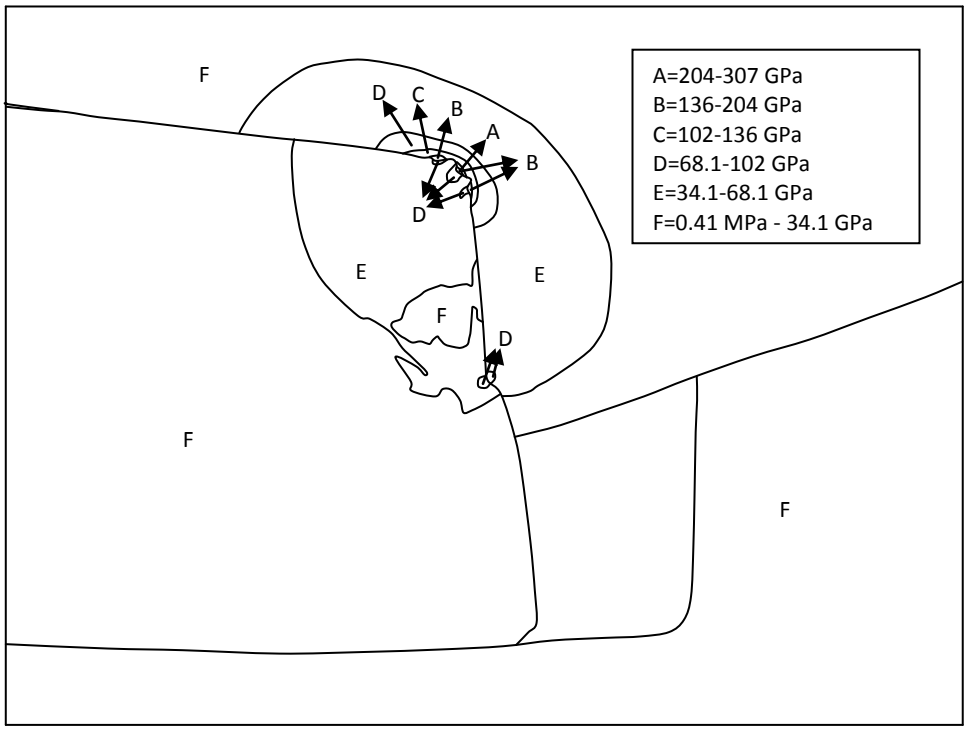

Figure 5.86. Stress contours at key and keyway corner (test no fa-3, T=1.25*Ty, fc=0.1)

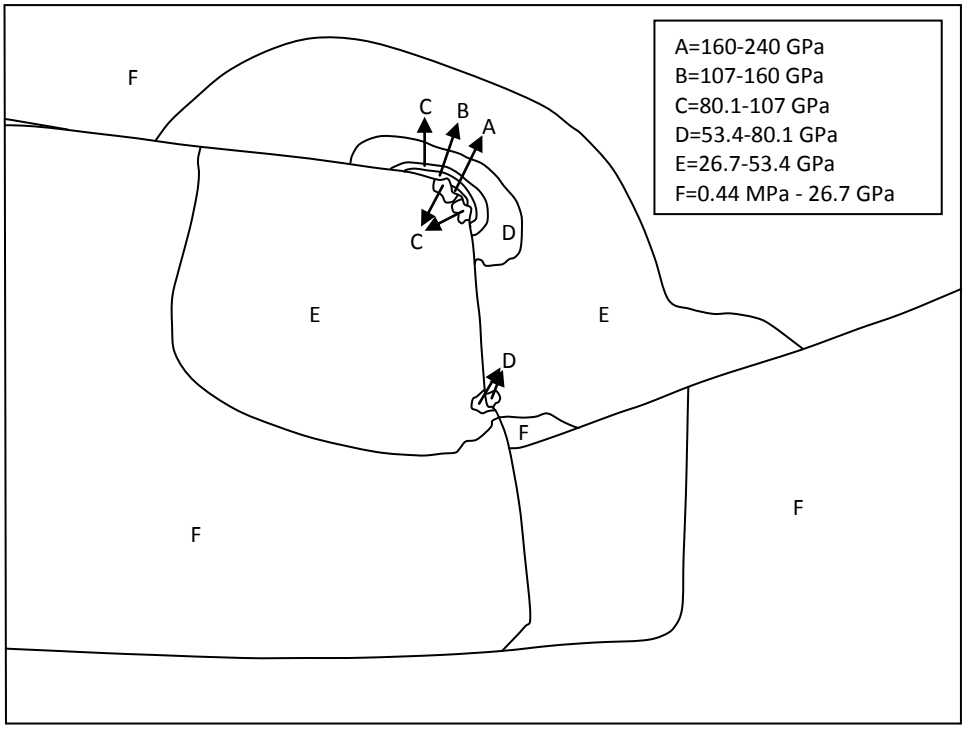

Figure 5.87. Stress contours at key and keyway corner (test no fa-4, T=1.25*Ty, fc=0.1)

When applying 1.25 of yield torque, stress contours of test no fa-4 become as given in Figure 5.87. High stresses are obtained at keyway fillet of the shaft and have a stress range between 160 GPa and 240 GPa.

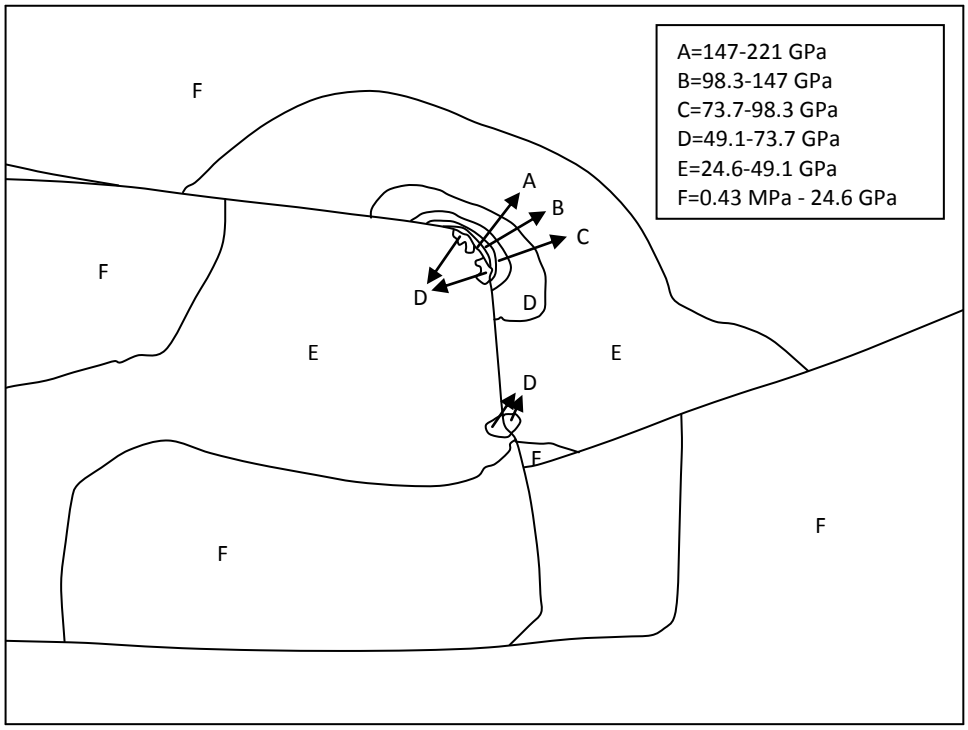

Figure 5.88. Stress contours at key and keyway corner (test no fa-5, T=1.25*Ty, fc=0.1)

Stress contours of test no fa-5 are shown in Figure 5.88 when applying 1.25 of yield torque. High stresses which have a stress range between 147 GPa and 221 GPa are obtained at keyway fillet of the shaft.

Stress contours of test no fe-6 are given in Figure 5.89 when applying 1.25 of yield torque. It is seen that high stresses are obtained at one of the key side and keyway of the shaft. They have a stress range from 122 GPa to 183 GPa.

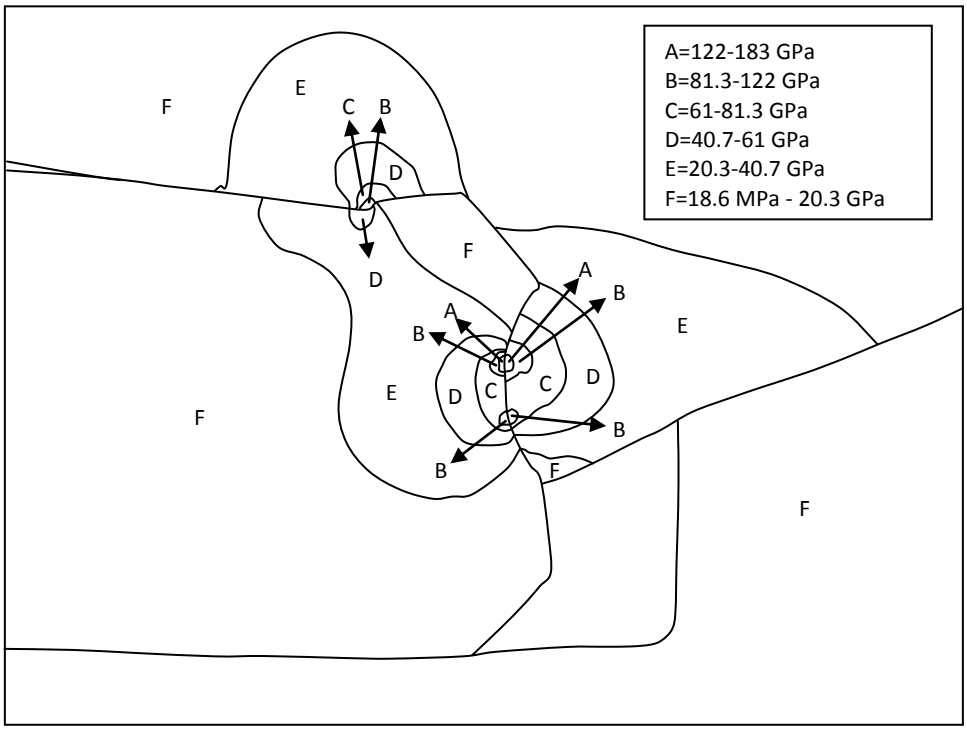

Figure 5.89. Stress contours at key and keyway corner (test no fa-6, T=1.25*Ty, fc=0.1)

5.5.7. Effect of sizes of chamfer at the point Sb with different torques

The effect of sizes of chamfer is investigated for point Sb with different torques. There is no experimental data for comparing with FEM results. But it is seen that general stress distribution values are decreasing when increasing the size of chamfer.

The effect of size of chamfer can be seen for point Sb in Figure 5.90 when applying 0.5 of yield torque. It is seen that stress indices are rapidly decreasing when starting to increase the chamfer size. Stress index of the smallest size chamfer result is nearly five times higher than the largest size chamfer result.

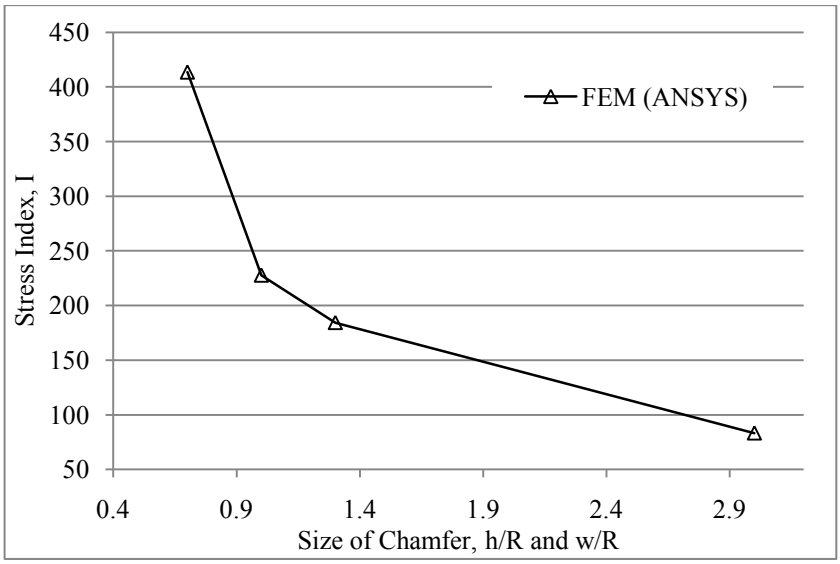

Figure 5.90. The effect of size of chamfer on stress at side of keyway, Sb, for $\gamma_k/\gamma_y = 0.5$

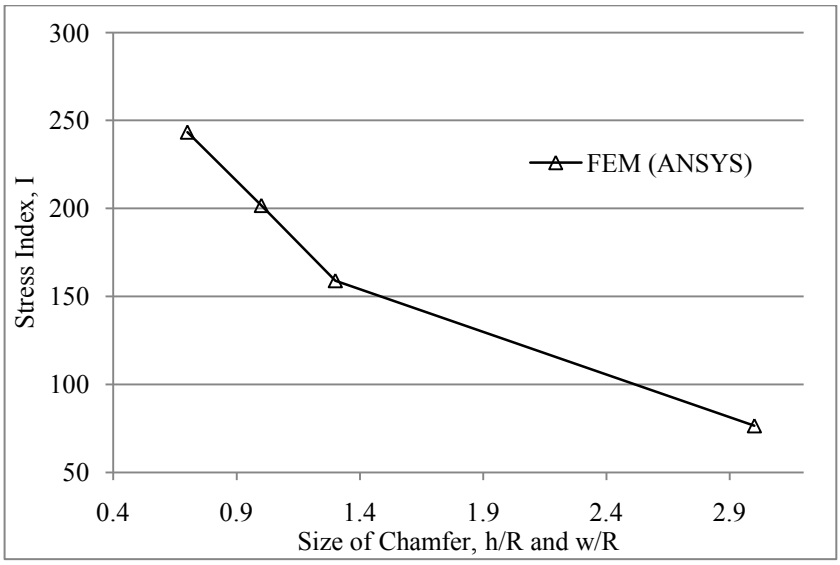

Figure 5.91. The effect of size of chamfer on stress at side of keyway, Sb, for $\gamma_k/\gamma_y = 0.75$

Stress indices can be seen in Figure 5.91, when 0.75 of yield torque is applied. Stress indices are decreasing when increasing the chamfer size of key edge.

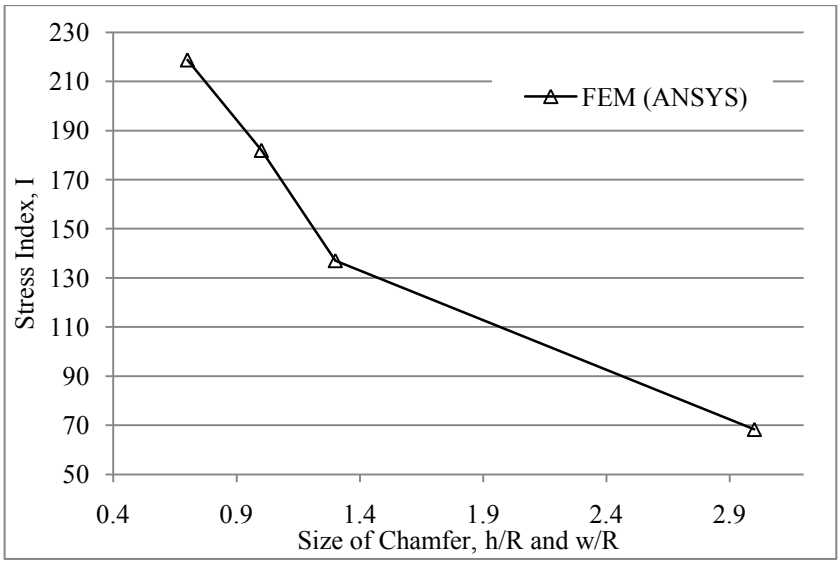

Figure 5.92. The effect of size of chamfer on stress at side of keyway, Sb, for $\gamma_k/\gamma_y = 1$

The effect of chamfer size can be seen in Figure 5.92 when applying yield torque. When increasing the size of chamfer, stress indices are decreasing at the point Sb.

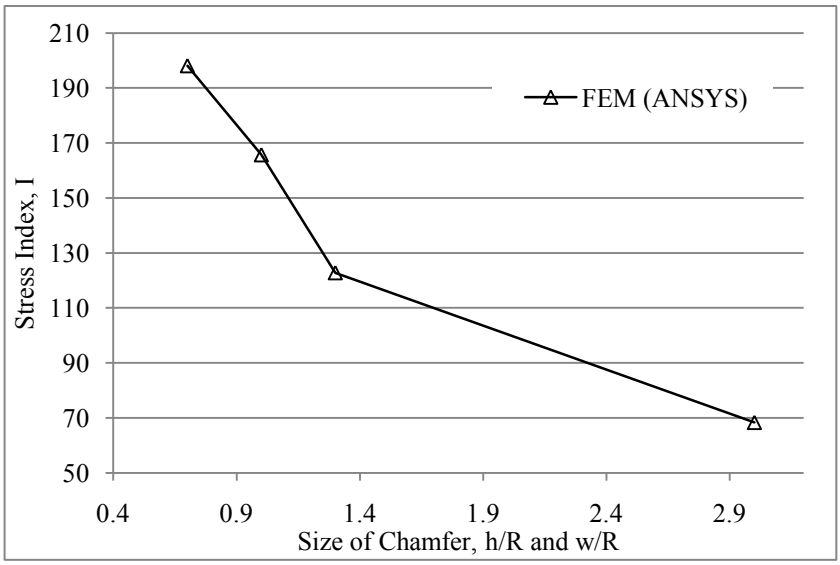

Figure 5.93. The effect of size of chamfer on stress at side of keyway, Sb, for $\gamma_k/\gamma_y = 1.25$

The effect of size of chamfer is given for point Sb in Figure 5.93 when applying 1.25 of yield torque. When increasing the size of chamfer, stress indices are decreasing.

It is seen that small size of chamfer geometries of key edges has higher stresses than big size chamfer key edges. Lowest stresses are obtained at chamfer size of h=3 mm and w=3 mm.

5.5.8. Effect of keyway edge radius at the point of Sr with different torques

The effect of keyway edge radius is investigated for point Sr with different torques. The FEM results are compared with experimental results.

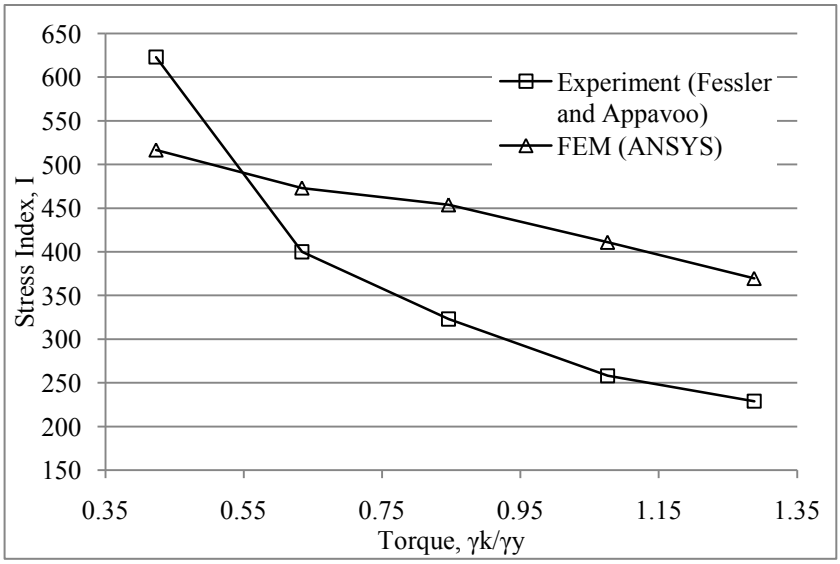

Figure 5.94. The effect of rounding key edge on stress at the centre point of keyway fillet for r/R =1

The effect of rounding key edge can be seen in Figure 5.94 for test no fa-7 and it is compared with the experimental result. When increasing the torque, stress indices of both FEM and experimental results are decreasing.

Stress contours of test no fa-7 can be seen in Figure 5.95 when applying 0.423 of yield torque. High stresses are obtained at the keyway fillet of the shaft and have a stress range from 81.7 GPa to 123 GPa.

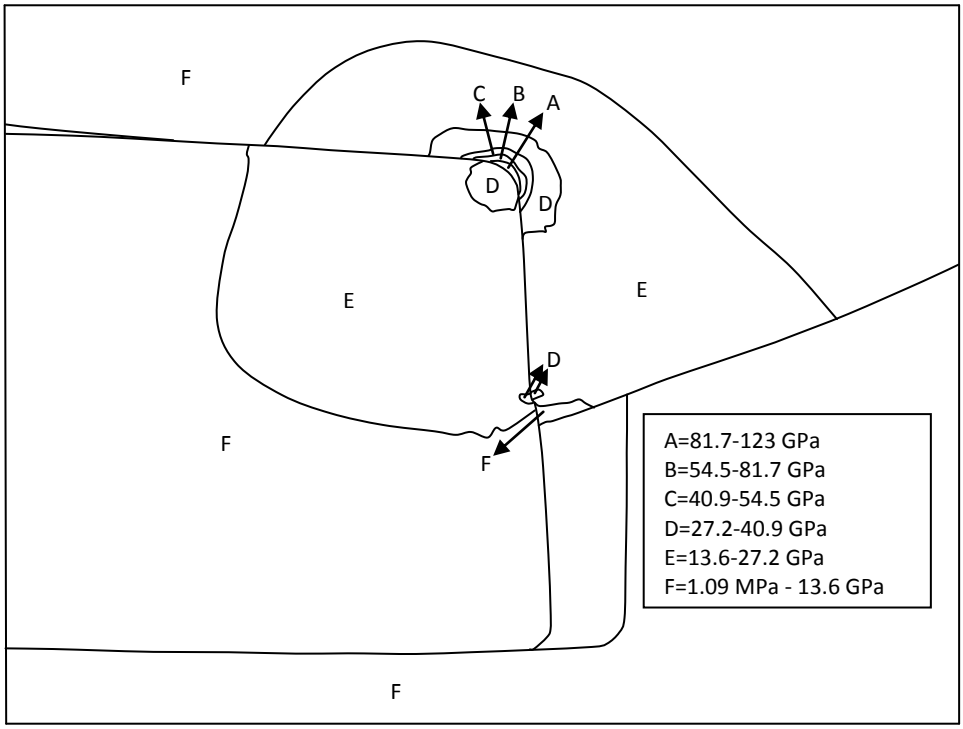

Figure 5.95. Stress contours at key and keyway corner (test no fa-7, T=0.423*Ty, fc=0.1)

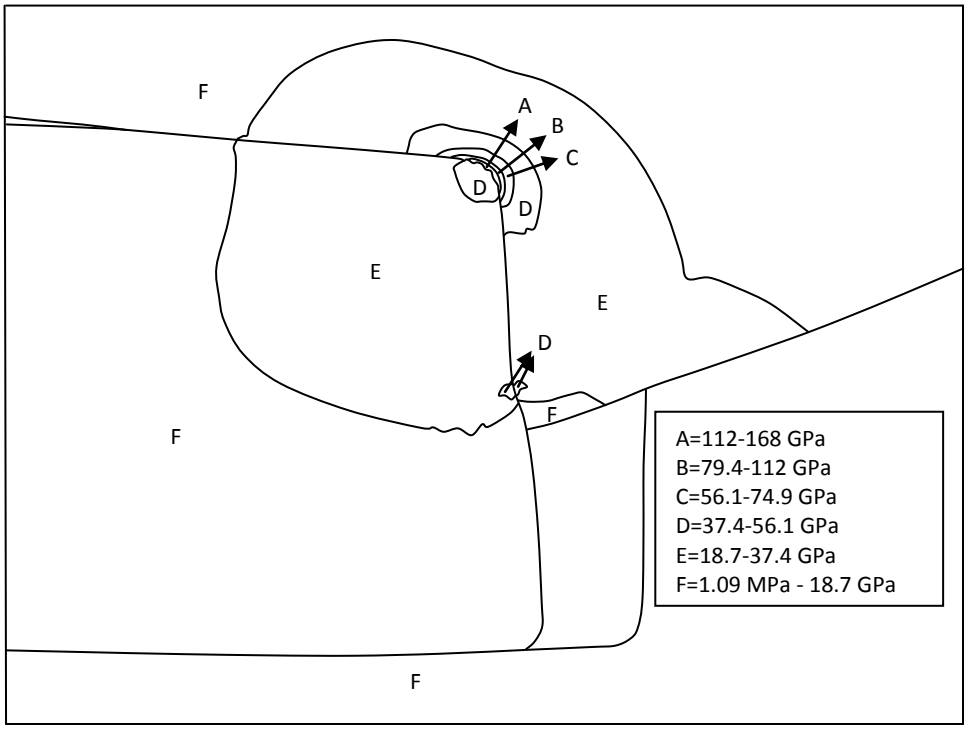

Figure 5.96. Stress contours at key and keyway corner (test no fa-7, T=0.634*Ty, fc=0.1)

When increasing the torque to 0.634 of yield torque, stresses are increasing and they can be seen in Figure 5.96. It is seen that high stresses are obtained at the keyway fillet of the shaft and have a stress range between 112 GPa and 168 GPa.

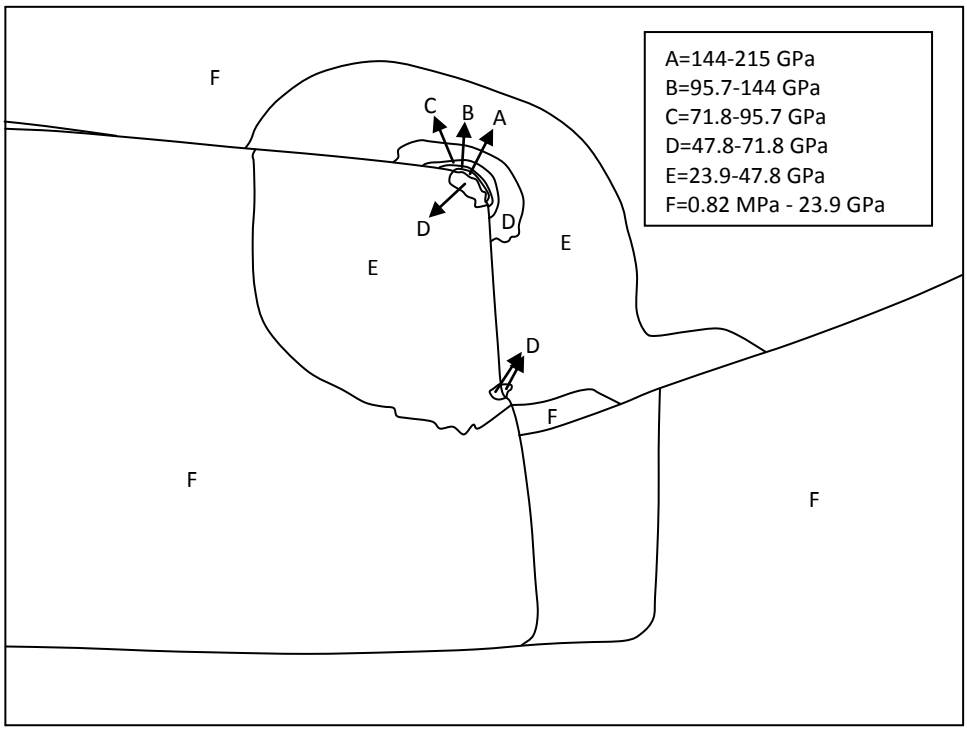

Figure 5.97. Stress contours at key and keyway corner (test no fa-7, T=0.846*Ty, fc=0.1)

Further increasing the torque to 0.846 of yield torque, stress contours become as given in Figure 5.97. High stresses are obtained at the keyway fillet of the shaft and have a stress range between 144 GPa and 215 GPa.

When applying 1.076 of yield torque, stresses are increasing and can be seen in Figure 5.98. High stresses have a stress range from 170 GPa to 255 GPa and they are obtained at the keyway fillet of the shaft.

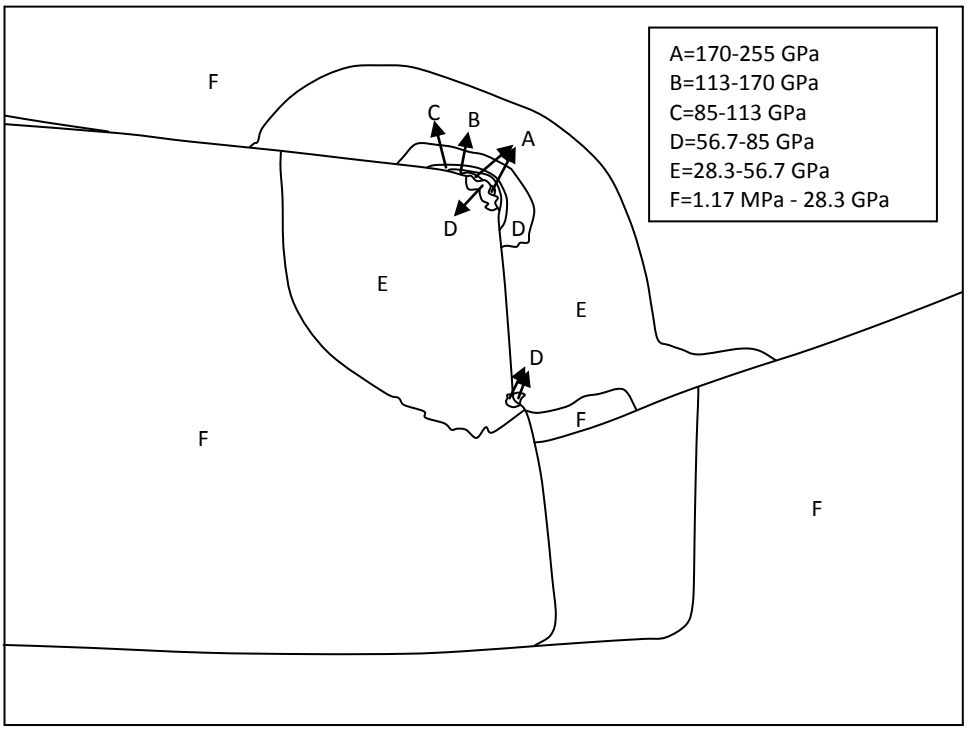

Figure 5.98. Stress contours at key and keyway corner (test no fa-7, T=1.076*Ty, fc=0.1)

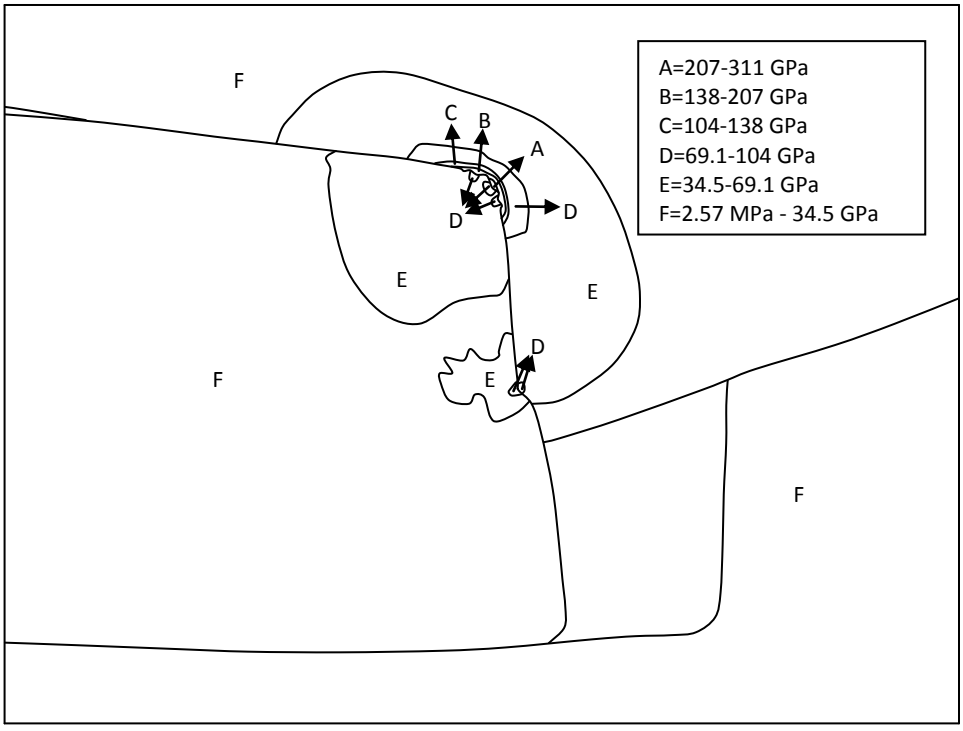

Figure 5.99. Stress contours at key and keyway corner (test no fa-7, T=1.288*Ty, fc=0.1)

Stress contours of test no fa-7 can be seen in Figure 5.99 when applying 1.288 of yield torque. High stresses are obtained at the keyway fillet of the shaft and have a stress range between 207 GPa and 311 GPa.

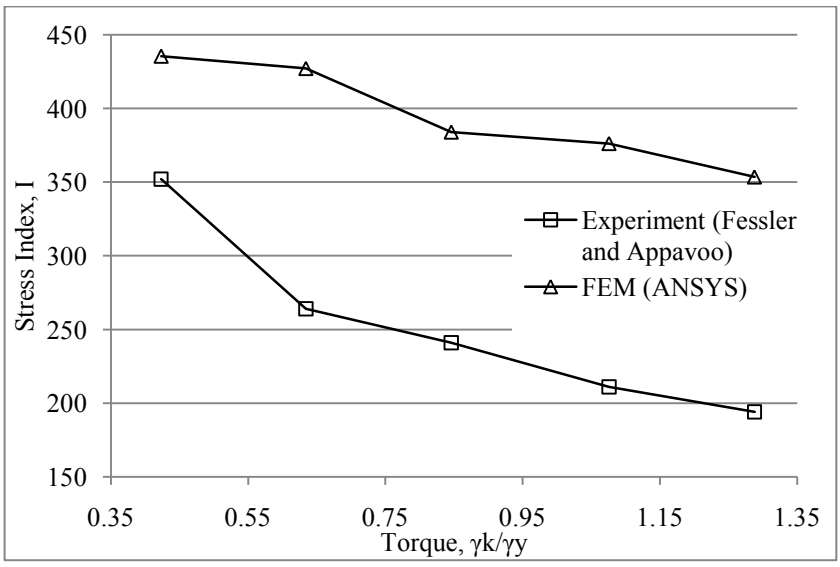

Figure 5.100. The effect of rounding key edge on stress at the centre point of keyway fillet for r/R =1.3

The effect of rounding the key edge can be seen for test no fa-8 in Figure 5.100. FEM results are higher than the experimental results. Both of FEM and experimental results are decreasing when increasing the torque.

Stress contours of FEM results have a wide stresses at the keyway fillet of the shaft and can be seen in Figure 5.101 when applying 0.423 of yield torque. High stresses are obtained at the keyway fillet of the shaft and have a stress range from 68.9 GPa to 103 GPa.

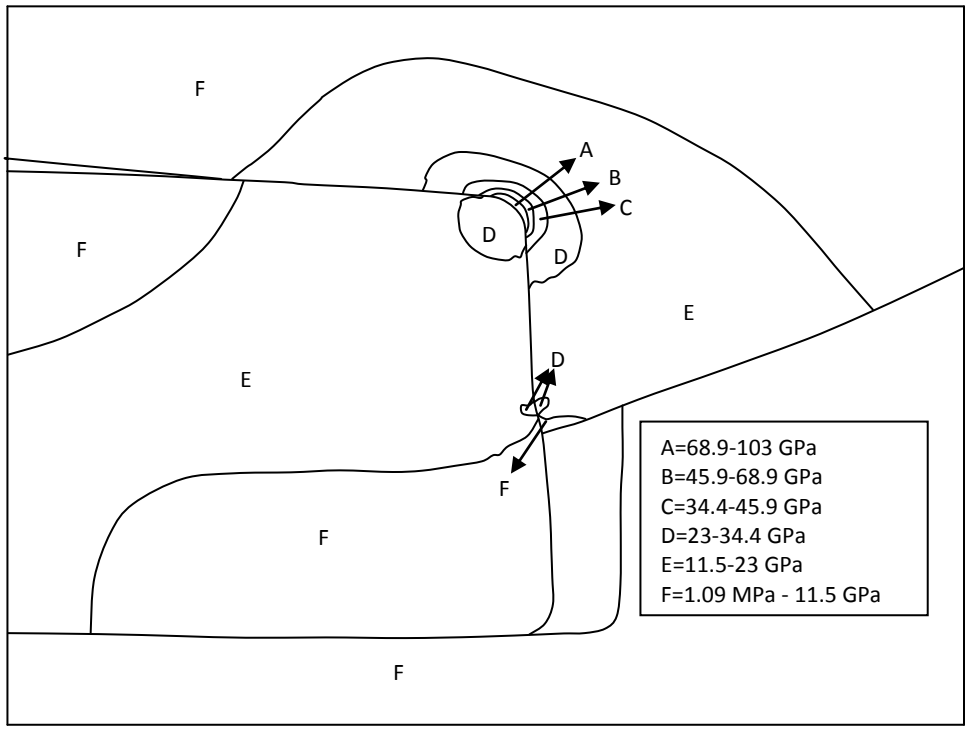

Figure 5.101. Stress contours at key and keyway corner (test no fa-8, T=0.423*Ty, fc=0.1)

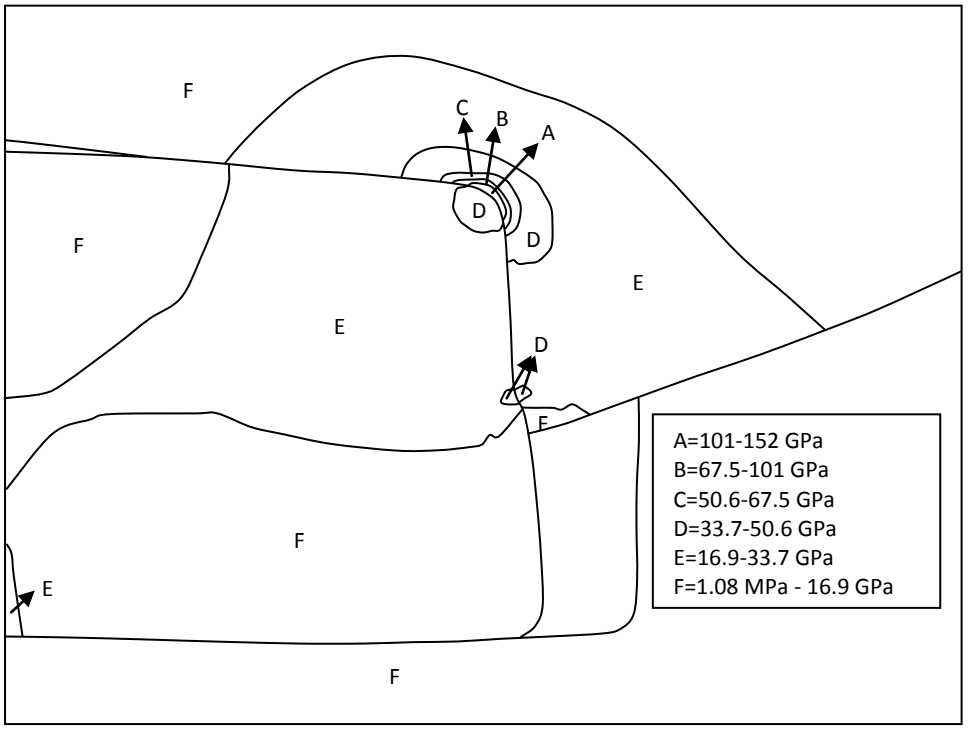

Figure 5.102. Stress contours at key and keyway corner (test no fa-8, T=0.634*Ty, fc=0.1)

When applying 0.634 of yield torque, stress contours become as given in Figure 5.102. Stresses are increasing. High stresses are obtained at the keyway fillet of the shaft. They have a stress range between 101 GPa and 152 GPa.

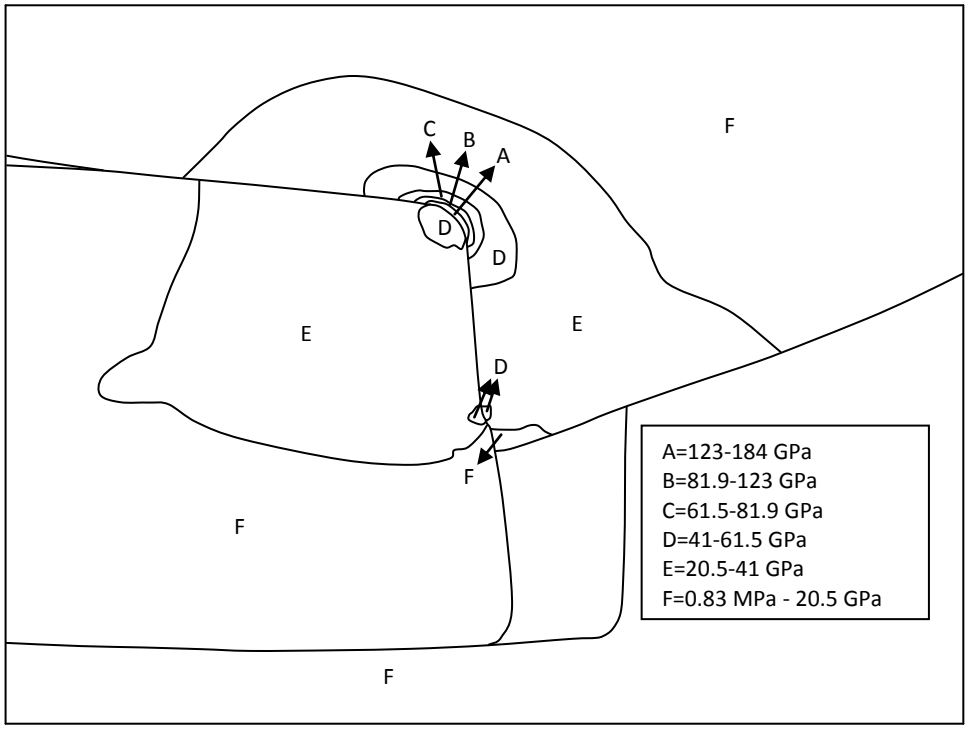

Figure 5.103. Stress contours at key and keyway corner (test no fa-8, T=0.846*Ty, fc=0.1)

Further increasing the torque to 0.846 of yield torque, stress contours become as given in Figure 5.103. High stresses are obtained at the keyway fillet of the shaft and have a stress range from 123 GPa to 184 GPa.

Stresses are increasing and can be seen in Figure 5.104 when applying 1.076 of yield torque. High stresses have a stress range from 151 GPa to 227 GPa and they are obtained at the keyway fillet of the shaft.

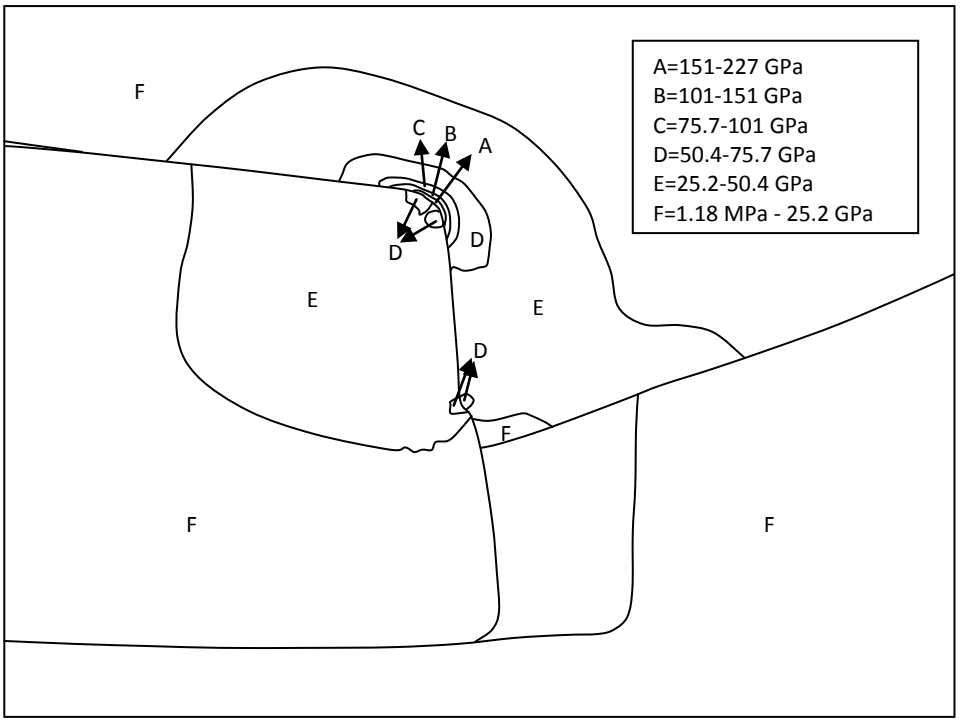

Figure 5.104. Stress contours at key and keyway corner (test no fa-8, T=1.076*Ty, fc=0.1)

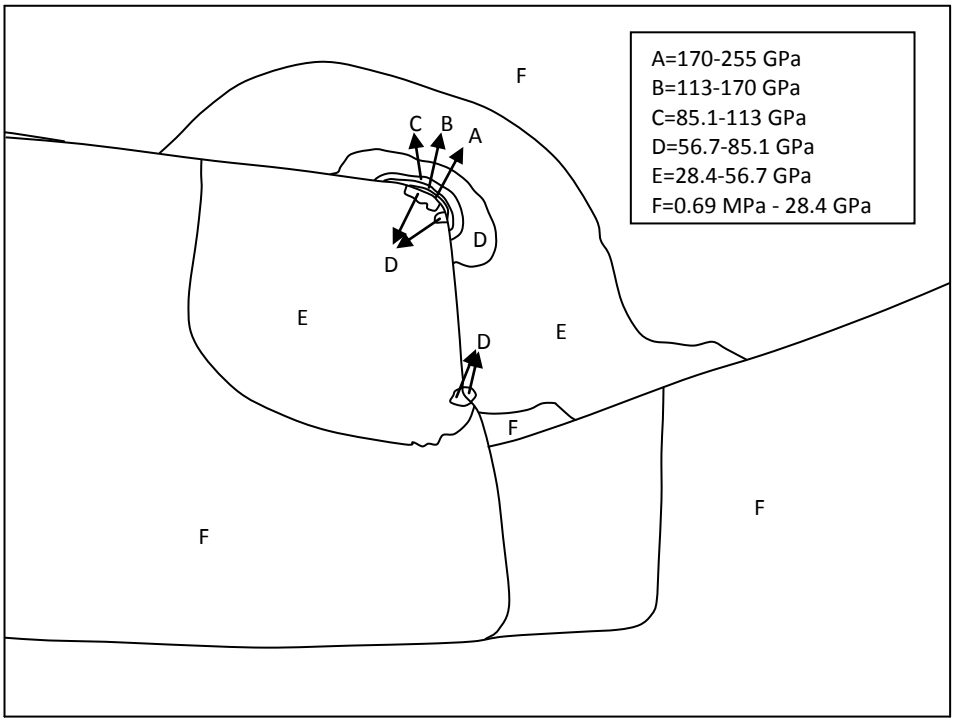

Figure 5.105. Stress contours at key and keyway corner (test no fa-8, T=1.288*Ty, fc=0.1)

Stress contours of test no fa-8 are given in Figure 5.105 when 1.288 of yield torque. High stresses are obtained at the keyway fillet of the shaft and have a stress range from 170 GPa to 255 GPa.

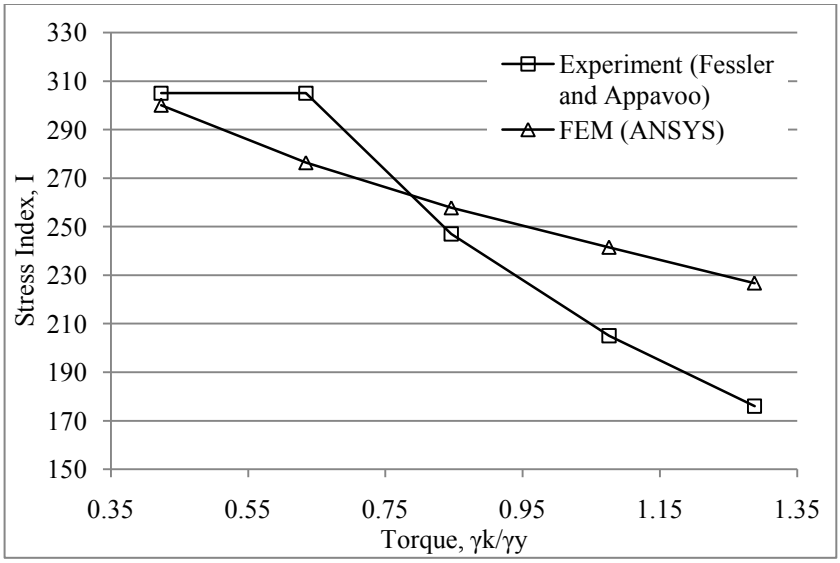

Figure 5.106. The effect of rounding key edge on stress at the centre point of keyway fillet for r/R =3

The effect of rounding key edge can be seen in Figure 5.106 for test no fa-9 when applying different torques. When increasing the torque, stress indices of FEM results are decreasing. But experimental study results are initially nearly constant then decreasing when increasing the torque.

When applying 0.423 of yield torque to test no fa-9, stress contours become as given in Figure 5.107. High stresses are obtained at the keyway fillet of the shaft and have stress range between 47.4 GPa and 71.2 GPa.

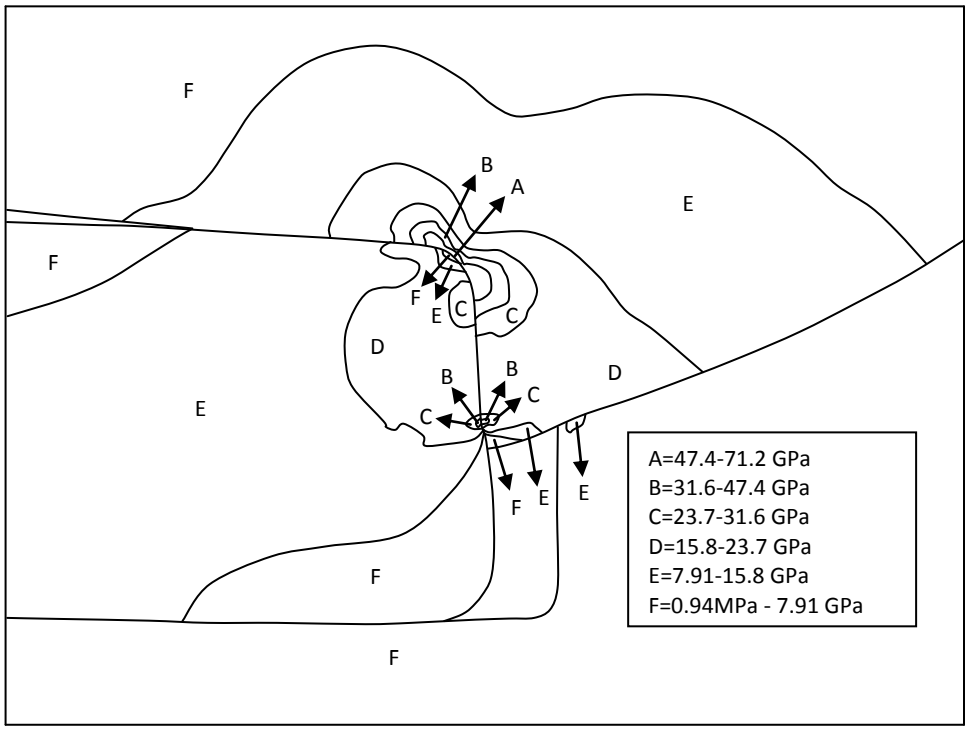

Figure 5.107. Stress contours at key and keyway corner (test no fa-9, T=0.423*Ty, fc=0.1)

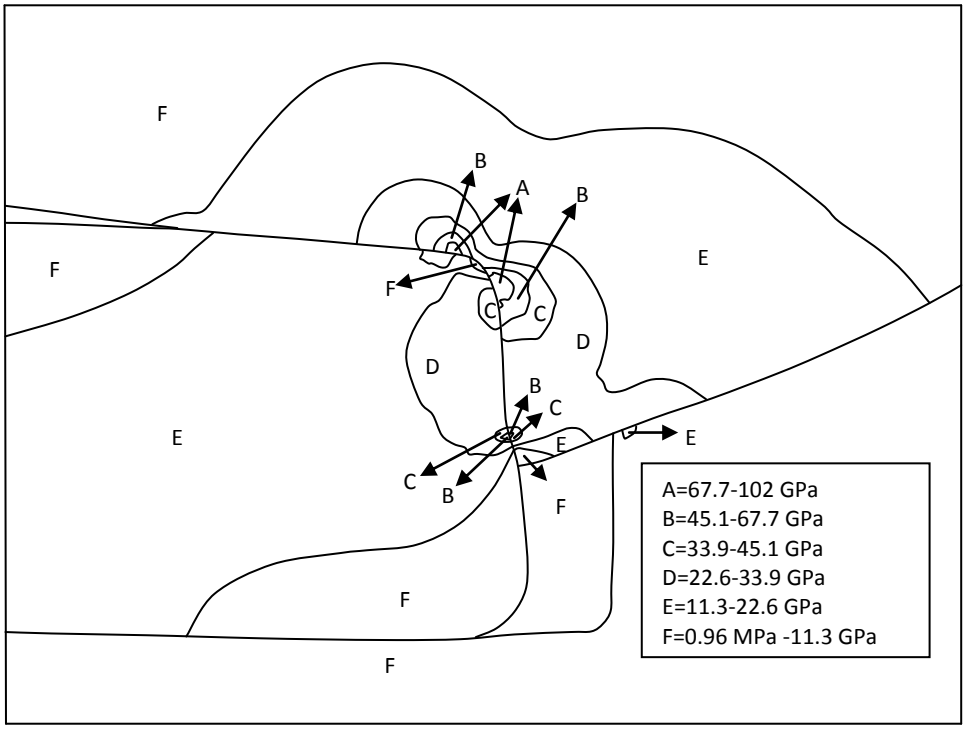

Figure 5.108. Stress contours at key and keyway corner (test no fa-9, T=0.634*Ty, fc=0.1)

Stress contours of test no fa-9 can be seen in Figure 5.108, when increasing the torque to 0.634 of yield torque. Keyway stresses of shaft have the highest stresses and have a stress range between 67.7 GPa and 102 GPa.

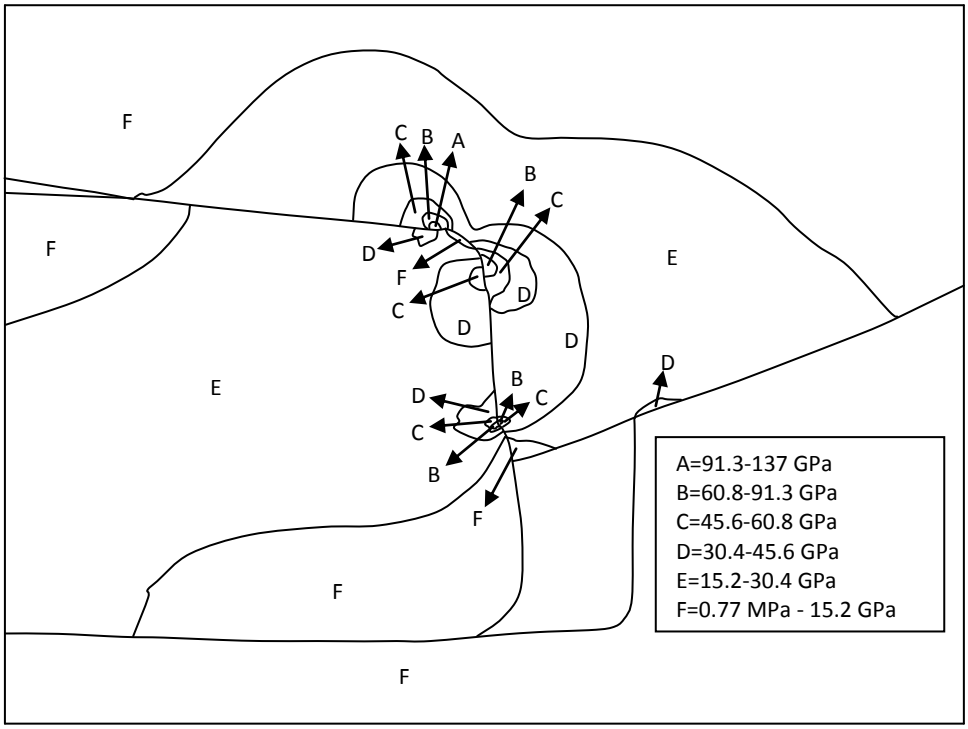

Figure 5.109. Stress contours at key and keyway corner (test no fa-9, T=0.846*Ty, fc=0.1)

Stress contours of test no fa-9 can be seen in Figure 5.109 when applying 0.846 of yield torque. High stresses are obtained at the keyway fillet of the shaft and have a stress range between 91.3 GPa and 137 GPa.

Stress contours can be seen in Figure 5.110 when applying 1.076 of yield torque. High stresses are obtained at the keyway fillet of the shaft and have a stress range from 105 GPa to 157 GPa.

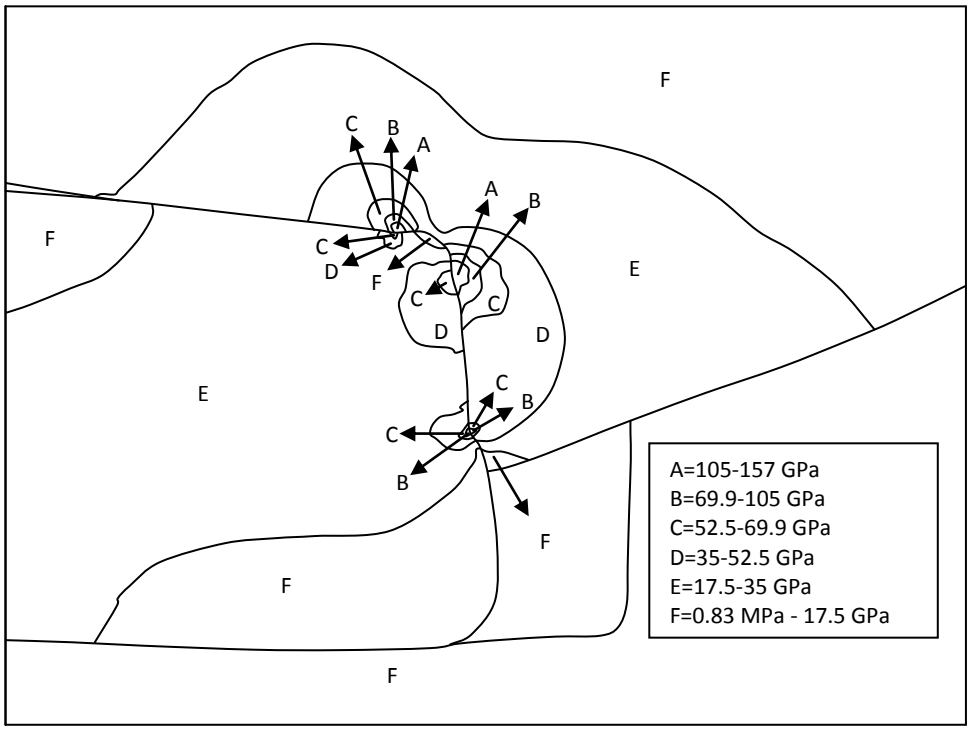

Figure 5.110. Stress contours at key and keyway corner (test no fa-9, T=1.076*Ty, fc=0.1)

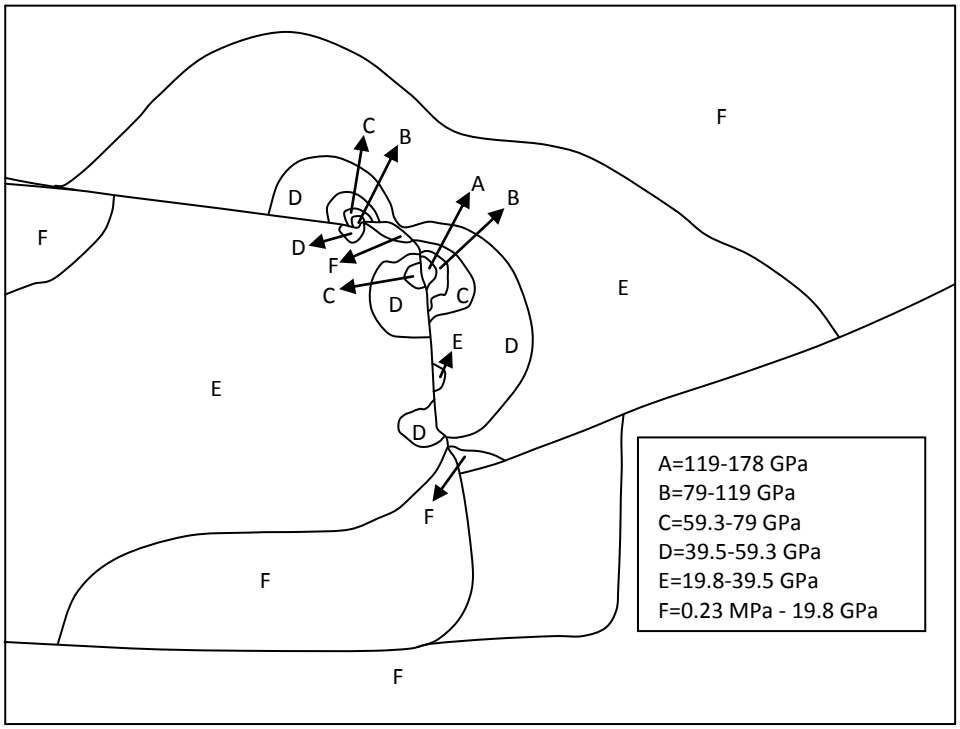

Figure 5.111. Stress contours at key and keyway corner (test no fa-9, T=1.288*Ty, fc=0.1)

Stress contours of FEM are given in Figure 5.111 when applying 1.288 of yield torque. High stresses are obtained at the shaft keyway and have a stress range between 119 GPa and 178 GPa.

5.5.9. Comparison of 2D and 3D analyses of effects of key geometry on stress distributions along keyway edge profile

2D and 3D of FEM results are given. The results are compared to see the difference between 2D and 3D analyses results.

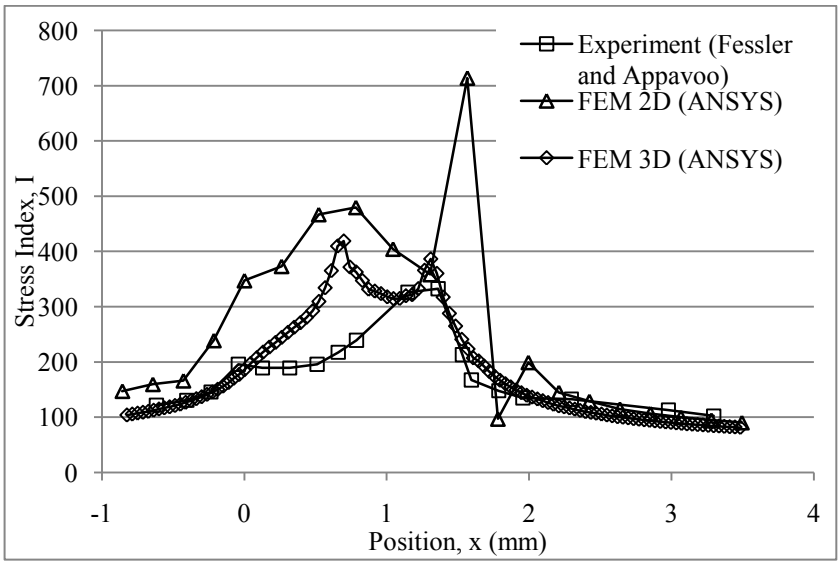

Figure 5.112. Comparison of 2D and 3D analysis for the stresses along keyway edge profiles (test no fa-1, T=Ty)

When comparing the 2D and 3D analyses, general stress distributions look same for key edge dimensions of w=1 mm and h=0.84 mm in Figure 5.112. However 3D analysis results are better than 2D analysis results for agreement with experimental results. Also 2D analyses results are not sensitive. Because few elements are used for convergence in 2D analyses.

2D and 3D stress analyses results can be seen in Figure 5.113 for key edge dimensions of w= 1 mm and h=3 mm. General stress distribution looks similar. However 3D stress analyses results are better than 2D stress analyses results.

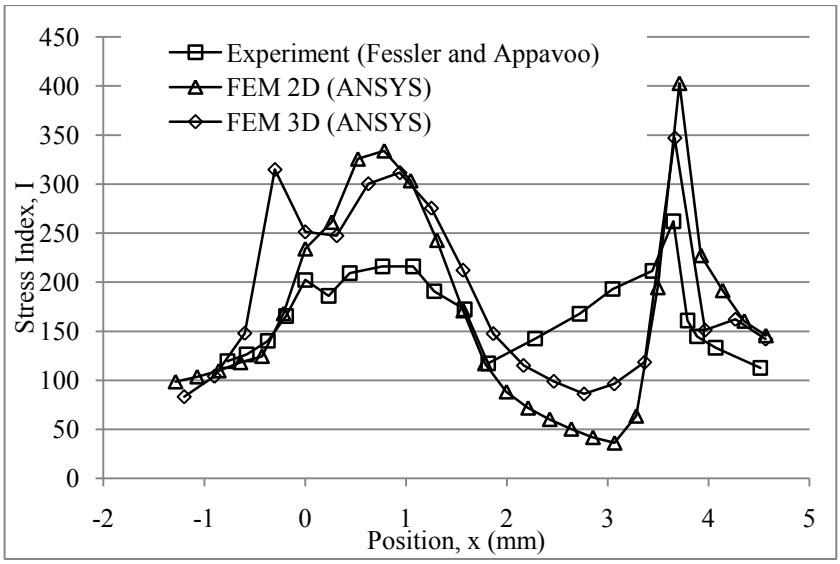

Figure 5.113. Comparison of the effect of friction coefficient in 2D analysis for the stresses along keyway edge profiles (test no fa-2, T=Ty)

5.5.10. Effect of interference fits and friction at the point Sb with different torques

The effect of interference fits and friction between parts are investigated at point Sb on shaft keyway. Different fits are friction coefficients are applied and their results are compared with suitable experimental results. Also some analyses are applied which are not applied before. Results of the analyses are given as stress indices.

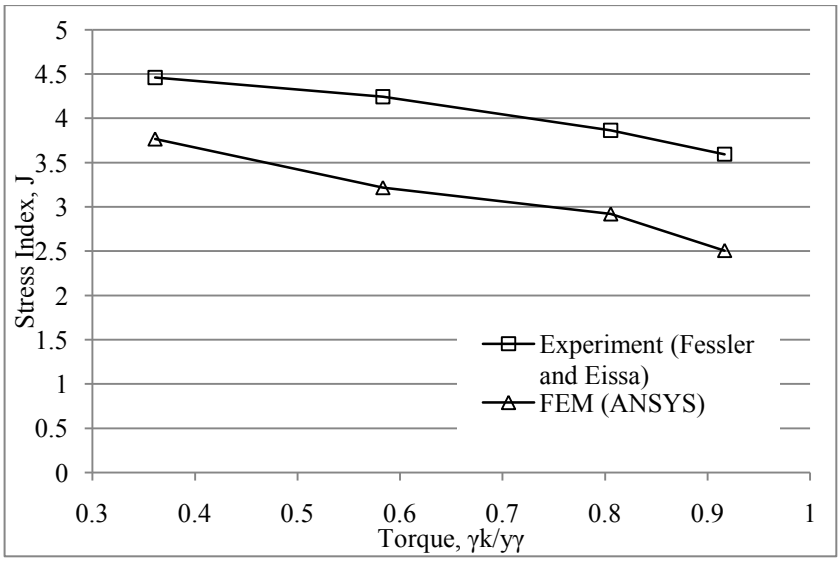

Figure 5.114. Variations of stress index, J at the point Sb for different torques (test no fe-1, fc=0.15)

The FEM stress indices at the point Sb can be seen in Figure 5.114 for test no fe-1 and they are compared with the experimental results. Properties of test no fe-1 can be shown in Table 3.2. The clearance between shaft and hub, key and shaft, key and hub are 0.06 mm, 0.06 mm and 0.31 mm respectively. The friction coefficient is 0.15 between all parts. FEM results are similar to experimental results. When increasing the torque, the stress indices are decreasing.

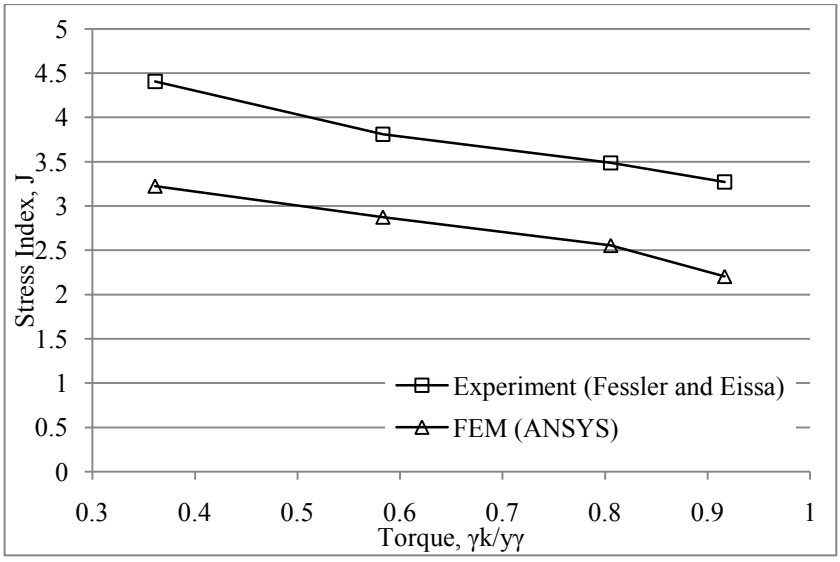

Figure 5.115. Variations of stress index, J at the point Sb for different torques (test no fe-2, fc=0.27)

Stress distribution of FEM results can be seen for test no fe-2 in Figure 5.115. The clearance between shaft and hub, key and shaft, key and hub are 0.06 mm, 0.06 mm and 0.31 mm respectively. The friction coefficient is 0.27 between all parts. The stress distribution of FEM is similar to experimental result. When increasing the torque, the stress indices are decreasing. This FEM analysis are similar to the test no fe-1 but only friction coefficient is changed. Hence the differences between test no fe-1 and test no fe-2 FEM analyses are occurred from friction effect. It is seen that when looking the Figure 5.114 and 5.115, the friction makes to decrease stress indices but does not change the stress distribution. When increasing the friction coefficient from 0.15 to 0.27, the stress indices are decreasing.

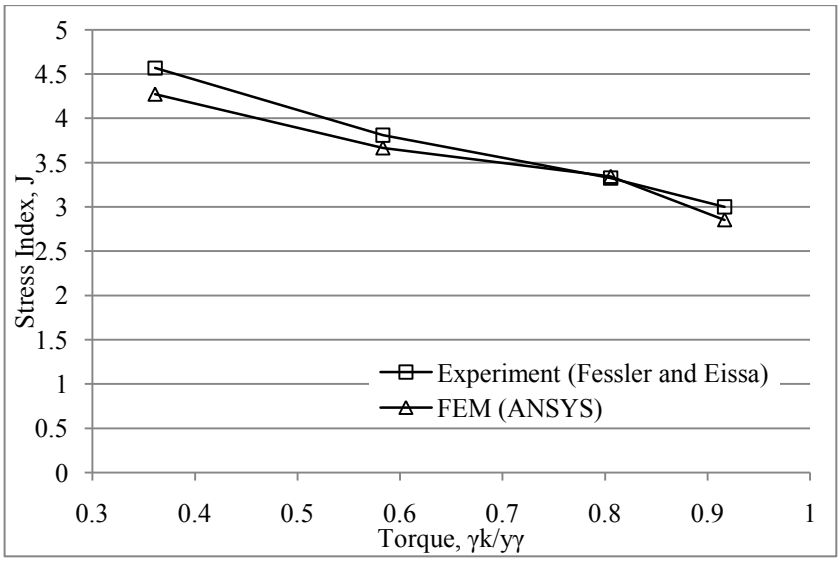

Figure 5.116. Variations of stress index, J at the point Sb for different torques (test no fe-3, fc=0.14)

The stress distribution of FEM can be seen in Figure 5.116 for test no fe-3. The clearance between shaft and hub, key and shaft, key and hub are 0.06 mm, -0.08 mm and 0.17 mm respectively. The friction coefficient is 0.14 between all parts. The FEM results are very similar to the experimental results. The friction coefficient is 0.14. Stress indices are getting higher by means of low friction coefficient. There is interference between shaft and key with a dimension of 0.08 mm.

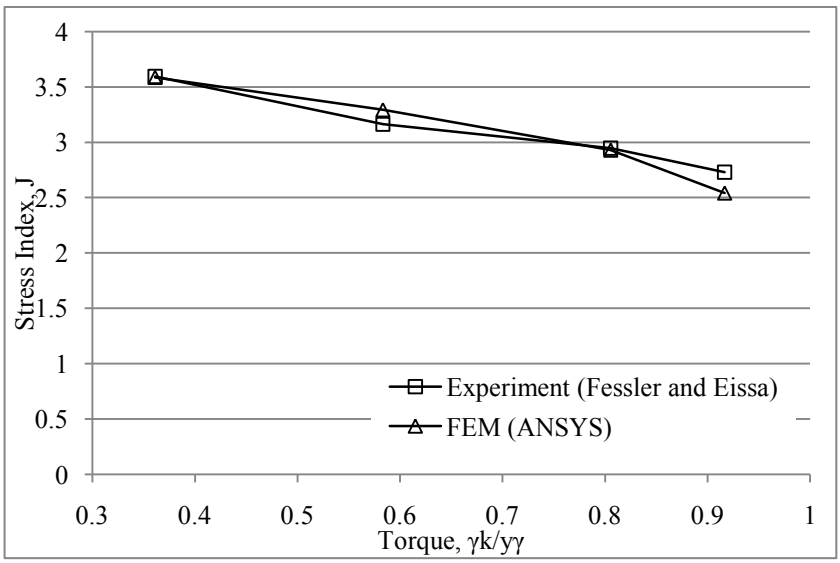

Figure 5.117. Variations of stress index, J at the point Sb for different torques (test no fe-4, fc=0.27)

Stress indices of FEM and experimental results can be seen in Figure 5.117. FEM results are very similar to experimental results. The clearance between shaft and hub, key and shaft, key and hub are 0.03 mm, -0.07 mm and 0.18 mm respectively. The friction coefficient is 0.27 between all parts. When increasing the torque, stress indices are decreasing.

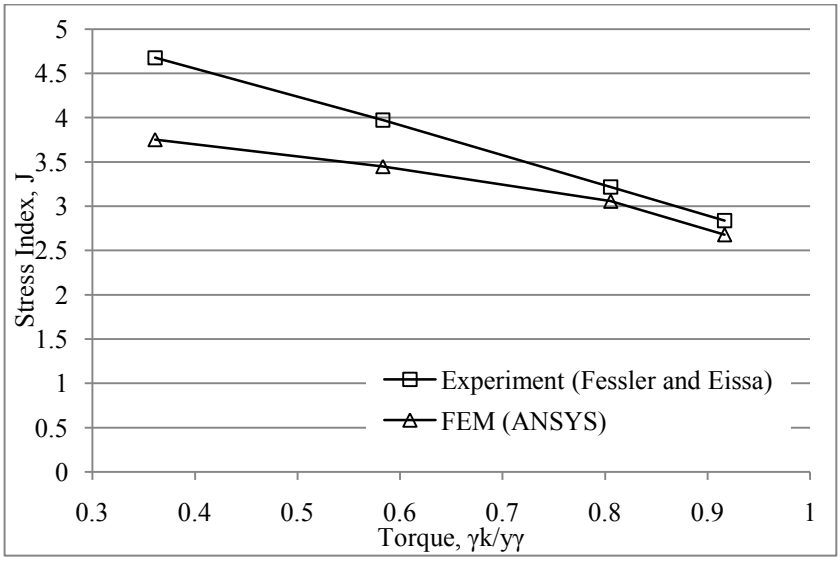

Figure 5.118. Variations of stress index, J at the point Sb for different torques (test no fe-5, fc=0.27)

The stress distribution of test no fe-5 can be seen in Figure 5.118. Clearance between shaft and hub, key and shaft, key and hub are 0.03 mm, -0.16 mm and 0.17 mm respectively. The friction coefficient is 0.27 between all parts. Test no fe-4 and test no fe-5 have nearly similar test conditions. Only the interference between shaft and key is different and it is higher at test no fe-5. Hence it is also seen that the stresses are getting higher, when interference of key and shaft is getting higher.

The stress distribution of test no fe-6 can be seen in Figure 5.119 and it is compared with experimental result. The clearance between shaft and hub, key and shaft, key and hub are -0.06 mm, 0.08 mm and 0.17 mm respectively. The friction coefficient is 0.35 between all parts. FEM result is higher than experimental result.

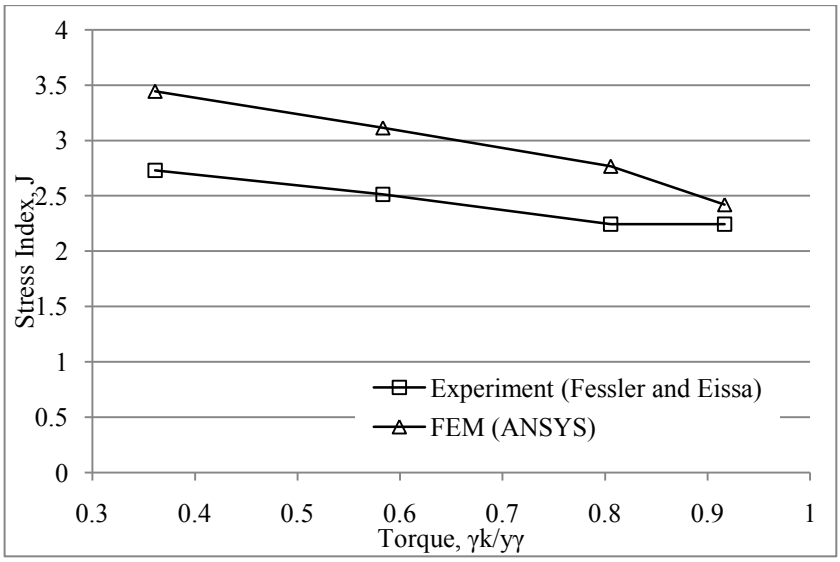

Figure 5.119. Variations of stress index, J at the point Sb for different torques (test no fe-6, fc=0.35)

The results of FEM analyses show that the stress indices are decreasing at point Sb when the torque is increasing. Also when the friction coefficient is decreasing, the stresses are getting higher. The interference between parts influences the stresses. Generally if the interference is getting higher, the stresses are getting higher. The dominant effect of increasing the stresses at point Sb may be caused from the interference between shaft and key.

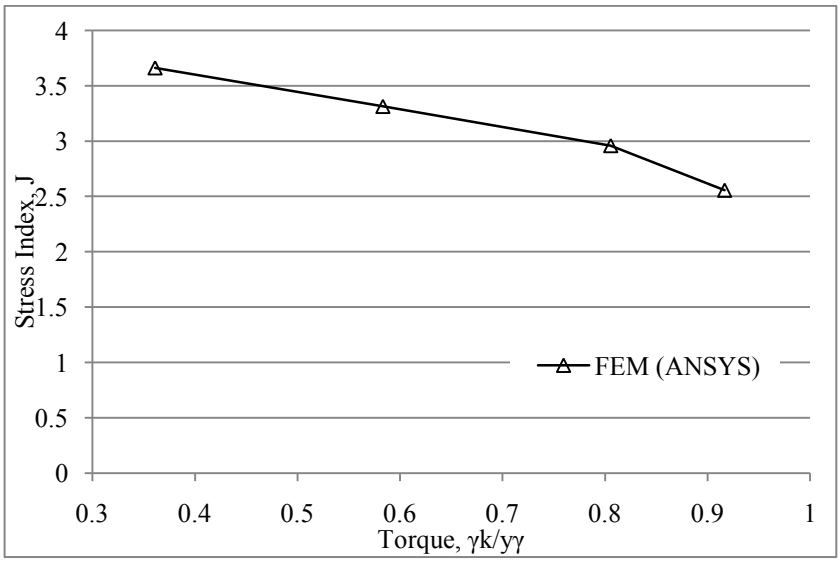

Figure 5.120. Variations of stress index, J at the point Sb for different torques (test no fem-1, fc=0.27)

Stress distribution of test no fem-1 can be seen in Figure 5.120. The clearance between shaft and hub, key and shaft, key and hub are -0.06 mm, -0.08 mm and 0.17 mm respectively. The friction coefficient is 0.27 between all parts. The conditions of test no fem-1 and test no fe-3 are similar. Only the difference is friction coefficient. Both of them have same stress distributions. However the stress distribution of test no fe-3 is higher than test no fem-1. It can be said that the friction coefficient can change the stress values. When the friction between parts is higher, stress indices are decreasing.

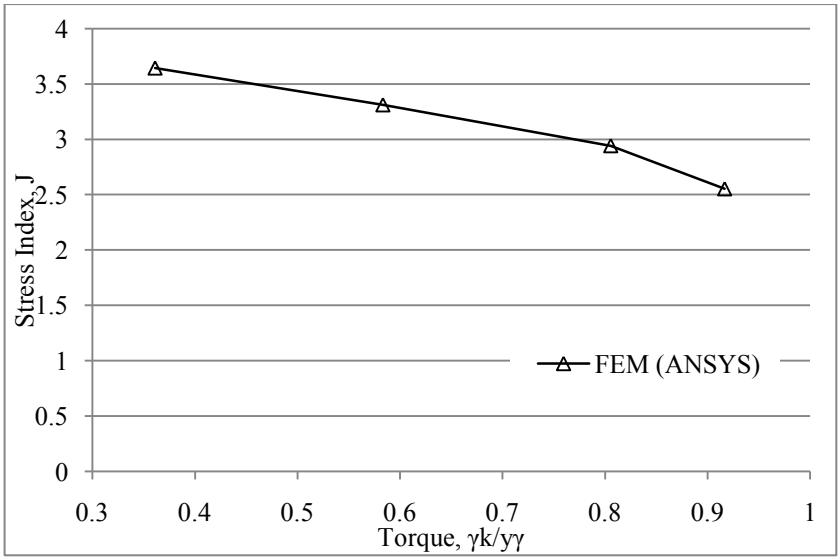

Figure 5.121. Variations of stress index, J at the point Sb for different torques (test no fem-2, fc=0.27)

The stress distribution of test no fem-2 can be seen in Figure 5.121. The clearance between shaft and hub, key and shaft, key and hub are -0.03 mm, -0.08 mm and 0.17 mm respectively. The friction coefficient is 0.27 between all parts. The test no fem-1 and test no fem-2 have similar conditions. Only the interference between shaft and hub is different. Friction coefficients of both tests are same. When the interference between shaft and key is decreasing, the stresses at point Sb are decreasing but not chancing dominantly.

The stress distribution of test no fem-3 can be seen in Figure 5.122. The clearance between shaft and hub, key and shaft, key and hub are 0.06 mm, -0.16 mm and 0.17 mm respectively. The friction coefficient is 0.14 between all parts. Test no fe-3 and

test no fem-3 have similar analyses conditions. Only the clearance between shaft and key is different. The stress results of test no fem-3 is higher than test no fe-3.

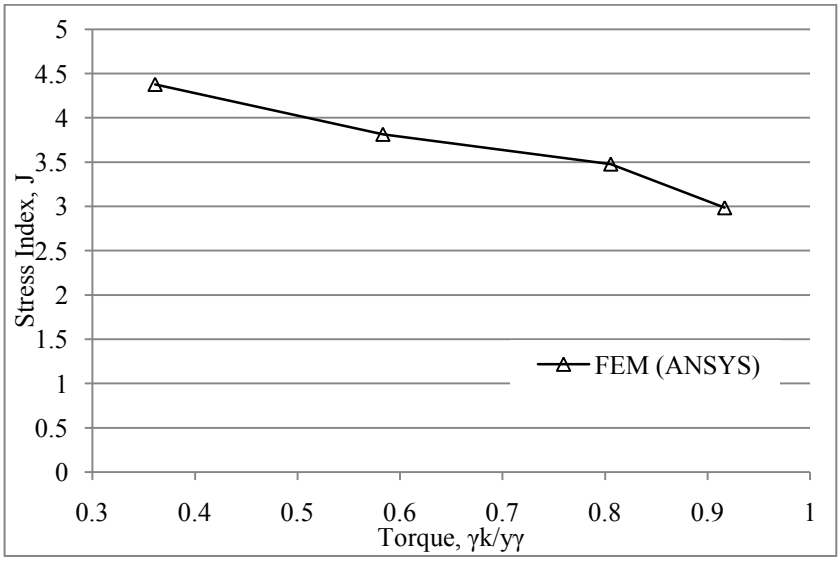

Figure 5.122. Variations of stress index, J at the point Sb for different torques (test no fem-3, fc=0.14)

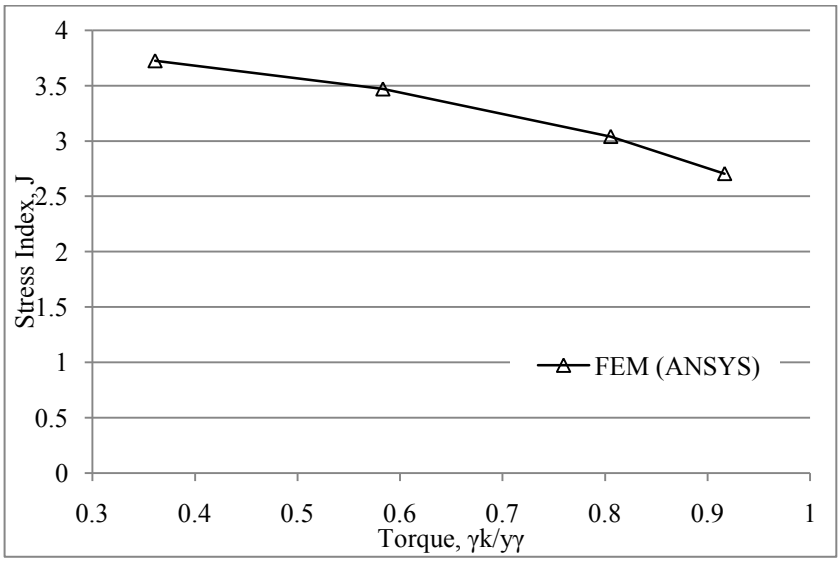

Figure 5.123. Variations of stress index, J at the point Sb for different torques (test no fem-4, fc=0.27)

The stress distribution of test no fem-4 can be seen in Figure 5.123. The clearance between shaft and hub, key and shaft, key and hub are 0.06 mm, -0.16 mm and 0.17 mm respectively. The friction coefficient is 0.27 between all parts. Test no fem-3 and test no fem-4 have nearly same analyses conditions. Only the difference is friction

coefficient. Test no fem-3 have higher stress results than test no fem-4. Because the friction coefficient of parts are different. When friction coefficient is getting higher, stress indices are decreasing.

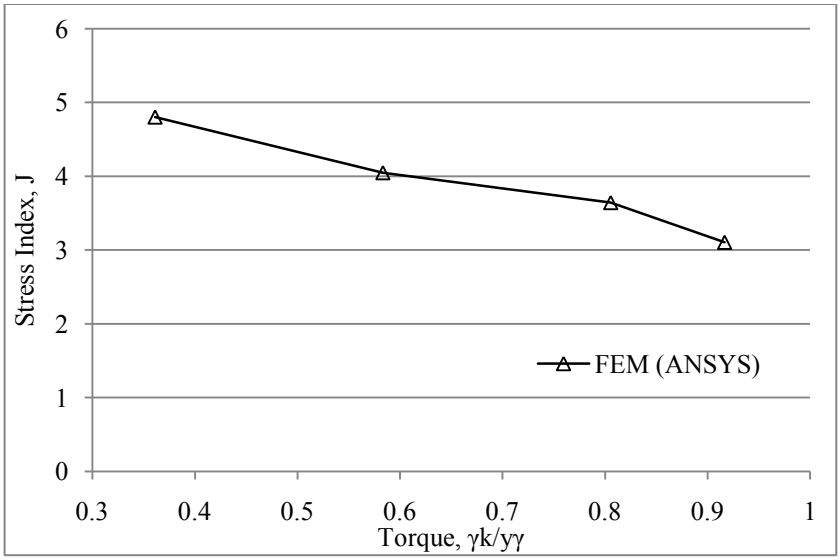

Figure 5.124. Variations of stress index, J at the point Sb for different torques (test no fem-5, fc=0.14)

The stress distribution of test no fem-5 can be seen in Figure 5.124. The clearance between shaft and hub, key and shaft, key and hub are 0.06 mm, -0.16 mm and -0.17 mm respectively. The friction coefficient is 0.14 between all parts. The test no fem-5 and test no fem-3 have same analyses conditions. But the clearance between key and hub is different. It is seen that the test no fem-5 have higher stress results than test no fem-3. The clearance and interference between key and hub also affects the stress results.

The stress distribution of test no fem-6 can be seen in Figure 5.125. The clearance between shaft and hub, key and shaft, key and hub are -0.03 mm, -0.08 mm and -0.06 mm respectively. The friction coefficient is 0.27 between all parts. The result of test no fem-6 looks similar to test no fe-5 FEM stress result. But their interferences of parts are different.

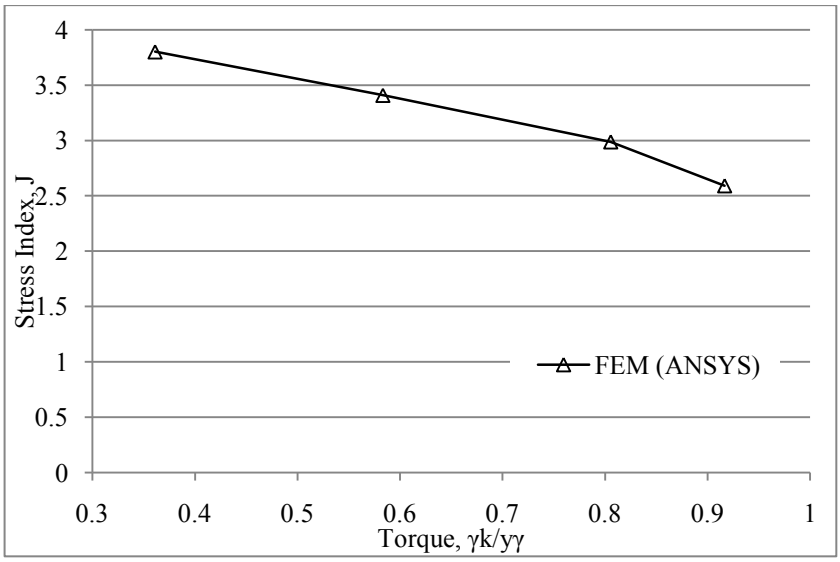

Figure 5.125. Variations of stress index, J at the point Sb for different torques (test no fem-6, fc=0.27)

In the most of the analyses of section 5.5.10 show that when increasing the torque, stress indices are getting decreasing. The friction can influence the solutions. When increasing the friction coefficient of the parts, stress indices are getting decreasing at point Sb. The interference between parts is also influencing the solutions. If the interference is increasing, the stresses are generally increasing.

5.5.11. Effect of interference fits and friction at the point Ss with different torques

Same analyses conditions of section 5.5.10 are valid for section 5.5.11. Only the stress results are taken for Ss point. The effect of interference and friction between parts are investigated for the point Ss.

The stress distribution of test no fe-1 can be seen in Figure 5.126 for the Ss point. The results are better at point Ss than point Sb for comparing with the experimental result for test no fe-1. When increasing the torque, stress indices are decreasing.

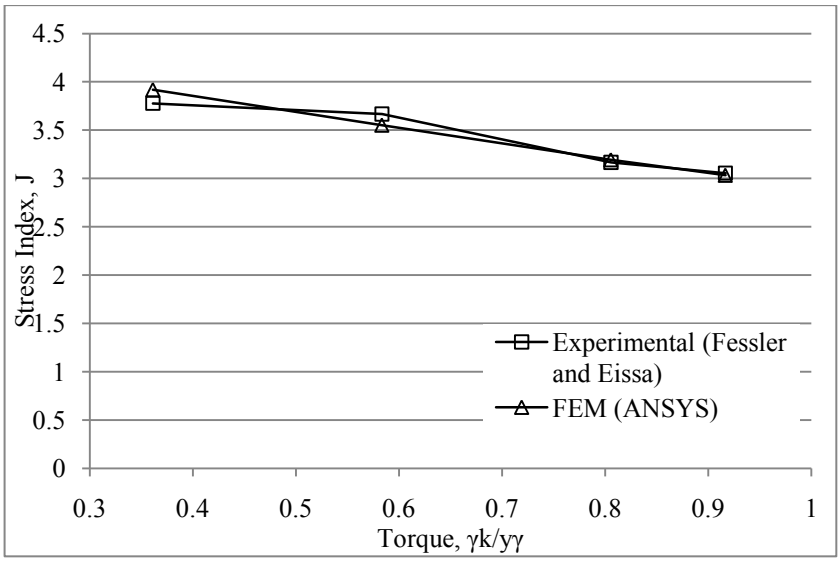

Figure 5.126. Variations of stress index, J at the point Ss for different torques (test no fe-1, fc=0.15)

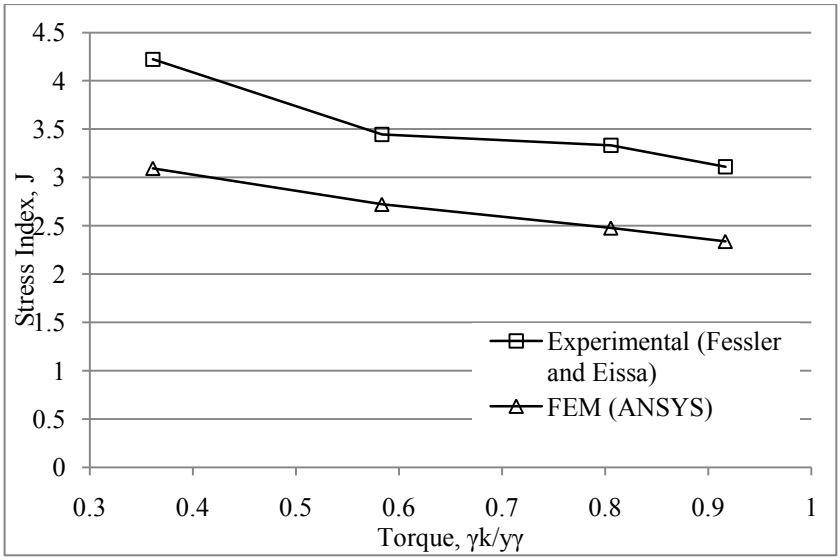

Figure 5.127. Variations of stress index, J at the point Ss for different torques (test no fe-2, fc=0.27)

Stress distribution of test no fe-2 is given in Figure 5.127 for point Ss. The FEM results are similar to the experimental results. However FEM results are less than experimental results. The difference between test no fe-1 and test no fe-2 is only the friction coefficient. When increasing the friction coefficient, stresses are decreasing.

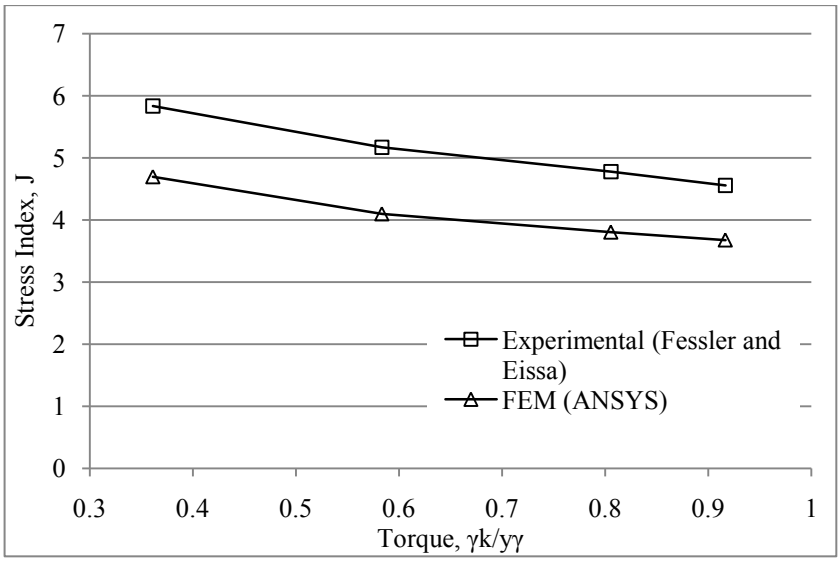

Figure 5.128. Variations of stress index, J at the point Ss for different torques (test no fe-3, fc=0.14)

Stress indices of FEM results are given in Figure 5.128 at the point Ss for test no fe-3. Stress distribution of FEM and experimental results are similar. The results are higher than test no fe-1 and test no fe-2 results at the point Ss. It may be caused from interferences and friction coefficients of parts. Especially there is an interference between shaft and key in test no fe-3. But test no fe-1 and test no fe-2 have clearances between shaft and key. It may influence the stresses.

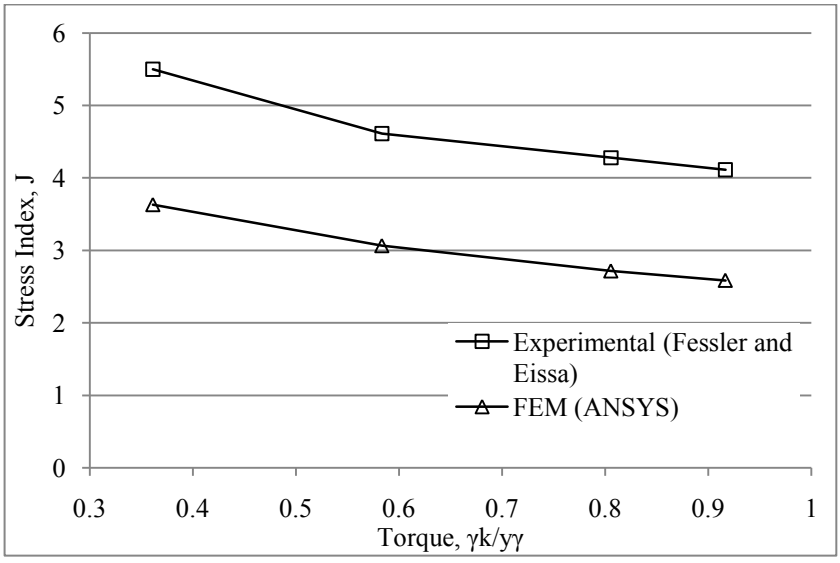

Figure 5.129. Variations of stress index, J at the point Ss for different torques (test no fe-4, fc=0.27)

The stress distribution of test no fe-4 is shown in Figure 5.129. FEM and experimental results are similar. However, FEM results are less than experimental results. The friction coefficient is the same as test no fe-2. The difference of FEM results between test no fe-2 and test no fe-4 may be caused from the interferences of parts. The interference between shaft and key is increasing the stresses.

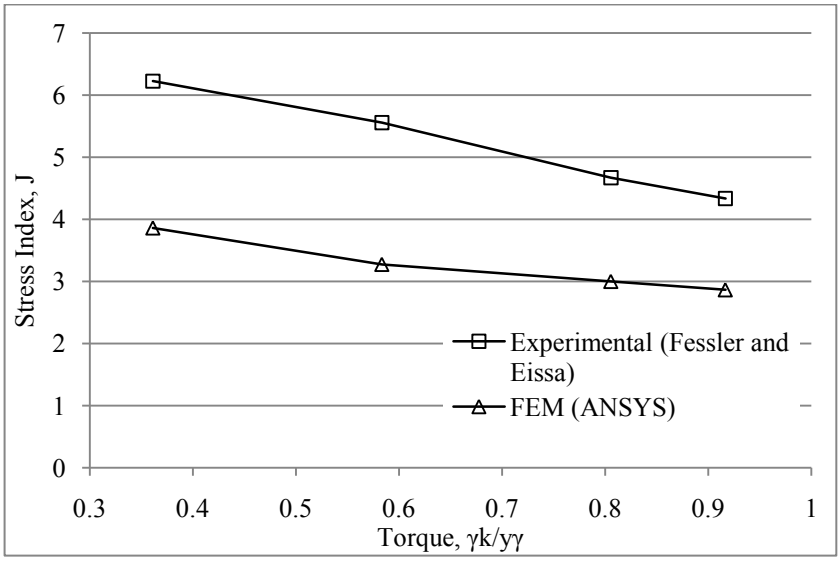

Figure 5.130. Variations of stress index, J at the point Ss for different torques (test no fe-5, fc=0.27)

Stress indices of test no fe-5 are given in Figure 5.130. Test no fe-4 and test no fe-5 have same friction coefficients. However the interference between key and shaft is different. Also the interference between key and hub is different but it is very small and can be neglected. It is seen that the stress indices are increasing when the interference between key and shaft is increasing.

Stress distribution of test no fe-6 can be seen in Figure 5.131. The FEM and experimental results are compared and it is seen that the distributions are similar but values are different. FEM results are less than experimental results.

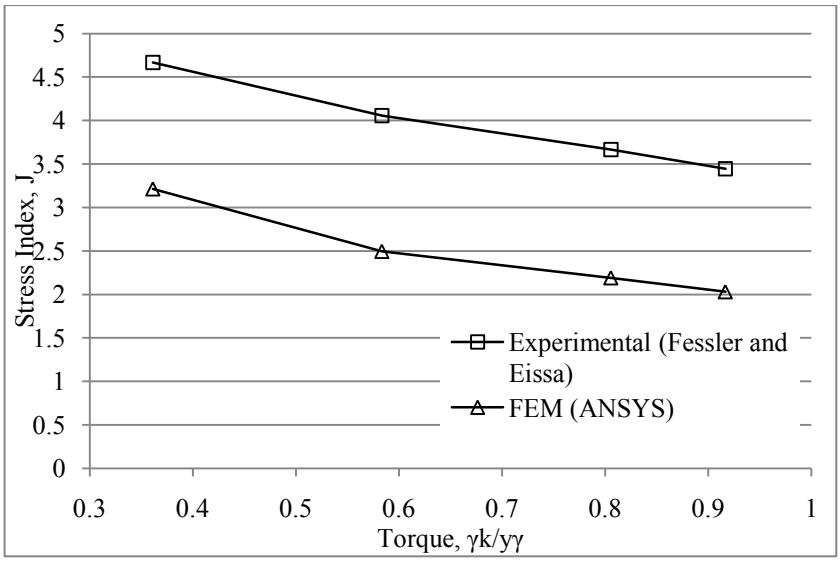

Figure 5.131. Variations of stress index, J at the point Ss for different torques (test no fe-6, fc=0.35)

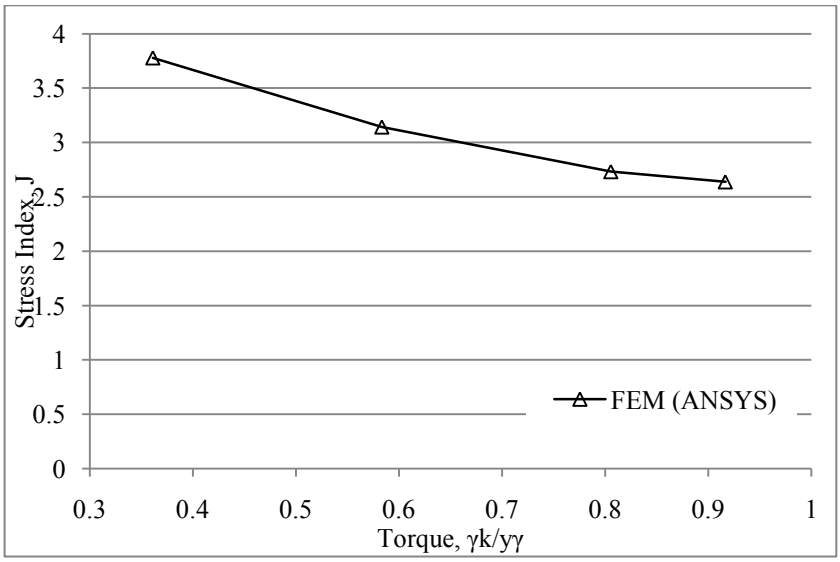

Figure 5.132. Variations of stress index, J at the point Ss for different torques (test no fem-1, fc=0.27)

Stress distribution of test no fem-1 at point Ss can be seen in Figure 5.132. Test no fem-1 and test no fe-3 are same without friction coefficient. It is seen that when comparing FEM results of Figure 5.132 and Figure 5.128, friction coefficient increment causes to decrease the stress indices.

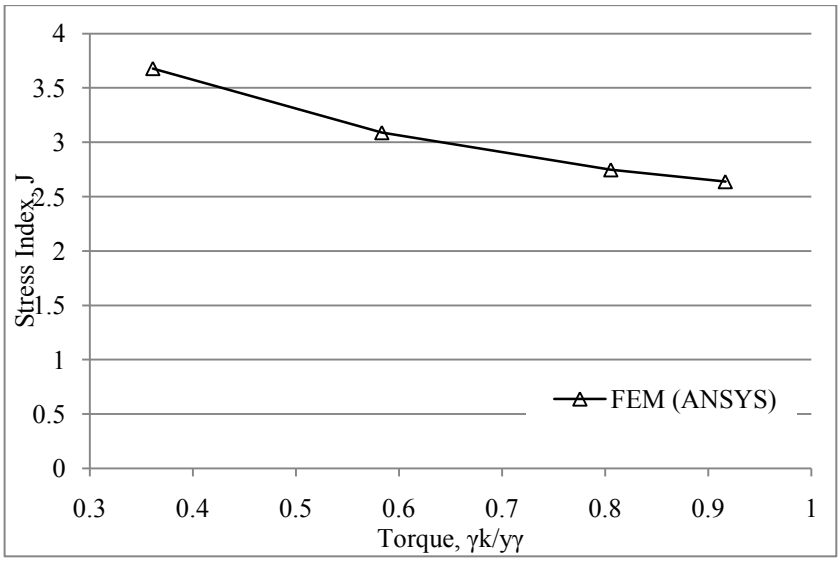

Figure 5.133. Variations of stress index, J at the point Ss for different torques (test no fem-2, fc=0.27)

Stress indices of test no fem-2 are shown in Figure 5.133 at point Ss. Test no fem-2 has same properties of test no fem-1. Only the interference between hub and shaft is different. When interference between hub and shaft is decreasing, stress indices are decreasing.

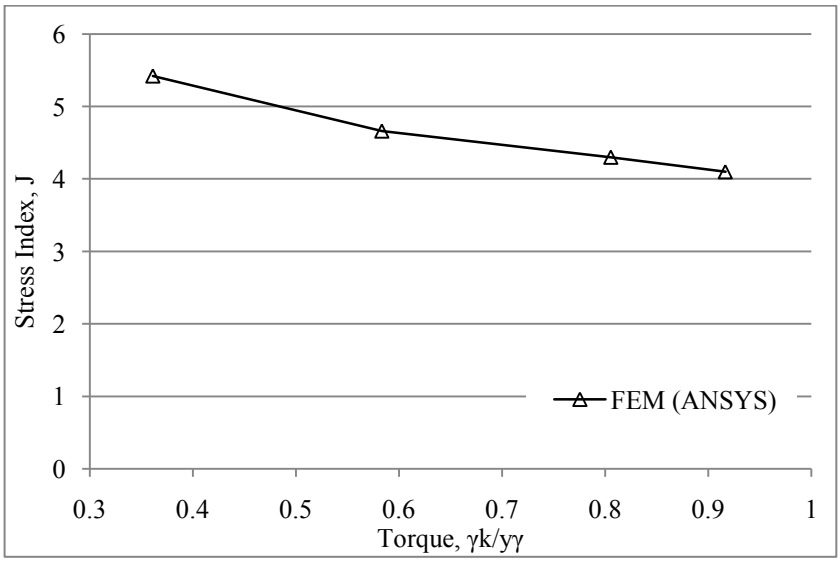

Figure 5.134. Variations of stress index, J at the point Ss for different torques (test no fem-3, fc=0.14)

Stress indices of test no fem-3 can be seen in Figure 5.134 at point Ss. Stress indices are decreasing when increasing the torque. Test no fe-3 and test no fem-3 have same geometries and frictions. Only the clearance between shaft and key is different. The

stress results of test no fem-3 are higher than test no fe-3. It may be caused from the interference between shaft and key in test no fem-3.

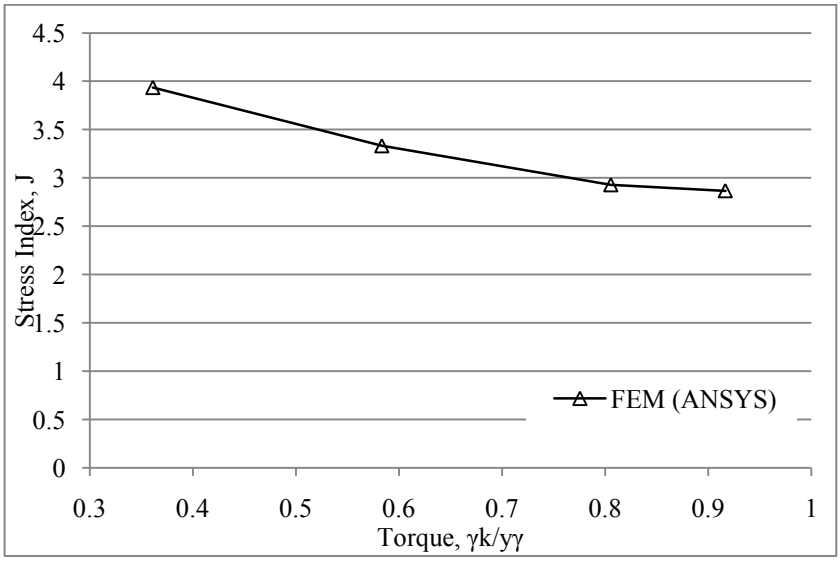

Figure 5.135. Variations of stress index, J at the point Ss for different torques (test no fem-4, fc=0.27)

Stress indices of test no fem-4 can be seen in Figure 5.135. Test no fem-4 results are compared with test no fem-3 results. Test no fem-3 and test no fem-4 have same analyses conditions. But friction coefficients are different. When increasing the friction coefficient, stress indices are decreasing.

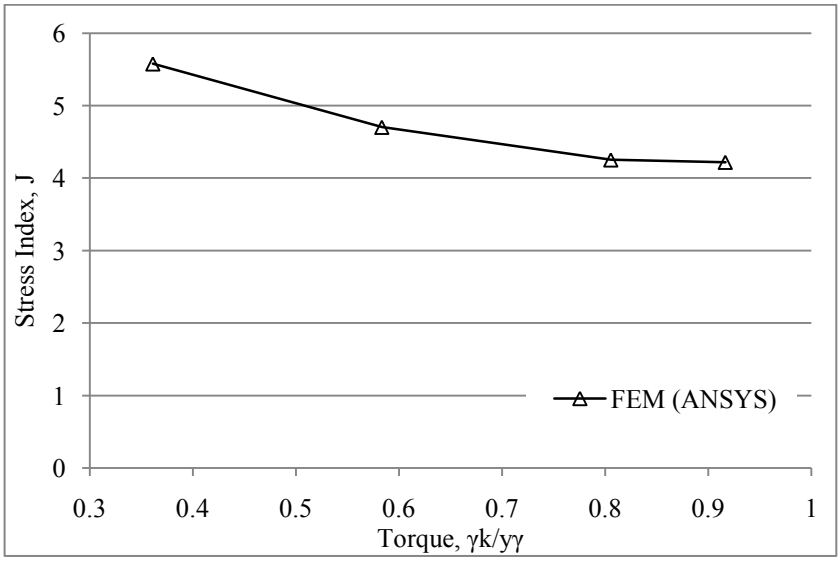

Figure 5.136. Variations of stress index, J at the point Ss for different torques (test no fem-5, fc=0.14)

Stress indices of test no fem-5 can be seen in Figure 5.136. The results of test no fem-5 are compared with test no fem-3. Both of them have same friction coefficients and geometrical conditions. Only the clearance between key and hub is different. Test no fem-5 has higher stresses than test no fem-3 but not high.

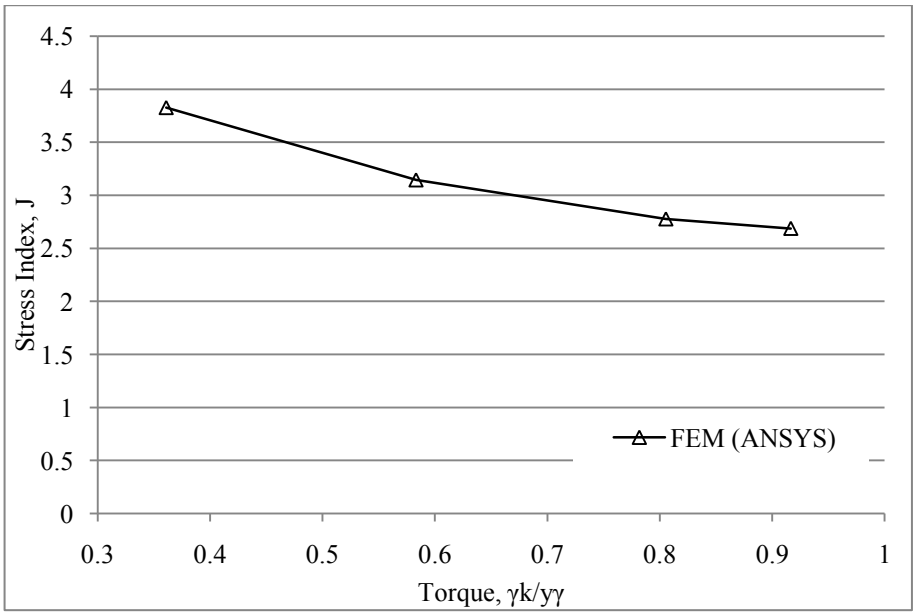

Figure 5.137. Variations of stress index, J at the point Ss for different torques (test no fem-6, fc=0.27)

The stress distribution of test no fem-6 can be seen in Figure 5.125. It is compared with test no fem-2 result which has same friction coefficients, clearances between shaft-hub and shaft-key. Only the clearance between key and hub is different. Test no fem-6 has higher stresses than test no fem-2. It may be occurred from interference between key and hub.

Same stress distributions are seen at point Ss like point Sb. When increasing torque, stress indices are generally decreasing. Friction coefficient and interference between parts influence the stress results. When increasing the friction coefficient, stress indices are decreasing. Also when increasing the interferences between parts, stress indices are generally increasing. In some cases, stress indices are nearly constant and not influence dominantly from interference and friction coefficient. The minimum stresses occur at test no fem-6 when comparing the interferences and friction coefficients in the Table 4.1. Test no fem-6 have clearances between shaft and hub,

key and shaft, key and hub are -0.03 mm, -0.08 mm and 0.17 mm respectively. Friction coefficient between parts is 0.15.

5.6. Analysis of hub, shaft and key interaction problem under torsion using 3D finite element models with different thicknesses

The stresses of hub, shaft and key interaction are investigated by chancing the keyway fillet ratio and torque under torsion. Also only a single shaft with keyway is investigated under torsion. The keyway fillet ratio and test properties are given in Table 3.3. The results are taken from keyway fillet of shaft and shown as stress concentration factor which is given in Equation 3.5.

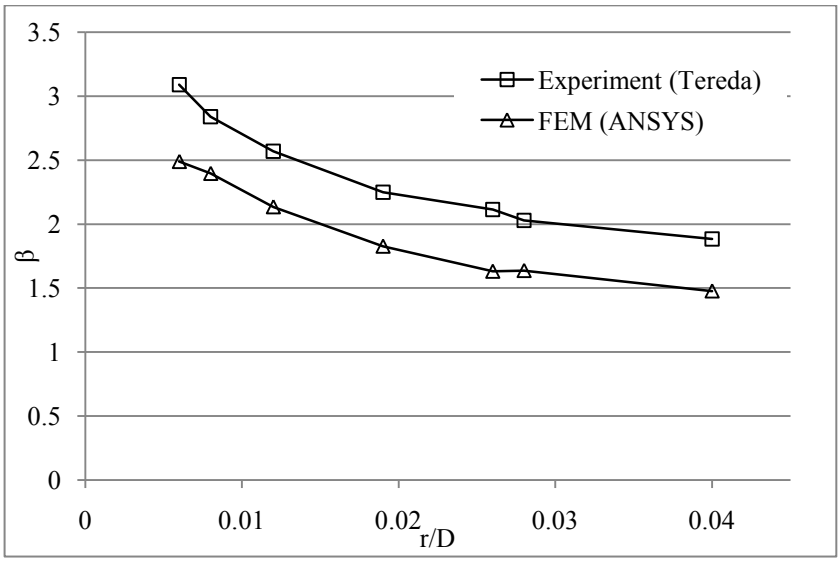

Figure 5.138. Variations of stress concentration factor, β, at keyway surface for different keyway fillet ratios (only a single shaft analysis)

Only a single shaft analyses results are given in Figure 5.138. The model geometries are given in Figure 3.7. It is seen that FEM and Terada's experimental stress distributions are similar. When keyway fillet ratio and torque increases, the stress concentration factor decreases. Also between test no oh-1 and test no oh-2, the torque is constant and only keyway fillet ratio is increasing. It is seen that when keyway fillet ratio is increasing, stress concentration factor is decreasing.

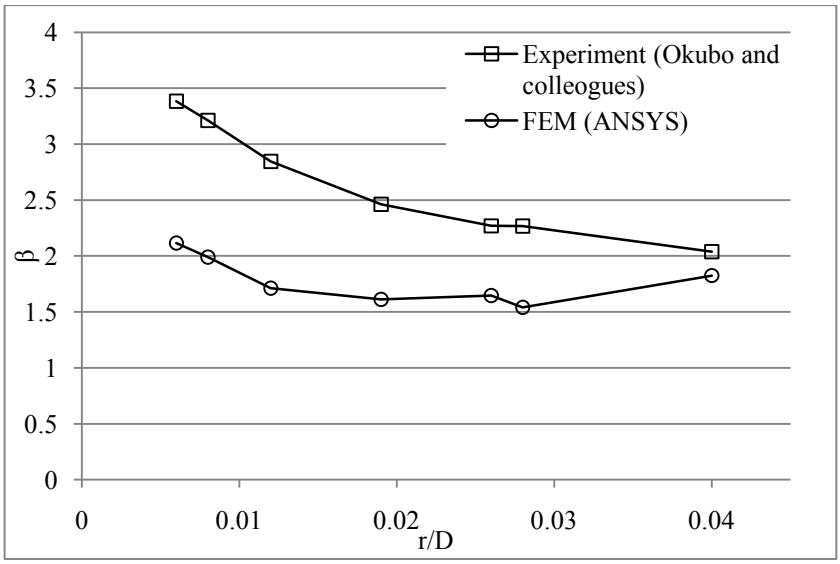

Figure 5.139. Variations of stress concentration factor, β, at keyway surface for different keyway fillet ratios (hub, shaft and key interaction analysis and fc=0.1)

The effect of the keyway fillet ratio and torque can be seen in Figure 5.139 for hub, shaft and key interaction analyses. Model geometries are given in Figure 3.6. The stress concentration factor decreases in experimental results. But stress concentration factor is firstly decreasing. Then becomes nearly constant and increases at the end in FEM.

5.7. Analysis of stepped shaft without keys under torsion using 3D finite element model

The keyway stresses of a stepped shaft are investigated under torsion. Stepped shaft geometry can be seen in Figure 3.5. Principal stress indices are calculated for different angles at the keyway fillet of the shaft and they are given in below Figures. Ex-1 and Ex-2 show the principal stress indices of experimental results of Fessler and colleagues [1]. FEM-1 and FEM-2 show the principal stress indices of FEM results.

Principal stress indices are shown in Figure 5.140 when angular coordinate (α) about shaft axis measured from plane of symmetry is 0^0. Stress indices are changing with respect to angular position (Φ) in keyway fillet. It is seen that nearly two symmetric stress distributions occur with respect to the Φ angle axis. FEM and experimental results are similar.

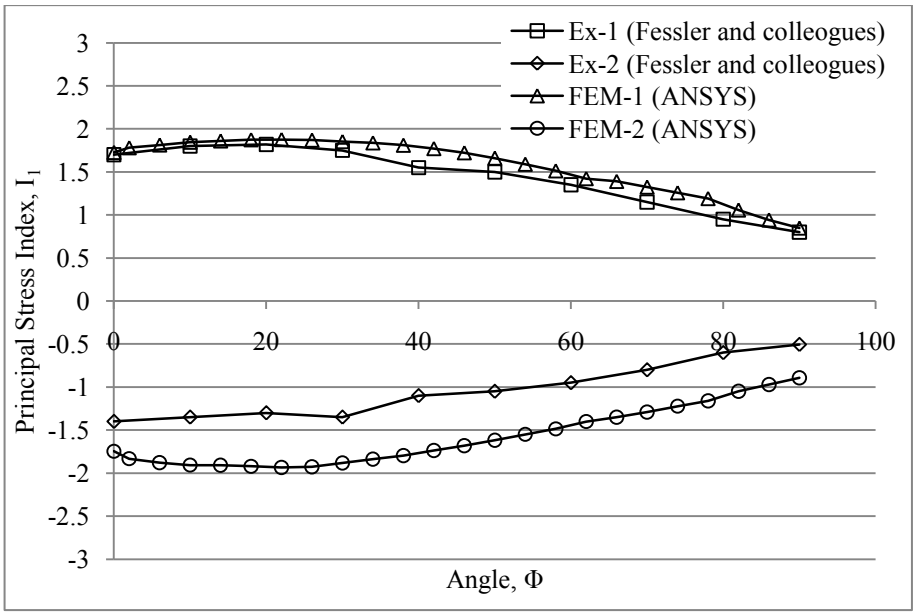

Figure 5.140. Stress indices in the keyway end for pure torsion when $\alpha=0^0$

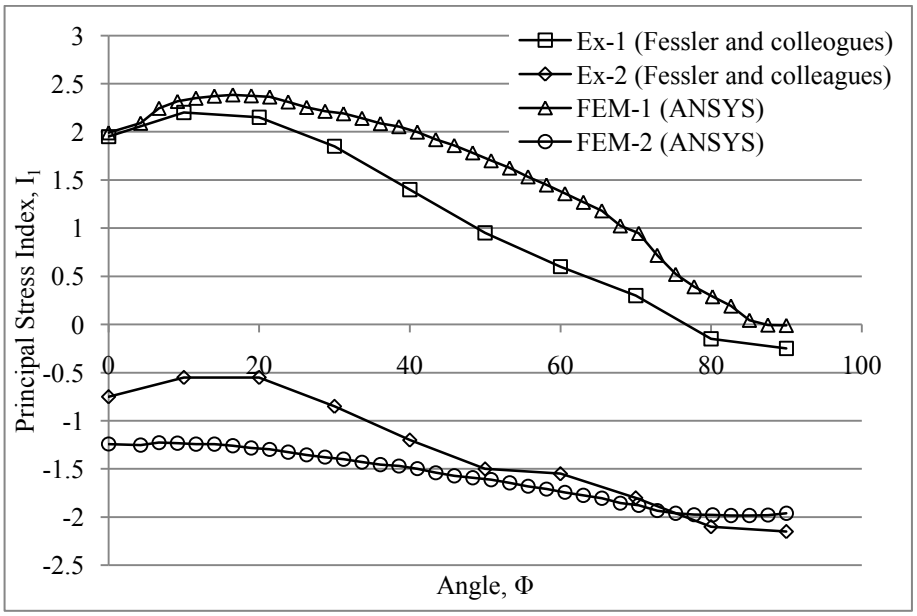

Figure 5.141. Stress indices in the keyway end for pure torsion when $\alpha=30^0$

The stress indices are shown in Figure 5.141 when angular coordinate (α) about shaft axis measured from plane of symmetry is 30^0. FEM-1 has the highest stress indices. The distribution of FEM and experimental results are similar.

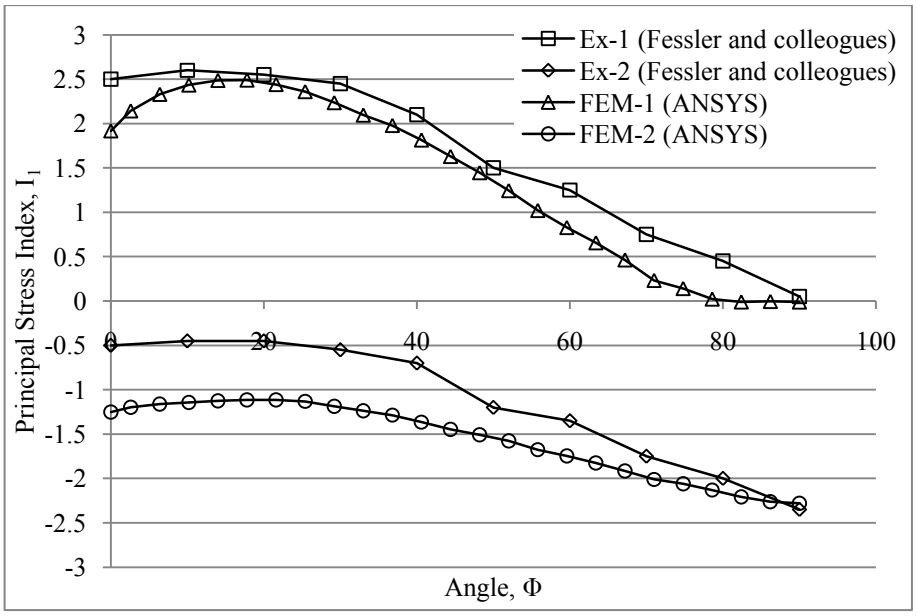

Figure 5.142. Stress indices in the keyway end for pure torsion when $\alpha=60^0$

The stress indices are shown in Figure 5.142 when angular coordinate (α) about shaft axis measured from plane of symmetry is 60^0. Stress distributions of FEM and experimental results are similar. Ex-1 results are higher than FEM-1 results.

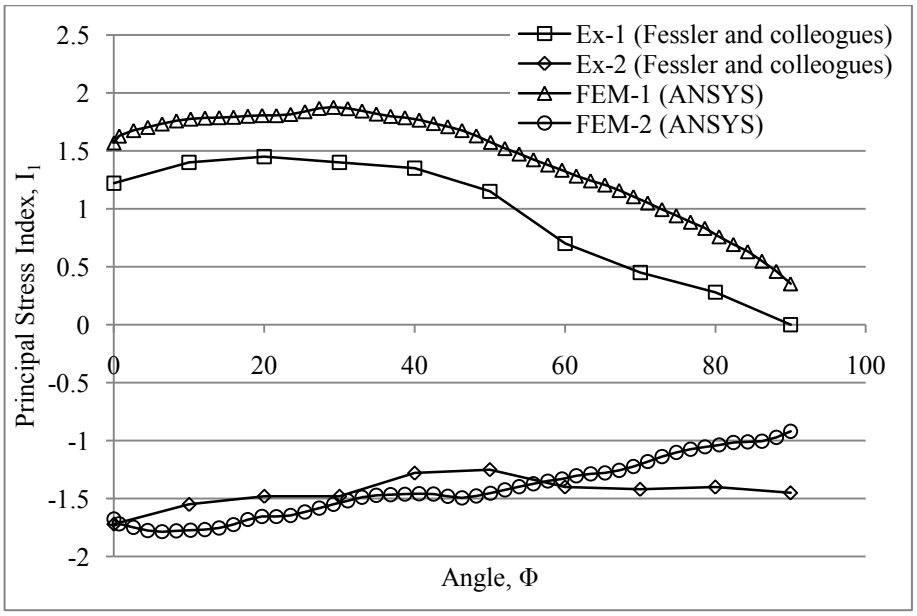

Figure 5.143. Stress indices in the keyway end for pure torsion when $\alpha=90^0$

The stress indices are shown in Figure 5.143 when angular coordinate (α) about shaft axis measured from plane of symmetry is 90^0. Stress distributions of FEM and experimental results are similar, but FEM-1 results are higher than Ex-1 results.

5.8. Analysis of plain shaft without keys under bending using 3D finite element model

A single shaft with keyway is investigated under bending and principal stress indices are calculated for different angles of keyway fillet. Bending model can be seen in Figure 3.4. The results are given by principal stress indices which are given in Equation 3.4. FEM results are compared with experimental results.

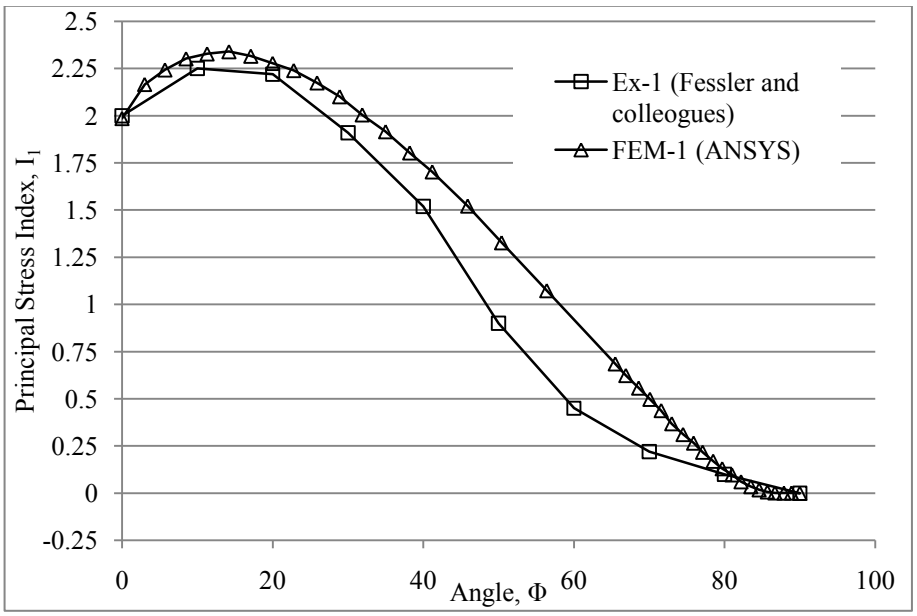

Figure 5.144. Stress indices in the keyway end for pure bending when $\alpha=0^0$

The stress indices are shown in Figure 5.144 when angular coordinate (α) about shaft axis measured from plane of symmetry is 0^0. Stress indices change with respect to angular position (Φ) in keyway fillet. FEM and experimental results are similar. FEM results have more data and more smooth than experimental results.

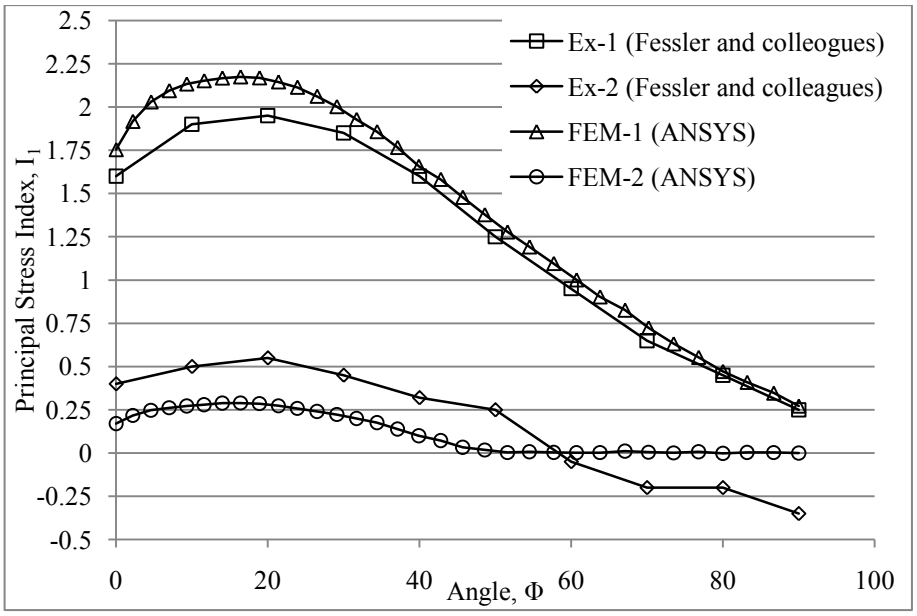

Figure 5.145. Stress indices in the keyway end for pure bending when $\alpha=30^0$

The stress indices are shown in Figure 5.145 when angular coordinate (α) about shaft axis measured from plane of symmetry is 30^0. FEM and experimental results are similar. Some differences exist between FEM-2 and Ex-2 results from 50^0 to 90^0.

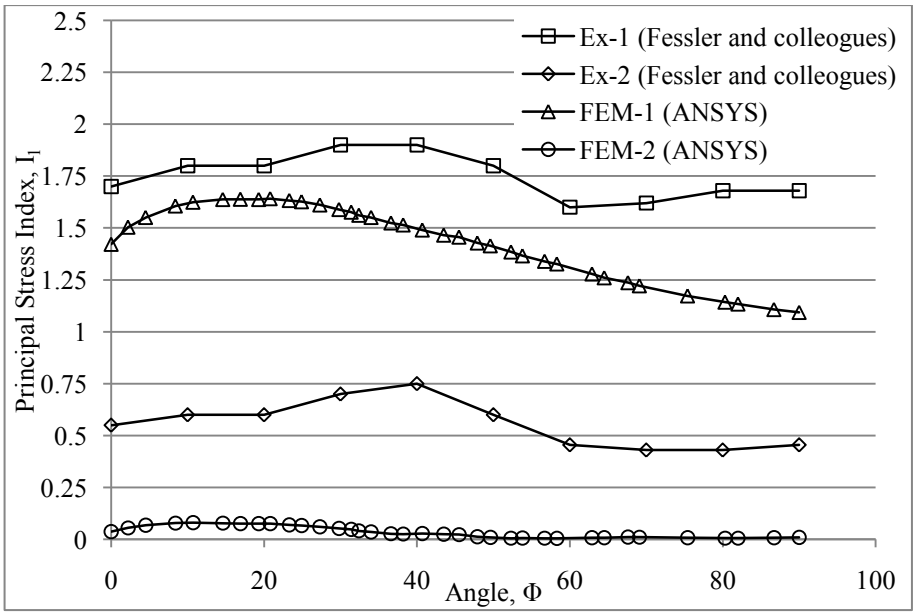

Figure 5.146. Stress indices in the keyway end for pure bending when $\alpha=60^0$

The stress indices are shown in Figure 5.146 when angular coordinate (α) about shaft axis measured from plane of symmetry is 60^0. FEM and experimental stress

distributions are similar but values are different. FEM-1 results are less than Ex-1 results. Also FEM-2 results are less than Ex-2 results.

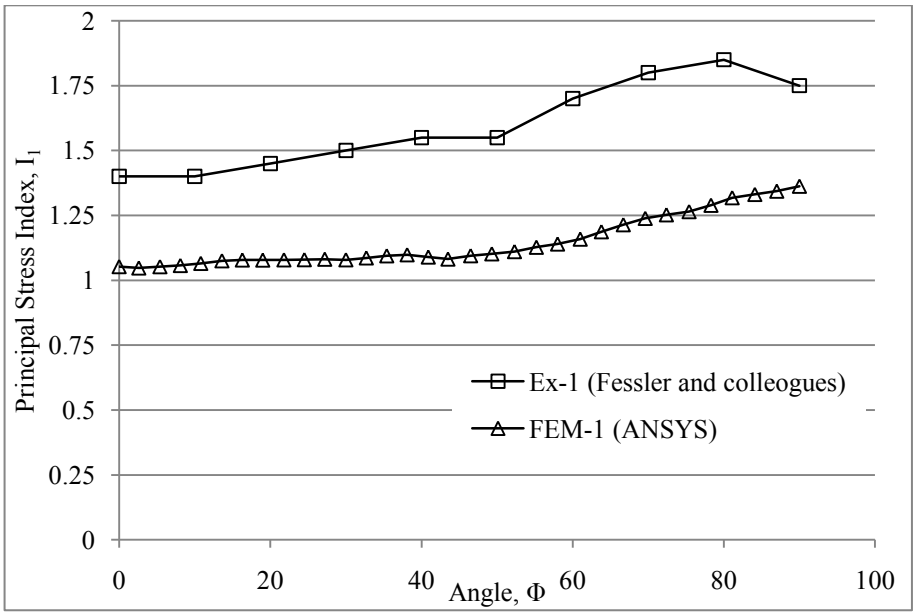

Figure 5.147. Stress indices in the keyway end for pure bending when $\alpha=90^0$

The stress indices are shown in Figure 5.147 when angular coordinate (α) about shaft axis measured from plane of symmetry is 90^0. FEM and experimental stress distributions are similar but FEM results are less than experimental results.

5.9. Analysis of hub, shaft and key interaction problem under bending using 3D finite element models with different thicknesses

Different types of loading can be seen in keyed connections. One of the loading types is bending. Different keyed connection models are investigated with FEM and their results are given in this topic.

There are no suitable experimental results for comparing the results of hub, shaft and key interaction analyses under bending. Stress values are taken from the centre of keyway fillet at Figure 4.7, Figure 4.9 and Figure 4.11 model analyses. Stress values are taken with respect to the angular coordinate (α) shaft axis and angular position (Φ) in keyway fillet at Figure 4.13, Figure 4.15 and Figure 4.17 model analyses. The results are given as principal stress indices.

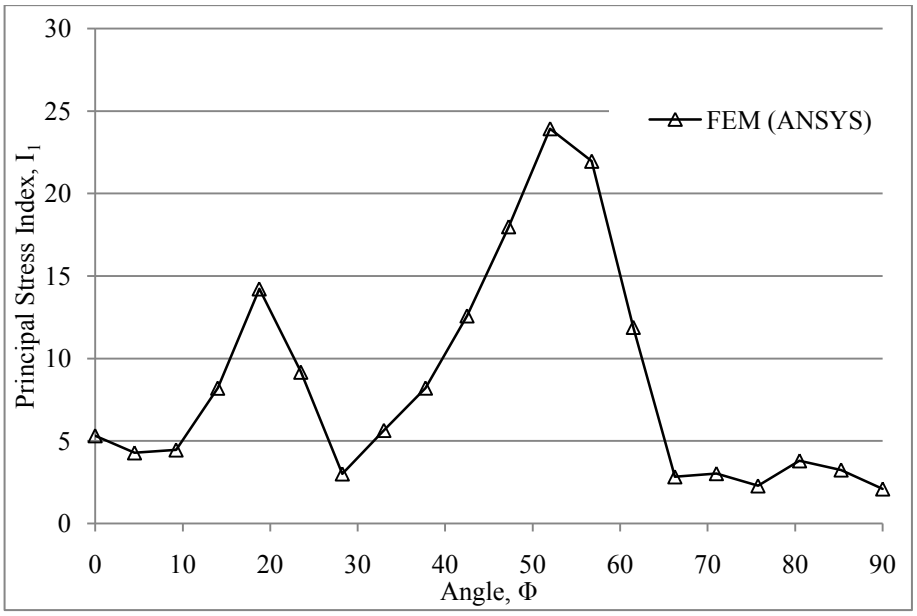

Figure 5.148. Principal stress indices in the keyway end for pure bending for Figure 4.7 model.

Principal stress indices of Figure 4.7 model can be seen in Figure 5.148. The results are taken from centre of keyway fillet. Stress indices are chancing with respect to angular position in keyway fillet, Φ. It is seen that two stress peak points are obtained at FEM results. The highest stress is obtained nearly at 50^0 of Φ.

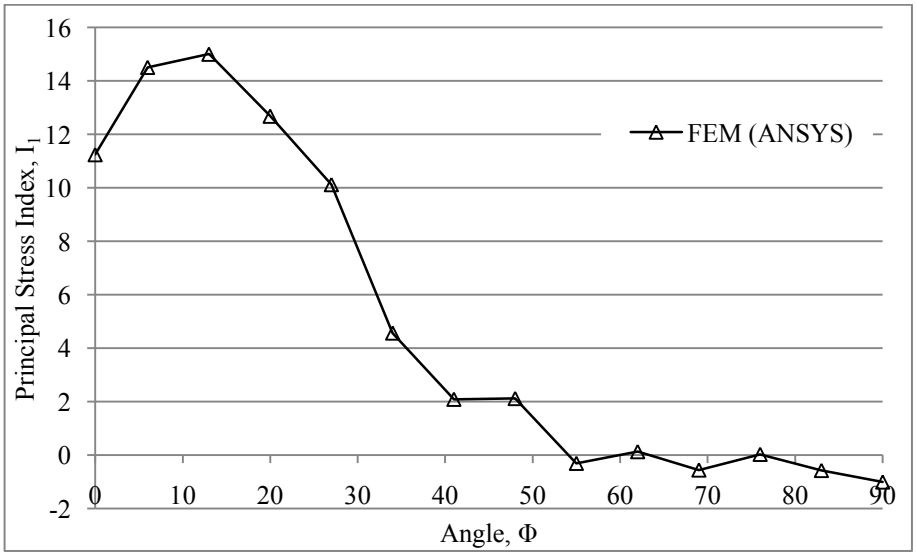

Figure 5.149. Principal stress indices in the keyway end for pure bending for Figure 4.9 model.

Principal stress indices of Figure 4.9 model can be seen in Figure 5.149. The results are taken from centre of keyway fillet. High stresses are obtained between 10^0 and 20^0 of Φ.

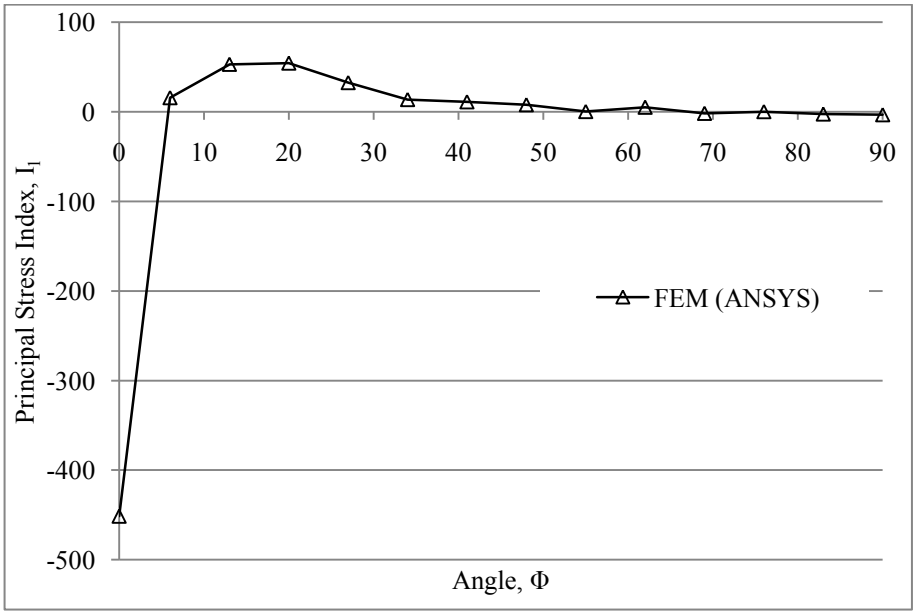

Figure 5.150. Principal stress indices in the keyway end for pure bending for Figure 4.11 model.

The results of Figure 4.11 model can be seen in Figure 5.150. Stress range is high and the highest stress is obtained at 0^0 of Φ.

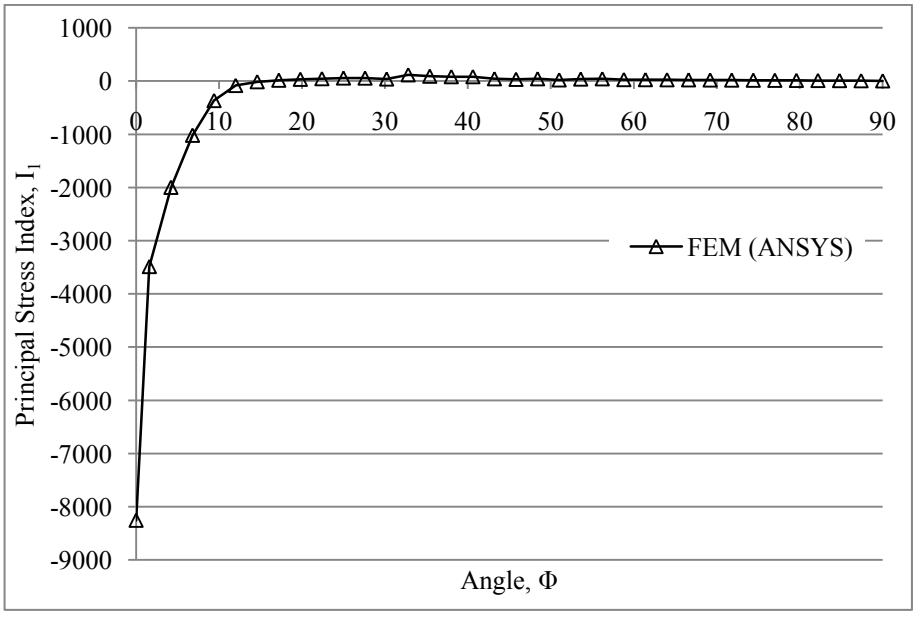

Figure 5.151. Principal stress indices in the keyway end for pure bending for Figure 4.13 model when $\alpha=0^0$

Principal stress indices of Figure 4.13 model are given in Figure 5.151 when α is 0^0. The highest stress is obtained at 0^0 of Φ.

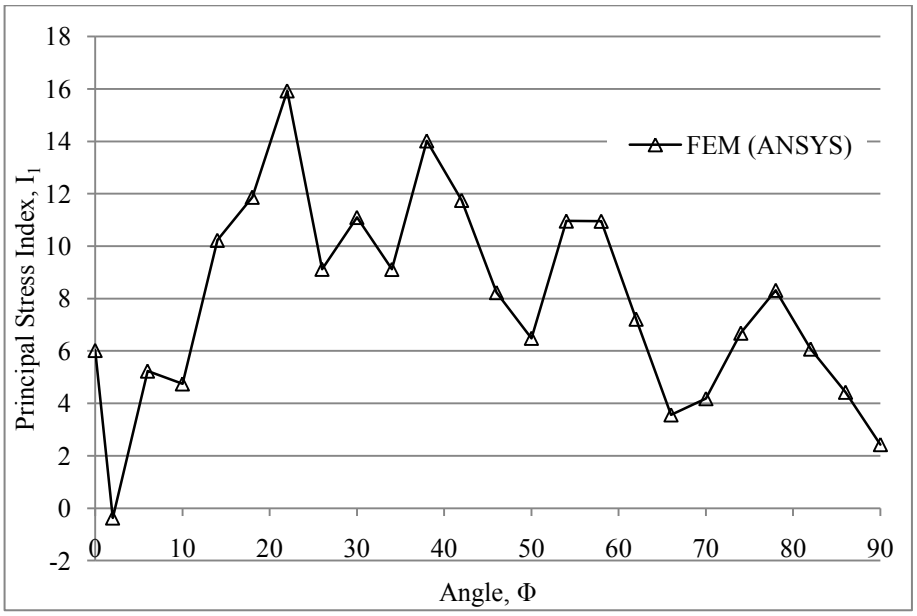

Figure 5.152. Principal stress indices in the keyway end for pure bending for Figure 4.13 model when $\alpha=30^0$

When α is 30^0, the result of Figure 4.13 model can be seen in Figure 5.152. Stress indices are obtained waved. The highest stress is obtained nearly at 20^0 of Φ.

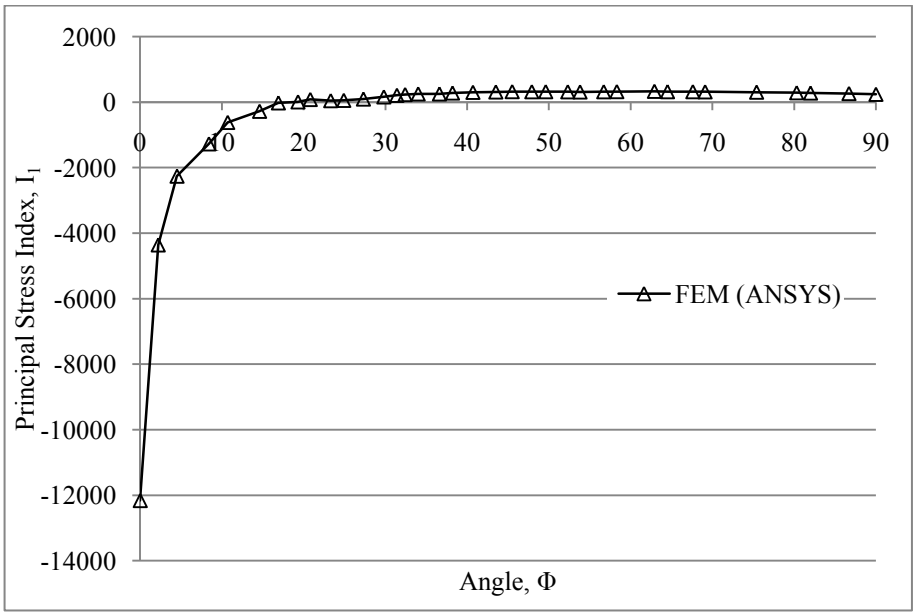

Figure 5.153. Principal stress indices in the keyway end for pure bending for Figure 4.13 model when $\alpha=60^0$

When α is 60^0, principal stress distribution becomes as given in Figure 5.153. The highest stress is obtained at 0^0 of Φ.

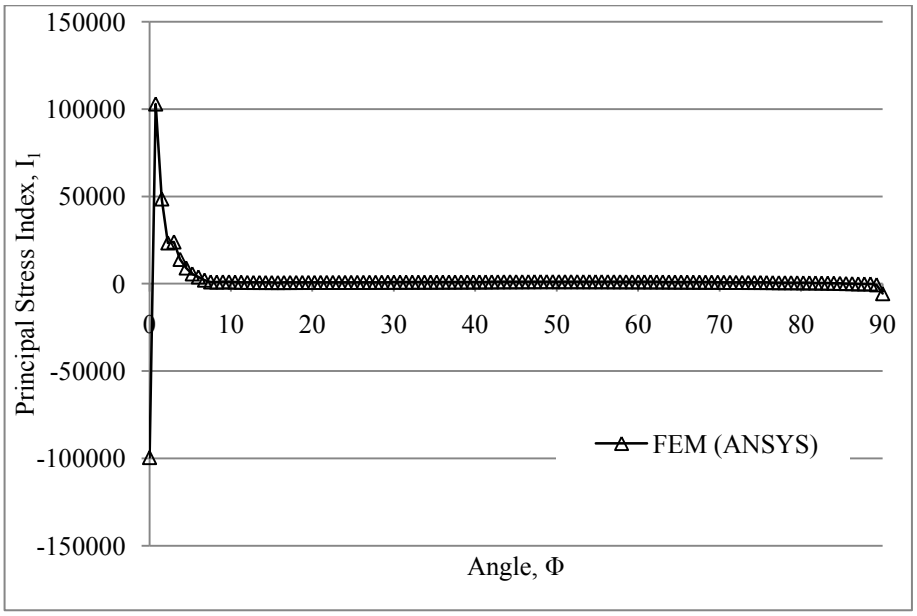

Figure 5.154. Principal stress indices in the keyway end for pure bending for Figure 4.13 model when $\alpha=90^0$

Principal stress indices for Figure 4.13 model are given in Figure 5.154 when α is equal to 90^0. It is seen that high stresses are obtained between 0^0 and 10^0 of Φ.

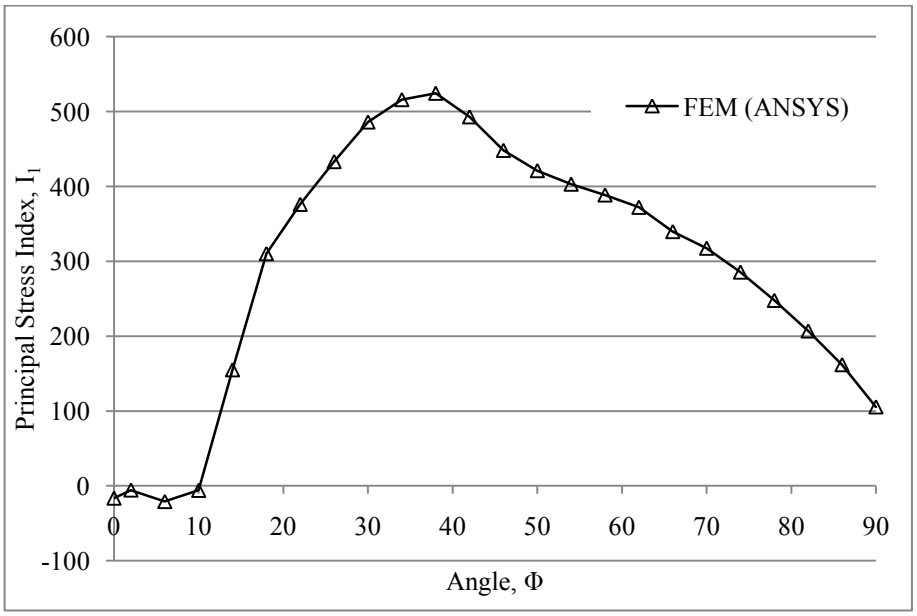

Figure 5.155. Principal stress indices in the keyway end for pure bending for Figure 4.15 model when $\alpha=0^0$

Principal stress distribution can be seen in Figure 5.155 when α is equal to 0^0. High stresses are obtained between 30^0 and 40^0 of Φ.

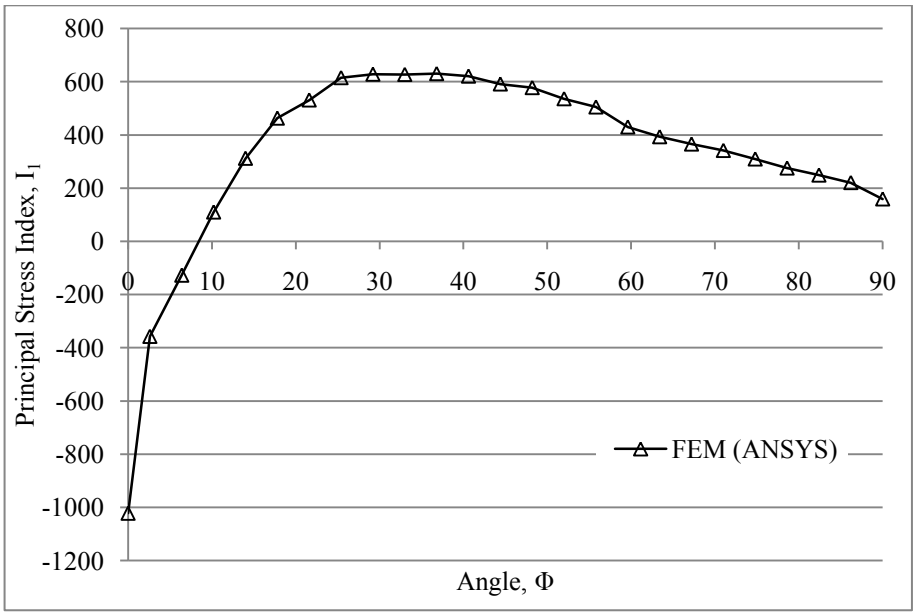

Figure 5.156. Principal stress indices in the keyway end for pure bending for Figure 4.15 model when $\alpha=30^0$

When α is equal to 30^0, stress distribution of Figure 4.15 model is given in Figure 5.156. High stresses are obtained between 30^0 and 40^0 of Φ.

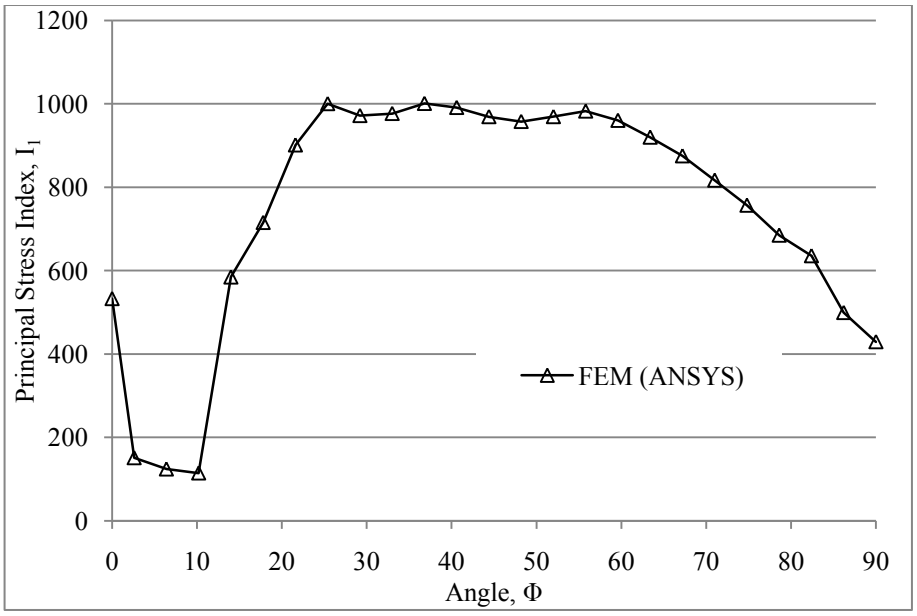

Figure 5.157. Principal stress indices in the keyway end for pure bending for Figure 4.15 model when $\alpha=60^0$

When α is 60^0, stress distribution can be seen in Figure 5.157. High stresses are obtained between 25^0 and 55^0 of Φ.

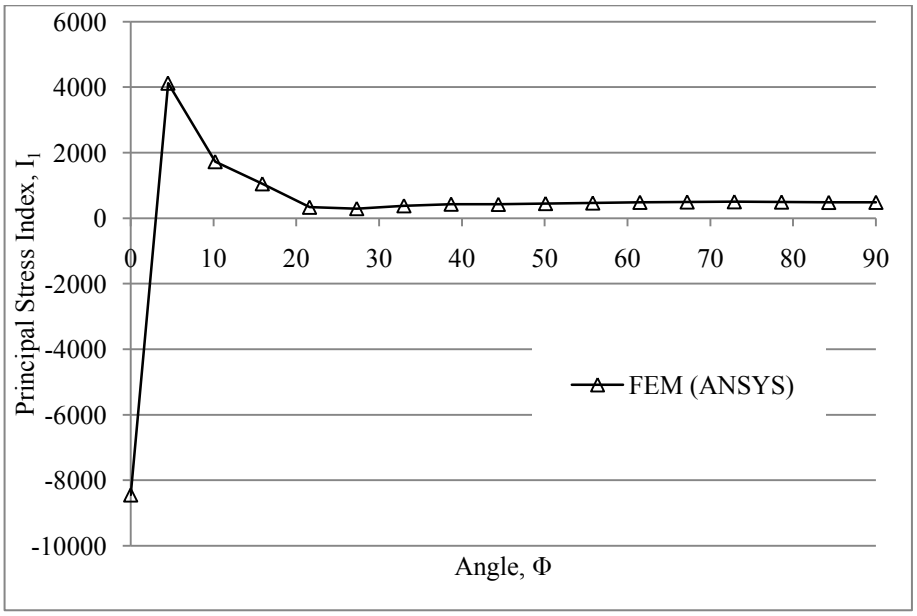

Figure 5.158. Principal stress indices in the keyway end for pure bending for Figure 4.15 model when $\alpha=90^0$

Principal stress distribution is given in Figure 5.158 when α is 90^0. High stresses are obtained between 0^0 and 20^0 of Φ.

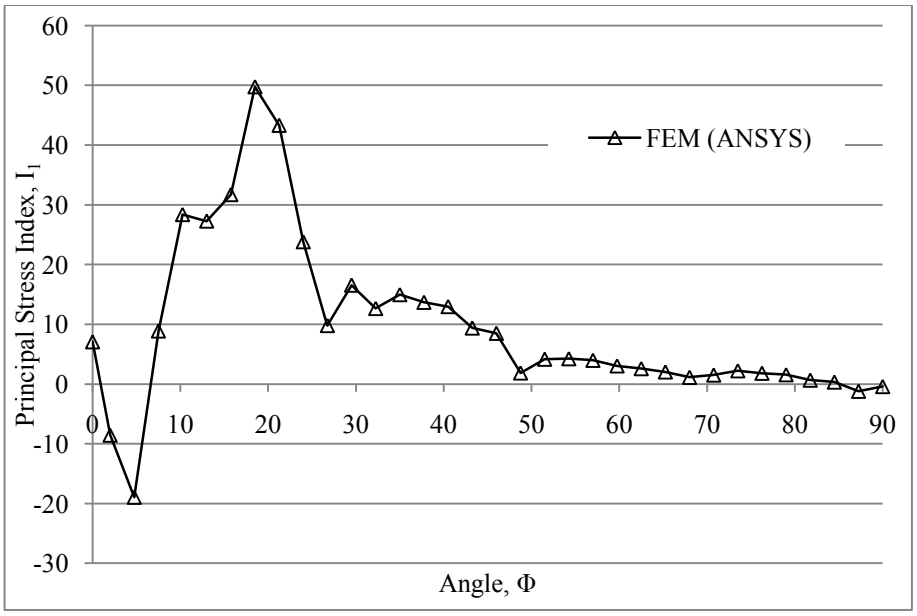

Figure 5.159. Principal stress indices in the keyway end for pure bending for Figure 4.17 model when $\alpha=0^0$

Principal stress indices is given in Figure 5.159 when α is 0^0. High stress indices are obtained between 15^0 and 25^0 of Φ.

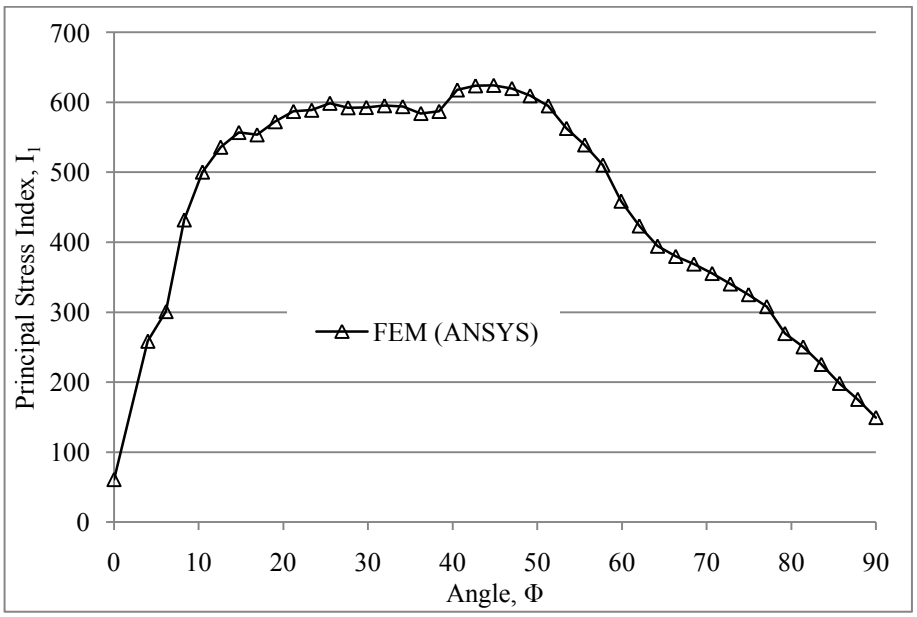

Figure 5.160. Principal stress indices in the keyway end for pure bending for Figure 4.17 model when $\alpha=30^0$

Principal stress indices can be seen in Figure 5.160 when α is 30^0. The highest stress indices are obtained between 40^0 and 50^0 of Φ.

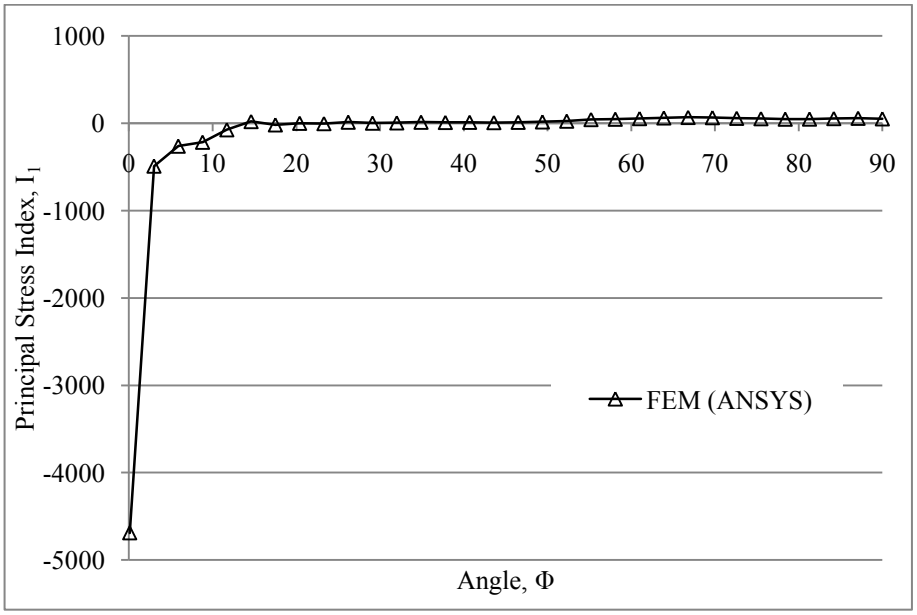

Figure 5.161. Principal stress indices in the keyway end for pure bending for Figure 4.17 model when $\alpha=60^0$

Principal stress indices are shown in Figure 5.161 when α is 60^0. Stress indices are rapidly changing when Φ is between 0^0 and 10^0. The highest stress is obtained at 0^0 of Φ.

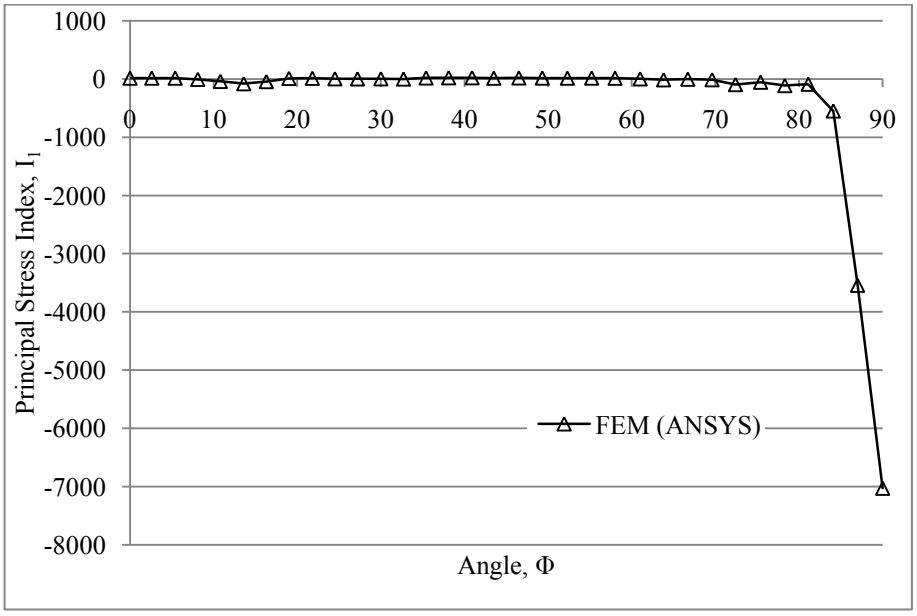

Figure 5.162. Principal stress indices in the keyway end for pure bending for Figure 4.17 model when $\alpha=90^0$

Principal stress indices can be seen in Figure 5.162 when α is 90^0. It is seen that the stress distribution is rapidly changing when Φ is between 80^0 and 90^0. The highest stress is obtained at 90^0 of Φ.

CHAPTER 6

CONCLUSIONS

In this thesis, keyed connections are analysed with finite element technique under torsion and bending loadings. Different key and keyway geometries of finite element models are used with different fit and friction conditions. The effect of key edge geometries, interferences and frictions between parts are researched and their results are presented.

In the finite element analyses of keyed connections under torsion, the following points are concluded:

- Augmented Lagrange contact algorithm gives the best results in 2D solutions.
- In 3D case, however, the Augmented Lagrange contact algorithm shows convergence problems. That's why, the Lagrange-Penalty contact algorithm is used in 3D solutions.
- Increasing the torque causes to convergence problems in all finite element solutions.
- The friction between parts directly influences the stresses. When increasing the friction coefficient between parts, the stresses at shaft keyway edge profile decreases. However, the characteristic of stress distribution is not influenced dominantly from the friction.
- The interference between parts slightly increases the stresses and its effect can be neglected. The clearances between parts decrease the stress indices but increase slipping.
- Key edge geometries directly influence the stresses. Big chamfered key edges cause less stresses. However, they cause more slipping. They also cause convergence problems in the finite element solutions. Small chamfered key edges cause higher stresses and smaller slipping.

- Generally the stress distributions obtained from finite element solutions are in good agreements with the experimental results.
- Contour plots of the stresses show that high stresses occur at the key edge corner contact points on the keyway.
- Contour plots also show that the stresses around the outside region of corners suddenly decrease.
- When the torque increases, the keyway profile stresses also increase. The stress indices, which are the ratio of the calculated stresses to the nominal stresses, generally decrease when increasing the torque.
- The slip of parts affects the stresses distributions. The contact points between key and keyways change when slip occurs. Hence, it causes changing the stress distributions.
- When the results of finite elements solutions are compared with experimental results, it is seen that the results of 3D models are better than 2D models.
- When increasing the fillet radius of keyway, stress concentration factors decreases in sled runner keyways.
- The highest principal stress indices are obtained when α is 60^0 at stepped shaft with end milled keyway under torsion.

In the finite element analyses of keyed connections under bending, the following conclusions are obtained:

- Keyways are modeled in two different ways; end milled keyways and sled runner keyways.
- The highest principal stress indices are obtained when α is 0^0 at the analysis of plain shaft with end milled keyway. In order to compare it with experimental results, the shaft is solved without key and hub.
- When key and hub are included in the models, there are not available experimental results. Therefore only the finite element solutions are discussed.
- The stresses obtained in the key, shaft and hub interaction model are generally much higher than the stresses obtained in the shaft without key and hub.

REFERENCES

[1] Fessler, H., Rogers, C.C. and Stanley, P. (1969). *Stresses at keyway ends near shoulders*. Journal of Strain Analysis, **4**, 267-277

[2] Okubo, H., Hosono, K. and Sakaki, K. (1968). *The stress concentration in keyways when torque is transmitted through keys*. Experimental Mechanics, **8**, 375-380

[3] Fessler, H., Rogers, C.C. and Stanley, P. (1969). *Stresses at end milled keyways in plain shafts subjected to tension, bending and torsion*. Journal of Strain Analysis, **4**, 180-189

[4] Fessler, H. and Eissa, M. (1982). *Elastic stresses due to torque transmitted through the prismatic part of keyed connections – Part I: effect of different fits and friction on standard shapes*. Journal of Strain Analysis, **17**, 103-111

[5] Fessler, H. and Eissa, M. (1982). *Elastic stresses due to torque transmitted through the prismatic part of keyed connections – Part II: effect of shape with usual fits and friction*. Journal of Strain Analysis, **17**, 215-222

[6] Fessler, H. and Eissa, M. (1983). *Three-dimensional elastic stress distribution in end-milled keyed connections*. Journal of Strain Analysis, **18**, 143-149

[7] Fessler, H. and Appavoo, T. (1989). *On the effect of key edge shape on keyway edge stresses in shafts in torsion*. Journal of Strain Analysis, **24**, 121-125

[8] Shaffer, B.W. (1994). *Bearing stress between a circumferential key and its keyway*. International Journal of Pressure Vessels and Piping, **58**, 1-8

[9] Fessler, H. and Warrior, N.A. (1999). *Advantages of cylindrical keys for torque transmission*. Journal of Strain Analysis, **34**, 225-233

[10] Çelik, M. (1999). *Comparison of three teeth and whole body models in spur gear analysis*. Mechanism and Machine Theory, **34**, 1227-1235

[11] Kanber, B. (2006). *Analysis of spur gears by coupling finite and boundary element methods*, Mechanics Based Design of Structures and Machines, **34**, 307–324

[12] Vogwell, J. (1998). *Analysis of a vehicle wheel shaft failure*. Engineering Failure Analysis, **5**, 271-277

[13] Berndt, F. and Bennekom, A.V. (2001). *Pump shaft failures a compendium of case studies*. Engineering Failure Analysis, **8**, 135-144

[14] Bhuamik, S.K., Rangaraju, R., Parameswara, M.A., Venkataswamy, M.A., Bhaskaran, T.A. and Krishnan, R.V. (2002). *Fatigue failure of a hollow power transmission shaft*. Engineering Failure Analysis, **9**, 457-467

[15] Parida, N., Tarafder, S., Das, S.K., Kumar, P., Das, G., Ranganath, V.R. and Bhattacharya, D.K. (2003). *Failure analysis of coal pulverizer mill shaft*. Engineering Failure Analysis, **10**, 733-744.

[16] Sekercioglu, T. (2006). *Fracture analysis of gear pump used for polymer production*. Engineering Failure Analysis, **13**, 835-842

[17] Göksenli, A. and Eryürek, I.B. (2009). *Failure analysis of an elevator drive shaft*. Engineering Failure Analysis, **16**, 1011-1019

[18] Vidner, J. and Leidich, E. (2007). *Enhanced Ruiz Criterion for the evaluation of crack initiation in contact subjected to fretting fatigue*. International Journal of Fatigue, **29**, 2040-2049

[19] Yang, D.C.H. and Tong, S. (2007). *On the profile design of transmission splines and keys*. Mechanism and Machine Theory, **42**, 82-87

[20] Terada, K. (1963). *Erneute untersuchung der formzahl für keilnuten*. Materialprüfung, **5**, 285-295